2021

DLL4 and JAG1 in the Glioblastoma Response to Temozolomide Chemotherapy

Bunston, Carly

UNIVERSITY OF PLYMOUTH

DLL4 AND JAG1 IN THE GLIOBLASTOMA RESPONSE TO TEMOZOLOMIDE CHEMOTHERAPY

By

CARLY BUNSTON

A thesis submitted to the University of Plymouth

in partial fulfilment for the degree of

DOCTOR OF PHILOSOPHY

Faculty of Health: Medicine, Dentistry and Human Sciences

July 2020

Acknowledgements

Firstly I would like to thank Professor Ji-Liang Li for giving me the opportunity to undertake this PhD and for his support and guidance throughout. I would also like to thank Professor Oliver Hanemann for taking over as my Director of Studies at the last hurdle, and Dr David Hilton (and the rest of the Neuropathology team) for sourcing patient samples and aiding in IHC analysis for this project. A sincere thank you goes to Dr Claudia Barros and Dr Jon Gil-Ranedo for supplying the U251 and CSC-5 cell lines, and to Professor Valentine Macauley for providing temozolomide during the foundation stages of this project.

To the JLL research group past and present, thank you for the help exchanged, the laughter shared, and for listening to my complaints when needed! It was a pleasure to teach and work alongside a number of placement students and it's a privilege to now see them pursuing their own scientific research careers.

A special thank you to Dr Paul Waines and Dr Claire Adams, two key individuals at JJB/DRF who are often overlooked! Thank you for your friendship, training, and guidance with lab management.

I would not have endured the past 4 years of this journey without the wonderful friends I met along the way. A huge thank you to "The Girls": Charlotte Illsley, Sarah Ellwood, Portia Maddick, Jemma Walker, Gabriela Wojcik, and Chloe Bolton. I cannot thank you all enough for the support, laughter, tears, and wine we all shared! It was a pleasure to share my PhD journey with you and wish you all the best for your respective futures. I hope in years to come we all look back on our time in Plymouth with fond memories.

Finally, none of this would have been possible without the unwavering love and support of my family who have always encouraged me to follow my ambitions. To my parents Janeen and Michael, grandparents Ivy and Bryan, and sister Alysha: this one's for you, diolch!

Author's Declaration

At no time during the registration for the degree of Doctor of Philosophy has the author been registered for any other University award without prior agreement of the Doctoral College Quality Sub-Committee.

Work submitted for this research degree at the University of Plymouth has not formed part of any other degree either at the University of Plymouth or at another establishment.

This study was financed with the aid of a studentship from PUPSMD and Brain Tumour Research.

Presentations at Conferences:

Oral and poster presentation at PUPSMD Annual Research Event, St Mellion, March 2017.

Poster presentation at PUPSMD Annual Research Event, University of Plymouth, March 2019.

Poster presentation at the 10th Brain Tumour Meeting, Berlin, May 2019.

Word count of main body of thesis: 57,611

Signed: 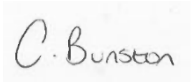

Date: 10/07/2020

Abstract

Name: Carly Bunston

Title: DLL4 and JAG1 in the glioblastoma response to temozolomide chemotherapy

Introduction: Glioblastoma multiforme is the most common aggressive primary malignant brain tumour in adults. The current gold standard treatment comprises of surgery followed by radiotherapy and adjuvant temozolomide (TMZ) chemotherapy. Prognosis is poor, with a median survival of 14.6 months following diagnosis. Treatment often fails due to intrinsic or acquired TMZ resistance of a small population of cells termed glioma cancer stem cells (GCSCs). A promising target for glioblastoma therapy is the Notch signalling pathway, which can be suppressed using gamma-secretase inhibitors such as dibenzazepine (DBZ). We investigated the effects of the Notch ligands, Delta-like 4 (DLL4) and Jagged-1 (JAG1) on tumour resistance to TMZ and GCSCs.

Methods: U87 and U251 glioblastoma cells were transduced with empty vector-, DLL4, and JAG1-encoded retroviruses. Cells were cultured under 2D, 3D, and CSC culture conditions and response to single (TMZ/DBZ) and combination (TMZ and DBZ) treatment was assessed. A patient derived GCSC line, CSC-5, was also used to evaluate the effect of single and combination treatment by neurosphere recovery assay.

Results: DLL4 and JAG1 overexpression promotes resistance by increasing the TMZ IC50. Neurosphere formation, recovery, and secondary neurosphere formation is increased following DLL4 and JAG1 overexpression and is reversed upon combination TMZ and DBZ treatment. TMZ has little effect on the self-renewal of GCSCs, however single DBZ and combination DBZ and TMZ treatment significantly reduces GCSC self-

renewal. Consequently, Notch inhibition reduces GCSC marker expression and may promote GCSC differentiation.

Conclusions: These data show the importance of the Notch pathway, in particular the ligands DLL4 and JAG1 in resistance to TMZ chemotherapy and GCSC self-renewal. The addition of Notch inhibitors to current treatment is a promising approach to overcome TMZ resistance and decrease brain tumour recurrence and encourages further translational and clinical studies.

Contents

Acknowledgements i

Author's Declaration iii

Abstract iv

List of Figures xiii

List of Tables xx

Abbreviations xxii

1 Introduction 2

1.1 Clinical Overview of Glioblastoma Multiforme 2

1.1.1 Epidemiology 5

1.1.2 Risk Factors 5

1.1.3 Clinical Presentation 8

1.1.4 Diagnosis and Screening 9

1.1.5 Pathological Classification 9

1.1.6 Glioblastoma Treatment 18

1.2 Cancer Stem Cells in Glioblastoma 48

1.2.1 Stem Cells 48

1.2.2 Cancer Stem Cell Hypothesis 49

1.2.3 Glioma Cancer Stem Cells 51

1.2.4 The Role of Glioma Cancer Stem Cells in Resistance and Tumour Progression 52

1.3 Notch Signalling Pathway 56

1.3.1 Biology 56
1.3.2 Notch Signalling 56
1.3.3 Notch Signalling in Neurogenesis 60
1.3.4 Notch Pathway Deregulation in Glioblastoma 62
1.3.5 Notch Pathway Deregulation in Glioma Cancer Stem Cells 71
1.3.6 Notch Signalling and Treatment Resistance 73
1.3.7 DLL4 and JAG1 in Glioblastoma 74
1.4 Thesis Aims 74
2 Materials and Methods 77
2.1 Cell Lines 77
2.2 Cell Culture and Maintenance 77
2.2.1 Preparation of Growth Medium for Cell Maintenance 77
2.2.2 Cell Maintenance 79
2.2.3 Passaging of Cells 79
2.2.4 Cell Counting 80
2.2.5 Cryopreservation of Cell Lines 81
2.2.6 3D Spheroid Culture 81
2.2.7 Neurosphere Culture 84
2.3 MTT Cell Viability Assay 87
2.3.1 IC50 Assay 87
2.4 Generation of Overexpression Cell Lines 89

2.4.1 Generation of Retroviral Constructs 89

2.4.2 Virus Packaging and Production 89

2.4.3 Retroviral Infection of Cell Lines 91

2.5 Generation of shRNA Knockdown Cell Lines 92

2.6 Quantitative Reverse Transcription Polymerase Chain Reaction (RT-qPCR) ... 94

2.6.1 Background 94

2.6.2 Total RNA Isolation 94

2.6.3 RNA Quantification 95

2.6.4 cDNA Synthesis 96

2.6.5 qPCR 97

2.7 Western blotting 100

2.7.1 Background 100

2.7.2 Cell Lysis 100

2.7.3 Protein Quantification 100

2.7.4 Protein Sample Preparation 101

2.7.5 Sodium Dodecyl Sulphate-Polyacrylamide Gel Electrophoresis (SDS-PAGE) 102

2.7.6 Electroblotting 103

2.7.7 Incubation with Antibodies 105

2.7.8 Development of Membrane 105

2.8 Immunofluorescence 107

2.8.1 Immunofluorescence Staining Method 107

2.8.2 Whole Mount Staining of Neurospheres 108

2.9 Immunohistochemistry 110

2.9.1 Background 110

2.9.2 Method 110

2.10 Statistical Analysis 114

3 DLL4 and JAG1 Increase Glioblastoma Resistance to Temozolomide Chemotherapy by Induction of Notch Signalling 117

3.1 Introduction 117

3.1.1 Mechanisms of Temozolomide Resistance 118

3.1.2 Notch in Glioblastoma 119

3.2 Methods 123

3.3 Results 126

3.3.1 DLL4 and JAG1 induce Notch Signalling in Glioblastoma Cell Lines 126

3.3.2 Increased Glioblastoma Resistance to Temozolomide by DLL4 and JAG1 in 2D Culture 130

3.3.3 Glioblastoma Resistance to Temozolomide by DLL4 and JAG1 is Reversed by Notch Inhibition by Dibenzazepine 132

3.3.4 DLL4 and JAG1 Have No Effect on Glioblastoma Cell Line Proliferation 138

3.3.5 Temozolomide and Dibenzazepine Co-treatment Significantly Reduces Glioblastoma Cell Line Proliferation 144

3.3.6 Combination Dibenzazepine and Temozolomide Treatment Reduces Growth in a 3D Spheroid Model 150

3.3.7 Increased Glioblastoma Resistance to Temozolomide by DLL4 and JAG1 in a 3D Spheroid Model 153

3.4 Discussion 162

4 DLL4 and JAG1 Increase Glioblastoma Resistance to Temozolomide Chemotherapy by Regulation of Glioma Cancer Stem Cells 168

4.1 Introduction 168

4.1.1 Glioma Cancer Stem Cells 168

4.1.2 Glioblastoma Cell of Origin 170

4.1.3 Markers of Glioma Cancer Stem Cells 172

4.1.4 Glioma Cancer Stem Cells and Treatment Resistance 173

4.1.5 Glioma Cancer Stem Cells and Notch Signalling 174

4.2 Methods 178

4.3 Results 183

4.3.1 DLL4 and JAG1-induced Notch signalling regulates the self-renewal of U87 and U251 glioblastoma neurospheres *in vitro* 183

4.3.2 DLL4 and JAG1 Increase Glioma Cancer Stem Cell Marker Expression .. 191

4.3.3 DLL4 and JAG1 induce Notch signalling in a Glioma cancer stem cell line, CSC-5. 202

4.3.4 DLL4 and JAG1 increase self-renewal in CSC-5 gliomas cancer stem cells 206

4.3.5 DLL4 and JAG1 Increase Glioma Cancer Stem Cell Marker Expression in the Patient-Derived GCSC Line CSC-5. 212

4.3.6 Single DBZ and Combination DBZ and TMZ treatment results in differentiation of CSC-5 glioma cancer stem cells 217

4.3.7 DLL4 and JAG1 knockdown reduces Notch signalling in the glioma cancer stem cell line, CSC-5. 246

4.3.8 DLL4 and JAG1 Knockdown Reduces CSC-5 Neurosphere Growth 246

4.4 Discussion 255

5 DLL4, JAG1, and Glioma Cancer Stem Cell Marker Expression in Paired Primary and Recurrent Glioblastoma 263

5.1 Introduction 263

5.1.1 Glioma Grading 263

5.1.2 Glioma Biomarkers 264

5.1.3 Notch Signalling in Glioblastoma 265

5.2 Methods 267

5.3 Results 269

5.3.1 DLL4 and JAG1 Staining 269

5.3.2 Correlation with Nestin Staining 271

5.3.3 Correlation with CD133 Staining 271

5.3.4 Correlation with MGMT Status 277

5.4 Discussion 281

6 Discussion 287

6.1 General Discussion 287

6.2 Experimental Limitations 296

6.3 Future Directions 298

6.4 Conclusions 301

7 References 302

8 Appendix 334

8.1 Analysis of Spheroid Volume using ImageJ 334

8.1.1 Macro 334

8.2 ΔΔCT Method for Analysing RT-qPCR Data 341

8.3 IHC Quantification 343

List of Figures

Figure 1.1: Relative frequency of Primary Brain and other Central Nervous System Tumours in adults.....3

Figure 1.2: Brain cells and brain tumours. 4

Figure 1.3: The effect of IDH1 and IDH2 mutations. 12

Figure 1.4: NICE recommendations for the management of newly diagnosed glioblastomas. 20

Figure 1.5: TMZ mechanism of action. 23

Figure 1.6: MGMT Mechanism of Action. 25

Figure 1.7: Mechanisms of DNA repair following DNA damage by TMZ chemotherapy. 29

Figure 1.8: Overall survival analysis of glioblastoma patients given radiotherapy alone versus radiotherapy plus TMZ. 35

Figure 1.9: The stochastic and hierarchical models of tumourigenesis. 50

Figure 1.10: Glioma cancer stem cells mediate resistance and tumour recurrence following TMZ treatment. 54

Figure 1.11: Domain organisation of human Notch receptors and DSL-family ligands. .57

Figure 1.12: The Notch signalling pathway. 59

Figure 2.1: 3D spheroid culture model. 83

Figure 2.2: Neurosphere recovery assay overview. 86

Figure 2.3: Assembly of the Western blot transfer apparatus. 104

Figure 3.1: Mechanisms of resistance to TMZ chemotherapy in glioblastoma. 120

Figure 3.2: Expression of DLL4 and JAG1 in U87 and U251 cells transduced with mDLL4 and mJAG1. 127

Figure 3.3: DLL4 and JAG1 expression in U87 cells following mDLL4 and mJAG1 retroviral transduction. 128
Figure 3.4: DLL4 and JAG1 expression in U251 cells following mDLL4 and mJAG1 retroviral transduction. 129
Figure 3.5: DLL4 and JAG1 induce Notch signalling in the U87 and U251 glioblastoma cell lines. 131
Figure 3.6: DLL4 and JAG1 confer U87 glioblastoma resistance to TMZ. 133
Figure 3.7: DLL4 and JAG1 confer U251 glioblastoma resistance to TMZ. 134
Figure 3.8: Expression of the Notch downstream target genes HES1, HEY1 and HEY2 in U87 cells following DBZ treatment. 136
Figure 3.9: Expression of the Notch downstream target genes HES1, HEY1 and HEY2 in U251 cells following DBZ treatment. 137
Figure 3.10: DBZ pre-treatment reduces TMZ IC50 in U87 cells. 139
Figure 3.11: DBZ pre-treatment reduces TMZ IC50 in U251 cells. 140
Figure 3.12: DLL4 and JAG1 have no effect on U87 and U251 cell proliferation. 141
Figure 3.13: DLL4 and JAG1 have no effect on U87 cell proliferation. 142
Figure 3.14: DLL4 and JAG1 have no effect on U251 cell proliferation. 143
Figure 3.15: U87 cell proliferation following single 25 nM DBZ/25 µM TMZ and combination 25 nM DBZ and 25 µM TMZ treatment. 145
Figure 3.16: The effect of single 25 nM DBZ/25 µM TMZ and combination 25nM DBZ and 25 µM TMZ treatment on Ki67 staining of U87 cells. 146
Figure 3.17: U251 cell proliferation following single 25 nM DBZ/25 µM TMZ and combination 25 nM DBZ and 25 µM TMZ treatment. 148
Figure 3.18: The effect of single 25nM DBZ/25 µM TMZ and combination 25nM DBZ and 25µM TMZ treatment on KI67 staining of U251 cells. 149

Figure 3.19: Development of the U87 3D spheroid model. 151
Figure 3.20: Development of the U251 3D spheroid model. 152
Figure 3.21: Combination DBZ and TMZ treatment significantly reduces U87 spheroid growth. 154
Figure 3.22: DLL4 and JAG1 confer TMZ resistance in a U87 3D spheroid model. 156
Figure 3.23: DLL4 and JAG1 confer TMZ resistance in a U251 3D spheroid model. 157
Figure 3.24: DBZ pre-treatment reduces TMZ IC50 in U87 spheroids. 159
Figure 3.25: DBZ pre-treatment reduces TMZ IC50 in U251 spheroids. 160
Figure 4.1: Glioblastoma cell of origin. 171
Figure 4.2: DLL4- and JAG1-induced Notch signalling regulates U87 primary neurosphere formation. 184
Figure 4.3: DLL4- and JAG1-induced Notch signalling regulates U251 primary neurosphere formation. 186
Figure 4.4: DBZ and TMZ combination treatment significantly reduces U87 neurosphere recovery. 187
Figure 4.5: DBZ and TMZ combination treatment significantly reduces U251 neurosphere recovery. 189
Figure 4.6: DBZ and TMZ combination treatment significantly reduces U87 secondary neurosphere formation. 190
Figure 4.7: DBZ and TMZ combination treatment significantly reduces U251 secondary neurosphere formation. 192
Figure 4.8: DLL4 and JAG1 increase GCSC marker expression in U87 primary neurospheres which is reversed upon combination DBZ and TMZ treatment. 194
Figure 4.9: DLL4 and JAG1 increase GCSC marker expression in U251 primary neurospheres which is reversed upon combination DBZ and TMZ treatment. 195

Figure 4.10: DLL4 and JAG1 increase GCSC marker expression in recovered U87 neurospheres which is reversed upon combination DBZ and TMZ treatment. 197
Figure 4.11: DLL4 and JAG1 increase GCSC marker expression in recovered U251 neurospheres which is reversed upon combination DBZ and TMZ treatment. 198
Figure 4.12: DLL4 and JAG1 increase GCSC marker expression in U87 secondary neurospheres which is reversed upon combination DBZ and TMZ treatment. 200
Figure 4.13: DLL4 and JAG1 increase GCSC marker expression in U251 secondary neurospheres which is reversed upon combination DBZ and TMZ treatment. 201
Figure 4.14: Expression of DLL4 and JAG1 in CSC-5 glioma cancer stem cells transduced with mDLL4 and mJAG1. 203
Figure 4.15: DLL4 and JAG1 expression in CSC-5 glioma cancer stem cells following mDLL4 and mJAG1 retroviral transduction. 204
Figure 4.16: DLL4 and JAG1 induce Notch signalling in CSC-5 glioma cancer stem cells. 205
Figure 4.17: DBZ and TMZ combination treatment significantly reduces CSC-5 primary neurosphere formation 207
Figure 4.18: DBZ and TMZ combination treatment significantly reduces CSC-5 neurosphere recovery following treatment. 209
Figure 4.19: DBZ and TMZ combination treatment significantly reduces CSC-5 secondary neurosphere formation following treatment 211
Figure 4.20: DLL4 and JAG1 increase GCSC marker expression in CSC-5 primary neurospheres. 213
Figure 4.21: DLL4 and JAG1 increase GCSC marker expression in recovered CSC-5 neurospheres. 214

Figure 4.22: DLL4 and JAG1 increase GCSC marker expression in CSC-5 secondary neurospheres. 216
Figure 4.23: Immunofluorescent staining of CD133 and GFAP of primary CSC-5 neurosphere formation following single DBZ/TMZ and combination DBZ and TMZ treatment. 219
Figure 4.24: Immunofluorescent staining of Nestin and β-III-tubulin of primary CSC-5 neurosphere formation following single DBZ/TMZ and combination DBZ and TMZ treatment. 221
Figure 4.25: Immunofluorescent staining of SOX2 and SOX10 of primary CSC-5 neurosphere formation following single DBZ/TMZ and combination DBZ and TMZ treatment. 224
Figure 4.26: Immunofluorescent staining of the proliferation marker Ki67 following single DBZ/TMZ and combination DBZ and TMZ treatment. 225
Figure 4.27: Immunofluorescent staining of CD133 and GFAP following CSC-5 neurosphere recovery following single DBZ/TMZ and combination DBZ and TMZ treatment. 228
Figure 4.28: Immunofluorescent staining of Nestin and β-III-tubulin following CSC-5 neurosphere recovery following single DBZ/TMZ and combination DBZ and TMZ treatment. 230
Figure 4.29: Immunofluorescent staining of SOX2 and SOX10 following CSC-5 neurosphere recovery following single DBZ/TMZ and combination DBZ and TMZ treatment. 232
Figure 4.30: Immunofluorescent staining of the proliferation marker Ki67 following CSC-5 neurosphere recovery following single DBZ/TMZ and combination DBZ and TMZ treatment. 234

Figure 4.31: Immunofluorescent staining of CD133 and GFAP following CSC-5 secondary neurosphere formation following single DBZ/TMZ and combination DBZ and TMZ treatment. 238
Figure 4.32: Immunofluorescent staining of Nestin and β-III-tubulin following CSC-5 secondary neurosphere formation following single DBZ/TMZ and combination DBZ and TMZ treatment. 240
Figure 4.33: Immunofluorescent staining of SOX2 and SOX10 following CSC-5 secondary neurosphere formation following single DBZ/TMZ and combination DBZ and TMZ treatment. 242
Figure 4.34: Immunofluorescent staining of the proliferation marker Ki67 following CSC-5 neurosphere secondary neurosphere formation. 244
Figure 4.35: Expression of DLL4 and JAG1 in CSC-5 glioma cancer stem cells transduced with shRNA lentiviral particles targeting DLL4 and JAG1. 247
Figure 4.36: DLL4 and JAG1 shRNA knockdown reduces Notch signalling in CSC-5 glioma cancer stem cells. 248
Figure 4.37: DLL4 and JAG1 shRNA knockdown significantly reduces CSC-5 primary neurosphere formation. 250
Figure 4.38: DLL4 and JAG1 shRNA knockdown significantly reduces CSC-5 neurosphere recovery. 251
Figure 4.39: DLL4 and JAG1 shRNA knockdown significantly reduces CSC-5 secondary neurosphere formation. 253
Figure 5.1: Representative IHC staining of the Notch ligand DLL4 in glioblastoma. 270
Figure 5.2: Representative IHC staining of the Notch ligand JAG1 in glioblastoma. 272
Figure 5.3: Comparison between DLL4 and JAG1 staining scores in (A) primary and (B) recurrent glioblastoma. 273

Figure 5.4: Representative IHC staining of the GCSC marker Nestin in glioblastoma. . 274

Figure 5.5: Comparison between staining scores for the Notch ligands DLL4 and JAG1 and the glioma cancer stem cell marker Nestin in primary and recurrent glioblastoma. 275

Figure 5.6: Representative IHC staining of the GCSC marker CD133 in glioblastoma. . 276

Figure 5.7: Comparison between the Notch ligands DLL4 and JAG1 and the glioma cancer stem cell marker CD133 in primary and recurrent glioblastoma. 278

Figure 5.8: Correlation of CD133 staining quantification in primary and recurrent glioblastoma samples. 279

Figure 5.9: Comparison between staining scores for the Notch ligands DLL4 and JAG1 and MGMT status in primary and recurrent glioblastoma. 280

Figure 8.1: ΔΔCT method used in this study to analyse qPCR data 342

Figure 8.2: Immunohistochemistry staining quantifications for primary and recurrent glioblastoma samples. 344

List of Tables

Table 1.1: Main familial tumour syndromes associated with brain tumours. 6

Table 1.2: Key characteristics of IDH-wildtype and IDH-mutant glioblastomas. 14

Table 1.3: Phase 2 and 3 trials of TMZ in malignant glioma. 33

Table 1.4: Expression pattern of Notch receptors and ligands in the adult brain. 60

Table 1.5: Examples of Cancer Clinical Trials involving Inhibitors of Notch Signalling 66

Table 2.1: Details of Cell Lines. 78

Table 2.2: Santa Cruz Biotechnology shRNA lentiviral particles 93

Table 2.3: cDNA synthesis reaction components 96

Table 2.4: cDNA synthesis cycling parameters. 96

Table 2.5: List of primers used for qPCR analysis 98

Table 2.6: qPCR reaction mix. 99

Table 2.7: qPCR cycling parameters. 99

Table 2.8: Components of the polyacrylamide resolving and stacking gels. 103

Table 2.9: 10X running buffer. 103

Table 2.10: Transfer buffer. 104

Table 2.11: List of primary and secondary antibodies used for Western Blot analysis 106

Table 2.12: List of primary and secondary antibodies used for immunofluorescence. 109

Table 2.13: Primary antibodies used for Immunohistochemistry. 112

Table 3.1: List of primers used in Chapter 3 124

Table 3.2: List of primary and secondary antibodies used for Western Blotting and Immunofluorescence in Chapter 3 125

Table 4.1: List of primers used in Chapter 4 180

Table 4.2: List of primary and secondary antibodies used for Western Blotting in Chapter 4. 181

Table 4.3: List of primary and secondary antibodies used for Immunofluorescence in Chapter 4. 182

Table 5.1: List of antibodies used for immunohistochemistry in Chapter 5 268

Abbreviations

5-ALA	5-Aminolevulinic acid
AA	Anaplastic astrocytoma
ABC	ATP-binding cassette
AD	Autosomal dominant
AE	Adverse event
ADAM	A disintegrin and metalloproteinase
AIC	4-Amino-5-imidazole carboxamide
AKT	Protein kinase B
ALT	Alternative lengthening of telomeres
AML	Acute myeloid leukaemia
ANK	Ankyrin
ANOVA	Analysis of variance
AP	Apurinic/apyrimidinic site
APC	Adenomatous polyposis coli
APE-1	AP endonuclease
APS	Ammonium persulphate
ATCC	American Type Culture Collection
ATP	Adenosine triphosphate
ATRX	Alpha thalassemia/mental retardation syndrome X-linked
BAX	Bcl-2 associated X
Bcl2	B-cell lymphoma-2
BCRP	Breast cancer resistance protein
BER	Base excision repair
bHLH	Basic helix-loop-helix
BMP	Bone morphogenic protein
BTSC	Brain tumour stem cell
CBTRUS	Central Brain Tumour Registry of the United States
CDKN	Cyclin-dependent kinase inhibitor
cDNA	Complementary DNA
Chk	Checkpoint response kinases
CNS	Central nervous system

CpG	Cytosine-phosphate-guanine
CRC	Cancer Research Campaign
CSC	Cancer stem cells
CSL	CBF1, Suppressor of Hairless, Lag1
CT	Computed tomography
Da	Daltons
DAB	3-3'-Diaminobenzidine
DAPI	4',6-Diamidino-2-phenylindole
DBZ	Dibenzazepine
DEPC	Diethylpyrocarbonate
DLL	Delta-like
DLT	Dose-limiting toxicities
DMEM	Dulbecco's modified Eagle medium
DMSO	Dimethylsulphoxide
DNA	Deoxyribonucleic acid
dsDNA	Double-stranded DNA
DSL	Delta-serrate-lag
EDTA	Ethylenediaminetetraacetic acid
EGFR	Epidermal growth factor receptor
ERK	Extracellular signal-related kinase
EV	Empty vector control
FBS	Foetal bovine serum
FEN-1	Flap endonuclease-1
FFPE	Formalin-fixed paraffin-embedded
FGF	Fibroblast growth factor
GABP	GA-binding protein
GalC	Galactosylceramidase
GAPDH	Glyceraldehyde 3-phosphate dehydrogenase
GBM	Glioblastoma multiforme
GCSC	Glioma cancer stem cells
GFAP	Glial fibrillary acidic protein
GSI	Gamma secretase inhibitor

Gy	Gray
H3K9	Histone H3 lysine 8
HD	Heterodimerisation domain
HEPES	4-(2-Hydroxyethyl)-1-piperazineethanesulfonic acid
HERP	Hes-related protein
HES	Hairy enhancer of split
HIF	Hypoxia inducible factor
HRP	Horseradish peroxidase
IDH	Isocitrate dehydrogenase
IF	Immunofluorescence
IGF	Insulin-like growth factor
IHC	Immunohistochemistry
IMR-1	Inhibitor of Mastermind recruitment-1
IRES	Internal ribosome entry site
JAG	Jagged
kDa	Kilodaltons
KDM	Lysine-specific histone demethylase
LNR	Lin-Notch repeats
MAML	Mastermind
MAP2	Microtubule-associated protein 2
MAPK	Mitogen-activated protein kinase
MGMT	O6-Methylguanine-DNA methyltransferase
miRNA	MicroRNA
MLH1	MutL homolog 1
MMR	Mismatch repair
MNNL	Module at the N-terminus of Notch ligands
MPG	N-methylpurine DNA glycosylase
MRI	Magnetic resonance imaging
MRP1	Multi-drug resistance protein 1
MSH2	MutS homolog 2
MSH6	MutS homolog 6
MTD	Maximum tolerated dose

MTIC	(5-[3-(2-Chloroethyl)triazen-1-yl]imidazole-4-carboxamide)
mTOR	Mammalian target of rapamycin
MTT	3-(4,5-Dimethylthiazol-2-yl)-2,5-diphenyl tetrazolium bromide
NAPDH	Nicotinamide adenine dinucleotide phosphate
NEAA	Non-essential amino acids
NECD	Notch extracellular domain
NES	Nestin
NF1	Neurofibromatosis 1
NF2	Neurofibromatosis 2
NICD	Notch intracellular domain
NICE	National Institute for Health and Care Excellence
NLS	Nuclear localisation signals
NOS	Not otherwise specified
NRR	Negative regulatory region
NSC	Neural stem cells
OLIG1	Oligodendrocyte transcription factor 1
OMM	Outer mitochondrial membrane
ORR	Objective/overall response rate
OS	Overall survival
PBS	Phosphate buffered saline
PCR	Polymerase chain reaction
PD	Drug pharmacodynamics
PDX	Patient-derived xenograft
PEST	Pro-Glu-Ser-Thr domain
PET	Positron emission tomography
PFS	Progression free survival
P-gp	P-glycoprotein
PI3K	Phosphoinositide 3-kinase
PMS2	PMS1 homolog 2
PTCH1	Patched 1 tumour suppressor
PVDF	Polyvinyl difluoride
qPCR	Quantitative PCR

RAM	RBPJ-associated molecule
RBPJ	Recombination signal binding protein for immunoglobulin kappa J region
RISC	RNA-induced silencing complex
RNA	Ribonucleic acid
RNAi	RNA interference
RPM	Rotations per minute
RT	Room temperature
RTK	Receptor tyrosine kinase
RT-qPCR	Quantitative reverse transcription polymerase chain reaction
SCID	Severe combined immunodeficient
SDS-PAGE	Sodium dodecyl sulphate-polyacrylamide gel electrophoresis
SGZ	Subgranular zone
shRNA	Short hairpin RNA
SNP	Single nucleotide polymorphism
SOX	SRY-Box Transcription Factor
SVZ	Subventricular zone
T-ALL	T-cell acute lymphoblastic leukaemia
TAD	Transcriptional activation domain
TEMED	N,N,N',N'-Tetramethylethane-1,2-diamine
TERT	Telomerase reverse transcriptase
TMZ	Temozolomide
TP53	Tumour protein p53
TSC	Tumour sclerosis complex
TUBB3	β-III-tubulin
VHL	von Hippel-Lindau
WHO	World Health Organisation

Chapter 1

1 Introduction

1.1 Clinical Overview of Glioblastoma Multiforme

Primary brain tumours are a heterogenous group of tumours arising from cells within the central nervous system (CNS). Brain tumours are characterised by high morbidity and mortality owing to their location and locally invasive growth. Gliomas are among the most common type of primary brain tumour accounting for 26% of all primary brain tumours, 81% of all malignant tumours (Figure 1.1), and are responsible for the majority of deaths from primary brain tumours (1, 2). Gliomas are tumours of neuroectodermal origin and are thought to arise from neurological stem or progenitor cells (3, 4). The classification of gliomas has undergone major restructuring with the release of the 2016 World Health Organisation (WHO) classification of tumours of the CNS (5). Gliomas are classified as astrocytomas, oligodendrogliomas, and ependymomas based on morphological similarities to the neuroglial cell types found in the brain (Figure 1.2). Recent advances in molecular biology has improved the understanding of glioma pathogenesis and has resulted in new concepts of glioma diagnosis, grading, and treatment.

Glioblastoma multiforme is a grade IV astrocytoma and is the most common primary malignant brain tumour in adults. The incidence of glioblastoma is estimated at 3.2 per 100,000 population with more than 10,000 cases annually diagnosed in the United States. The incidence of glioblastoma increases with age, with a median age of diagnosis of 65 years (1). Glioblastomas arise *de novo* as primary tumours in more than 90% of cases, with no clinical or histological evidence of a less malignant precursor.

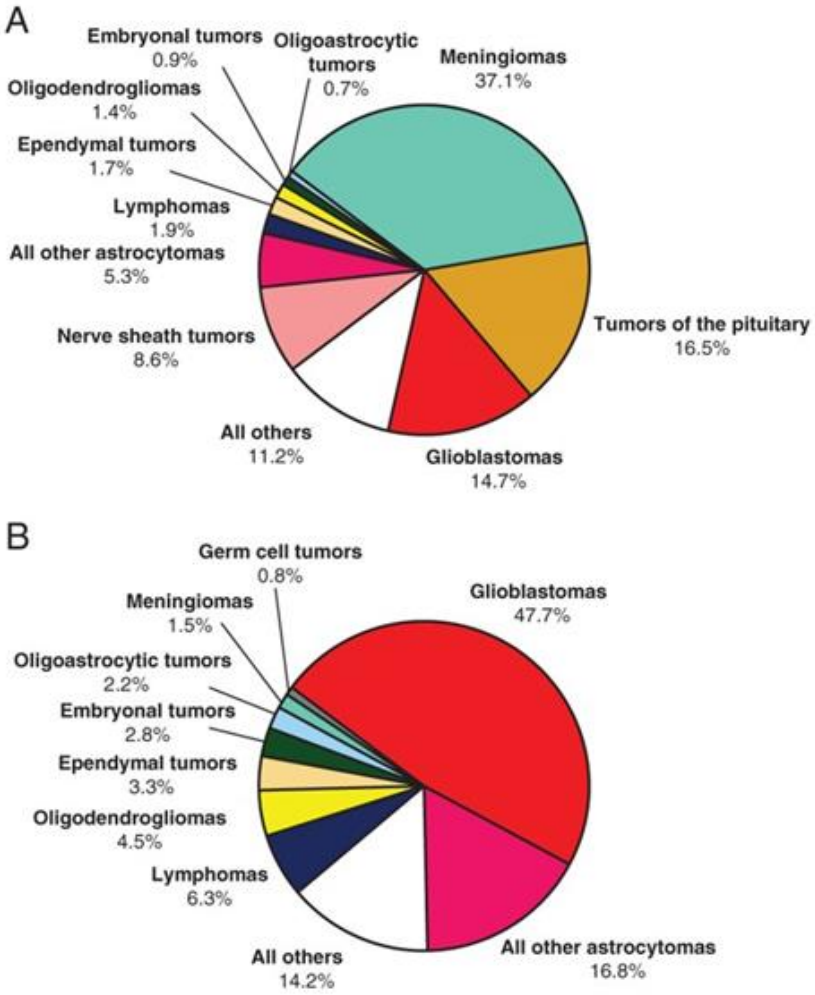

Figure 1.1: Relative frequency of Primary Brain and other Central Nervous System Tumours in adults.

(A) The distribution of primary brain and other central nervous system histologies. Gliomas account for 26% of primary brain tumours diagnosed in the United States, with glioblastomas accounting for approximately half of all gliomas diagnosed (n = 392,982). **(B)** The distribution of malignant brain and other central nervous system tumours by histology. Glioblastomas account for 47.7% of malignant brain tumours diagnosed in adults (n = 121,277). Diagram adapted from (1).

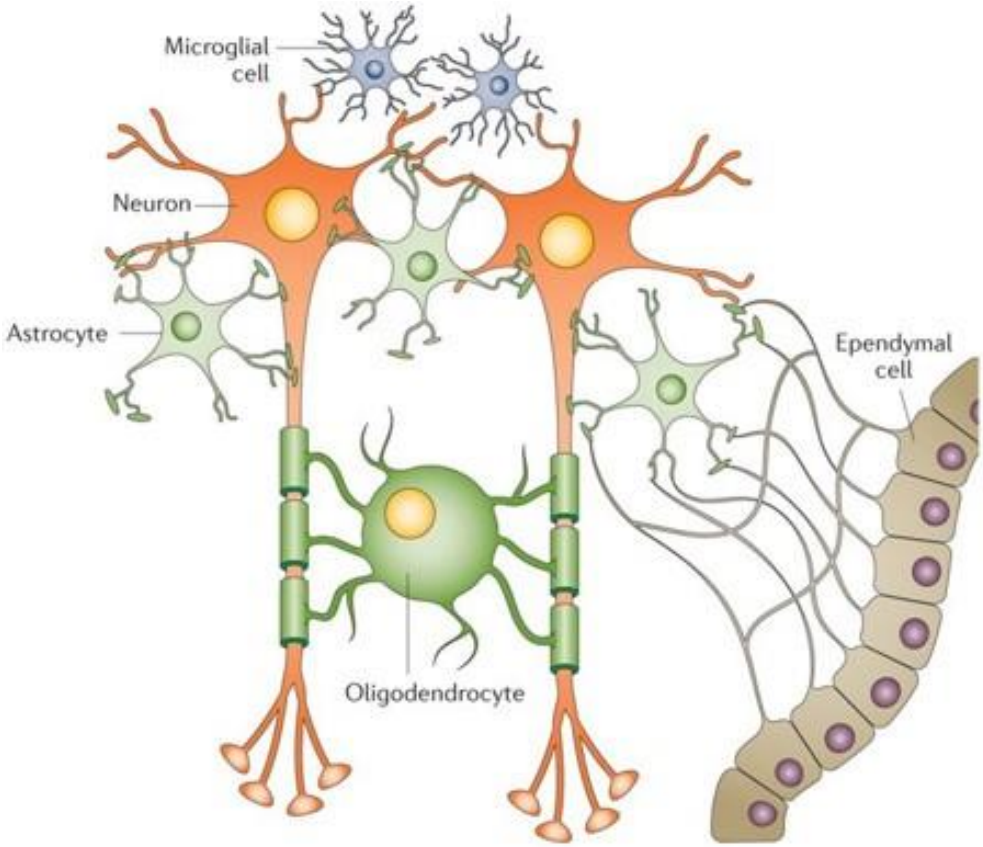

Figure 1.2: Brain cells and brain tumours.

Gliomas are classified histologically into astrocytomas, oligodendrogliomas, mixed astrocytic gliomas, or ependymomas based on morphological similarities to the neuroglial cell types found in the brain. Neurons form extensive networks and serve to control the main functions of the brain, including regulation of homeostasis, circadian rhythms, and all higher nervous system functions. Astrocytes are supportive glial cell components in neural tissue, forming the main connective tissue of the brain. Oligodendrocytes serves the function of providing support and insulation to CNS axons by wrapping them with myelin. Microglial cells exert limited immune function and have roles in tissue repair and restoration. Diagram taken from (6).

Secondary glioblastoma progresses from lower grade astrocytomas and are more prevalent in younger patients (7). Glioblastoma primarily manifests in the cerebral hemispheres, but may occur in the cerebellum, brainstem, or spinal cord. Patients with glioblastoma present with a variety of symptoms including seizures, focal neurological deficits, confusion, memory loss, and personality changes (8). Prognosis for patients is poor, with a progression-free survival of 7-8 months, median survival of 14.6 months, and a 5 year overall survival (OS) of just 9.8% (9).

1.1.1 Epidemiology

The 2018 Central Brain Tumour Registry of the United States (CBTRUS) found primary brain tumours account for approximately 2% of all cancers, with an annual incidence of 21.4 per 100,000 individuals. Gliomas represent approximately 26% of all primary brain tumours, and glioblastoma accounts for 56.6% of all gliomas diagnosed (Figure 1.1) (1).

The incidence of glioblastoma varies with sex, age, and ethnic origin. Glioblastoma occurs slightly more frequently in men than women (1.4:1) and incidence is higher in Caucasians relative to other ethnicities. Glioblastoma primarily presents in older adults, with a median age of 65 years at diagnosis, but can occur at any age, including childhood (1).

1.1.2 Risk Factors

For the majority of patients with glioblastoma, there is no known cause of the disease and risk factors other than age are poorly defined (6). A small subset of glioblastomas (less than 5%) are due to genetic predisposition syndromes (Table 1.1), and fewer than 20% of patients have a strong family history of cancer (10, 11).

The only well-established causative is exposure from ionising radiation (12, 13); however, only a small minority of brain tumours caused by radiation exposure are

Table 1.1: Main familial tumour syndromes associated with brain tumours.

	Gene	Inheritance	CNS Tumours
Neurofibromatosis type 1	*NF1*	50% AD; 50% *de novo*	15-20% optic pathway glioma; 4% low grade glioma (brainstem glioma); 1% glioblastoma*.
Neurofibromatosis type 2	*NF2*	50% AD; 50% *de novo*	80% schwannoma; 50% intracranial meningioma; 20% spinal meningioma; 30% spinal ependymoma.
Schwannomatosis	*SMARCB1, LZTR1*	AD	Meningioma; non vestibular schwannomas.
Li-Fraumeni	*TP53*	80% AD; 20% *de novo*	Wide range of brain tumours reported in 20-60%; glioblastoma; medulloblastoma; choroid plexus carcinoma.
Von Hippel-Lindau	*VHL*	80% AD; 20% *de novo*	80% haemangioblastoma; (cerebellum/spinal cord/retina).
Turcot type 1 (brain tumour-polyposis syndrome 1, hereditary non-polyposis cancer syndrome [HNPCC], constitutional mismatch repair cancer syndrome or deficiency, Lynch syndrome)	MMR genes: *MLH1, PMS2, MSH2, MSH6, EPCAM*		3% glioblastoma.
Turcot type 2 (brain tumour-polyposis syndrome 2, familial adenomatous polyposis [FAP], Gardner syndrome)	*APC*	85% AD, 15% *de novo*	Medulloblastoma (WNT activated).

Gorlin syndrome (nevoid basal cell carcinoma)	*PTCH1; SUFU*	75% AD; 25% *de novo*	5% medulloblastoma (SHH-activated); meningioma.
Tuberous sclerosis complex	*TSC1; TSC2*	85% AD; 25% AD	10% subpendymal giant cell astrocytoma; subependymoma.
Melanoma-astrocytoma (familial atypical multiple mole melanoma [FAMMM])	*CDKN2A; CDKN2B; P14/ARF*	AD	Astrocytoma; pleomorphic xanthoastrocytoma; meningioma.
Breast cancer (BRCA)	*BRCA-1; BRCA-2*		Glioma.
Cowden syndrome (multiple hamartoma syndrome)	*PTEN*	50% AD, 50% *de novo*	Dysplastic gangliocytoma of the cerebellum (Lhermitte-Duclos syndrome)
DICER1 syndrome (pleuropulmonary blastoma familial tumour and dysplasia syndrome)	*DICER1*	AD	Pineoblastoma; pituitary blastoma.
Multiple endocrine neoplasia type 1 (Werner syndrome)	*MEN1*	AD	Pituitary adenoma; ependymoma.

*Prevalence of high-grade gliomas is 10-50 times higher in NF1 patients than the general population (14). AD = autosomal dominant. TP53 = tumour protein p53. NF1 = neurofibromatosis type 1. NF2 = neurofibromatosis type 2. MMR = mismatch repair. APC = adenomatous polyposis coli. PTCH1 = patched 1 tumour suppressor. TSC = tuberous sclerosis complex. CDKN = cyclin-dependent kinase inhibitor. VHL = von Hippel-Lindau tumour suppressor. Table adapted from (10).

glioblastomas (13). Exposure to radiofrequency electromagnetic fields via mobile phone use has gained significant attention as a potential risk factor for brain tumour development. Despite multiple large studies, no conclusive causative role for radiofrequency electromagnetic fields has been established for brain tumours. However, cumulative evidence suggests a slight increased risk of glioma with long term (>10 year) mobile phone use (15-17). In 2011, radiofrequency electromagnetic fields were classified by both the WHO and International Agency for Research on Cancer as possibly carcinogenic (18), and were upgraded to probably carcinogenic in 2015 (19). Still, the association remains controversial and additional research is required.

1.1.3 Clinical Presentation

The presentation of a patient with glioblastoma can vary greatly depending on tumour size, location, and anatomical structures of the brain involved. Patients often present with symptoms of increased intracranial pressure, including headaches, nausea, drowsiness, blurred vision, and focal or progressive neurological deficits. A seizure occurs as the presenting symptom in approximately 25% of patients, and can occur in up to 50% of patients who are at a later stage of the disease (20, 21).

Tumours present in functional areas of the brain will cause more obvious focal neurological deficits than in other areas. Tumours of the frontal lobe may cause weakness or dysphasia; parietal lobe tumours may cause numbness, hemineglect, or spatial disorientation; and tumours involving the optic radiations in the temporal, parietal, or occipital lobe may result in visual field defects. Conversely, tumours located in the prefrontal lobe, temporal lobe, or corpus callosum often result in more subtle cognitive dysfunctions including personality changes, mood disorders, and

short-term memory deficits. Infratentorial tumours can cause a combination of cranial-nerve palsies, cerebellar dysfunction, and long-tract signs (10).

1.1.4 Diagnosis and Screening

Brain tumours commonly present with the development of neurological deficits over a period of weeks to months or the onset of seizures in a previously healthy individual. These symptoms require a neurological work-up that includes a neuroimaging assessment. The National Institute for Health and Care Excellence (NICE) recommends patients are offered a standard structural magnetic resonance imaging (MRI) without and with contrast enhancement as the initial diagnostic test for suspected glioma, unless MRI is contraindicated (22). The clinical value of other imaging techniques, such as magnetic resonance spectroscopy or positron emission tomography (PET), remains to be established. However, PET appears to be of value in tumour grading and can be used to aid surgical planning (6, 23).

1.1.5 Pathological Classification

A definitive diagnosis of glioblastoma can only be made by histology. Histological diagnoses based on tumour resections are more reliable than those based on biopsies due to limited tissue, the risk of sampling error, and possible under grading. Many features inherent to morphology-based histological classification provide a useful stratification to enable clinicians to define risk groups. However, a classification system based on morphology alone leaves much unknown and incomplete, especially due to the recent advances in determining the molecular markers of gliomas.

1.1.5.1 WHO Classification of Tumours of the Central Nervous System 2016

Tumours of the CNS are classified and diagnosed based on a system devised by the WHO. Until recently, primary CNS tumours were defined on the basis of histological

criteria and assigned a grade (from I to IV). This system was originally built on the histopathological and microscopic features of haematoxylin and eosin stained sections, such as cell type, level of differentiation, and presence of lineage-specific markers (24).

Studies over the past two decades have clarified the genetic basis of tumorigenesis, and in 2016, the WHO released its update to the 2007 classification of tumours of the CNS. This updated classification incorporates signature molecular genetic alterations to the classic histology. This combined genotypic and phenotypic classification has resulted in integrated diagnoses, where the histopathological name is followed by the genetic features of the tumour, e.g. glioblastoma, *IDH*-wildtype. In cases of discordant results from histology and molecular genetic features, the genotype is considered to be more informative than the histological phenotype (5). The integration of molecular parameters improves both diagnostic objectivity and accuracy, and results in more precise determination of prognosis and treatment responses.

1.1.5.2 Glioma Grading

Prior to the 2016 WHO update, all astrocytic tumours were grouped together (24). As of 2016, gliomas have been separated into circumcised gliomas (WHO grade I) and diffusely infiltrating gliomas (WHO grades II-IV; whether astrocytic or oligodendroglial) based on their growth pattern and the absence/presence of isocitrate dehydrogenase (*IDH*) mutation (5). Circumcised gliomas represent tumours regarded as benign and curable by total resection. These gliomas do not have an *IDH* mutation and have frequent *BRAF* mutations and fusions, for example, pilocytic astrocytoma and pleomorphic xanthoastrocytoma (5, 10).

Conversely, diffuse gliomas are in most cases never cured by resection alone, are graded using histopathological criteria, and are classified according to diagnostic

molecular markers. According to the WHO's current histological definition grade II (low grade) diffuse astrocytomas display nuclear atypia (defined as variation in nuclear shape or size with accompanying hyperchromasia), tumours that also show anaplasia and increased mitotic activity (i.e. anaplastic astrocytomas) are considered grade III, whilst grade IV glioblastomas show additional microvascular proliferation, necrosis, or both (5). As a result of the 2016 classification, grade II-IV gliomas are further stratified into three diagnostic and prognostic subgroups based on their *IDH,* alpha thalassemia/mental retardation syndrome X-linked *(ATRX)*, and 1p/19q status (5, 10). The NICE recommends analysis of the following molecular markers to determine prognosis and guide treatment as described below (22).

1.1.5.2.1 Isocitrate Dehydrogenase Mutation

Mutations in *IDH* are key diagnostic and prognostic markers in gliomas (5, 25). IDH enzymes catalyse the oxidative decarboxylation of isocitrate to α-ketoglutarate, and in doing so, generate nicotinamide adenine dinucleotide phosphate (NAPDH) from NAPD+. IDH1 is the principle source of NAPDH in the brain (26), with NAPDH required to protect against oxidative damage (27). *IDH* mutation results in a loss of function of α-ketoglutarate production, but a gain of function to produce 2-hydroxyglutarate, a putative oncometabolite. 2-hydroxyglutarate has been found to competitively inhibit the activities of α-ketoglutarate-dependent dioxygenases, including histone demethylases and the ten-eleven translocation family of 5-methylcytosine hydroxylases. This results in genome-wide histone and DNA methylation alterations which may contribute to tumorigenesis (Figure 1.3) (28, 29).

IDH1 and *IDH2* mutations are thought to be an early event in gliomagenesis and are more commonly found in lower grade gliomas (>70% of grade II-III astrocytomas and

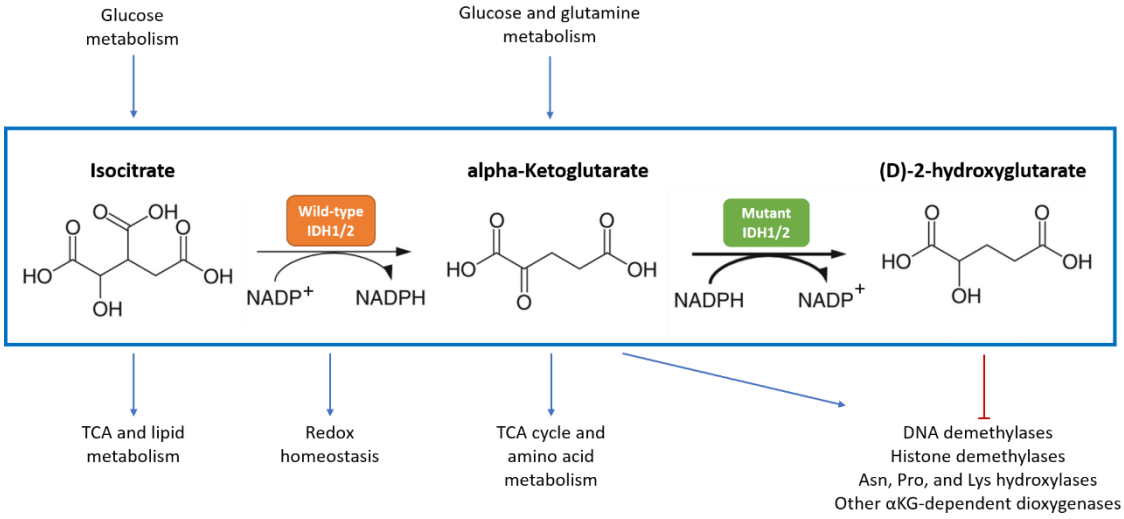

Figure 1.3: The effect of IDH1 and IDH2 mutations.

Wild-type IDH1 and IDH2 normally catalyse the reversible $NADP^+$-dependent oxidative decarboxylation of isocitrate to alpha-ketoglutarate in either the cytosol (IDH1) or mitochondria (IDH2). However, the mutant IDH enzyme loses oxidative activity and instead reduces alpha-ketoglutarate to (D)-2-hydroxyglutarate consuming one molecule of NAPDH in the process. Multiple cellular pathways are affected by mutations in IDH1 and IDH2. Metabolites involved in these reactions are critical for glucose, glutamine, NAPDH, amino acid, and lipid metabolism as well as epigenetic regulation. Diagram adapted from (30)

all oligodendrogliomas) than in glioblastomas (10, 31-33). In the 2016 CNS WHO glioblastomas are divided into:

1. Glioblastoma, *IDH*-wildtype (approximately 90% of cases), which corresponds more frequently with the clinically defined primary or *de novo* glioblastoma and predominates in patients over 55 years of age. The designation of *IDH*-wildtype should be applied to a glioblastoma when both R132H-mutant *IDH1* immunohistochemistry and subsequent *IDH1/2* sequencing reveal wildtype sequences at *IDH1* codon 132 and *IDH2* codon 172 (Table 1.2) (5).
2. Glioblastoma, *IDH*-mutant (approximately 10% of cases), which corresponds closely to secondary glioblastoma, in which patients have a history of prior lower grade diffuse glioma and preferentially arises in younger patients (Table 1.2).
3. Glioblastoma, NOS (not otherwise specified), is a diagnosis reserved for tumours in which full *IDH* evaluation cannot be performed (5, 7).

Diffuse gliomas which harbour *IDH1/2* mutations are associated with a better prognosis compared to *IDH*-wildtype gliomas (5).

Table 1.2: Key characteristics of IDH-wildtype and IDH-mutant glioblastomas.

	***IDH*-wildtype glioblastoma**	***IDH*-mutant glioblastoma**
Synonym	Primary glioblastoma, *IDH*-wildtype	Secondary glioblastoma, *IDH*-mutant
Precursor lesion	Not identifiable; develops *de novo*	Diffuse astrocytoma Anaplastic astrocytoma
Proportion of glioblastomas	~90%	~10%
Median age at diagnosis	~62 years	~44 years
Male-to-female ratio	1.42:1	1.05:1
Mean length of clinical history	4 months	15 months
Median overall survival - **Surgery + radiotherapy** - **Surgery + radiotherapy + chemotherapy**	 9.9 months 15 months	 24 months 31 months
Location	Supratentorial	Preferentially frontal
Necrosis	Extensive	Limited
TERT promoter mutations	72%	26%
TP53 mutations	27%	81%
ATRX mutations	Exceptional	71%
EGFR amplification	35%	Exceptional
PTEN mutations	24%	Exceptional

Table adapted from (5).

1.1.5.2.2 1p/19q Codeletion

Codeletion of chromosomes 1p and 19q results from the t(1:19)(q10:p10) non-balanced centrometric translocation (34). This codeletion alongside an *IDH* mutation is required for the diagnosis of oligodendroglioma, *IDH*-mutant and 1p/19q codeleted (5). It also has a prognostic value as codeletion is associated with better prognosis in oligodendroglial tumours and has been shown to be predictive of an increased response to alkylating chemotherapy (5, 32, 35).

1.1.5.2.3 Histone H3 Lys27Met Mutation

The novel entity of diffuse midline glioma, H3 Lys27Met-mutant (WHO grade IV), is molecularly defined by mutations in the genes encoding histone proteins H3.3 (*H3F3A*) or H3.1 (*HIST1H3B*) resulting in a lysine to methionine substitution at amino acid 27 (Lys27Met or K27M) (36-38). The H3 Lys27Met mutation is mutually exclusive with *IDH* mutations and is believed to be an early event in gliomagenesis (39, 40). Amongst all diffuse gliomas, H3 Lys27Met-mutant tumours confer the poorest prognosis (2-year survival <10%). As a result, they are considered WHO grade IV even if their histology appears low-grade or anaplastic (5). A predictive value for this mutation has yet to be identified (10).

1.1.5.2.4 O^6-methylguanine-DNA methyltransferase Promoter Methylation

O^6-methylguanine-DNA methyltransferase (MGMT) is a DNA repair protein involved in repairing damage induced by alkylating agents such as temozolomide (TMZ). Methylation of the *MGMT* associated 5'-cytosine-phosphate-guanine (CpG) island results in transcriptional gene silencing and sensitivity to alkylating agent chemotherapy, and has become one of the most studied biomarkers in neuro-oncology. Previous clinical trials have shown tumour response to TMZ is significantly

ameliorated when expression of *MGMT* is low due to promoter methylation (9, 41, 42). As highlighted by Hegi *et al., MGMT* promoter methylation results in a better outcome for patients receiving TMZ. Median OS of patients with *MGMT* promoter methylation is 18.2 months, compared to just 12.2 months for patients without *MGMT* methylation (42). However, its testing generally does not impact treatment as alkylating chemotherapy is the standard of care for all glioblastomas. *MGMT* promoter methylation also confers a favourable prognosis in both glioblastomas (9, 42) and anaplastic astrocytomas (43, 44). *MGMT* promoter methylation is commonly found in approximately 30-50% of primary, *IDH*-wildtype, glioblastomas, and in oligodendrogliomas (>90%), but it much less common in lower grade astrocytomas (45).

1.1.5.2.5 BRAF Mutation

B-raf is a protein kinase which regulates the RAS-RAF-MEK-ERK signalling pathway. Alterations in *BRAF*, such as $BRAF^{V600E}$ mutation or KIAA1549-BRAF fusion result in activation of the pathway leading to tumour growth and maintenance (46). The $BRAF^{V600E}$ mutation is more commonly found in circumcised gliomas, including 60-80% of pleomorphic xanthroastrocytoma (47), 30% of dysembryoplastic neuroepithelial tumours, 25% of gangliogliomas (48), and around 5-15% of pilocytic astrocytomas (47). The mutation is also found in approximately half of all *IDH*-wildtype epithelioid glioblastomas (47, 49). The KIAA1549-BRAF fusion is almost exclusively found in 75% of pilocytic astrocytomas (50), and is predictive of an indolent course (46, 47).

1.1.5.2.6 Telomerase Reverse Transcriptase Promoter Mutations

Telomeres are nucleoprotein complexes found at the end of all eukaryotic chromosomes and are composed of several hundred nucleotide repeats which

progressively shorten with each cycle of cell division. Telomerase is a ribonucleoprotein enzyme complex that requires a catalytic component (i.e. the telomerase reverse transcriptase [TERT]) and an RNA template for elongation of telomeres by adding hexameric 5'-TTAGGG-3' tandem repeats at chromosomal ends (51, 52). In normal somatic cells, the length of telomeres shorten at the end of each cycle of cell division (53, 54). When the chromosome ends reach a critical length, cells are directed towards senescence and apoptosis (55). Tumours are able to maintain their telomere length by either re-activation of telomerase or through telomerase-independent mechanisms collectively called alternative lengthening of telomeres (ALT), enabling indefinite proliferation and cell immortalisation (56-58). The promoter region of *TERT* contains two hotspots for point mutations (C228T and C250T), with the majority of glioblastomas (approximately 70%) carrying these mutations (59). *TERT* promoter mutations lead to the recruitment of multimeric GA-binding protein (GABP) transcription factor specifically to the mutant promoter, leading to increased TERT expression (60). *IDH*-mutant glioblastomas exhibit ALT due to concurrent loss-of-function mutations in *ATRX* (61, 62).

It has been reported that TERT promoter mutations are inversely correlated with *IDH* mutations, which is a well-defined molecular marker for a favourable prognosis (63). For example, the presence of *TERT* promoter mutations is associated with favourable outcomes in patients with *IDH*-mutant, 1p/19p-codeleted oligodendrogliomas, and with unfavourable outcomes among *IDH*-wildtype astrocytomas (64).

1.1.5.2.7 Alpha Thalassemia/Mental Retardation Syndrome X-Linked Mutation

ATRX gene mutations result in loss of ATRX expression and function. These inactivating mutations correlate with the ALT phenotype and are associated with telomere

dysfunction and other mutations including *IDH1* and *TP53,* but are mutually exclusive from 1p/19q codeletion (65, 66). A study by Abedalthagafi *et al.* has shown the ALT phenotype is associated with loss of ATRX expression in both paediatric and adult astrocytomas, suggesting ATRX loss to be a highly specific biomarker of tumours with an astrocytic lineage (67). *ATRX* mutations can be used to identify *IDH*-mutant astrocytomas and glioblastomas. However, it is only a characteristic of these tumours and its identification is not required for diagnosis (5).

1.1.6 Glioblastoma Treatment

In newly diagnosed glioblastoma patients, initial treatment is maximal safe resection, with the goals to achieve accurate histological diagnosis, establish the tumours molecular genotype, and improve the patient's quality of life and OS. The extent of tumour resection is largely dependent on the tumour location, surgeons experience, and the use of pre-operative and intra-operative techniques. A longer OS is seen in patients with a greater extent of tumour resection (68). However, glioblastomas are highly invasive tumours and commonly infiltrate the surrounding brain parenchyma, making full resection difficult. To improve the extent of resection, fluorescent imaging can be utilised during surgery. Fluorescent dyes such as 5-aminolevulinic acid (5-ALA) are preferentially taken up by tumour cells enhancing visualisation of the tumour during surgery. Fluorescence guided surgery has resulted in a significantly higher rate of complete resections in malignant gliomas (69), however, it is not clear if it improves OS (70, 71).

Following surgery, most glioblastoma patients with good performance status (Karnofsky performance status > 70) will undergo 6 weeks of radiotherapy (to either 60 Gy or 40 Gy depending on patient age) with concomitant daily TMZ chemotherapy.

This is followed by at least 6 cycles of TMZ chemotherapy, 5 days over a 21 day cycle (Figure 1.4) (22). Radiotherapy forms the mainstay of treatment, resulting in an increase in median survival from three to four months, to around nine to ten months (72). Concurrent radiotherapy and TMZ administration improves OS compared to radiotherapy alone (9). However, prognosis for glioblastoma patients is still very poor and median survival is just 14.6 months.

1.1.6.1 Temozolomide

1.1.6.1.1 Background

TMZ was first synthesised at Aston University in the 1980s as one of a series of novel imidazotetrazinones (73). Unlike the previously synthesised bicyclic triazenes which contained only two adjacent nitrogen atoms, imidazotetrazinones were structurally unique as they contained three adjacent nitrogen atoms conferring unique physiochemical properties along with a much greater anti-tumour activity (73, 74). The most potent anti-tumour compound of the imidazotetrazinones, mitozolomide, showed significant anti-tumour activity in a number of murine tumour model systems (75). Mitozolomide is a prodrug which undergoes spontaneous decomposition to a highly reactive metabolite MCTIC (5-[3-(2-chloroethyl)triazen-1-yl]imidazole-4-carboxamide), which causes DNA interstrand cross-linking resulting in cytotoxicity (76, 77). Phase 1 clinical trials revealed some activity against malignant melanoma and small-cell carcinoma of the lung. However, mitozolomide also produced severe thrombocytopenia which limited its use. As a result, further clinical development of mitozolomide was withdrawn (78).

A 3-methyl derivative of mitozolomide, TMZ, was found to exhibit less toxicity than mitozolomide but had comparable anti-tumour activity in murine models (79). Further

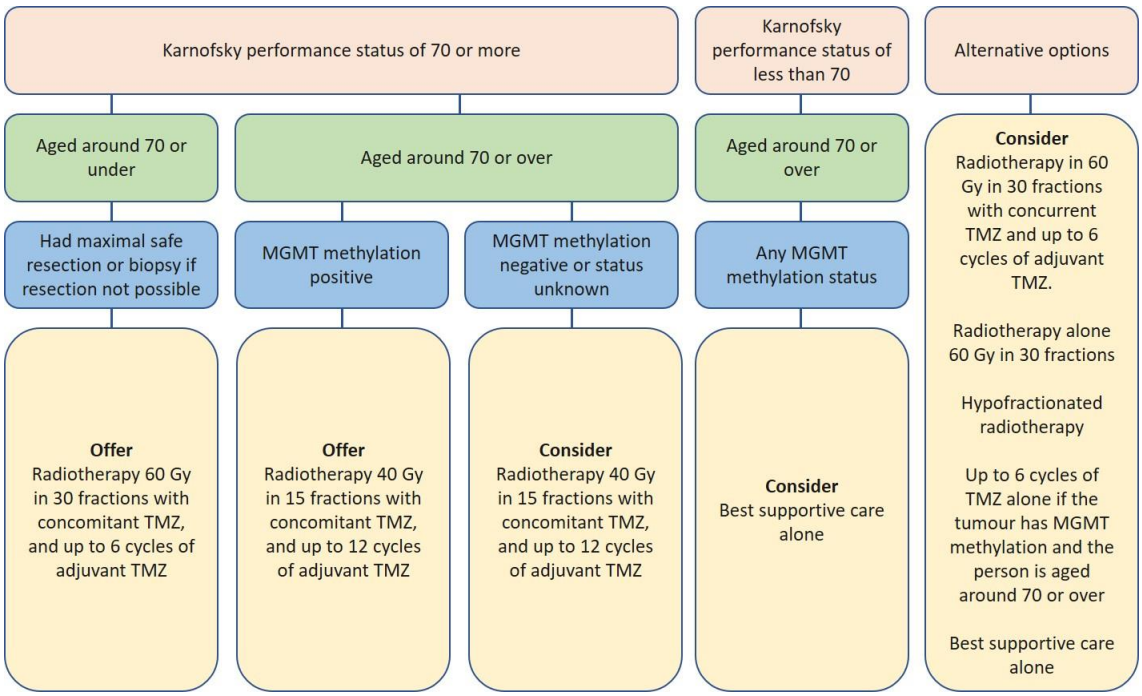

Figure 1.4: NICE recommendations for the management of newly diagnosed glioblastomas.

NICE recommended management options for patients with newly diagnosed grade IV glioma (22).

development and clinical evaluation of TMZ in cancer patients was undertaken due to the drugs wide tissue distribution including penetration into the murine brain, 100% bioavailability following oral administration, and no requirement for enzymatic conversion to its potent anti-tumour metabolite (74, 80).

1.1.6.1.2 Pharmacokinetics

The pharmacokinetics, safety, and anti-tumour activity of TMZ was initially evaluated in a Phase 1 clinical trial sponsored by the Cancer Research Campaign (CRC; London, UK) after animal studies demonstrated even tissue distribution, predictable drug kinetics, and tolerability. This trial included a total of 51 patients, nearly all of which had melanoma (81). Following oral administration, TMZ is rapidly and completely absorbed reaching peak serum concentration within 1-2 hours (82). Peak TMZ concentrations in the plasma and brain extracellular fluid are approximately 5.5 ± 3.2 µg/ml (11.8 – 44.8 µM) and 0.6 ± 0.3 µg/ml (1.55–4.64 µM), respectively. The mean time to reach peak level in the brain is around 2 hours (83). Once absorbed, TMZ binds minimally to plasma proteins limiting its interactions with other drugs administered concurrently in patients. As a small lipophilic molecule, TMZ readily penetrates the blood brain barrier and as such, is one of the few drugs with CNS activity (84). Dose modifications are not required for either liver or renal dysfunction since cytochrome P450 enzymes and the kidneys are not required for TMZ metabolism. Like absorption, TMZ elimination is equally as rapid, with a plasma half-life ranging from 1.6 to 1.8 hours, and a whole body clearance of 12 L/hour (81). Adverse events from TMZ administration are predictable and toxicities are normally reversible and not severe. During clinical trials, myelotoxicity was found to be the dose-limiting side effect, however compared to mitozolomide, it was less frequent and less severe. Mild to

moderate nausea and vomiting was also found to be dose related but is easily controlled with antiemetic medications (81).

1.1.6.1.3 Mechanism of Action

TMZ is a small (194 Da), lipophilic prodrug which undergoes spontaneous hydrolysis and is converted to the active metabolite intermediate 5-(-3-methyl-1-triazeno)imidazole-4-carboxamide (MTIC) by non-enzymatic chemical conversion at physiological pH. This spontaneous conversion is initiated by the effect of water at the highly electropositive C^4 position of TMZ. This activity opens the ring releasing CO_2, resulting in the generation of MTIC. MTIC is then irreversibly degraded to 4-amino-5-imidazole carboxamide (AIC) and a highly reactive methyldiazonium cation. The methyldiazonium cation formed by the breakdown of MTIC readily methylates guanine residues in DNA and is the principal mechanism responsible for TMZ cytotoxicity in malignant cells (Figure 1.5).

The most common lesion produced in DNA following TMZ treatment is methylation at the N^7 position of guanine (N^7-methylguanine; 60-80%), followed by methylation of the O^3 position of adenine (O^3-methyladenine; 10-20%), and O^6 position of guanine (O^6-methylguanine; 5-10%) (85). Despite being the least frequent, the formation of O^6-methylguanine is critical for TMZ cytotoxicity (86-88). In normal cells, direct repair of O^6-methylguanine by the enzyme MGMT effectively removes the methyl adduct, restoring guanine (Figure 1.6) (89). However, in MGMT deficient cells, methylation of the O^6 position of guanine leads to the insertion of a thymine instead of a cytosine adjacent to the methylguanine during subsequent DNA replication. This alerts the DNA mismatch repair (MMR) pathway, a protein complex including MutS homolog 2

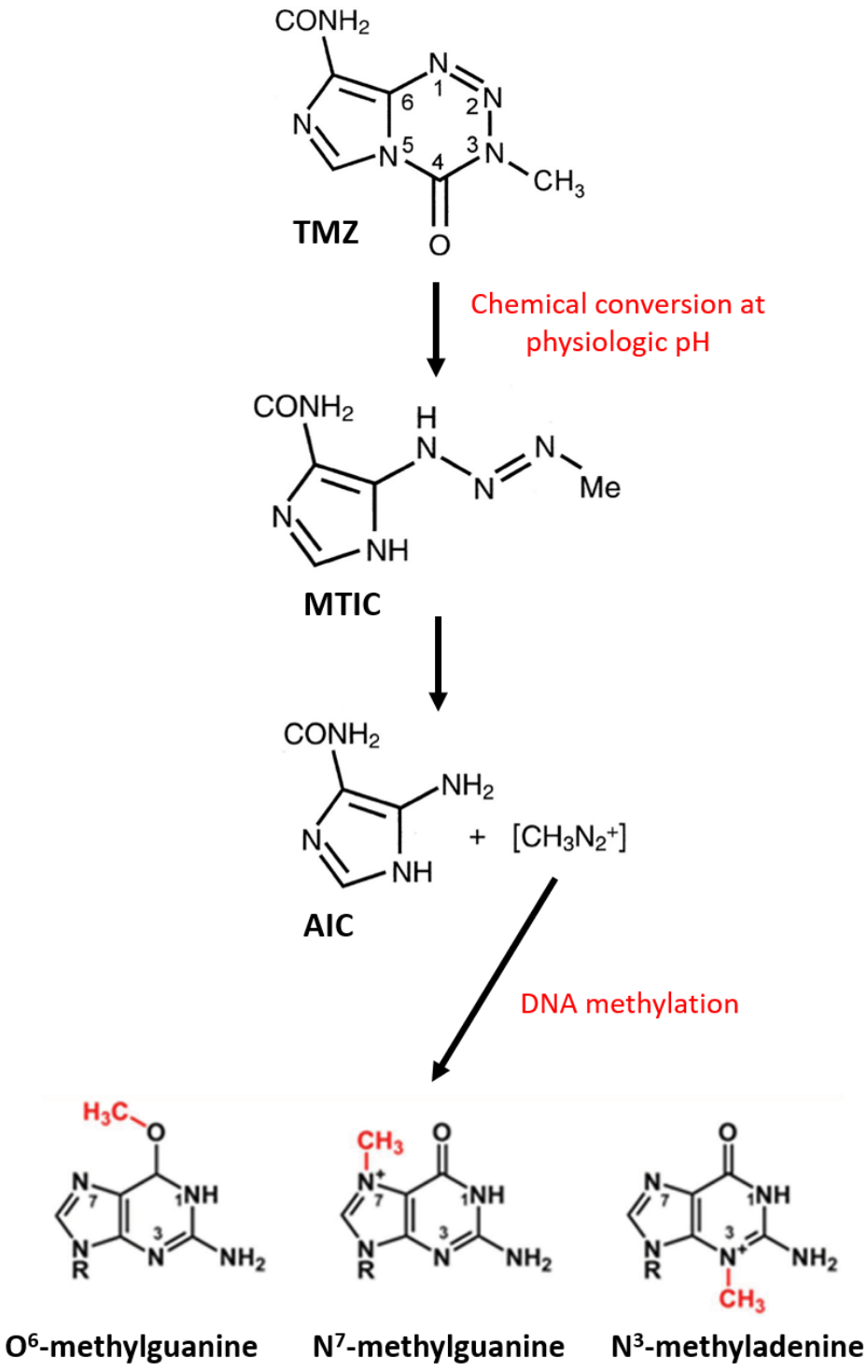

Figure 1.5: TMZ mechanism of action.

TMZ is converted to 5-(3-methyltriazen-l-yl)imidazole-4-carboximide (MTIC) following chemical conversion at physiological pH. MTIC is broken down to 5-aminoimidazole-4-carboxamide (AIC) and a highly reactive methyldiazonium cation. AIC is excreted via the kidneys and the methyldiazonium cations deliver methyl groups to DNA. Diagram adapted from (74).

(MSH2), MutS homolog 6 (MSH6), MutL homolog 1 (MLH1), and PMS1 homolog 2 (PMS2) which exclusively recognise the mispaired thymine on the daughter strand and excises it. However, if O^6-methylguanine persists in the template strand, thymine can still be misincorporated opposite O^6-methyguanine. This results in futile cycles of thymine reinsertion and excision during the S phase of the cell cycle. This process replication fork collapse and subsequent DNA double strand break that leads to G2/M arrest and ultimately cellular apoptosis (90). MMR-deficient cells are unable to detect alkylation adducts and are therefore resistant to TMZ, even when they lack MGMT (91). TMZ is therefore most cytotoxic in cells with low levels of MGMT and intact MMR (92).

1.1.6.1.4 Temozolomide and DNA Repair

There are several mechanisms to correct or prevent alkylation-induced DNA damage induced by TMZ. These mechanisms include direct repair which is achieved by removing only the abnormal alkyl group, without removing the affected base or nucleotide, and excision repair whereby a single base/nucleotide or a segment of the damaged DNA strand is excised, and the gap is filled by a combination of DNA polymerase and ligase. Two well-known excision repair systems used to detect and correct DNA damage resulting from TMZ treatment include base excision repair (BER) and MMR.

1.1.6.1.4.1 Direct Repair

Direct repair of the effects of TMZ is performed by the enzyme MGMT, a small 22 kDa protein able to remove the methyl group from the O^6-methylguanine adduct (88). The O^6 methyl group is transferred from guanine to an internal cysteine reside (Cys 145) of MGMT in a one-step reaction which does not rely on co-factors or enzymes (Figure 1.6)

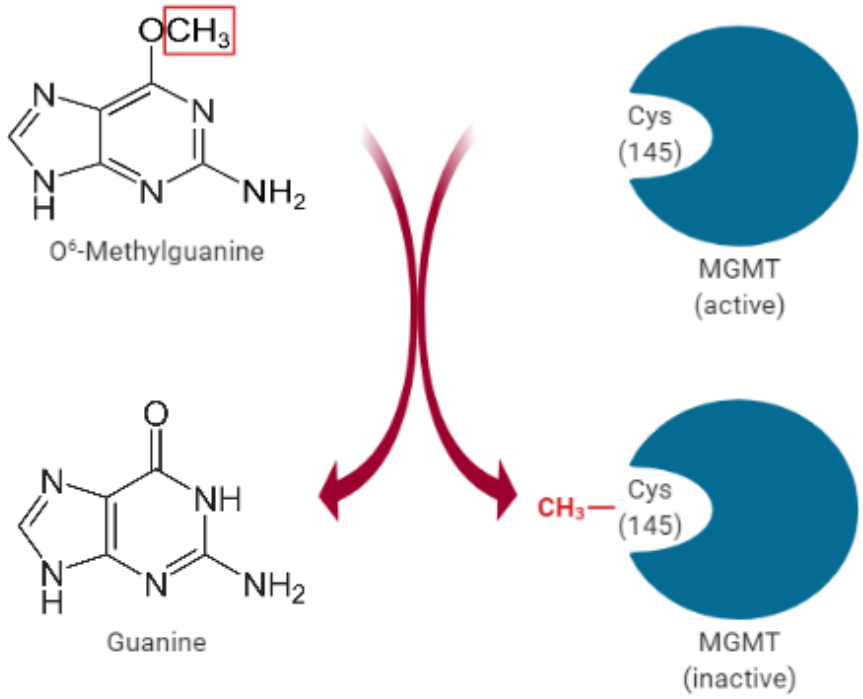

Figure 1.6: MGMT Mechanism of Action.

MGMT acts to transfer the alkyl group from O^6-methylguanine to an internal 145 cysteine residue of the MGMT protein. Diagram adapted from (93).

(94). This process is able to remove alkyl molecules at a 1:1 ratio, restoring guanine and thus eliminating further DNA strand breaks. As such, MGMT acts as an acceptor molecule by sequestering the methyl group from O^6-methylguanine (95). The enzyme then becomes inactivated and is degraded by ubiquitination (96). For this reason, MGMT is often referred to as a suicide enzyme.

Despite protecting healthy cells from alkylating carcinogens, MGMT also protects cancer cells from the same kind of chemical genotoxicity. This non-discriminatory effect of MGMT on both healthy and cancer cells is of concern since it counteracts the effect of TMZ treatment (93).

In some glioblastoma patients, reduced MGMT expression occurs due to epigenetic silencing of its gene. Conversely, some patients may display increased MGMT activity when compared to corresponding healthy tissue, therefore presenting an increase in tumour resistance to TMZ treatment (95). As such, low-level MGMT expression is considered a favourable predictive maker in TMZ-treated glioblastoma patients (42).

1.1.6.1.4.2 Base Excision Repair

BER is the major pathway involved in the excision and repair of modified or damaged nucleotides, abasic sites, and DNA single strand breaks generated by ionising radiation, reactive oxygen species, and alkylating agents. The overall estimate of 10^4 base damages per mammalian cell per day underlies the importance of BER (97). The two major lesions resulting from TMZ treatment, N^7-methylguanine and N^3-methyadenine, are both recognised and repaired by BER (88).

Damaged bases are recognised by lesion-specific glycosylases which hydrolytically cleave the N-glycosidic bond resulting in the generation of an internal abasic apurinic/apyrimidinic (AP) site. AP endonuclease (APE-1) then cleaves the

phosphodiester backbone on the 5’ side of the AP site, leaving a 3’-OH and 5’-deoxyribosephosphate termini at the DNA strand break. The terminal 5’-deoxyribose phosphate is then removed by exonuclease or DNA-deoxyribophosphodiesterase, resulting in a nucleotide gap. Further repair proceeds via one of two pathways: short patch which involves the replacement of a single nucleotide; and long patch which involves the replacement of 2 to 10 nucleotides. In short patch BER the single nucleotide gap is filled by DNA polymerase and the nick is sealed by DNA ligase III. Whereas in long patch BER, the DNA strand may become displaced resulting in the formation of a flap. Flap endonuclease-1 (FEN-1) cleaves the flap and the DNA ends are sealed by DNA ligase I (98, 99).

1.1.6.1.4.3 Mismatch Repair

If not repaired by MGMT, the O^6-methylguanine adduct produced by TMZ results in a structural distortion of DNA which can be recognised by MMR. MMR is the recognition and correction of mispaired bases and insertion/deletion loops generated during DNA synthesis. The MutSα complex (comprising of MSH2 and MSH6) recognises and binds to the mismatch lesion. MutSα binds to base to base mismatches and insertion/deletion loops of one or two nucleotides. The MSH2/MSH6 heterodimer undergoes an ATP-dependent conformational change recruiting the MLH1/PMS2 heterodimer, which coordinates the interplay between the mismatch recognition complex and additional proteins (including exonuclease-1, helicases, proliferating cell nuclear antigen, single strand DNA binding protein, DNA polymerase δ and ε) required for the removal and replacement of the mismatched base (88).

Following TMZ treatment, MMR can correct the error by replacing O^6-methylguanine with guanine or leave single strand breaks which can in turn generate potentially lethal

double-strand breaks during DNA replication. The MMR pathway recognises the mispaired thymine on the daughter strand and excises it. However, if O^6-methylguanine persists in the template strand, thymine can still be misincorporated opposite O^6-methyguanine. This results in futile cycles of thymine reinsertion and excision during the S phase of the cell cycle. This process triggers replication fork collapse and subsequent DNA double strand break that leads to G2/M arrest and ultimately cellular apoptosis (90). A successful MMR system is therefore required for TMZ cytotoxicity, and cells deficient in MMR are resistant to TMZ treatment (100, 101).

A diagrammatic overview of the mechanisms of DNA repair following TMZ induced DNA damage is given in Figure 1.7.

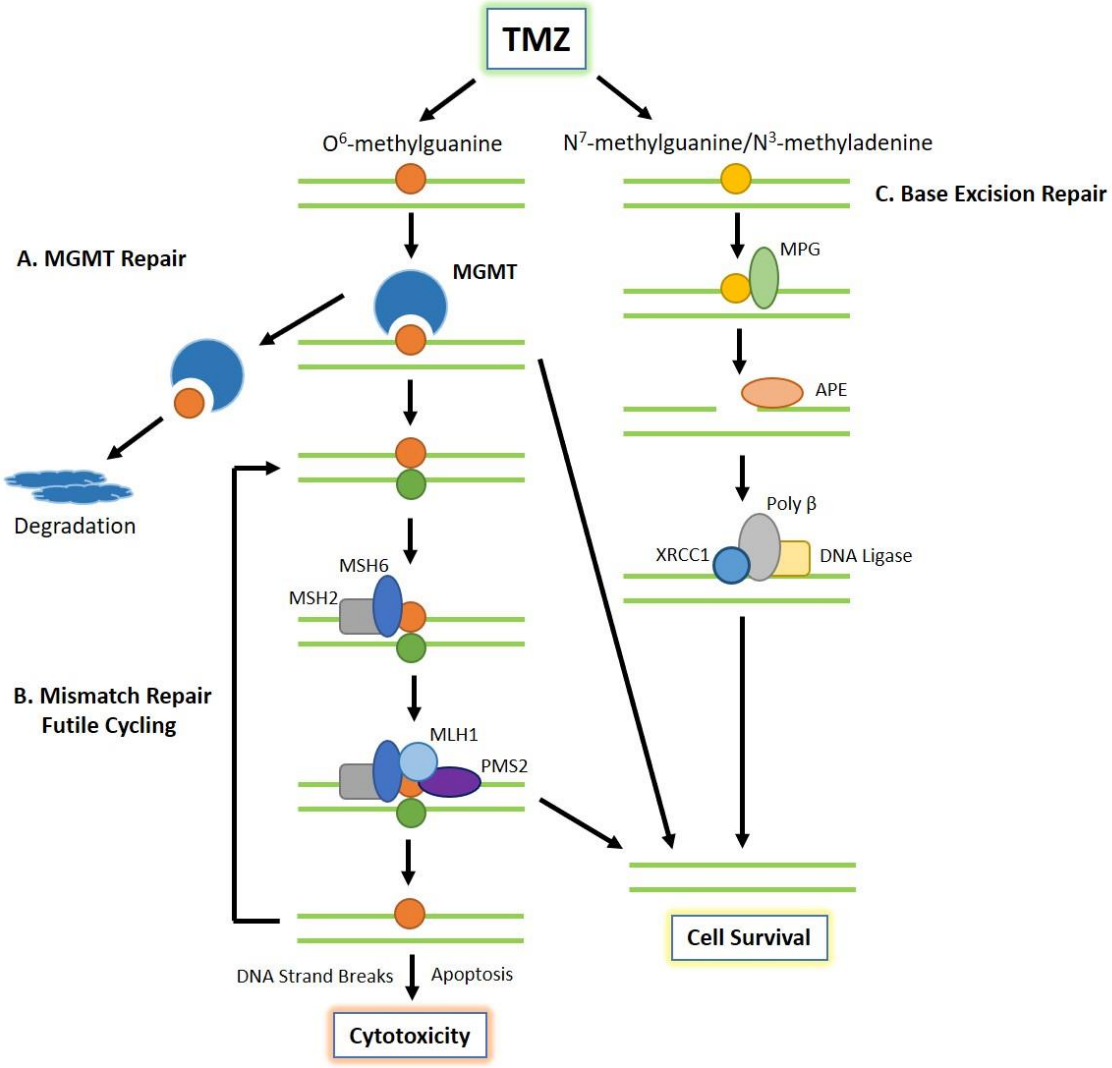

Figure 1.7: Mechanisms of DNA repair following DNA damage by TMZ chemotherapy.

TMZ chemotherapy results in the formation of cytotoxic DNA lesions including O^6-methylguanine (orange circle) and N^7-methylguanine/N^3-methyladenine (yellow circle). **(A)** MGMT removes the O^6-methylguanine adduct through transfer of the alkyl group to the conserved active site cysteine, restoring guanine. Following receipt of the methyl group, MGMT is inactivated and subjected to ubiquitin-mediated degradation. **(B)** If O^6-methylguanine escapes MGMT repair, it forms a base pair with thymine (green circle) during DNA replication. The mismatched base pair is recognised by the mismatch repair pathway, resulting in futile cycles of repair leading to cell death. **(C)** N^7-methylguanine/N^3-methyladenine adducts are efficiently repaired by the base excision repair pathway, however they contribute little to the cytotoxicity of TMZ. Diagram adapted from (102).

1.1.6.1.5 Clinical Trials with Temozolomide in Glioma

1.1.6.1.5.1 Phase 1 Clinical Trials

During the initial phase 1 clinical trial conducted by the CRC, a total of 51 patients with advanced cancer received a single oral dose of TMZ. This study initially evaluated the safety, pharmacokinetics and anti-tumour activity. TMZ demonstrated 100% bioavailability and peak plasma concentration occurred within 0.33-2 hours following oral administration. Drug elimination was shown to be equally as rapid, with a plasma half-life of 1.6-1.8 hours. The study showed the pharmacokinetics of TMZ to be linear and reproducible, with little variation between patients (81).

Due to the schedule-dependent anti-tumour activity of TMZ observed in preclinical studies, an additional 42 patients were given a single 150 mg/m^2 oral dose of TMZ and escalated to 240 mg/m^2 for 5 days in a 4-week cycle if no myelosuppression was detected. The dose limiting toxicity of TMZ was mild-to-moderate myelosuppression (neutropenia and thrombocytopenia), which was predictable and easy to control. The maximum tolerated dose was found to be 200 mg/m^2 per day (81). As a result, for Phase 2 studies the authors recommended a dosage of 150 mg/m^2 for the initial course, followed by 200 mg/m^2 for subsequent courses in the absence of major myelosuppression (74, 81).

As shown in preclinical evaluations of TMZ (103), Phase 1 studies demonstrated the anti-tumour activity of TMZ in numerous difficult-to-treat cancers. The CRC Phase 1 trial showed clinical responses were observed in patients with melanoma, mycosis fungoides, and high-grade glioma. The high-grade glioma patients enrolled in the study had good partial responses on CT scans with dramatic clinical improvements after prior

surgery and radiotherapy (81). This initial Phase 1 study warranted the further evaluation of TMZ in Phase 2 studies in melanoma, lymphoma, and gliomas.

1.1.6.1.5.2 Phase 2 and 3 Clinical Trials

Although previously used alkylating agents such as procarbazine had activity in the treatment of malignant glioma, the use of these agents was associated with high levels of toxicity and only a moderate improvement in patient OS. As such, there was an unmet clinical need for new effective chemotherapy agents that can be used in combination with other drugs or radiation to overcome resistance. The acceptable safety profile and clinical activity of TMZ observed in patients with malignant glioma in Phase 1 clinical trials prompted Phase 2 and 3 studies to confirm the efficacy of TMZ in these malignancies. The CRC conducted a number of these studies, in which the activity of TMZ in newly diagnosed and recurrent gliomas was established (Table 1.3).

A Phase 2 trial conducted by O'Reilly *et al.* evaluated the efficacy of TMZ in 28 patients with primary brain tumours. TMZ was given at an initial oral dose of 150 mg/m^2 once daily for 5 days (total dose 750 mg/m^2), escalating to 200 mg/m^2 for 5 days (total dose 1000 mg/m^2) for subsequent courses at 28-day intervals if no significant myelosuppression occurred. Of the 10 evaluable patients with recurrent astrocytoma after radiation therapy, 5 showed significant improvement on CT scan alongside complete resolution of clinical symptoms that persisted for 3 to 6 months. Three other patients showed a slight reduction or no change on CT, however their neurological condition improved. Major improvement on CT was also reported for 2 of the 9 evaluable patients treated with two courses of TMZ prior to radiotherapy for newly diagnosed high-grade astrocytomas; 2 others showed slight improvement. Three additional patients with primary brain tumours, including one with recurrent

medulloblastoma following radiotherapy and chemotherapy, showed major improvement on CT that was maintained for six month (104). The study was then extended to 75 patients, 48 with recurrent disease and 27 newly diagnosed patients. Improvements on CT was observed in 25% of patients with recurrent disease and 30% of newly diagnosed patients. A total 22% of patients with recurrent tumours and 43% with newly diagnosed tumours survived to one year. The study confirmed the efficacy of TMZ against gliomas in patients who have previously failed to response to intensive radiotherapy (105).

A pivotal Phase 3 trial by Stupp *et al*. compared radiotherapy alone with radiotherapy plus TMZ, given concomitantly with and after radiotherapy in patients with newly diagnosed glioblastoma. The trial contained a total of 573 patients from 85 centres who all underwent randomisation. Patients were randomly assigned to receive radiotherapy alone (fractionated focal conformal irradiation in daily fractions of 2 Gy given 5 days per week for 6 weeks, totalling 60 Gy) or radiotherapy plus continuous daily TMZ (75 mg/m^2 per day from the first to last day of radiotherapy), followed by six cycles of adjuvant TMZ (150 to 200 mg/m^2 for 5 days during each 28 day cycle). Median survival was 14.6 months with radiotherapy plus TMZ and 12.1 months with radiotherapy alone (Figure 1.8). The study concluded the addition of TMZ to radiotherapy for newly diagnosed glioblastoma resulted in both a clinically meaningful and statistically significant survival benefit for patients with minimal toxicity (9). As a result, radiation with concomitant TMZ was readily accepted as the standard of care for newly diagnosed glioblastoma patients in both Europe and the United States.

Table 1.3: Phase 2 and 3 trials of TMZ in malignant glioma.

Study	Pathology	Dosage Schedule	Enrolment	Response	Comments
O'Reilly (104)	Primary brain tumours.	150 mg/m^2/day p.o. for 5 days (total dose 750 mg/m^2), escalated to 200 mg/m^2/day p.o. for 5 days (total dose 1000 mg/m^2) every 28 days.	28	CT response in 5/10 recurrent anaplastic astrocytomas (50%) and 4/7 neoadjuvant anaplastic astrocytomas (57%).	Improved CT, neurological signs and symptoms of 3 to 6 month duration.
Newlands (105)	AA and GBM.	150 mg/m^2/day p.o. for 5 days (total dose 750 mg/m^2), escalated to 200 mg/m^2/day p.o. for 5 days (total dose 1000 mg/m^2) every 28 days.	75 (48 recurrent, 27 neoadjuvant)	12 recurrent patients had partial response (25%), and 8 neoadjuvant patients had partial response (30%).	Survival advantage not shown.
Bower (106)	Progressive or recurrent AA, and GBM.	200 mg/m^2/day p.o. for 5 days (total dose 1000 mg/m^2) every 28 days.	103	11 (11%) objective response.	48 (47%) stable disease; median response 4 to 6 months.
Yung (107)	GBM at first relapse.	TMZ: 150 mg/m^2/day p.o. for 5 days (total dose 750 mg/m^2), escalated to 200 mg/m^2/day p.o. for 5 days (total dose 1000 mg/m^2) every 28 days.	225	TMZ: partial response (5.4%); stable disease (40.2%). Procarbazine: partial response (5.3%); stable disease (27.4%).	TMZ PFS: 21% at 6 months; median 2.89 months. TMZ OS: 60% at 6 months; median 7.34 months

		Procarbazine: 150 mg/m^2/day for 28 days every 56 days.			Procarbazine PFS: 8% at 6 months; median 1.88 months. Procarbazine OS: 44% at 4 months; median 5.66 months.
Yung (108)	AA at first relapse.	150 mg/m^2/day p.o. for 5 days (total dose 750 mg/m^2), escalated to 200 mg/m^2/day p.o. for 5 days (total dose 1000 mg/m^2) every 28 days.	162	13 complete response (8%), 57 complete response or partial response (35%), 101 complete response, partial response, or stable disease (62%).	PFS: 46% at 6 months; 24% at 12 months. Median OS: 13.6 months.
Friedman (109)	Newly diagnosed AA and GBM.	200 mg/m^2/day p.o. for 5 days (total dose 1000 mg/m^2) every 28 days.	38 (33 GBM and 5 AA)	3 complete response (9%) and 14 partial response (43%).	No survival data. MGMT protein expression may identify TMZ resistant tumours.

AA, anaplastic astrocytoma; GBM, glioblastoma multiforme; OS, overall survival; PFS, progression-free survival. Table adapted from (74).

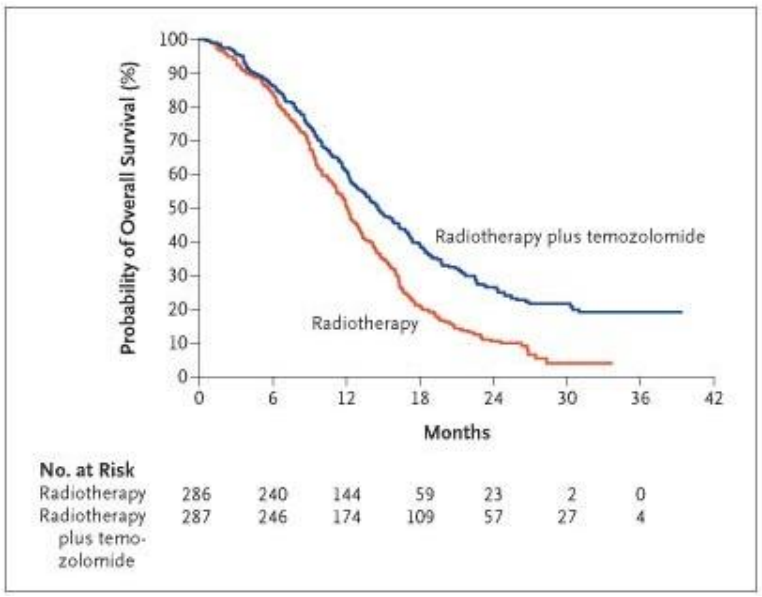

Figure 1.8: Overall survival analysis of glioblastoma patients given radiotherapy alone versus radiotherapy plus TMZ.

Kaplan-Meier overall survival was 14.6 months with radiotherapy plus TMZ compared to 12.1 months with radiotherapy alone. Diagram taken from (9).

1.1.6.2 Mechanisms of Resistance to Temozolomide Chemotherapy

Despite being the standard of care for glioblastoma patients, at least 50% of patients do not respond to TMZ chemotherapy due to resistance. Drug resistance can generally be categorised as either acquired or intrinsic. Intrinsic drug resistance refers to a tumour that shows insignificant or no response to chemotherapy at the onset of treatment, whilst acquired drug resistance occurs when a tumour that initially responded to treatment is no longer sensitive to the chemotherapeutic agent. Acquired drug resistance emerges by Darwinian evolution as a result of selective pressure in the presence of a given drug. Acquired resistance may arise because of drug-induced genetic and epigenetic changes in tumour cells, inducing and selecting genes that confer a survival advantage, or results from selection of pre-existing clones within a tumour. During treatment of initially heterogeneous tumours, chemotherapy eliminates drug-sensitive malignant cells allowing the survival of drug-resistant cells which advance to seed more resistant tumours. Within glioblastomas, populations of cells with stem cell-like properties termed glioma cancer stem cells (GCSCs) have been associated with tumour-initiating capacity and resistance to treatment. As a result, tumours demonstrating resistance to multiple chemotherapeutic agents with distinct mechanisms of action may emerge. Multidrug resistance is a major factor contributing to treatment failure. Mechanisms which confer resistance to chemotherapeutic agents include mechanisms involving epigenetic, transcriptomic, proteomic aberrations as well as alterations in receptor tyrosine kinase activity, drug efflux transporters, apoptosis and autophagy processes, adaptation of the tumour microenvironment, alongside the emergence of GCSCs. The consequence of such is the survival and proliferation of malignant cells resistant to drug-induced apoptosis.

1.1.6.2.1 DNA Damage Repair

1.1.6.2.1.1 MGMT

The primary mechanism for the majority of TMZ resistance is *MGMT* gene silencing. Repression of *MGMT* gene transcription is achieved by methylation of the CpG-rich islands located in the promoter region (41). It has been estimated approximately 45% of newly diagnosed glioblastoma patients have *MGMT* promoter methylation, and thus gene silencing is the strongest prognostic marker for OS (42). Whilst the unmethylated *MGMT* phenotype represents the primary mechanism for intrinsic TMZ resistance, its role in acquired resistance has only partially been assessed. Few studies have verified whether *MGMT* promoter methylation can change following chemotherapy. By undertaking methylation-specific polymerase chain reaction (PCR), studies have identified that methylation of the *MGMT* promoter remains largely stable during the disease course in approximately 75%-89% of patients (110, 111). Conversely, other studies have documented adaptive epigenetic changes can occur following TMZ chemotherapy. Conversions from methylated to unmethylated *MGMT* promoter i.e. acquired chemoresistance, was observed in a study by Christmann *et al*., 39.1% of pre-treatment tumours exhibited MGMT promoter methylation compared to just 5.3% of recurrences (112). Therefore, these studies suggest *MGMT* gene silencing plays a role in both intrinsic and acquired TMZ resistance.

1.1.6.2.1.2 Mismatch Repair

Aside from MGMT-mediated direct DNA repair, MMR results in the recognition, excision, and re-synthesis of the affected DNA. There is growing evidence to suggest disruption of the MMR system is a major contributor to acquired TMZ resistance. Deficiencies of MMR can result in tolerance to the O^6-methylguanine:thymine

mispairing which consequently results in a state of microsatellite instability and hypermutability. As previously discussed, in the absence of MGMT expression resultant base mismatch invokes the MMR pathway. The MMR proteins MSH2, MSH6, MLH1 and PMS2 recognise and bind to the mismatched guanine resulting in cells entering a cycle of DNA repair. Mismatches in the newly synthesised DNA daughter strands are repaired whilst methyl adducts persist in the parental DNA strand in the absence of MGMT. This results in futile cycles of repair followed by mismatching which eventually induces DNA double strand break formation, cell cycle arrest and apoptosis. MMR is therefore essential to repair TMZ-induced cytotoxicity. Comparison of MMR protein expression in 80 paired primary and recurrent glioblastoma samples treated with the current standard of care revealed consistent downregulation of the MMR proteins MSH2, MSH6 and PMS2 in recurrent glioblastomas (111). *In vitro* knockdown of *MSH6*, *MLH1* and *PMS2* in glioblastoma cell lines showed enhanced cell survival to cytotoxic doses of TMZ, and when *MSH6* was reintroduced, TMZ sensitivity was restored (113, 114). As such, it is apparent that mutations of the MMR system are unlikely to account for gliomagenesis or primary chemoresistance but contribute to acquired TMZ resistance. Interestingly, these mutations have been shown to occur primarily among recurrent *MGMT*-promoter methylated glioblastomas, suggesting initial sensitivity to TMZ may exert a selective pressure for mutations of MMR proteins.

1.1.6.2.1.3 Base Excision Repair

Whilst the MMR system is primarily responsible for the repair of the O^6-methylgunaine lesion resulting from TMZ treatment, the BER system is the principal reason why TMZ-induced N^7-methylguanine and N^3-methyladenine lesions possess limited genotoxicity. Should the system be inhibited, N^3-methyladenine, the more toxic of the adducts, can

trigger DNA replication fork collapse and induce DNA double-strand breaks, potentiating the cytotoxic effect of TMZ (115, 116). Supporting the contribution of BER in TMZ resistance, increased expression of N-methylpurine DNA glycosylase (MPG; responsible for cleavage of the N-glycosidic bond during BER) was found to be negatively correlated with OS in glioblastoma patients with *MGMT*-promoter methylation. The study by Agnihotri *et al*. also identified re-introduction of MPG in TMZ sensitive glioblastoma cell lines conferred resistance to TMZ both *in vitro* and in an *in vivo* orthotopic xenograft mouse model (117). Additionally, APE-1, a key BER enzyme that cleaves DNA at cytotoxic abasic sites, has been shown to mediate resistance to alkylating chemotherapy and may be a useful predictor of tumour progression following adjuvant therapy in a subset of gliomas (118). Further molecular studies of APE-1 in TMZ resistant glioblastoma cell lines demonstrated inhibition of APE-1 expression results in restoration of TMZ sensitivity (119, 120).

1.1.6.2.2 Epigenetic Alterations

1.1.6.2.2.1 microRNA

Aside from canonical DNA repair mechanisms, posttranscriptional epigenetic regulation of gene expression by microRNAs (miRNAs) has also been suggested to play a role in TMZ resistance in glioblastoma. miRNAs are a class of short, single-stranded, non-coding endogenous RNAs of 19-25 nucleotides in length. They play an important regulatory role by targeting specific mRNAs for degradation or translation repression (121). The most extensively studied miRNA in glioblastoma is miRNA-21 (miR-21). miR-21 is consistently upregulated and plays a role in numerous oncogenic processes including proliferation, apoptosis, and tumour invasion (122).

In terms of chemoresistance, miR-21 has been shown to decrease expression of the pro-apoptotic protein Bcl-2 associated X (BAX) and caspases, resulting in a reciprocal increase in anti-apoptotic B-cell lymphoma-2 (Bcl-2) expression (123). Increased expression of miR-21 is associated with reduced chemosensitivity to TMZ in glioblastoma cell lines, and its inhibition is able to re-sensitise glioblastoma cells to TMZ treatment (124).

Numerous miRNAs have since been predicted to mediate acquired TMZ resistance in glioblastoma through a number of mechanisms. For example, some miRNAs can function as tumour suppressors with their downregulation resulting in resistance. miR-128 is commonly downregulated and has been shown to be responsible for tumour progression by its negative regulation of cell proliferation, migration, invasion, and GCSC self-renewal (125). Reduced miRNA activity following TMZ treatment is also associated with increased drug efflux transporter expression (miR-1268a) (126), reduced MGMT promoter methylation (miR-101) (127), and enhanced DNA repair (miR-29c) (128).

1.1.6.2.2.2 Histone Modifications

There are multiple mechanisms by which transcription is epigenetically regulated. In relation to TMZ resistance in glioblastoma, aside from *MGMT* promoter CpG island hypermethylation and adaptive differential expression of miRNAs, another recently proposed mechanism is chromatin remodelling (129). Histones are subjected to modifications that can either repress or activate transcription. Chromatin is the condensed combination of histones and DNA in the cell nucleus. The fundamental unit of chromatin is the nucleosome, composed of an octamer core of histone proteins wrapped in DNA. All histone proteins possess an amino-terminal tail protruding from

the surface of the nucleosome that are targets for a variety of posttranslational modifications (130). These modifications include acetylation, methylation, ubiquitylation, or glycosylation on lysine; methylation on arginine; phosphorylation on serine, threonine, or tyrosine; and diphosphate ribosylation or carbonylation on adenosine (131). The type of modification regulates the stability of the bonds between the octamer core and its surrounding DNA. These modifications determine if the chromatin conforms to a closed or open configuration for transcription. Each histone modification process is catalysed by reciprocal families (e.g. responsible for acetylation as opposed to deacetylation) that have been shown to influence numerous cellular processes such as proliferation, apoptosis, DNA repair, drug efflux pump expression, cell cycle, and signal transduction pathway regulation in glioblastoma (131).

Concerning TMZ resistance, in glioblastoma xenograft models, increased lysine acetylation of histone H3 lysine 9 (H3K9) was shown to upregulate MGMT expression in TMZ resistant specimens independent of methylation (132). Another study by Banelli *et al.* has shown histone tail lysine demethylation is associated with TMZ resistance as displayed by increased KDMA (lysine demethylase) levels, and KDM5A expression in an acquired TMZ resistant glioblastoma cell line. The same study also showed by reducing KDM5A expression, glioblastoma cells can be re-sensitised to TMZ treatment (133). Adaptive chromatin remodelling has also been shown to drive GCSC plasticity and drug tolerance by upregulating the histone demethylases KDM6A/B following treatment, potentially contributing to relapse (134).

1.1.6.2.3 Drug Efflux

The active efflux of drugs across the tumour cell membrane by adenosine triphosphate (ATP)-dependent transporters is considered to be a major contributor to

chemoresistance (135). ATP-binding cassette (ABC) transporters regulate the ATP-dependent efflux of toxic endogenous molecules and drugs out the cell. Among the 49 discovered human ABC transporters, P-glycoprotein (P-gp), multi-drug resistance protein 1 (MRP1), and breast cancer resistance protein (BCRP) are three major proteins that constitute the ABC family (136). Increased expression of P-gp, the most widely studied ABC transporter, has been observed in TMZ resistant glioblastoma cell lines, and the protein has six predicated TMZ binding sites within its intracellular region (137). A single nucleotide polymorphism (SNP) in the gene encoding P-gp has been identified in glioblastoma patients who are unresponsive to TMZ chemotherapy. Analysis of the exon12 C1236T P-gp SNP showed patients with the C/C genotype had a 2 year OS of 37% compared to 8% and 10% for patients with the C/T and T/T genotypes respectively, suggesting genetic variants of P-gp are associated with glioblastoma patient OS (138). Similarly, BCRP protein expression has been identified as an indicator of OS in glioblastoma; high BCRP expression has been associated with significantly shorter OS compared to patients with low expression (139). ABC transporters have not only shown to be upregulated at the tumour cell membrane but are also widely distributed at the blood-brain barrier limiting drug delivery to the CNS. A study by Agarwal *et al*. identified P-gp and BCRP are two key ABC transporters involved in drug efflux at the blood-brain barrier. Inhibition of both P-gp and BCRP was shown to drastically increase drug delivery to the tumour core, rim, and normal brain, highlighting the impact that active efflux at the blood-brain barrier has on the delivery of chemotherapeutic drugs in glioblastoma (140).

1.1.6.2.4 Apoptosis and Autophagy

Apoptosis, a major mechanism of programmed cell death, is the final step by which TMZ elicits its cytotoxic effect. In glioblastoma, TMZ-induced apoptosis activates the intrinsic (mitochondrial-dependent) apoptosis pathway. TMZ disturbs cellular homeostasis by inducing DNA damage. As such, this intracellular stress signal is recognised by several intracellular proteins and results in an imbalance of pro- and anti-apoptotic proteins of the Bcl-2 superfamily. This imbalance results in the loss of integrity of the outer mitochondrial membrane (OMM) and releases cytochrome c and other mitochondrial proteins into the cytosol (141).

Modulation of apoptosis is a known mechanism by which cells become resistant to TMZ. In studies of paired (pre- and post-TMZ treatment) glioblastoma patient tumour samples, significant upregulation of the anti-apoptotic proteins Bcl-2, Bcl-X and Mcl-1 is observed, whilst there is a downregulation of pro-apoptotic BAX. This imbalance of pro- and anti-apoptotic proteins results in a shift towards apoptosis evasion in recurrent glioblastomas (142).

Autophagy is the process by which damaged cytoplasmic organelles and misfolded and dysfunctional proteins are degraded by the lysosomal pathway. As a catabolic process, autophagy is cytoprotective as it enables maintenance of metabolic homeostasis during periods of hypoxia, oxidative stress, and nutrient depletion by producing ATP alongside other metabolic precursors (143). Recently, autophagy has been identified as a novel cell survival mechanism in glioblastoma (141). In cultured glioblastoma cells, autophagy is frequently activated as a response to stress following treatment with chemotherapeutic agents, with cells exposed to increasing TMZ doses having been confirmed to stimulate autophagy (144, 145). As a potential mechanism of resistance,

in vitro studies revealed that subsequent exposure of glioblastoma cell lines to inhibitors of autophagy (e.g. bafilomycin A1) results in enhanced TMZ cytotoxicity by inducing apoptosis (144, 146). Some clinical trials have adopted chloroquine (an inhibitor of autophagy) in combination with TMZ and have produced encouraging results (141, 147). Significant research is required to elucidate the role of autophagy in acquired TMZ resistance, however some data suggests the process may be regulated epigenetically by miRNA and histone modification mechanisms.

1.1.6.2.5 Receptor Tyrosine Kinase Signal Transduction Pathway Activation

Receptor tyrosine kinases (RTKs) play a significant role in numerous cellular processes including growth, motility, differentiation, and metabolism. As such, aberrant RTK signalling results in the development and progression of various malignancies. Abnormal RTK activation in cancer is mediated by four principal mechanisms: genomic amplification, gain-of-function mutations, chromosomal rearrangements, and/or autocrine activation (148).

In glioblastoma, the most studied RTK is epidermal growth factor receptor (EGFR). Upon activation, EGFR triggers the intracellular Ras/mitogen-activated protein kinase/extracellular signal-related kinase (Ras/MAPK/ERK) and phosphoinositide 3-kinase/protein kinase B/mammalian target of rapamycin (PI3K/AKT/mTOR) pathways (149). EGFR-mediated signal transduction results in tumour cell proliferation, migration, invasion, angiogenesis, and GCSC maintenance (150). In primary glioblastoma, EGFR amplification is the most frequent genetic mutation occurring in 65% of tumours, with the most common form being the constituently active EGFR variant III detected in approximately 54% of tumours (149). Co-expression of EGFR and

EGF ligand in glioblastoma also implies an autocrine/paracrine loops also plays a role in disease progression (150).

A number of studies have identified mechanisms by which EGFR signalling contributes to TMZ resistance. EGFR signalling has been shown to inhibit TMZ-induced apoptosis by inducing the expression of anti-apoptotic proteins including Bcl-X_L and subsequent inhibition of caspase-3-like protease activation (151). A significant number of GCSCs have been shown to have elevated EGFR signalling, suggesting their dependence on EGFR signalling to induce TMZ chemoresistance (152). EGFR is an appealing drug target due to its high degree of selectivity in glioblastoma, as in comparison to glioma cells, normal adult neural cells (except for neuroglial stem cells located at the hippocampus and subventricular zone) do not express EGFR. Several targeted therapies are currently being investigated in clinical trials including small molecule inhibitors, monoclonal antibodies, and vaccines, however these have shown limited success (150, 153).

An alternative RTK pathway believed to be involved in mediating TMZ resistance in glioblastomas is the insulin-like growth factor (IGF) signalling axis. The pathway has been implicated in the development of chemoresistance in numerous malignancies including breast, prostate, colon, and ovarian cancer (154). A study by Maris *et* al. revealed in a cohort of glioblastoma patients, IGF-1 expression is increased in 25% of tumours, and IGF-1 expression is an independent prognostic factor associated with decreased OS (155). Metformin, a drug commonly used for the treatment of Type 2 diabetes, has been found to reverse or reduce chemoresistance by inhibition of IGF-1 signalling (156), and in glioblastoma reduces TMZ resistance (157, 158). There is considerable crosstalk between both the EGFR and IGF-1 signalling pathways, including the PI3K/AKT/mTOR pathway. Currently, there is evidence to suggest IGF-1 signalling

contributes to acquired TMZ resistance, and crosstalk between pathways may explain why therapies targeting EGFR have failed to improve patient survival in clinical trials (153).

1.1.6.2.6 Tumour Microenvironment

1.1.6.2.6.1 Hypoxia

One of the hallmarks of the tumour microenvironment in glioblastoma is chronic hypoxia which results from an imbalance between uncontrolled tumour cell proliferation and oxygen supply. At the tumour core, oxygen partial pressure can be as low as 1% of arterial blood, triggering adaptive responses driven by selective pressure (159). Hypoperfusion of the tumour causes a significant reduction of drug delivery resulting in chronic sub-cytotoxic concentrations of chemotherapeutic agents favouring the development of drug resistance (160).

In terms of hypoxia-mediated growth of glioblastoma, the most extensively studied mechanism is increased expression of the transcription factor hypoxia-inducible factor 1 (HIF-1), composed of α and β subunits (159). During normoxia, cytosolic HIF-1α has a short half-life and undergoes hydroxylation and proteasomal degradation. However during periods of hypoxia, HIF-1α escapes this fate and it transfers from the cytosol to the nucleus where it dimerises with HIF-1β and becomes transcriptionally active (159, 161). Studies have shown chronic hypoxia results in the activation of numerous downstream pathways involved in cell survival, enhanced glycolysis (162, 163), tumour invasion (164), cytoprotective autophagy (165), and GCSC proliferation (166, 167).

The activity of HIF-1α is believed to play a role in TMZ resistance in glioblastoma (168). Cycling hypoxia (characterised by periodic patterns of hypoxia and reoxygenation) has been shown to induce acquired TMZ resistance by increasing expression of anti-

apoptotic proteins including Bcl-2 and Livin (169, 170), alongside increased expression of drug efflux ABC transporters (171). Direct inhibitors of HIF-1α have shown limited efficacy in reducing tumour proliferation, however studies suggest TMZ re-sensitisation can be accomplished when given in combination with TMZ (172, 173).

1.1.6.2.6.2 Glioma Cancer Stem Cells

There is significant evidence to suggest a subpopulation of cells in glioblastoma possess properties shared by neural stem cells (NSCs) such as self-renewal, proliferative capacity, and multipotency (174). The discovery of this population, termed GCSCs, was substantiated by their expression of stem cell markers including CD133, SOX2, and Nestin, their ability to form neurospheres in serum-free conditions, and tumour growth in orthotopic xenograft mouse models. These xenograft tumours recapitulated the histopathological phenotype of the parent tumour, suggesting this subpopulation of cells can give rise to the full heterogenous population of cells present within the tumour (3, 4, 175).

It is believed by many researchers in the field that the intrinsic resistance of GCSCs to chemotherapy drives tumour repopulation and recurrence following treatment. Several mechanisms have been identified to explain GCSC chemoresistance including upregulation of anti-apoptotic proteins (e.g. Bcl-2), inhibitors of apoptosis, and drug efflux transporters (176), enhanced expression of DNA damage checkpoint response kinases (e.g. Chk1 and Chk2) (177), increased EGFR activity (178), and increased MGMT expression. For the latter, studies have shown MGMT expression amongst CD133+ tumour cells is significantly increased compared to CD133- cells, suggesting a robust intrinsic direct DNA repair mechanism in GCSCs (179).

1.2 Cancer Stem Cells in Glioblastoma

1.2.1 Stem Cells

Stem cells are defined as undifferentiated cells of a multicellular organism which are capable of giving rise to indefinitely more cells of the same type, and from which other cells arise by differentiation. They are best known for their role in embryonic development (embryonic stem cells), but also reside in adult tissues where they are responsible for maintaining tissue homeostasis. Normal adult stem cells are tissue-specific and have the ability to self-renew and differentiate into all cell types of the tissue of origin. As stem cells divide asymmetrically to produce an identical daughter cell and another cell of more differentiated progeny, this enables stem cells to generate cellular diversity without depleting the stem cell pool.

The classical definition of a stem cell requires that it possesses two key properties:

1. Self-renewal: the ability to generate daughter cells identical to their mother.
2. Potency: the ability to produce progeny with more restricted potential (differentiated cells). A multipotent stem cell sits at the apex of a lineage hierarchy and can generate multiple types of differentiated cells (180, 181).

Within normal tissues, organogenesis and tissue homeostasis occur following a strict hierarchical organisation. The cellular heterogeneity of tissues reflects a hierarchical programme of differentiation in which multiple mature cell types are derived from a common multipotent stem cell through intermediate progenitors, resulting in the complex architecture of tissues. In a similar fashion, it has been hypothesised that some cancers may mirror this same complex hierarchical organisation, with cancer stem cells (CSCs) being capable of generating a wide array of phenotypically diverse cells within a single tumour (182).

1.2.2 Cancer Stem Cell Hypothesis

It has become increasingly clear from studies of intratumoral heterogeneity that tumours encompass a complex ecosystem of cell types. Until recently, the clonal evolution model (stochastic model) was the primary hypothesis for tumour heterogeneity. This model, first proposed by Peter Nowell in 1976 (183), suggests tumours arise from a single mutated cell, accumulating additional mutations as the tumour progresses. These genetic changes give rise to additional subpopulations, and each of these have the ability to divide and mutate further (Figure 1.9A) (184).

The more recent CSC hypothesis (hierarchical model) is now more widely accepted to explain the cellular hierarchy observed in tumours. The hypothesis states that within a population of tumour cells, there is only a small subset of cells that are tumourigenic, and these cells are termed CSCs. CSCs reside at the apex of the hierarchy and possess the ability to self-renew and differentiate into non-tumourigenic progeny, giving rise to the variety of cells that comprise a tumour (Figure 1.9B) (185). As tumour cells differentiate, their ability to undergo self-renewal is reduced and they lose their "stemness". The hierarchy is dynamic with respect to cell type (CSCs and non-CSCs) and is maintained by the balance between self-renewal and differentiation. As a result, tumours can be viewed as an aberrant organ comprising heterogenous cell types derived from CSCs, rather than simply a collection of diverse neoplastic clones (182). The CSC population is currently defined by functional parameters based on experimental observations. Firstly, these cells must have the ability for long term self-renewal, having limitless regenerative potential to support the growth of the tumour. Secondly, the cells must possess the capacity to differentiate, giving rise to tumorigenesis and tumour heterogeneity. Finally, these cells must also have the ability

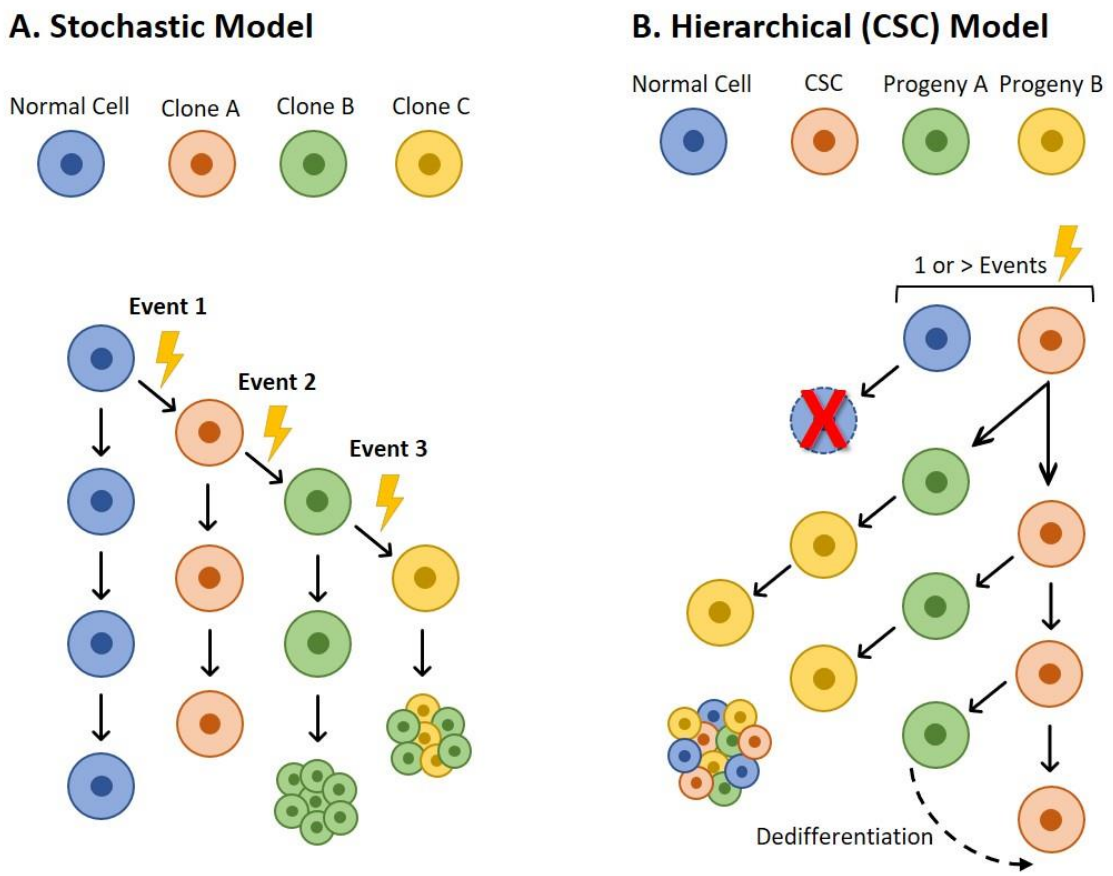

Figure 1.9: The stochastic and hierarchical models of tumourigenesis.

(A) The stochastic model assumes a cell can become tumourigenic under certain conditions. This is initiated by a deleterious event such as a mutation, but a single event is unlikely to initiate tumourigenesis. Instead, an accumulation of mutations forms a cancer cell that expands to form the bulk of the tumour. This model predicts both homogeneous and heterogeneous tumour types. **(B)** The hierarchical model predicts tumours arise when a tumourigenic event occurs in a specific cell type which gains the ability to self-renew and continuously produce the progeny that form the tumour bulk (e.g. a CSC). CSCs are highly tumourigenic with the ability to establish new tumours. CSCs divide asymmetrically to form new CSCs and progenitor cells that in turn, give rise to differentiated cancer cells that form the bulk of the tumour. This model supports the heterogeneity of all CSC-driven tumours. Diagram adapted from (186).

to form tumours that are histopathologically identical to the parent tumour following xenotransplantation, and can be expanded in culture whilst maintaining a high percentage CSC population (187).

The concept of CSCs originated in 1994, with the observation by Dick and colleagues that a fraction of CD34+ CD38- cells in acute myeloid leukaemia (AML) could be transplanted into severe combined immune-deficient (SCID) mice, engraft, and disseminate consistent with human disease, whilst other populations could not (188). This subpopulation demonstrated self-renewal and reconstituted both the leukaemic cell hierarchy and the clinical disease state *in vivo* following xenotransplantation. Following the identification of CSCs in AML and other blood cancers, CSCs were later discovered to exist in various solid tumours including those of the breast, prostate, colon, lung, brain, and liver (175, 189-192).

1.2.3 Glioma Cancer Stem Cells

The presence of CSCs in primary glioblastomas was initially reported by two independent groups (3, 4). Singh *et al*. isolated a subpopulation of cells from glioblastomas based on selection for the cell surface marker CD133, a glycoprotein found on numerous adult stem cell populations. In culture, this cell population demonstrated capabilities of NSCs including neurosphere forming capacity, self-renewal, high proliferative potential, and multipotency. In addition, implantation of CD133+ cells into SCID mice produced a tumour which recapitulated the histopathological phenotype of the parent tumour, suggesting this subpopulation can give rise to the full heterogeneous complement of cell present within the tumour (4). Similarly, Galli *et al*. isolated and identified glioblastoma cells, which possessed all the defining features of somatic stem cells including *ex vivo* multipotency and the ability to

establish and expand glioblastoma-like tumours. These tumours reproduced the intraparenchymal invasion patterns typical of human glioblastomas and also exclusively contained cells expressing astroglial markers (3).

The functional definition of a brain tumour stem cell (BTSC), and thus GCSCs, was constructed by Peter Dirks and colleagues to counteract the inconsistencies that arise due to the heterogeneity in approaches by various groups to isolate these cells. A BTSC should be multipotent, highly proliferative, and capable of self-renewal. Second, a BTSC should be tumourigenic; capable of giving rise to a histologically identical tumour following xenotransplantation. Finally, a BTSC should give rise to a tumour capable of propagation, either by dissociation and cell culture of the tumour mass, or by transplantation into an immunocompromised host (174, 193, 194).

1.2.4 The Role of Glioma Cancer Stem Cells in Resistance and Tumour Progression

The addition of TMZ to radiotherapy in glioblastoma increased median survival by several months, however lineage tracing in mouse models has demonstrated GCSCs repopulate tumours following TMZ treatment. A study by Chen *et al*. identified a putative endogenous stem cell located at the apex of a cellular hierarchy responsible for tumour maintenance and recurrence following TMZ chemotherapy (195). GCSCs have not only been implicated in tumour initiation, but also tumour recurrence and progression. Liu *et al.* found the percentage of CD133+ cells is markedly increased in recurrent gliomas compared to newly diagnosed patients with the same tumours. Additionally, CD133+ cells have been shown to be more resistant than other cells to treatment with a panel of chemotherapeutics including TMZ (179). This suggests their role in tumour recurrence is likely to be mediated by their resistance to chemotherapy. Eramo *et al*. provided the first demonstration of GCSC chemoresistance by measuring

viability of glioblastoma-derived tumour neurospheres, compared with Jurkat cells and small-cell lung CSCs following treatment with an array of chemotherapeutic agents. GCSCs showed increased viability compared to other cell types, alongside an enhanced capacity to proliferate following cessation of treatment (196).

Numerous mechanisms have been identified to mediate the therapeutic resistance of GCSCs to TMZ and include upregulation of anti-apoptotic proteins (e.g. Bcl-2), inhibitors of apoptosis, and drug efflux transporters (176), enhanced expression of DNA damage checkpoint response kinases (e.g. Chk1 and Chk2) (177), increased EGFR activity (178), and increased MGMT expression (179). There is significant evidence to suggest neural developmental signalling pathways including Notch (197), bone morphogenic protein (BMP) (198), NF-κB (199), and Wnt signalling (200) are deregulated in glioblastoma, and play a role in mediating TMZ resistance in GCSCs.

As a result of the role of GCSCs in resistance to treatment, alongside their tumourigenic potential, there is an urgent need to target GCSCs therapeutically (Figure 1.10). One such way to achieve this is to identify and target specific signalling pathways involved in the maintenance of GCSCs. The Notch pathway plays an important role in neural development, functioning to inhibit neural differentiation and maintain the neural stem and progenitor cell pool. In glioblastoma, the Notch pathway is hijacked by GCSCs in order to maintain the stem cell population and plays a role in mediating resistance and tumour recurrence following treatment.

Excessive and grossly disorganised blood vessel formation is one of the hallmarks of glioblastoma. This aberrant vascularity was initially believed to be important for satisfying the high demand for nutrients of the rapidly growing tumour. However, the existence of GCSCs alongside the discovery of vascular stem cell niches in the normal

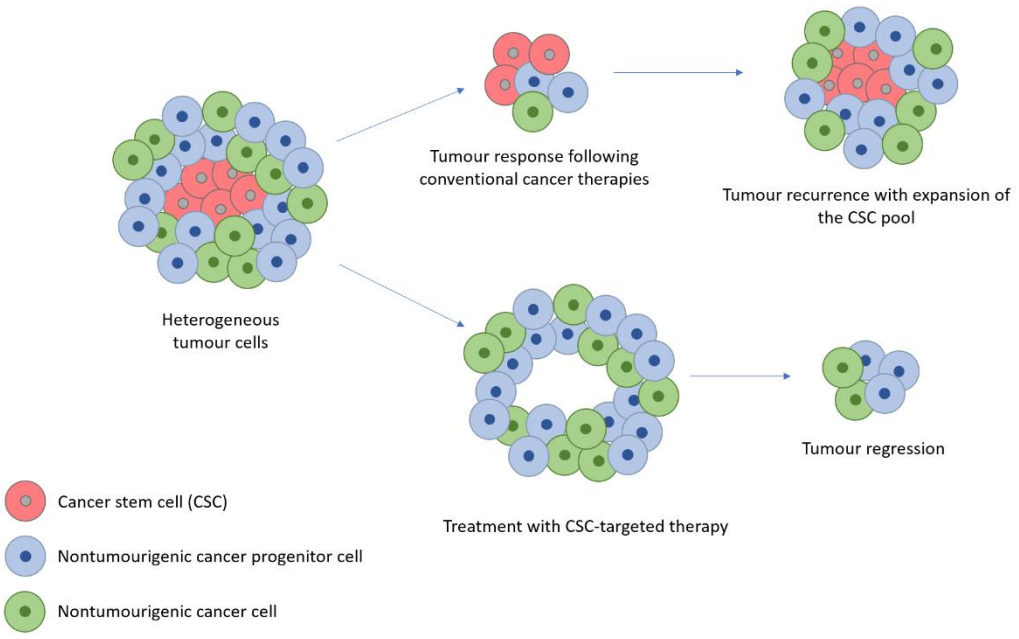

Figure 1.10: Glioma cancer stem cells mediate resistance and tumour recurrence following TMZ treatment.

The cancer stem cell (CSC) hypothesis suggests tumour growth is driven by a subpopulation of cells that are capable of proliferation and self-renewal. CSCs are multipotent and can give rise to the diverse population of cells that make up a tumour. Inherent within this hypothesis is the assumption that current treatments can considerably diminish the bulk of the tumour, but have no effect on CSCs, which are later capable of driving tumour recurrence and regrowth. Nontumorigenic cancer progenitor cells are capable of cell division, but their capacity to divide is limited, and they are unable to match the rates of tumour cell apoptosis and senescence. To achieve cancer remission or cure, it is necessary to develop novel target therapies that are cytotoxic to CSCs. Diagram adapted from (194).

brain suggested the tumour vascular bed is responsible for maintaining GCSCs. GCSCs reside in this protective vascular niche which contributes to cell fate decisions and survival. Interactions between CSCs and the vascular niche confer a survival advantage following chemotherapy, as well as maintaining the stem cell population, and thus, the ability to re-populate the tumour following treatment (201). Hovinga *et al*. has shown inhibition of Notch signalling in glioblastoma targets GCSCs via an endothelial cell intermediate. Using a novel organotypic explant culture system, Notch inhibition decreased the number of endothelial cells within the tumour, alongside decreased proliferation and self-renewal of tumour cells (202). The findings support a role for tumour endothelial cells in GCSC maintenance, mediated by Notch signalling. These studies demonstrate the role of Notch signalling in the regulation and self-renewal of GCSCs, and GCSCs are believed to mediate TMZ resistance and tumour recurrence following treatment.

1.3 Notch Signalling Pathway

1.3.1 Biology

Notch signalling is an evolutionary conserved pathway in multicellular organisms that regulates cell-fate determination during development, and maintains adult tissue homeostasis (203). The *Notch* locus was first described by Thomas Hunt Morgan in a strain of *Drosophila,* as partial loss-of-function (haploinsufficiency) results in notches at the fly wing margin (204). In 1991, the first human Notch gene was identified, and in the same study, linked to cancer (205).

1.3.2 Notch Signalling

1.3.2.1 Receptors and Ligands

In mammals, there are four Notch receptors (Notch1-4) and five canonical ligands of the Delta-Serrate-Lag (DSL) family (Jagged-1 [JAG1] and JAG2, and delta-like 1 [DLL1], DLL3 and DLL4). The four Notch receptors consist of 29 to 36 EGF-like repeats in the Notch extracellular domain (NECD), which are post-translationally modified by a variety of glycans (206). The NECD is followed by the negative regulatory region (NRR) composed of three cysteine rich Lin-Notch repeats (LNR) and the heterodimerisation domain (HD) (207, 208). The Notch intracellular domain (NICD) consists of a recombination signal binding protein for immunoglobulin kappa J region (RBPJ)-associated molecule (RAM) domain, ankyrin (ANK) repeats flanked by two nuclear localization signals (NLS): a transcriptional activation domain (TAD) and a C-terminal Pro Glu Ser Thr (PEST) domain. Both the RAM and ANK domains are essential for interacting with the DNA binding protein CSL (CBF1, Suppressor of Hairless, Lag1) in the nucleus (209) (Figure 1.11A).

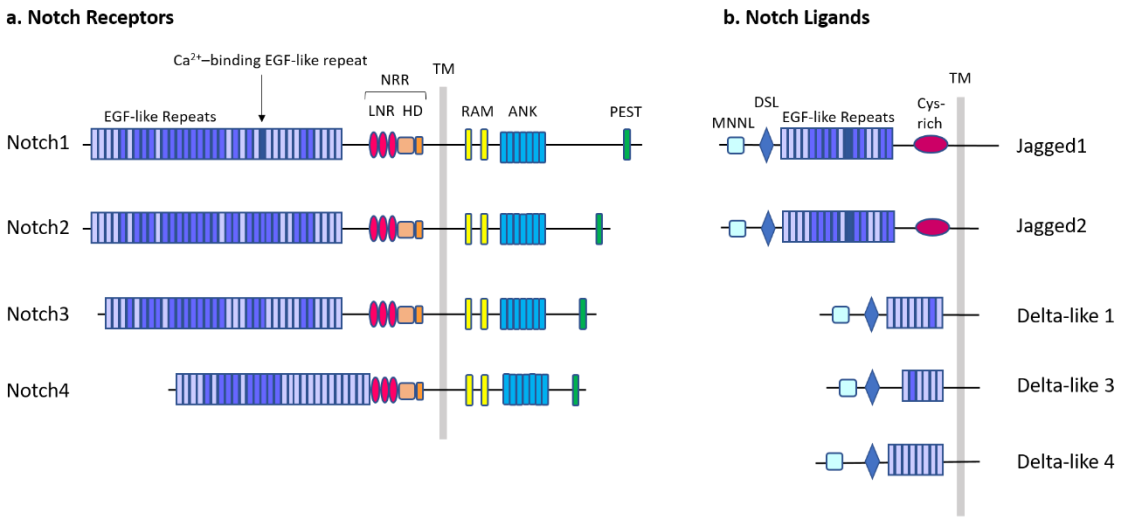

Figure 1.11: Domain organisation of human Notch receptors and DSL-family ligands.

(A) Human Notch receptors consist of epidermal growth factor (EGF)-like repeats in the Notch extracellular domain (NECD), which are post-translationally modified by glycans. The NECD is followed by the negative regulatory region (NRR) composed of Lin-Notch repeats (LNR) and the heterodimerisation domain (HD). The Notch intracellular domain (NICD) consists of a RBPJ-associated molecule (RAM) domain, ankyrin (ANK) repeats flanked by two nuclear localisation signals: a transcriptional activation domain and a C-terminal Pro Glu Ser Thr (PEST) domain. **(B)** The Delta-Serrate-Lag (DSL) Notch ligands contain an extracellular domain containing EGF-like repeats and a cysteine-rich N terminal DSL domain. Preceding this is a module at the N-terminus of Notch ligands (MNNL). Both JAG1 and JAG2 contain an additional cysteine-rich domain. TM denotes transmembrane domain. Diagram adapted from (210).

The DSL ligands of Notch are transmembrane proteins with an extracellular domain containing EGF-like repeats and a cysteine-rich N-terminal DSL domain required for receptor-ligand interaction. Preceding this is a disulphide-bond stabilised module at the N-terminus of Notch ligands (MNNL). Additionally, both JAG1 and JAG2 contain an extra cysteine-rich domain (Figure 1.11B) (211, 212).

1.3.2.2 Signalling

The interaction between Notch and its ligands can occur in two ways: *in trans*, when the receptor and ligand are present on neighbouring cells, or *in cis*, when the receptor and ligand are present on the same cell (213, 214). *In trans*, binding results in pathway activation, whilst *in cis* the interaction inhibits signalling (208). Notch receptors are expressed on the cell surface as a processed heterodimer resulting from a Furin-dependent cleavage (S1 cleavage) in the NECD, occurring during trafficking through the Golgi complex (215). During synthesis and secretion, the NECD undergoes O-linked glycosylation crucial for proper folding of the Notch receptor and interaction with its ligand (206). The Notch receptor on the signal-receiving cell directly binds to ligands located on the opposing signal-sending cell (207, 208). Receptor-ligand binding triggers a second NECD cleavage (S2 cleavage) by ADAM10 (a disintegrin and metalloproteinase domain containing protein-10) or ADAM17. This facilitates a further crucial signalling cleavage within the Notch transmembrane domain by γ-secretase (S3 cleavage) (216). The released NICD translocates to the nucleus, where it forms a transcriptional activation complex with CSL, Mastermind (MAML) and several transcriptional co-activators which drive the expression of the Hairy-Enhancer of Split (HES) and Hes-related protein (HERP) gene families (Figure 1.12) (207, 208, 210).

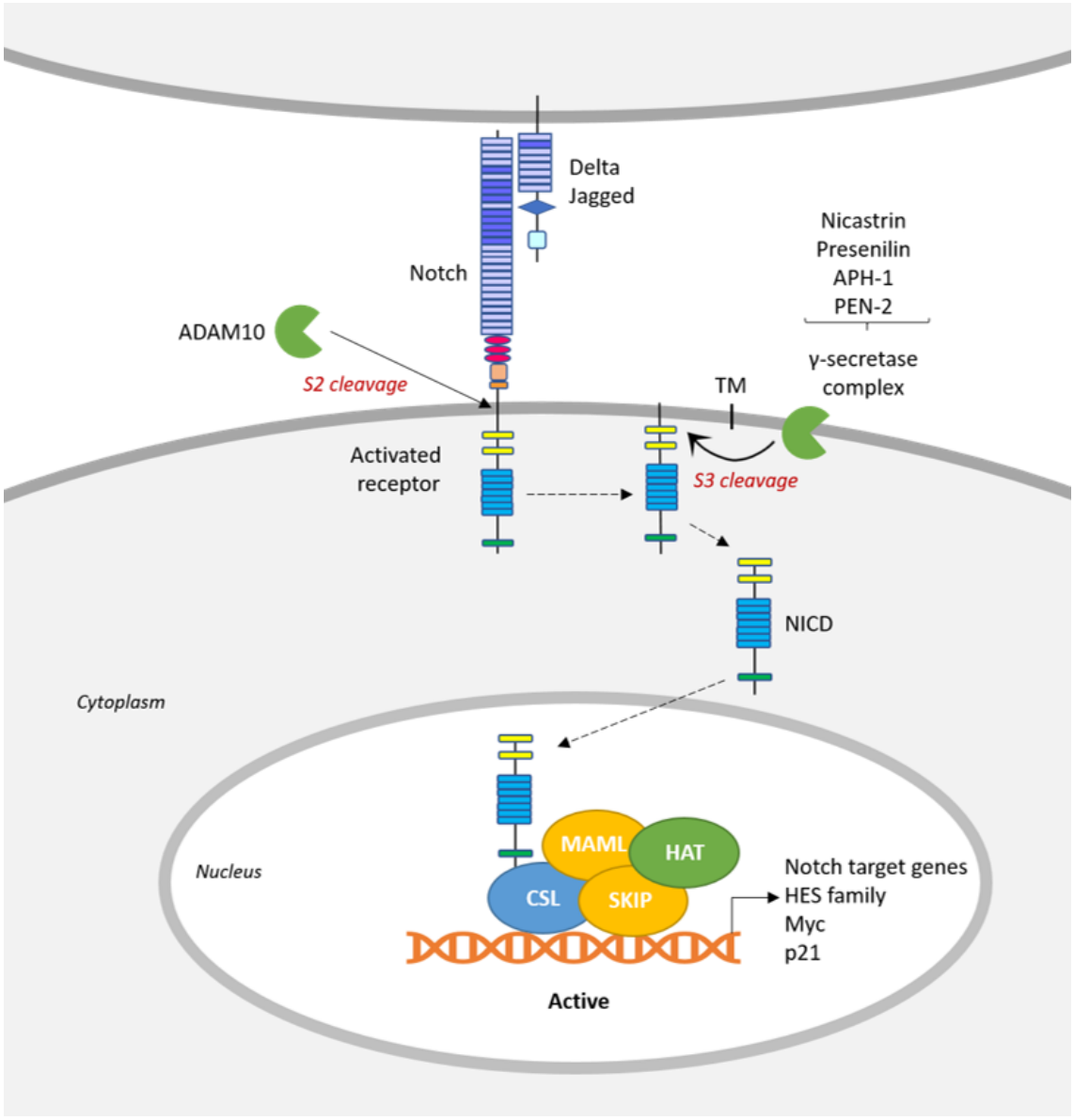

Figure 1.12: The Notch signalling pathway.

The Notch receptor on a signal-receiving cell directly binds to ligands located on the opposing signal-sending cell. Receptor-ligand binding results in cleavage of the Notch extracellular domain (NECD; S2 cleavage) by ADAM10, facilitating a further cleavage within the Notch transmembrane domain by γ-secretase (S3 cleavage). The Notch intracellular domain (NICD) is released and translocates to the nucleus, where it forms a transcriptional activation complex with CSL (CBF1, Suppressor of Hairless, Lag1), Mastermind (MAML) and several transcriptional co-activators to drive the expression of Notch target genes. Diagram adapted from (217).

1.3.3 Notch Signalling in Neurogenesis

The development of the CNS is an intricate, precisely regulated process. The Notch signalling pathway plays a key role in neurogenesis in both the embryonic and adult brain. Despite members of Notch signalling showing differential expression patterns throughout the brain (Table 1.4), they are master regulators of neurogenic niches, specialised microenvironments able to modulate stem cell properties including stem cell number, self-renewal, and fate decision, to prevent the depletion of the NSC pool (218, 219). Being the initiators of neurogenesis, NSCs are extremely important. NSCs are found in two distinct niches and give rise to new neurons throughout life; the subventricular zone (SVZ) of the lateral ventricle (219) and the subgranular zone (SGZ) of the dentate gyrus (220).

Table 1.4: Expression pattern of Notch receptors and ligands in the adult brain.

Notch Pathway Protein	Expression Pattern
Notch1	Neurons, astrocytes, precursor cells, ependymal cells, endothelium
Notch2	Precursor cells, neuron
Notch3	Precursor cells
Notch4	Endothelium
DLL1	Intermediate neural progenitors, postmitotic neurons
DLL3	Intermediate neural progenitors
DLL4	Endothelium
Jagged-1	Precursor cells, intermediate neural progenitors, neurons
Jagged-2	Neurons

Table adapted from (221) and (222).

During the neurogenic phase of brain development (embryonic neurogenesis), NSCs have to divide to generate differentiated progeny but also maintain the stem cell

population. It has been demonstrated that inhibition of Notch signalling induces the proliferation of NSCs, resulting in exit from the cell cycle and neural differentiation (223). Conversely, high levels of Notch signalling results in growth arrest, and can even induce quiescence (224, 225). The cell-fate regulation of quiescent NSCs is as a result of RBPJ activity, by Notch2- and Notch3-induced signalling (226, 227). Notch1 however appears to be essential for the active proliferation of the NSC pool, which diminishes with age (219, 220). In addition, the reduction or loss of RBPJ function results in depletion of progenitor cells in both the postnatal SVZ and DG, alongside reduced neurogenesis (220, 228). Therefore, it is plausible to conclude Notch signalling plays a key role in the regenerative capacity of the adult brain.

In order to execute their functions, neurons require glial cells to surround and insulate them providing support. Similar to neurons, glial cells differentiate from NSCs (229, 230). Notch signalling prevents equipotent cells from acquiring identical fates, and this is accomplished by lateral inhibition; a process in which a cell that stochastically acquires enhanced ligand expression and stimulates neighbouring cells to differentiate. The *in-cis* inhibition of Notch on the ligand-expressing cell renders the interaction unilateral. During neurogenesis, the signal-sending cell will differentiate into a neuronal precursor, whilst the signal-receiving cell will remain an uncommitted progenitor (229). For glial differentiation, NSCs are exposed to a Delta signal and tend to resist prevailing neurogenic signals, activating Notch signalling resulting in glial differentiation (231, 232). Thus, Notch signalling plays an instructive role in gliogenesis, promoting the differentiation of many glial subtypes, whilst differentiation towards an oligodendrocyte fate appears to be inhibited by Notch activation (233).

As discussed, the relevance of Notch signalling in the developing brain is in part due to its role in maintaining NSCs and progenitor cells, as well as stimulating their glial differentiation at the expense of their neuronal fate. Notch1 knock-out mice die before E11.5, at the approximate time of neuronal maturation, among other reasons due to a loss of neuroblasts and premature neuronal differentiation (234, 235). The essential role of Notch signalling in the maintenance of NSCs and the control of their fate suggests that Notch may also play a key role in GCSCs.

1.3.4 Notch Pathway Deregulation in Glioblastoma

Due to the central role of Notch in differentiation, its deregulation has been shown to lead to multiple malignancies. The first indication of the tumourigenic role of Notch was the identification of the t(7;9)(q34;q34.3) translocation in T-cell acute lymphoblastic leukaemia (T-ALL). This translocation results in a constitutively active Notch1 receptor under the control of the T-cell receptor-β promoter (205, 236). Subsequently, numerous components of the Notch pathway have been found to be deregulated in several haematological malignancies and solid tumours, including gliomas (237).

Notch signalling is a major pathway involved in the development of glioblastoma, and expression of Notch receptors and their ligands are critical markers of glioblastoma patient survival. Increased expression of Notch1. Notch4, DLL1, DLL4, JAG1, RBPJ, Hey1, Hey2, and Hes1 is observed in glioblastoma tumour cells compared to normal brain (238-240). A study by Kanamori *et al*. showed the Notch signalling pathway is deregulated at multiple points in nearly 75% of glioblastomas, and inhibition of one member of the Notch family can suppress glioblastoma growth. Notch1 is overexpressed in the majority of primary glioblastomas, and elevated levels of cleaved,

activated NICD is also observed in 80% of primary glioblastomas (238). The expression of Notch pathway components exhibits a positive correlation with glioma progression, and high expression is reported to be an independent predictor of poor survival (241, 242). This suggests increased activation of Notch signalling promotes a more undifferentiated and aggressive tumour phenotype.

Activation of the Notch pathway is considered to be a key characteristic of glioblastoma pathogenesis. Numerous studies have shown increased Notch pathway activation in primary glioblastomas compared with low grade gliomas (243), secondary glioblastomas (244) and normal brain tissue (238-240). Increased Notch signalling is associated with Hanahan *et al.*'s "hallmarks of cancer", including self-sufficiency in growth signals, insensitivity to anti-growth signals, evasion of apoptosis, limitless replicative potential, sustained angiogenesis, and tissue invasion and metastasis. As a result of its role in tumour biology, to date, several classes of Notch inhibitors have been developed including gamma secretase inhibitors (GSIs), other small molecule inhibitors, as well as targeted monoclonal antibodies (245, 246). Many of these studies have shown inhibition of Notch signalling can successfully reverse these hallmarks of cancer.

1.3.4.1 Inhibitors of Notch Signalling

Given that Notch signalling is frequently aberrantly expressed in cancer and has a well-established role in tumourigenesis, there has been a growing interest in therapeutically targeting Notch signalling in a number of cancers. Due to extensive research on the regulation of Notch signalling, three main strategies of therapeutically inhibiting Notch have emerged:

1. Inhibiting the proteolytic cleavage/activation of the receptor using small molecule gamma-secretase inhibitors.

2. Inhibiting the initial ligand-receptor interaction using neutralising monoclonal antibodies.

3. Suppressing the transcriptional coactivator role of Notch in the nucleus.

1.3.4.1.1 Inhibition of Gamma Secretase

Gamma secretase is a membrane-bound aspartyl protease complex which consists of a catalytic subunit presenilin and three other subunits including nicastrin, anterior pharynx defective-1, and presenilin enhancer-2 (247). Gamma secretase is an enzyme responsible for the crucial S3 cleavage within the Notch transmembrane domain, which results in the release of the NICD which is then able to translocate to the nucleus and form the transcription activation complex (248). Besides its role in mediating Notch signalling, the gamma secretase complex is also involved in the proteolytic cleavage of more than 90 other membrane-bound protein substrates including ErbB4, E-cadherin, CD44, and amyloid precursor protein indicating the varied physiological role of the enzyme (249). For example, the sequential cleavage of amyloid precursor protein results in the release of β-amyloid peptides that accumulate as insoluble amyloid plaques in Alzheimer's disease (250). Small-molecule GSIs were initially developed for the treatment of Alzheimer's disease, but due to the role of gamma secretase in Notch signalling activation, a number of these drugs are being repurposed as anti-cancer agents to prevent the canonical activation of Notch signalling.

One of the most studied GSIs is RO4929097. Initially developed by Roche for the treatment of Alzheimer's disease, its on-target effects on the Notch signalling pathway

led to its repurposing as a novel anti-cancer therapy. Several preclinical studies demonstrated RO4929097 has anti-tumour efficacy in a number of cancer types including lung and breast cancer, melanoma, and glioblastoma (251-255). A multitude of Phase I clinical trials have indicated RO4929097 has good tolerability as a single therapeutic agent (256-258), and it can also be used safely in combination with chemotherapy agents, radiotherapy, and other molecular-targeted therapies (259-262) (Table 1.5).

Dibenzazepine (DBZ; also known as LY-411575) was initially developed by Eli Lilly and had shown promise for significantly reducing brain and cerebral spinal fluid levels of Aβ-peptides though its inhibition of gamma secretase (263). DBZ has been shown to strongly inhibit Notch signalling *in vitro* as shown by reduced protein levels of activated NICD and the Notch target Hes1 in endothelial cells. Tumour growth in response to Notch inhibition with DBZ has also been shown to be significantly reduced alongside increased survival in mice bearing xenograft tumours following treatment (264). However, DBZ has yet to be used in a clinical trial as a potential cancer treatment.

A derivative of DBZ known as crenigacestat (LY-3039478) also developed by Eli Lilly has been utilised in a number of Phase I clinical trials (Table 1.5). Crenigacestat has been shown to inhibit Notch signalling in cell lines representing a number of different solid tumour and leukaemia including T-ALL. In xenograft models, crenigacestat demonstrated significant activity against human ovary, colon, and non-small-cell lung cancers (265). A first-in-human study of crenigacestat as an oral Notch signalling inhibitor in advanced or metastatic cancer determined crenigacestat is well tolerated and associated with target engagement, with evidence of clinical activity in a number of patients (266).

Table 1.5: Examples of Cancer Clinical Trials involving Inhibitors of Notch Signalling

Drug Class	Drug	CT Identifier	Study	Phase	Primary Endpoint	Status	Clinical Output Met?	Reference
Gamma Secretase Inhibitor	**RO4929097**	-	Molecular and Clinical Effects of Notch Inhibition in Glioma Patients: A Phase 0/I Trial.	0/I	PD	Completed	Yes	(252)
		NCT01218620	Gamma-Secretase/Notch Signalling Pathway Inhibitor R04929097 in Treating Patients with Advanced Solid Tumours	I	PD	Completed	-	No results published.
		NCT01189240	RO4929097 and Bevacizumab in Treating Patients with Progressive or Recurrent Malignant Glioma	I	DLT, MTD	Terminated (drug development ceased)	-	(262)
		NCT01232829	Gamma Secretase Inhibitor RO4929097 in Previously Treated Metastatic Pancreas Cancer	II	OS	Completed	No	(267)
	Crenigacestat (LY-3039478)	NCT01695005	A Study of LY3039478 in Participants with Advanced Cancer	I	DLT, ORR	Completed	Yes	(268)
		NCT02784795	A Phase 1b Study of LY3039478 in Combination with Other Anticancer Agents in Patients With Advanced or Metastatic Solid Tumours	I	MTD	Completed	Yes	No results published.
DLL4 Antibody	**Demcizumab**	NCT02722954	A Phase 1b Study of Demcizumab Plus Pembrolizumab in Locally Advanced or Metastatic Solid Tumours	Ib	DLT	Completed	Yes	(269)

		NCT01952249	A Study of Demcizumab Plus Paclitaxel in Subjects with Platinum Resistant Ovarian (SIERRA)	Ib	DLT, MTD	Completed	Yes	(270)
	Enoticumab (REGN421)	NCT00871559	A Multiple-Ascending-Dose Study of the Safety and Tolerability of REGN421 (SAR153192) in Patients with Advanced Solid Malignancies	I	DLT	Completed	Yes	(271)
	MEDI0639	NCT01577745	A Phase 1 Study to Evaluate the Safety, Tolerability, and Pharmacokinetics of MEDI0639 in Advanced Solid Tumours	I	DLT, MTD	Completed	Yes	(272)
Notch Receptor Antibody	**Brontictuzumab (OMP-52M51)**	NCT01778439	A Dose Escalation Study of OMP-52M51 in Subjects with Solid Tumours	I	DLT	Completed	Yes	(273)
		NCT01703572	A Dose Escalation Study of OMP-52M51 in Subjects with Lymphoid Malignancies	I	DLT	Completed	Yes	(274)
	Tarextumab (OMP-59R5)	NCT01277146	A Dose Escalation Study of OMP-59R5 in Subjects with Solid Tumours	I	AE, DLT	Completed	Yes	(275)
		NCT01647828	A Phase 1b/2 Study of OMP-59R5 in Combination with Nab-Paclitaxel and Gemcitabine in Subjects With Previously Untreated Stage IV Pancreatic Cancer	I/II	I: DLT II: PFS	Completed	I: Yes II: No	I: (276) II: (277)
Notch Transcription Complex Inhibitor	**CB-103**	NCT03422679	Study of CB-103 in Adult Patients with Advanced or Metastatic Solid Tumours and Haematological Malignancies	I/II	I: DLT II: Efficacy	Ongoing	-	(278)

AE: adverse events, DLT: dose-limiting toxicities, MTD: maximum tolerated dose, ORR: objective/overall response rate, OS: overall survival, PD: drug pharmacodynamics, PFS: progression-free survival.

1.3.4.1.2 Inhibiting the Receptor-Ligand Interaction

Antibody inhibitors remain a prominent means for blocking receptor-ligand interactions or part of a protein structure, and therefore represent one such modality to inhibit Notch signalling. A potential advantage of antibody inhibitors is their specificity, enabling targeting of individual Notch receptors or ligands compared to GSIs which inhibit Notch signalling as a whole (245). The Notch ligand DLL4 is important in vascular development, and in the context of cancer, its upregulation has been demonstrated in both tumour cells and tumour associated blood vessels (240, 279). DLL4 inhibition results in non-productive angiogenesis and tumour necrosis, resulting in inhibition of tumour growth which has been demonstrated in numerous *in vivo* cancer models (264, 279, 280). Several anti-DLL4 monoclonal antibodies (demcizumab, enoticumab, and MEDI0639) have been developed and are in clinical trials for advanced solid tumours (Table 1.5).

Another strategy is the development of monoclonal antibodies directed specifically at the Notch receptor. Brontictuzumab (OMP-52M51) is a humanised IgG2 antibody which targets the LNR and NRR domains of the Notch1 receptor (281). It has shown efficacy in T-ALL and mantle cell lymphoma *in vitro* and in vivo models, and in leukaemia patient-derived xenograft (PDX) models harbouring two common Notch1 activating mutations (HD and PEST domains) (282, 283). Another antibody, tarextumab (OMP-59R5), has been developed by OncoMed which selectively targets both Notch2 and Notch3. In preclinical studies tarextumab has shown anti-tumour efficacy when combined with gemcitabine and nanoparticle albumin-bound-paclitaxel in PDX models of several solid tumour types including breast, lung, pancreatic, and ovarian cancer (284). In a Phase I dose-escalation study in the treatment of advanced solid tumours,

tarextumab was reported to be well-tolerated and biomarker analysis indicated the clinical doses were adequate to inhibit Notch gene signalling (275). Examples of clinical trials utilising these therapeutic antibodies can be found in Table 1.5.

1.3.4.1.3 Inhibiting the Notch Transcriptional Activation Complex

Efforts have also been directed to target the further downstream signalling activities of intracellular Notch, rather than inhibiting the activation of Notch itself. Uniquely, this allows Notch signalling to be inhibited regardless of any genetic activating mutations of the Notch receptors. As previously discussed (Introduction 1.3.2.2), once cleavage of the Notch receptor occurs, the NICD is released and translocates to the nucleus where it forms a transcription activation complex with CSL DNA-binding protein and MAML adaptor protein. The Notch transcription activation complex binds to DNA resulting in the activation of Notch target genes such as the HES and HERP gene families (207, 208, 210).

SAHM1, a synthetic cell-permeable α-helical peptide, has been developed to block MAML recruitment with high affinity for the interface on the Notch-CSL/RBPJ transactivation complex. In both culture of leukaemic cells and a mouse model of Notch1 driven T-ALL, direct antagonism of the Notch transcriptional program by SAHM1 results in potent, Notch-specific anti-proliferative effects (285). Whilst this approach has efficacy in pathologies such as asthma and eye disorders (286, 287), there is currently a lack of pharmacokinetic and pharmacodynamic data supporting its use as an anti-cancer therapeutic. Aside from a peptide-based approach, a first-in-class small molecule inhibitor named Mastermind recruitment 1 (IMR-1) has been identified from *in silico* screening of over 1.5 million compounds. IMR-1 prevents recruitment of MAML to the Notch transcription activation complex on chromatin with a dose-

dependent decrease in Notch target gene transcription observed similar to GSI treatment. IMR-1 demonstrated efficacy in xenograft tumour models, minus any adverse effects on animal weight and other vital parameters (288). Despite promising preclinical data, IMR-1 is awaiting further preclinical evaluation.

Currently, only one inhibitor of the Notch transcription complex has undergone clinical trials in cancer patients. CB-103 is a first-in-class orally available small molecule protein-protein interactor and pan-Notch inhibitor that interrupts the assembly of the Notch transcription complex on the DNA within the nucleus, resulting in the downregulation of Notch transcriptional effectors including *MYC*, *CCND1*, and *HES1*. *In vitro* pharmacodynamic studies of CB-103 indicated an inhibition of Notch signalling in a dose-dependent manner. In a panel of more than 120 cell lines, CB-103 showed efficacy in 24 cell lines spread across a number of haematological (leukaemias and lymphomas) and solid malignancies (lung, breast, and sarcoma), in *in vivo* PDX models, in addition to an excellent safety profile (289, 290). A first-in-man Phase I/IIa multicentre open-label dose-escalation trial with an expansion study to determine preliminary anti-tumour efficacy is currently ongoing, with the aim to recruit 165 patients with advanced, refractory, or metastatic solid tumours (including glioblastoma), or haematological malignancies for whom no standard therapy exists (278).

The Notch inhibition strategies described above represent an attractive therapeutic approach in cancer treatment, however further clinical research is required to determine the effectiveness of these agents. In CSC-driven tumours like glioblastoma, Notch inhibition may prove useful in targeting the sub-population of GCSCs responsible for treatment resistance and tumour relapse.

1.3.5 Notch Pathway Deregulation in Glioma Cancer Stem Cells

Until recently, it was believed that glioblastoma originates solely from glial cells, i.e. astrocytes and oligodendrocytes residing in the brain parenchyma. However the discovery of proliferating cells in the brain led to a modification of this hypothesis (291). Studies performed in genetically modified mouse models suggest gliomas arise from the normal reservoirs of neural stem and progenitor cells within the brain. These models support the idea in that a diverse range of glioma-relevant mutations targeted to NSCs *in vivo* (e.g. inactivation of p53), readily produce gliomas with high fidelity and penetrance (292, 293).

Significant similarities have been identified between neural stem cells and GCSCs with regards to the signalling pathways controlling their self-renewal, survival, and cell-fate determination. On the top of this list are key developmental pathways controlled by Notch, Wnt, and Hedgehog (294). The Notch pathway has been extensively studied in the development and adult nervous system for its pleiotropic functions maintaining the pool of neural stem and progenitor cells, and to direct lineage specification (295). Many studies have identified Notch signalling promotes self-renewal and survival of neural stem and progenitor cells and blocks differentiation (296, 297). On the other hand, withdrawal of Notch signalling leads to diminished pools of progenitor cells and increased neuronal differentiation (296, 297).

Members of the Notch signalling pathway are expressed in neurogenic regions of the adult CNS (298), including the SVZ, where they maintain the NSC pool , and as previously mentioned, are involved in cell fate determination. A study by Lee *et al*. identified glioblastoma cells lines established under NSC culturing conditions match the phenotype and genotype of the original tumour, compared to glioblastoma cell

lines established in the presence of serum. In addition, the NSC-cultured glioblastoma cell lines clustered together with normal NSCs in global gene expression profiling. These cell lines expressed high levels of genes involved in CNS function and development, as well as stem cell associated genes such as Notch1 and Notch4, and DLL1 and DLL3 (299). Overexpression of NICD in a glioma cell line has also been shown to enhance proliferation alongside increased colony and sphere-forming potential. The sphere-forming cells displayed increased GCSC characteristics including the expression of the NSC marker Nestin, and the ability to differentiate into all three neuronal lineages based on immunofluorescence staining for GFAP, MAP2, and GalC (300). These studies support the idea that Notch signalling plays a role in regulating key GCSC characteristics.

Notch signalling also plays a role in the microenvironment of GCSCs. Within a tumour, the various cellular compartments provide both physical and chemical cues to maintain the CSC population, induce proliferation, and promote tumour heterogeneity. It has been identified that CSC fate is determined by juxtacrine or paracrine signalling from neighbouring cells (301, 302). In glioblastoma, GCSCs are often located regions of hypoxia and perivascular areas. Zhu *et al*. have reported in perivascular regions, Notch ligands present on endothelial cells could increase the GCSC phenotype in neighbouring tumour cells, whilst also enhancing their capacity for self-renewal. Coculture of human brain microvascular endothelial cells or Notch ligand with glioblastoma neurospheres promoted glioma cell growth and increased GCSC self-renewal, suggesting targeting GCSCs via Notch may provide a novel treatment strategy in glioblastoma (303).

1.3.6 Notch Signalling and Treatment Resistance

The current gold standard treatment in glioblastoma comprises of surgery followed by radiotherapy and adjuvant TMZ chemotherapy. However, approximately 50% of primary glioblastomas including most recurrent tumours are resistant to TMZ. Treatment failure in glioblastoma leads to a high mortality rate, therefore, there is a great need for novel treatments to improve clinical management and disease outcome.

The role of Notch signalling in glioma treatment resistance and recurrence was first examined by Gilbert *et al*. whereby inhibition of Notch signalling by a GSI enhanced glioma treatment by inhibiting neurosphere repopulation of cultured patient samples and xenograft recurrence in mice (197). In a murine orthotopic mouse model, Chu *et al*. examined the effects of Notch inhibition on glioblastoma xenografts. Weekly oral delivery of the GSI MRK003 resulted in significant inhibition of Notch pathway activity, tumour growth, CSC marker expression and clonogenicity (304). A more recent study has shown Notch inhibition combined with the current standard of care has an anti-GCSC effect, which provides and improved survival benefit in a glioblastoma orthotopic mouse model (255). A Phase I clinical trial conducted by Krop *et al*. assessed both the pharmacology and pharmacodynamics of the GSI MK-0752 in patients with solid tumours who had failed to respond to standard therapies. Dose-dependent inhibition of Notch signalling by MK-0752 was observed. A complete response was observed in a patient with anaplastic astrocytoma, and stable disease in 10 patients with glioblastoma. The study observed MK-0752 has a modest level of activity in patients with gliomas, and provides the first clinical evidence validating Notch as a therapeutic target in gliomas (305). These studies show the importance of Notch signalling in

tumour response to treatment, however, little is known about the importance of specific Notch ligands.

1.3.7 DLL4 and JAG1 in Glioblastoma

Both DLL4 and JAG1 are two key Notch ligands which have been previously implicated in tumour angiogenesis. In glioblastoma, both ligands are upregulated, however their relative effects and interactions in tumour biology, particularly in tumour response to therapeutic intervention remains unclear. Oon *et al*. have recently identified both DLL4 and JAG1 promote tumour growth by modulating angiogenesis, and both mediate tumour resistance to anti-VEGF therapy with bevacizumab (306). In glioblastoma, DLL4 expression in endothelial cells correlates with peritumoural brain oedema and poor prognosis (307, 308). Similarly, JAG1 expression in tumour and endothelial cells is associated with reduced time to progression and OS in primary glioblastoma patients (309). There is significant evidence to suggest Notch signalling regulates the self-renewal of GCSCs in glioblastoma (303, 310), and GCSCs are generally believed to mediate tumour recurrence and resistance to treatment (197). However, whether DLL4 and/or JAG1 are involved in the regulation of GCSCs, tumour recurrence, or TMZ chemoresistance remains to be elucidated.

1.4 Thesis Aims

Cancer stem cells have been identified as the drivers of tumourigenesis in glioblastoma, promoting angiogenesis, treatment resistance, and ultimately, tumour recurrence. The current prognosis for glioblastoma patients is poor, and in order for this to improve, GCSCs need to be targeted. There is significant evidence to suggest Notch signalling regulates the self-renewal of GCSCs, however, whether DLL4 and/or

JAG1 are involved in the regulation of GCSCs, TMZ resistance and tumour recurrence remains to be elucidated.

We hypothesise that DLL4 and JAG1 expression on endothelial cells and/or tumour cells may increase tumour resistance to chemotherapy with TMZ by induction of Notch signalling (DLL4-Notch/JAG1-Notch) in neighbouring tumour cells. Additionally, tumour resistance to TMZ chemotherapy is likely to be mediated through regulation of GCSCs by DLL4-Notch/JAG1-Notch signalling.

Project Aims:

Aim 1: To investigate if DLL4-Notch and JAG1-Notch signalling mediates tumour resistance to TMZ chemotherapy.

Aim 2: To dissect the underling molecular mechanisms of how DLL4/JAG1 or DLL4-Notch/JAG1-Notch signalling confer TMZ resistance at cellular and molecular levels.

Aim 3: To provide the rationale for developing clinical intervention strategies against glioblastoma (i.e. develop and optimal combination therapy).

Chapter 2

2 Materials and Methods

2.1 Cell Lines

The human glioblastoma cell lines U87MG (U87), U251MG (U251), Phoenix-AMPHO viral packaging cell line, and a patient-derived GCSC cell line, CSC-5, were used during this study. The U87 and U251 glioblastoma cell lines were chosen for this study as they are the two most commonly used cell lines used in glioblastoma research, and previous studies have identified both these cell lines have increased expression of Notch ligands and receptors when compared to other glioblastoma cell lines (238, 255, 311). Full details of cell origins and characteristics are given in Table 2.1. The U87, U251, and Phoenix AMPHO cell lines were purchased previously from the American Type Culture Collection (ATCC), whilst the CSC-5 cell line was kindly provided by Dr Claudia Barros (University of Plymouth, UK). The GCSC line was derived at the Department of Molecular Biology, Autonomous University of Madrid (312).

2.2 Cell Culture and Maintenance

2.2.1 Preparation of Growth Medium for Cell Maintenance

U87, U251, and Phoenix AMPHO cell lines were maintained in Dulbecco's modified Eagle medium (DMEM; D5796, Sigma Aldrich) containing 4500 mg/L glucose, L-glutamine, and sodium bicarbonate, and supplemented with 10% (v/v) foetal bovine serum (FBS; F7524, Sigma Aldrich), 1% non-essential amino acids (NEAA; 11140035, Gibco), 1% sodium pyruvate (11360070, Gibco) and 1% antibiotic-antimycotic solution (15240096, Gibco).

CSC-5 cells were maintained in a CSC medium consisting of DMEM/Ham's F12 nutrient mixture (D6421, Sigma Aldrich) containing 15 mM HEPES and sodium bicarbonate, and

Table 2.1: Details of Cell Lines.

Cell Line	Species	Origin	Morphology	Histology	Image
U87MG	*Homo sapiens*	Male, age unknown	Epithelial	Likely glioblastoma	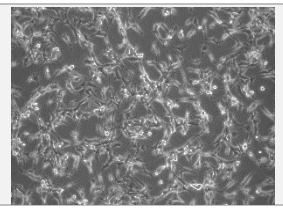
U251MG	*Homo sapiens*	Male, age 75	Fibroblastic	Glioblastoma, astrocytoma	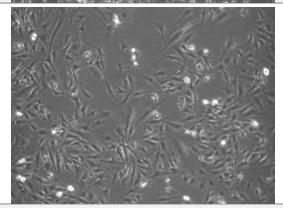
CSC-5	*Homo sapiens*			Glioblastoma	
Phoenix AMPHO	*Homo sapiens*	Embryonic kidney	Epithelial		

U87, U251, and Phoenix AMPHO cell lines were purchased previously from the American Type Culture Collection (ATCC), whilst the CSC-5 cell line was kindly provided by Dr Claudia Barros (University of Plymouth, UK).

supplemented with 10 ng/mL human EGF (E9644, Sigma Aldrich), 10 ng/mL recombinant human FGF-basic (154 amino acids; 100-18B, Preprotech), 1% N2 supplement (17502048, Gibco), 2 µg/mL heparin (Sigma Aldrich), 1% GlutaMAX supplement (35050061, Gibco), 1% NEAA, 1% sodium pyruvate, and 1% antibiotic-antimycotic solution.

2.2.2 Cell Maintenance

Cells were maintained in T75 flasks (11884235, ThermoFisher Scientific) or 100 mm dishes (11815275, ThermoFisher Scientific) in an incubator at 37 ^{o}C with 5% carbon dioxide. All tissue culture was performed following aseptic techniques with autoclaved and sterile equipment inside a class II laminar flow cabinet. U87, U251, and Phoenix AMPHO cells were maintained in the supplemented medium as previously described and routinely sub-cultured upon reaching 80-90% confluence. Confluence was gauged visually by assessing cell coverage of the surface of the culture dish under a light microscope (Motic AE2000 Inverted Light Microscope).

CSC-5 cells were fed three/four times weekly with 10-20% volume of fresh CSC medium. Under these conditions, neurospheres developed within one to two weeks. Neurosphere size was assessed visually and when the size reached 200-300 µm, neurospheres were enzymatically dissociated with 1X trypsin-ethylenediaminetetraacetic acid (EDTA) solution (15400054, Gibco) and re-seeded.

2.2.3 Passaging of Cells

Upon reaching 80-90% confluence, the medium of the adherent cell lines was aspirated and the cells washed once with sterile phosphate buffered saline (PBS). Adherent cells were detached by the addition of 2-3 mL trypsin-EDTA (1X) and incubated at 37 ^{o}C for several minutes. Cells were visualised to confirm detachment of

the cell monolayer before an equal volume of DMEM containing 10% FBS was added to neutralise the trypsin-EDTA solution. The cell suspension was then transferred to a 15 mL tube (11755075, Fisher Scientific) and centrifuged for 5 minutes at 1200 RPM. The supernatant was discarded, and the cell pellet was resuspended in an appropriate volume of medium. Cells were then either counted for use in experiments or transferred to a sterile 100 mm dish/T75 flask for sub-culture.

For CSC-5 cells, once neurospheres reached a size of 200-300 µm, spheres were collected in a 15 mL tube and centrifuged at 1200 RPM for 5 minutes. The supernatant was removed and 1-2 mL trypsin-EDTA was used to dissociate the spheres and incubated for 5 minutes at room temperature (RT). Following incubation an equal volume of DMEM containing 10% FBS was added to neutralise the trypsin-EDTA, and the cell suspension was centrifuged at 1200 RPM for 5 minutes. The supernatant was discarded, and the cell pellet was gently resuspended in CSC medium ensuring a single cell suspension, before being either counted for use in experiments or transferred to a sterile 100 mm dish for sub-culture.

2.2.4 Cell Counting

For counting, cells were mixed with trypan blue solution (final concentration 0.2%; 15250061, Gibco) (1:1 v/v). Trypan blue utilises the fact that live cells possess intact cell membranes, and therefore will not take up the dye. Dead cells have compromised cell membranes and as such will take up the dye, allowing them to be excluded from the viable cell count. Viable cells were manually counted using a BRAND counting chamber (BR719520, Sigma Aldrich). Briefly, the chamber was prepared by affixing the coverslip to the chamber and 10 µL of the trypan blue treated cell suspension was loaded onto the chamber. Using an inverted microscope, the grid lines of the chamber

were focussed on with a 10X objective. The counting chamber consists of 9 large squares, each subdivided into 16 square areas, of which 4 of the large squares were counted. To determine cell concentration, the following equation was used:

$$\text{Cells per mL} = (\text{average number of cells per large square}/2) \times (1 \times 10^4)$$

This calculation enabled the correct estimation of cell densities to be seeded during experiments.

2.2.5 Cryopreservation of Cell Lines

Cells were collected and spun down as previously described in section 2.2.3. The resulting cell pellet was resuspended in FBS containing 10% dimethyl sulfoxide (DMSO; D2650, Sigma Aldrich) for U87, U251 and Phoenix AMPHO cells, or for CSC-5 cells resuspended in CSC medium containing 10% DMSO and added to cryovials. Cells were then slowly frozen to -80^{o}C using a Nalegene Mr. Frosty^{TM} freezing container (51000001, ThermoFisher Scientific). The following day, frozen cells were transferred to liquid nitrogen tanks for long-term storage.

To revive cryopreserved cells, cells were thawed at 37 ^{o}C and immediately diluted 10X with DMEM containing 10% FBS. Cells were then spun down and plated as previously described in section 2.2.3.

2.2.6 3D Spheroid Culture

In contrast to 2D cell culture systems, 3D cell culture is believed to represent more accurately the microenvironment where cells reside in tissues, and as such, the behaviour of cells cultured in 3D is more reflective of the *in vivo* cellular response. Unlike 2D tumour cell culture, 3D tumour spheroid cultures are of intermediate complexity containing many elements found in tumours including regions of chronic

hypoxia, extracellular matrix, cell–cell and cell–extracellular matrix interactions, metabolite/catabolite gradients, necrosis and pH gradients (313). As such, we utilised a 3D spheroid culture system for glioblastoma in this study.

We exploited a rapid method of initiating glioblastoma spheroids using Ultra-Low Attachment 96-well plates. Briefly, 8000 cells in 100 µL DMEM containing 10% FBS were seeded per well in a Corning Costar 96-well Ultra-Low Attachment Plate (CLS7007, Corning). These plates have a round-shaped bottom with an ultra-low attachment surface consisting of a covalently bound hydrogel layer that is both hydrophilic and neutrally charged to prevent cell attachment. Cells were subjected to centrifugation at 1400 x g for 10 minutes. Plates were then returned to the cell culture incubator. One spheroid per well formed 48 h after seeding. Forty-eight h post seeding, the first phase contrast images were taken for all spheroids using a light microscope (Leica DM IL LED microscope with an attached Leica DFC3000G camera), and sphere volume was analysed using ImageJ software and an accompanying macro (Appendix 8.1.1 Analysis of Spheroid Volume using ImageJ). Following image acquisition, treatment regimens were administered (DMSO control, 25 nM DBZ only, 25 µM TMZ only, and 25 nM DBZ plus 25 µM TMZ). Spheroids were treated twice, once at day 0 and again at day 7 (Figure 2.1). TMZ (S1237, Selleck Chemicals) was diluted in DMSO and stored as a 100 mM stock at -80 ^{o}C, similarly DBZ (209984-56-5, Syncom) was also diluted in DMSO and stored as a 0.5 mM stock and stored at -80 ^{o}C. Spheres were monitored for a total of 21 days; imaged every 2 days and medium changed every 3/4 days.

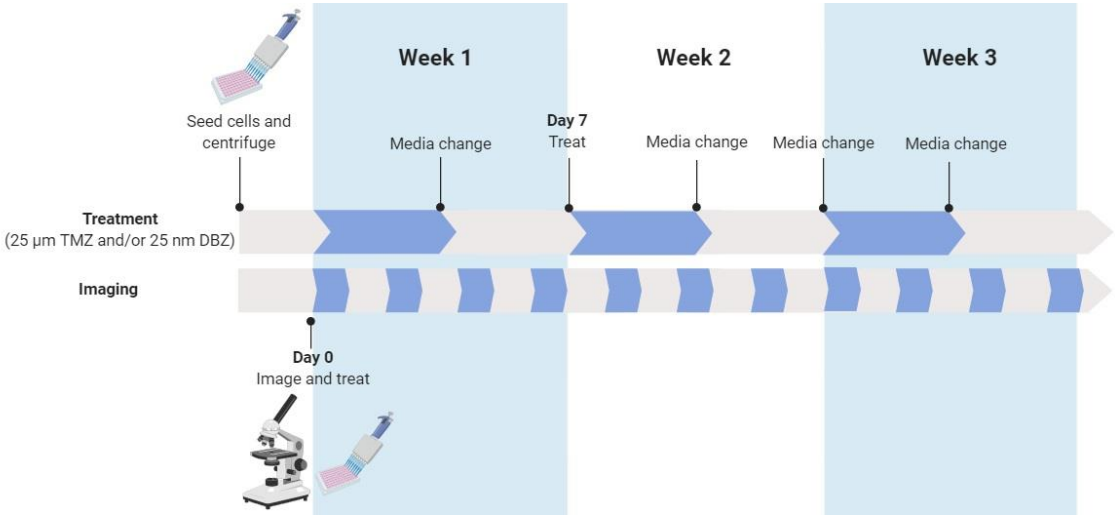

Figure 2.1: 3D spheroid culture model.

Spheroid culture was initiated and 48 h later, the first phase contrast images were taken. Spheroids were then treated with single DBZ/TMZ, or combination DBZ and TMZ treatment. Treatment was repeated again at day 7. Imaging was performed every two days, and media changed every three to four days.

2.2.7 Neurosphere Culture

2.2.7.1 Background

Neurosphere cultures were primarily developed for the propagation of free-floating clusters of NSCs and provide a method to investigate neural precursor cells *in vitro* (314). These methods have since been applied to glioma cell culture (175). Cells are suspended in a medium lacking adherent substrates but contain necessary growth factors such as EGF and FGF. This enables the stem cells to form characteristic 3D clusters. Neurosphere cultures have been shown to maintain genetic profiles similar to patient tumours and form invasive intracranial xenografts in immunocompromised mice (4, 299, 315).

2.2.7.2 Neurosphere Culture

To convert the adherent serum culture of the U87 and U251 cell lines to neurosphere culture, cells were detached as previously described (section 2.2.3) and immediately plated in serum-free, defined CSC medium consisting of DMEM/Ham's F12 nutrient mixture containing 15 mM HEPES and sodium bicarbonate, and supplemented with 10 ng/mL human EGF, 10 ng/mL recombinant human FGF-basic, 1% N2 supplement, 2 µg/mL heparin, 1% GlutaMAX supplement, 1% NEAA, 1% sodium pyruvate, and 1% antibiotic-antimycotic solution. Cultures were supplemented three/four times weekly with 10-20% volume of fresh CSC medium. Neurospheres generally formed within 1 to 2 weeks.

2.2.7.3 Neurosphere Recovery Assay

We utilised a neurosphere recovery assay developed by Gilbert *et al*. (197), which measures neurosphere formation at three time points to assess the ability of the culture to repopulate following treatment. First, we assess the ability of the cells to

form neurospheres shortly after treatment. Second, the number of neurospheres that form during a one-week recovery period are counted to determine if the surviving cells resume neurosphere formation. Finally, neurospheres are dissociated and the number of secondary neurospheres that form are counted to measure self-renewal. This assay provides a quantitative assay to assess culture repopulation following drug treatment (Figure 2.2).

Cells were plated at a concentration of 12,000 cells per well in a 6-well plate in 2 mL CSC medium. Immediately following plating, cells were treated with DMSO control, 25 nM DBZ, 25 µM TMZ, or 25 nM DBZ and 25 µM TMZ. Neurospheres were imaged on day 7 using a light microscope (Leica DM IL LED microscope with an attached Leica DFC3000G camera) and the number of neurospheres formed was counted using ImageJ software. At this timepoint, 2ml CSC medium was added and the spheres were left for another seven days. At day 14, neurosphere recovery was assessed by imaging neurospheres with a light microscope (as above), and the number of neurospheres was again counted. Neurospheres were then dissociated to single cells as previously described in section 2.2.3. Cells were then re-plated at a concentration of 12,000 cells per well in a 6-well plate and incubated under standard cell culture conditions for a further seven days. Secondary neurosphere formation was finally assessed at day 21 by imaging using a light microscope and the number of neurospheres formed was counted.

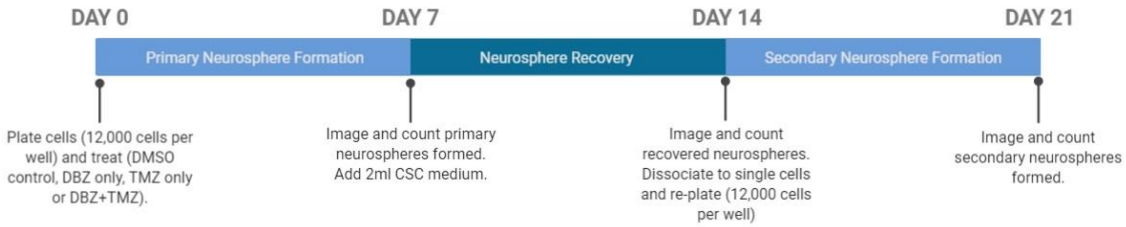

Figure 2.2: Neurosphere recovery assay overview.

A neurosphere recovery assay developed by Gilbert et al. (197) was utilised to assess primary neurosphere formation, neurosphere recovery, and secondary neurosphere formation following single DBZ/TMZ, and combination DBZ and TMZ treatment.

2.3 MTT Cell Viability Assay

The MTT (3-(4,5-dimethylthiazol-2-yl)-2,5-diphenyl tetrazolium bromide) cell viability assay is a colorimetric assay that measures the reduction of yellow MTT by mitochondrial succinate dehydrogenase. Viable cells with active metabolism convert MTT into an insoluble, purple coloured formazan product, which can then be solubilised with an organic solvent, e.g. DMSO, and the released, solubilised product can be measured spectrophotometrically. Since the reduction of MTT can only occur in metabolically active cells, the level of activity is a measure of cell viability.

MTT (M6494, ThermoFisher Scientific) was prepared as a 5 mg/mL stock solution in sterile PBS. For cell viability experiments, U87 cells were typically plated at a density of 4000 cells per well, and U251 at 2000 cells per well in a 96-well plate in 200 µL media. Briefly, 20 µL of stock solution was added per well and incubated at 37 ^{o}C for 4 h to allow formazan crystal formation. Following incubation, the medium was removed and replaced with 100 µL DMSO, and crystals were dissolved by pipetting before plate shaking for 10 minutes. Absorbance readings were taken at 562 nm and corrected by subtracting a reference measurement at 650 nm. Absorbance measurements were taken with the TECAN GENios V4.62-07/01 microplate reader (Tecan, Reading, UK) running XFLUOR4 Version V 4.51 software (Tecan), or the FLUOstar® Omega plate reader (Firmware version: 1.43) running the Omega software (Software version: 5.11).

2.3.1 IC50 Assay

To determine the IC50 of TMZ at several timepoints, U87 (4000 cells per well) and U251 (2000 cells per well) cells were plated in a 96-well plate. Twenty-four h later, cells were treated with 0 to 2 mM TMZ. Following 72 h, 96 h and 120 h TMZ treatment, cytotoxicity was determined by MTT assay as described above. To determine the effect

of DBZ pre-treatment on TMZ IC50, cells were plated as described and immediately treated with 25 nM DBZ followed by 0 to 2 mM TMZ treatment 24 h later. Cytotoxicity was again determined by MTT assay at the three timepoints (72 h, 96 h and 120 h post-TMZ treatment). For data analysis, non-linear regression analysis was performed to fit a dose-response curve to determine LogIC50 and IC50 values for given treatments using GraphPad Prism (version 6.01, GraphPad Software Inc., San Diego, USA).

2.4 Generation of Overexpression Cell Lines

2.4.1 Generation of Retroviral Constructs

Retroviral constructs containing mDLL4 and mJAG1 were previously established and provided by Li *et al.* (264, 316). Briefly, the cDNA of DLL4 and JAG1 was cloned from murine cDNA, followed by TA cloning into pGEM-T easy vector (A1360, Promega). Cloning accuracy was verified by DNA sequencing. Full-length mDLL4 and mJAG1 were released from pGEM-T easy vectors using *BamHI* and *EcoRI* restriction enzymes and ligated into the retroviral plasmid LZRSpBMN-linker-IRES-EGFP. This vector contains an internal ribosomal entry sites (IRES) that enables cap-independent translation of enhanced green fluorescent protein marker (eGFP), alongside a puromycin resistance gene. Ligation sites were sequenced, and accuracy of insertion verified.

2.4.2 Virus Packaging and Production

For viral packaging and production, the Phoenix AMPHO cell line was used. This cell line is a second-generation retrovirus producer line for the rapid generation of helper free amphotrophic retroviruses. It is based on the 293T cell line, a human embryonic kidney cell line transformed with adenovirus E1a and carrying a temperature sensitive T antigen co-selected with neomycin (317, 318). Transformation of 293T cells was achieved by the insertion of approximately 4.5 kb of viral genome into human chromosome 19; introducing constructs capable of producing viral gag-pol and env protein for amphotrophic viruses. One of the unique features of the Phoenix cell line is that it is highly transfectable with either calcium phosphate mediated transfection or lipid-based transfection protocols. It is suggested that a single transfection experiment can generate sufficient virus to infect millions of target cells (319).

The cell line utilises two non-retroviral promoters in the gag-pol and env expression constructs, with co-selectable resistance to hydromycin and diphtheria toxin, respectively. This enables easy and reliable selection of the packaging functions. The gag-pol gene product is coupled to a CD8α surface marker via an internal ribosome entry site (IRES) for direct monitoring of gag-pol production by flow cytometry. Expression of env may be assessed with available antisera (320).

Phoenix AMPHO cells were grown to 50% confluency in 6-well plates and transfected with retroviral constructs (5 µg) using Lipofectamine3000 (L3000015, Invitrogen) for 24 h following the manufacturers protocol. In brief, 250 µL Opti-MEM-I (31985062, Gibco) and 15 µL Lipo3000 was added to microcentrifuge tube 1, whilst 250 µL Opti-MEM-I, 10 µL p3000 and 5 µg plasmid was added to microcentrifuge tube 2. Tube 1 and 2 were then mixed and then left to incubate at RT for 15 minutes. Following incubation, medium was removed from the Phoenix AMPHO cells and the DNA-lipid complex was added, along with 3.5 mL DMEM containing 10% FBS.

The following day, medium was removed and fresh complete DMEM containing 2 µg/mL puromycin (15490717, Fisher Scientific) was added and incubated for 24 h. Cells were then split into a 6-well plate at three increasing cell densities in DMEM containing 2 µg/mL puromycin and left for 24 h. The following day, the medium was changed to DMEM containing 10% FBS. Following 24 h incubation, the cells were washed with PBS and cultured in Opti-MEM-I for 24 h. The virus containing culture supernatant was filtered (0.45 µm) and added with polybrene (4 ng/ml; TR-1003-G, Sigma Aldrich) to the cells to be transfected.

2.4.3 Retroviral Infection of Cell Lines

2.4.3.1 U251 Cell Line

U251 cells were grown to 50% confluency in a 6-well plate. Viral supernatant (0.5 mL) containing polybrene (4 ng/mL) was added to the cells and left to incubate under standard conditions for 3-5 h. The medium was then diluted (1:3) with DMEM containing 10% FBS and polybrene (4 ng/ml). Viral transduction was repeated three times over three consecutive days. Green fluorescent protein (GFP) expression of positively transduced cells was visualised using a Leica DMi8 S inverted microscope and the accompanying Leica LAS software.

2.4.3.2 CSC-5 Cell Line

For viral infections, 0.5 x 10^6 cells were seeded into a 10 cm dish in CSC medium and left overnight. The following day, 2 mL viral particles and polybrene (4 ng/ml) were added and incubated overnight. Viral infection was completed a total of three times over three consecutive days. Following viral transduction, cells were collected and spun down to remove the viral supernatant before being cultured as previously described. GFP expression of positively transduced cells was visualised using a Leica DMi8 S inverted microscope and Leica LAS software.

2.5 Generation of shRNA Knockdown Cell Lines

A short hairpin RNA (shRNA) is an artificial RNA molecule with a tight hairpin turn that can be utilised to silence gene expression by RNA interference (RNAi). In this study we utilised shRNA lentiviral particles purchased from Santa Cruz Biotechnology (Table 2.2), which are provided as pools of three to five expression constructs each encoding a target-specific 19-25 nucleotide (plus hairpin loop) shRNA.

Following viral transduction and integration of the vector into the host genome, the shRNA is transcribed in the nucleus by polymerase II or polymerase III depending on the promoter. The resulting product mimics pri-microRNA and is processed by Drosha. The resultant pre-shRNA produced is exported from the nucleus by Exportin 5 and is then processed by Dicer and loaded into the RNA-induced silencing complex (RISC). The sense strand is degraded whilst the antisense (guide) strand directs RISC to mRNA that has a complementary sequence. As a result of perfect complementarity, RISC cleaves the mRNA, however in cases of imperfect complementarity, RISC represses mRNA translation. In both cases, this results in silencing of the target gene (321).

shRNA knockdown of DLL4 and JAG1 was performed in CSC-5 cells. Briefly, cells were seeded at 0.25 x 10^6 cells per well alongside 2 mL CSC medium in a 6-well plate and left to incubate overnight. The following day, 15 µL lentiviral particles (Table 2.2) was added to the cells alongside 4 µg/mL polybrene and incubated for 24 h. The next day, cells were subjected to 0.5 µg/mL puromycin in order to select for cells stably expressing shRNA.

Table 2.2: Santa Cruz Biotechnology shRNA lentiviral particles

ShRNA	**Product Code**
Delta-4 shRNA (h) Lentiviral Particles	sc-39667-V
Jagged1 shRNA (h) Lentiviral Particles	sc-37202-V
Control shRNA Lentiviral Particles-A	sc-108080

2.6 Quantitative Reverse Transcription Polymerase Chain Reaction (RT-qPCR)

2.6.1 Background

RT-qPCR is a sensitive technique enabling the detection of small quantities of complementary DNA (cDNA) within a sample whilst determining an accurate copy number of the target gene being amplified. RT-qPCR uses real-time fluorescence to measure the quantity of specific DNA targets present in a sample during a PCR. SYBR® Green I is one of the most commonly used fluorescent dyes for qPCR and was utilised during this study. The fluorescent dye is a double-stranded DNA (dsDNA)-binding dye that intercalates non-specifically into dsDNA, allowing measurement of the amount of PCR product. As amplification proceeds, the amount of DNA product increases, and therefore the number of SYBR® Green I molecules incorporated into DNA also increases. As the increase in fluorescence is proportional to the amount of product amassed, qPCR using SYBR® Green I can be used for relative DNA quantification.

In RT-qPCR, the sample RNA template is first converted into cDNA using reverse transcriptase. The cDNA is then used as the template for amplification during qPCR. RT-qPCR can be performed in a one-step or two-step assay. One-step assays combine reverse transcription and PCR in a single tube and buffer, using a reverse transcriptase along with a DNA polymerase. Whereas in two-step assays, the reverse transcription and PCR steps are performed separately. In this study, a two-step assay was utilised: the Applied Biosystems High Capacity cDNA Reverse Transcription kit for cDNA synthesis and the Roche LightCycler 480 II system for qPCR.

2.6.2 Total RNA Isolation

Total RNA was extracted following the acid guanidinium thiocyanate-phenol-chloroform extraction protocol using TRI reagent (AM9738, Invitrogen). Cultured cells

were washed twice using sterile PBS and 1 mL TRI reagent was added. The reagent aids detachment of the monolayer and induces cell lysis. After 5 minutes at RT, a cell scraper was used to physically removed the cell monolayer into the TRI reagent, and the lysate was transferred to a 1.5 mL microcentrifuge tube. Samples were then vortexed and incubated for 5 minutes at RT before the addition of 100 µL 1-bromo-3-chloropropane (B9673, Sigma Aldrich). Samples were mixed well and incubated on ice for 10 minutes before centrifugation at 12,000 x g for 10 minutes at 4 ^{o}C. Following centrifugation, the homogenate separates into three distinct phases: the lower pink organic phase contains protein, the white inter phase contains DNA, and the upper aqueous phase contains RNA. The aqueous phase was collected and 500 µL 2-propanol (I9516, Sigma Aldrich) added. Samples were mixed and incubated on ice for 10 minutes prior to centrifugation at 12,000 x g for 8 minutes at 4 ^{o}C. As RNA is insoluble in isopropanol, this step precipitates RNA out of solution forming a visible pellet. The supernatant was removed, and the resulting pellet was washed in 1 mL 75% ethanol (10644795, Fisher Scientific) and centrifuged for 5 minutes at 12,000 x g at 4 ^{o}C. Ethanol was removed, and the resulting RNA pellet was allowed to briefly air-dry prior to being resuspended in 10 µL diethylpyrocarbonate (DEPC)-treated distilled water (10245203, Fisher Scientific).

2.6.3 RNA Quantification

Purified RNA was quantified using a NanoDrop^{TM} 2000 UV-Vis Spectrophotometer (Thermo Scientific). RNA quality was assessed by analysing the 260/280 and 260/230 ratios and corresponding graphs, which indicates the presence of contaminants. RNA was then diluted to a concentration of 1 µg/µL.

2.6.4 cDNA Synthesis

Reverse transcription was performed using a High Capacity cDNA Reverse Transcription kit (4368814, Applied Biosystems) following the manufacturers protocol. Briefly, 1 µg of total RNA was reverse transcribed using the Multiscribe™ Reverse Transcriptase polymerase and random hexamer primers as detailed in Table 2.3.

Table 2.3: cDNA synthesis reaction components

Component	**1X Reaction (µL)**
10X RT buffer	2.0
25X dNTP mix (100 mM)	0.8
10X random primers	2.0
Multiscribe™ Reverse Transcriptase	1.0
Nuclease free water	13.2
RNA sample (1 µg/µL)	1.0
Total	20

Samples were then placed in a Veriti™ Thermal Cycler 96 well (Applied Biosystems) and the temperature parameters given in Table 2.4 were applied.

Table 2.4: cDNA synthesis cycling parameters.

	Annealing	**Elongation**	**Denaturation**	**Final hold**
Temperature (°C)	25	37	85	4
Time	10 minutes	120 minutes	5 minutes	∞

The generated cDNA samples were then diluted 1:50 in DEPC-treated water and stored at -20 °C until required.

2.6.5 qPCR

qPCR was performed using the Roche LightCycler 480 DNA SYBR® Green I Master kit (4707516001, Roche Diagnostics) using the Roche LightCycler 480 II system. Primers were designed against the coding sequence for each gene, provided by NCBI gene (http://www.ncbi.nlm.nih.gov/gene/) using the Primer 3 website (http://biotools.umassmed.edu/bioapps/primer3_www.cgi). Primer binding sites and predicted product sizes were verified using NCBI Primer-Basic Local Alignment Search Tool (BLAST) (www.ncbi.nlm.nih.gov/tools/primer-blast/). Primers were designed to give an amplicon length that reduces the risk of dimers and hairpins. If possible, primers were designed to cross an exon in order to negate the issue of genomic DNA contaminants being amplified. A list of primers used in this study are given in Table 2.5.

cDNA samples were combined with LightCycler 480 DNA SYBR® Green I Master mix and appropriate primers totalling 10 µL or 20 µL (Table 2.6) depending on whether a 96-well (05102413001, Roche Diagnostics) or 384-well (05102430001, Roche Diagnostics) reaction plate was used.

Samples were loaded into the appropriate qPCR plate and sealed with an optically clear microseal. The qPCR plate was then briefly centrifuged at 1000 RPM for 2 minutes, before being loaded into the Roche LightCycler 480 II instrument and the programme conditions in Table 2.7 were applied.

Table 2.5: List of primers used for qPCR analysis

Gene		Primer Sequence (5' →3')	Product size (bp)
CD133	Forward	CCTCTGGTGGGGTATTTCTT	210
	Reverse	CAGTTTCCGACTCCTTTTGA	
DLL4	Forward	ACAACTTGTCGGACTTCCAG	77
	Reverse	CAGCTCCTTCTTCTGGTTTG	
GAPDH	Forward	GACCCCTTCATTGACCTCAAC	134
	Reverse	TGGACTGTGGTCATGAGTCC	
GFAP	Forward	GAGCAGGAGGAGCGGCAC	164
	Reverse	TAGGTGGCGATCTCGATGTCC	
HES1	Forward	AGTGAAGCACCTCCGGAAC	107
	Reverse	CGTTCATGCACTCGCTGA	
HEY1	Forward	CGAGCTGGACGAGACCAT	76
	Reverse	GGAACCTAGAGCCGAACTCA	
HEY2	Forward	GTACCATCCAGCAGTGCATC	65
	Reverse	GGAACCTAGAGCCGAACTCA	
JAG1	Forward	TGGGCTTTGAGTGTGAGTGT	93
	Reverse	CCCCGTGGGAACAGTTATTA	
mDLL4	Forward	AGGTGCCACTTCGGTTACAC	62
	Reverse	GGGAGAGCAAATGGCTGATA	
mJAG1	Forward	TCTCTGACCCCTGCCATAAC	169
	Reverse	TTGAATCCATTCACCAGATCC	
NES	Forward	ATAGAGGGCAAAGTGGTAAGCAG	177
	Reverse	TTCTAGTGTCTCATGGCTCTGGTT	
OLIG1	Forward	GTCATCCTGCCCTACTCAGC	107
	Reverse	CTGCCCAGCAGTAGGATGTAG	
SOX2	Forward	GGGAAATGGGAGGGGTGCAAAAGAGG	151
	Reverse	TTGCGTGAGTGTGGATGGGATTGGTG	
TUBB3	Forward	CCAAGGGTCACTACACGGAG	187
	Reverse	ATGATGCGGTCGGGATACTC	

Table 2.6: qPCR reaction mix.

Component	1X Reaction (96-well)	1X Reaction (384-well)
Mastermix, 2X	10	5
Forward primer	0.5	0.25
Reverse primer	0.5	0.25
Water, PCR grade	4	2
cDNA (5ng)	5	2.5
Total	20	10

Table 2.7: qPCR cycling parameters.

	Step 1: Initiation	Step 2: Denaturation	Step 3: Annealing	Step 4: Extension	Step 5: Cooling
Temperature (°C)	95	95	58	72	40
Time	10 minutes	15 seconds	30 seconds	30 seconds	10 seconds
Cycles	1	45			1

GAPDH was used as a control in order to normalise the data. Results were analysed using the ΔΔCT method (also known as the Livak method) in Microsoft Excel (Version 1808; Microsoft Corporation, Washington, USA). An overview of qPCR data analysis using the ΔΔCT method is given in Appendix 8.2 **(**ΔΔCT Method for Analysing RT-qPCR Data). PCR amplification was assessed to ensure appropriate amplification curves and annealing temperature was obtained. Generated results were exported into GraphPad Prism (Version 6.01; Graphpad Software Inc., California, USA) for statistical analysis.

2.7 Western blotting

2.7.1 Background

Western blotting is an analytical technique used to detect specific proteins in a sample. It utilises gel electrophoresis to separate denatured proteins by their size before the proteins are transferred to a polyvinylidene difluoride (PVDF) membrane. The membrane is then probed using antibodies specific for the protein of interest before detection using chemiluminescence.

2.7.2 Cell Lysis

Cell culture medium was removed, and cells were washed with ice cold sterile PBS three times on ice. Ice cold RIPA Lysis and Extraction buffer (containing protease and phosphatase inhibitors; 89900, Pierce) of an appropriate volume was added to cells and left to incubate on ice for 5 minutes. A cell scraper was then used to detach the cells from the surface of the dish and samples were transferred to a sterile 1.5 mL microcentrifuge tube. Samples were then placed on a microcentrifuge tube rotator for 30 minutes at 4 ^{o}C, before being centrifuged at 16,000 x g for 20 minutes at 4 ^{o}C. The resultant supernatant was transferred to a sterile 1.5 mL microcentrifuge tube and stored at -20 ^{o}C until further analysis.

2.7.3 Protein Quantification

Total protein was quantified using the Bicinchoninic Acid (BCA) Protein Assay kit (23225, Pierce) following the manufacturer's instructions. This assay is used to determine the total protein concentration of a sample by comparison to a known set of standards. A standard curve was produced from a set of nine protein standards. Standards were made from a 2 mg/mL BSA standard and serially diluted in PBS to yield the following protein concentrations: 0, 25, 125, 250, 500, 750, 1000, 1500 and 2000

µg/ml. Twenty-five microliters of each standard was used to produce the standard curve of the assay. Protein samples were diluted 1:10 in PBS to minimise usage of the sample, and 25 µL was taken for protein quantification. The BCA working reagent was then prepared as described following the manufacturers protocol. Briefly, the working reagent was prepared by mixing 50 parts of BCA Reagent A with 1 part of BCA Reagent B (50:1 reagent A:B). Two-hundred microliters of the BCA working reagent was added to 25 µL of protein standard or sample in a 96-well plate in triplicate. The plate was gently shaken for 1 minute before being wrapped in foil and samples were left to incubate for 30 minutes at 37 ^{o}C. Following incubation, the absorbance of each well was measured at 592 nm using a FLUOstar® Omega plate reader (Firmware version: 1.43) and the Omega software (Software version: 5.11). The absorbance values of the standards were used to plot a linear regression curve and its associated equation. The equation was then utilised to calculate the protein concentration of each sample.

2.7.4 Protein Sample Preparation

Prior to separation by electrophoresis, proteins were first denatured. Samples were diluted in 4X Lamelli sample loading buffer (composed of 4% w/v SDS, 20 % v/v glycerol, 120 mM TRIS pH 6.8, 1.54 % w/v DTT and 0.01% w/v bromophenol blue; 15405809, Alfa Aesar) before being denatured by heating at 95 ^{o}C for 10 minutes. SDS is an anionic detergent which causes complex secondary, tertiary, and quaternary proteins to be denatured and applies a negative charge to the proteins in proportion to their mass. Consequently, when an electrical field is applied each protein will migrate towards the anode. DTT further denatures proteins by reducing disulphide bonds. Glycerol increases the density of the sample making it easier to load into the

wells, and bromophenol blue is a tracking dye which allows the visualisation of the migration of the proteins through the polyacrylamide gel.

2.7.5 Sodium Dodecyl Sulphate-Polyacrylamide Gel Electrophoresis (SDS-PAGE)

SDS-PAGE is a method used to separate protein according to their size. All SDS-PAGE gels were prepared in a gel casting apparatus (Bio-Rad Laboratories). For SDS-PAGE, two polyacrylamide gels are made: a resolving gel and a stacking gel. The resolving gel is basic (pH 8.8) and has a higher percentage of acrylamide, therefore making the pores in the gel smaller and consequently proteins are separated based on their size, as the smaller proteins travel more rapidly and easily through the gel. The percentage of acrylamide in the resolving gel is dependent on the molecular weight of the protein of interest. As the acrylamide percentage increases, the pore size decreases and thus smaller proteins are resolved better. The upper stacking gel is acidic (pH 6.8) with a lower percentage of acrylamide and consequently larger pores. The stacking gel functions to enable the proteins to stack into one band at the interface between the two gels, allowing protein to migrate into the resolving gel at the same time.

A 10% resolving gel was prepared to separate proteins (Table 2.8). Reagents were added in order from largest to smallest, with APS and TEMED added last to trigger polymerisation of the acrylamide. The solution was inverted several times to mix and then pipet and left to set between the glass plates. Water was pipette on top of the gel to ensure the gel set straight with no bubbles. Once set, the water was removed, and the stacking gel was prepared and added on top of the resolving gel. A 10-well comb was inserted into the gel and the stacking gel was left to set for 30 minutes.

Once the gels had set, the gel was placed into an electrophoresis tank (Mini-PROTEAN, Bio-Rad Laboratories) and submerged in 1X running buffer (Table 2.9). The comb was

removed, and 20-40 µg protein samples were loaded into the wells of the polyacrylamide gel alongside a pre-stained protein ladder (10-250 kDa; 26619, ThermoFisher Scientific) for reference. Proteins were resolved at 80 V for 30 minutes, before being increased to 120 V for 1 h.

Table 2.8: Components of the polyacrylamide resolving and stacking gels.

Constituent	Stacking gel	Resolving gel
Deionised H_2O	3.4 mL	4Ml
30% Acrylamide solution	830µL	3.3mL
1.0M Tris-HCl (pH 6.8)	630µL	
1.5M Tris-HCl (pH 6.8)		2.5mL
10% (w/v) SDS	50µL	100µL
10% (w/v) APS	50µL	100µL
TEMED	5µL	6µL

The components and volumes of both the stacking (5%) and resolving (10%) gels. SDS, sodium dodecyl sulphate; APS, ammonium persulphate; TEMED, tetramethylethylenediamine.

Table 2.9: 10X running buffer.

Constituent	Weight (g)
Tris-base	30
Glycine	144
SDS	10

The constituents of the running buffer were made up in 1 L of deionised water and diluted 1:10 before running the gels.

2.7.6 Electroblotting

Following SDS-PAGE, wet electroblotting was used to transfer proteins from the gel to a 0.2 µm or 0.45 µm PVDF membrane (10600029, GE Healthcare) depending on the size of the protein of interest. The PVDF membrane was soaked in methanol (10284580, Fisher Scientific) prior to assembling the blotting cassette. Both the gel and

the PVDF membrane were sandwiched between pre-soaked blotting paper and foam pads and encased within the blotting cassette (Figure 2.3). The cassette was placed into a wet electroblotting tank (Mini-PROTEAN, Bio-Rad Laboratories), the tank was filled with transfer buffer (Table 2.10) and an ice pack was added. Proteins were transferred for 2 h at 200 mA.

Table 2.10: Transfer buffer.

Constituent	Weight (g)
Tris-base	3
Glycine	14.4

The constituents were added to 800ml water and 200ml methanol. The buffer was stored on ice before use.

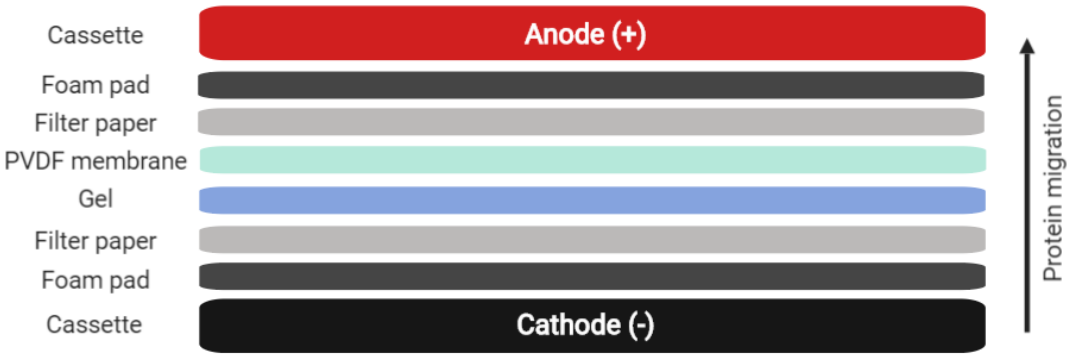

Figure 2.3: Assembly of the Western blot transfer apparatus.

The PVDF membrane is placed between the gel and the positive anode to enable negatively charged proteins to transfer from the gel to the membrane.

2.7.7 Incubation with Antibodies

Following transfer, the gel was discarded and the PVDF membrane was blocked by incubating in 5% (w/v) skimmed milk powder (10651135, ThermoFisher Scientific) in PBS-Tween (0.1% v/v) at RT for 1 h. The membrane was then incubated with the primary antibody in 5% milk in PBS-Tween (0.1% v/v) overnight at 4 ^{o}C. The membrane was washed 3 times for 5 minutes each in PBS-Tween (0.1% v/v) before incubating in a horseradish peroxidase (HRP)-conjugated secondary antibody diluted in 5% milk in PBS-Tween (0.1% v/v) for 1 h at RT. The membrane was again washed in PBS-Tween (0.1% v/v) 3 times for 5 minutes to remove any unbound antibody before protein detection. A list of primary and secondary antibodies used during this study is given in Table 2.11.

2.7.8 Development of Membrane

In order to detect protein bands, the Enhanced Chemiluminescence (ECL) Western Blotting Substrate kit (32106, Pierce) was used. Briefly, detection reagents 1 and 2 were mixed at a ratio of 1:1 and added directly to the PVDF membrane. Blots were imaged using a Syngene PXi imaging system and the accompanying software.

Table 2.11: List of primary and secondary antibodies used for Western Blot analysis

Primary Antibodies						
Name	**Species**	**Specificity**	**Molecular Weight (kDa)**	**Supplier**	**Product Code**	**Dilution**
Anti-β-tubulin	M	C, Dg, H, M, Mk, R, Rb	51	ThermoFisher Scientific	MA5-16308	1:2000
Anti-Cleaved Notch-1 (NICD)	R	H, M, R	120	Cell Signalling Technology	4147	1:1000
Anti-DLL4	R	H, M	74	Abcam	AB7280	1:1000
Anti-GAPDH (GA1R)	M	B, C, Dg, H, Hm, I, Rb, R, Y	37	ThermoFisher Scientific	MA5-15738	1:2000
Anti-HES1	R	H, M, Mk, R	30	Cell Signalling Technology	11988	1:1000
Anti-JAG1 (28H8)	R	H, M	180	Cell Signalling Technology	2620	1:1000

Secondary Antibodies				
Name	**Species**	**Supplier**	**Product Code**	**Dilution**
Anti-rabbit IgG HRP conjugate	G	ThermoFisher Scientific	65-6120	1:5000
Anti-mouse IgG HRP conjugate	G	ThermoFisher Scientific	31430	1:5000

B: bacteria, C: chicken, Dg: dog, G: goat; H: human, Hm: hamster, I: insect; M: mouse, Mk: monkey, R: rat, Rb: rabbit, Y: yeast.

2.8 Immunofluorescence

Immunofluorescence (IF) is a technique which combines the use of antibodies with fluorescence imaging techniques to visualise target antigens within fixed cell or tissue samples. This technique can reveal the localisation, relative expression, and even the activation states of target proteins. The power of IF is that it provides data that is both graphical and quantifiable.

Proteins of interest are detected using either primary antibodies covalently conjugated to fluorophores (direct detection), or a two-step approach with an unlabelled primary antibody followed by a fluorophore-conjugated secondary antibody (indirect detection). Both methods enable combinations of multiple fluorophores (multiplex analysis), and as such IF is ideal for investigating protein co-localisation, changes in cellular localisation, differential activation of proteins within a cell, identification of different cell types, and other analyses.

2.8.1 Immunofluorescence Staining Method

Samples were fixed in 4% paraformaldehyde in PBS and incubated for 20 minutes at RT or overnight at 4 ^{o}C. Samples were then washed twice in 0.1% Triton X-100 in PBS for 5 minutes each. To prevent non-specific binding of antibodies samples were blocked using 5% donkey serum (D9663, Sigma Aldrich), 0.25% gelatine (G7765, Sigma Aldrich), and 0.25% bovine serum albumin (BSA; A2153, Sigma Aldrich) in PBS for 1 h. Samples were once again washed twice in in 0.1% Triton X-100 in PBS for 5 minutes each prior to incubation with primary antibodies overnight (Table 2.12). The following day, primary antibody was removed and samples were again washed twice in 0.1% Triton X-100 in PBS for 5 minutes each, before incubation with secondary antibodies (Table 2.12) for 2 h at RT. Nuclei were counterstained with 2 µg/mL 4’,6-diamidino-2-

phenylindole (DAPI) (D9542, Sigma-Aldrich) for 5 minutes at RT, followed by two final washes with 0.1% Triton X-100 in PBS for 5 minutes each. IF staining was imaged using a Leica DMI 5500 Q confocal microscope with a Leica TCS SPE attachment running Leica LAS AF software, or Leica DMi8 inverted microscope running Leica LAS AF software.

2.8.2 Whole Mount Staining of Neurospheres

Neurospheres were collected and centrifuged at 1200 RPM for 5 minutes. The medium was discarded and neurospheres were washed twice using sterile PBS. Neurospheres were then resuspended in 4% paraformaldehyde in PBS and fixed for 20 minutes at RT, or overnight at 4 ^{o}C. Spheres were then washed once using PBS and then twice in sterile water before being resuspended in an appropriate volume of sterile water. Neurospheres were pipette onto a Polysine Adhesion Microscope Slide (J2800AMNZ, Thermo Scientific) and allowed to attach by drying for approximately 1-2 h at RT. Once attached, neurospheres were rehydrated with PBS before being permeabilised with 0.5% Triton X-100 in PBS for 1 h at RT. Neurospheres were washed once in PBS, and to prevent non-specific binding of antibodies, slides were blocked using 5% donkey serum, 0.25% gelatine, and 0.25% bovine serum albumin in PBS for at least 3 h at RT. Following blocking, neurospheres were incubated in primary antibody (Table 2.12) diluted in 0.5% Triton X-100 in PBS for 24 h at 4 ^{o}C. The following day, spheres were washed for 3 h in PBS before being incubated in secondary antibody (Table 2.12) diluted in 0.5% Triton X-100 in PBS overnight at 4 ^{o}C. Slides were then washed for 3 h before being counterstained with 2 µg/mL DAPI for 20 minutes at RT. Slide were again washed in PBS before being mounted with Dako fluorescence mounting medium (S3023, Agilent) with a glass coverslip prior to imaging. IF staining was imaged using a

Leica DMI 5500 Q confocal microscope with a Leica TCS SPE attachment running Leica LAS AF software.

Table 2.12: List of primary and secondary antibodies used for immunofluorescence.

Primary Antibodies						
Name	**Species**	**Specificity**	**Supplier**	**Product Code**	**Dilution**	**Whole Mount Staining Dilution**
Anti-β-III-tubulin	M	C, Dg, H, M, NHP, R, Rb	R&D Systems	MAB1195	N/A	1:250
Anti-CD133 (W6B3C1)	M	H	Miltenyi Biotec	130-092-395	N/A	1:50
Anti-DLL4	Rb	H, M	Abcam	AB7280	1:1000	1:250
Anti-GFAP (28H8)	M	H, R	Sigma Aldrich	G3893	N/A	1:250
Anti-JAG1	Rb	H, M	Cell Signalling Technology	2620S	1:1000	1:250
Anti-Ki67	Rb	H	Abcam	AB15580	1:2000	1:1000
Anti-Nestin	Rb	H, M, R	Sigma Aldrich	N5413	N/A	1:250
Anti-SOX2	Rb	H, M	Abcam	AB97959	N/A	1:250
Anti-SOX10	M	H, R	R&D Systems	MAB2864	N/A	1:250

Secondary Antibodies				
Name	**Species**	**Supplier**	**Product Code**	**Dilution**
Anti-mouse IgG Alexa Fluor 568	D	ThermoFisher Scientific	A10037	1:1000
Anti-rabbit IgG Alexa Fluor 647	G	ThermoFisher Scientific	A21245	1:1000

B: bacteria, C: chicken, D: donkey, Dg: dog, G: goat, H: human, Hm: hamster, I: insect; M: mouse, Mk: monkey, R: rat, Rb: rabbit, Y: yeast.

2.9 Immunohistochemistry

2.9.1 Background

Immunohistochemistry (IHC) allows the qualitative identification by light microscopy of antigens in sections of formalin-fixed paraffin-embedded (FFPE) tissue, via sequential steps with interposed washing. Sections are subjected to antigen/epitope retrieval prior to staining as fixation generally generates methylene bridges which cross link proteins and can therefore mask the antigen of interest. Endogenous peroxidase activity is blocked using hydrogen peroxide to prevent non-specific staining. The section is subsequently incubated with optimally diluted primary antibody, followed by incubation with a biotinylated HRP-conjugated secondary antibody. Sections are further incubated with the substrate/chromogen, 3-3'-diaminobenzidine (DAB), whereby reaction with the peroxidase produces a visible brown precipitate at the site of the antigen. Sections are then counterstained with haematoxylin and mounted. Results are then interpreted using a light microscope and can aid in the differential diagnosis of pathophysiological processes, which may/may not be associated with a particular antigen.

2.9.2 Method

Paired primary and recurrent glioblastoma patient samples were provided by the Brain Archive and Information Network UK (BRAIN UK) with ethical approval by the South West Research Ethics committee (REC number: 14/SC/0098; BRAIN UK reference: 17/002).

FFPE tissue sections were cut (4 µm) by the Department of Cellular and Anatomical Pathology at University Hospitals Plymouth. For each antibody staining, 10 biological repeats were cut for paired primary and recurrent grade IV glioblastoma. Optimisation

of primary antibody was performed on tonsil sections. Staining of DLL4, JAG1, KI67, CD133 and Nestin was performed by the Department of Cellular and Anatomical Pathology ay University Hospitals Plymouth. To eliminate the possibility of false positive immunostaining due to nonspecific binding of secondary antibody, negative controls were completed in parallel on tonsil and normal brain by omission of primary antibody. Tonsil sections were also used as a positive control and routinely stained during each antibody run (data not shown).

FFPE sections (4 μm) were de-paraffinised in Xylene (Sigma Aldrich) twice for 5 minutes each, followed by a further two washes in 100% ethanol for 5 minutes each. Slides were then washed in running tap water for 5 minutes. Endogenous peroxidases were blocked using a 3% hydrogen peroxide in methanol solution for 30 minutes. Slides were then washed in running tap water for 5 minutes. Antigen retrieval was performed by boiling samples in a microwave (900W) with either citrate buffer or EDTA buffer depending on the primary antibody for 30 minutes (Table 2.13). Slides were then washed in running tap water for 5 minutes.

A ring was drawn around the tissue samples using an ImmEdge pen (H-4000, Vector Laboratories) to create a hydrophobic barrier. In order to visualise the localisation of the primary antibody, one of two kits were utilised (either the Vector Laboratories VECTASTAIN Elite ABC HRP Kit or Leica Novolink Polymer Detection System) depending on the primary antibody (Table 2.13). Briefly, for the VECTASTAIN Elite ABC HRP kit (PK-6100, Vector Laboratories) sections were blocked with 1:100 normal horse serum in 0.05 M Tris-HCl for 30 minutes at RT. Slides were drained and primary antibody was applied at an optimised dilution in 0.05 M Tris-HCl and was left to incubate overnight in a moist, sealed chamber at RT. Slides were then washed twice in 0.05 M Tris-HCl by

Table 2.13: Primary antibodies used for Immunohistochemistry.

Primary Antibody	Host	Dilution	Company	Product Code	Antigen Retrieval Method	Detection Kit
CD133/1 (W6B3C1)	Mouse	1:100	Milteyni Biotech	130-092-395	EDTA	Novalink Polymer Detection System
Nestin (10C)	Mouse	1:2000	ThermoFisher Scientific	MA1-110	Citrate	VECTASTAIN Elite ABC HRP Kit
DLL4	Rabbit	1:3000	Abcam	Ab7280	Citrate	VECTASTAIN Elite ABC HRP Kit
JAG1 (28H8)	Rabbit	1:150	Cell Signalling Technology	#2620	EDTA	VECTASTAIN Elite ABC HRP Kit

immersion for 5 minutes each. For the secondary antibody, 1:50 normal horse serum was added to 0.05 M Tris-HCl followed by 1:50 Biotinylated Universal Antibody (200 µl per slide) and applied and incubated at for 30 minutes. Slides were then washed in 0.05 M Tris-HCl twice by immersion for 5 minutes each. Next the Streptavidin/Biotin Complex (ABC) was made by adding 1:50 Reagent A and 1:50 Reagent B to 0.05 M Tris-HCl (200 µL per slide). This was made up no less than 30 minutes before use as it requires at least 30 minutes reaction time. ABC was added and incubated at RT for 30 minutes. Slides were once again washed in 0.05 M Tris-HCl twice by immersion for 5 minutes each. DAB visualisation medium was prepared by dissolving 1 DAB tablet (D4293, Sigma Aldrich) in 5 mL deionised water, followed by the addition of 1 urea tablet and filtered with Whatman No.1 filter paper (1001-055, GE Healthcare) before use. Slides were then treated with DAB visualisation medium for 5 minutes at RT.

The Novolink Polymer detection system utilised as novel controlled polymerisation technology in order to prepare HRP-linker antibody conjugates. Therefore, the problem of non-specific staining which can occur with Streptavidin/Biotin detection systems due to endogenous biotin does not occur. For the Novolink Polymer detection system (RE7200-CE, Leica) primary antibody (Table 2.13) was added at an optimised dilution in 0.05M Tris-HCl overnight in a moist, sealed chamber at RT. Slides were washed twice in 0.05M Tris-HCl by immersion for 5 minutes each. The Post Primary Block was then applied and left for 30 minutes at RT. Slides were again washed twice in 0.05 M Tris-HCl by immersion for 5 minutes each. The Novolink Polymer was then applied to the slides and left to incubate for 30 minutes at RT. Slides were washed twice in 0.05 M Tris-HCl by immersion for 5 minutes each. Fifty microlitres of DAB

Chromogen was added to 1 mL Novolink DAB Substrate buffer and applied to the slides for 5 minutes.

Following visualisation in DAB, slides were washed in running tap water for 5 minutes. Slides were then immersed in a copper sulphate solution (DAB enhancer) to enhance the DAB reaction product for 5 minutes, followed by briefly washing in running tap water. Nuclei were then lightly counterstained in Mayers' haematoxylin solution (MHS1, Sigma Aldrich) for 1-2 minutes, then washed in tap water and briefly incubated in Scott's tap water substitute (consisting of 10 g magnesium sulphate and 0.67 g sodium bicarbonate dissolved in 1 L deionised water) before being briefly washed in running tap water. Slides were finally dehydrated by submerging the slides in 100% alcohol twice, and once briefly in xylene to remove the wax from the ImmEdge pen. Slides were finally mounted, and coverslip added using DPX mounting media (06522, Sigma Aldrich).

Images were acquired using a Leica DMRB and the intensity of staining was assessed semi-quantitatively with the help of consultant neuropathologist, Dr David Hilton (Department of Cellular and Anatomical Pathology at University Hospitals Plymouth).

2.10 Statistical Analysis

All data were presented as mean ± standard deviation (SD) or standard error of the mean (SEM) and analysed using GraphPad Prism (version 6.01, GraphPad Software Inc., San Diego, USA). Unpaired t-test was used to compare the means of two groups where the populations follow a normal distribution and it is assumed the variance is the same for the two populations. For multiple comparisons a one-way analysis of variance (ANOVA) was used to compare the means of three or more groups. This statistical test was used in conjunction with Tukey's multiple comparison post-hoc test,

which compares every mean with every other mean, or Dunnett's post-hoc test which compares every mean with a control. Both tests enable for any unequal sample sizes and accounts for the scatter of the groups. A two-way ANOVA was used to analyse data with two grouping variables (e.g. cell line and treatment), this was used again in conjunction with Tukey's multiple comparison post-hoc test, Dunnett's post-hoc test, or Sidak's post-hoc test to correct for multiple comparisons. For IC50 analysis, non-linear regression analysis was performed to fit a dose-response curve to determine LogIC50 and IC50 values for given treatments. In all cases a confidence interval of 95% was used and a *p* value of < 0.05 was regarded as statistically significant. Statistical significance was indicated by asterisks (* $p < 0.05$, ** $p < 0.01$, *** $p < 0.001$, and **** $p < 0.0001$).

Chapter 3

3 DLL4 and JAG1 Increase Glioblastoma Resistance to Temozolomide Chemotherapy by Induction of Notch Signalling

3.1 Introduction

Although it is the most common primary malignant brain tumour in adults, limited progress has been made in glioblastoma treatment, with many clinicians considering the disease incurable. The current standard of care involves maximal safe resection of the tumour followed by radiotherapy and concomitant and adjuvant TMZ chemotherapy (9). Despite advances in our understanding of glioblastoma from glioma pathogenesis to its molecular classification, translational breakthroughs in improving patient overall survival have been few and far between.

More than a decade since the addition of TMZ to the standard of care for glioblastoma, it is still the only effective chemotherapeutic agent to confer a consistent, modest improvement in patient OS. Upon tumour recurrence, it has been shown there is minimal consensus for second-line therapy with agents such as procarbazine, lomustine, carboplatin, and bevacizumab which have a limited effect on improving patient OS (322). Some clinicians even re-challenge tumours with TMZ in order to overcome acquired TMZ resistance, however this has shown varying degrees of success (323).

Glioblastoma patients who initially respond to TMZ treatment will inevitably experience tumour relapse during treatment or after its cessation. When tumour response to treatment reaches a plateau due to chemoresistance, understanding the mechanisms of this is critically important to overcome this major clinical challenge. Due to the limited therapeutic options for patients with recurrent glioblastoma,

research is now significantly focussed on dissecting mechanisms of TMZ chemoresistance. Many studies have solely focused on the role of DNA repair in TMZ resistance. However, our current understanding of this topic has advanced significantly beyond genetic mechanisms with numerous discoveries made in epigenetics, transcriptomics, and proteomics.

3.1.1 Mechanisms of Temozolomide Resistance

As previously discussed in Chapter 1 (1.1.6.1), TMZ, an imidazole derivative, is a second-generation alkylating chemotherapy agent. TMZ is a prodrug which undergoes spontaneous hydrolysis and is converted to its active metabolite MITC. TMZ is efficiently absorbed following oral administration, has schedule dependent anti-tumour activity, and readily crosses the blood brain barrier (81). Conversion of TMZ to MITC results in the formation of a highly reactive methyldiazonium cation which readily methylates the O^6 position of guanine. Formation of O^6-methylguanine initiates a sequence of DNA MMR events leading to cellular apoptosis (74, 324).

Direct repair by MGMT is believed to be the main mechanism of resistance in glioblastoma. MGMT is enzyme ubiquitously expressed in the nucleus where it removes an alkyl group from O^6-MeG. Hypermethylation of the *MGMT* promoter, which has been detected in approximately 40-68% of patient tumours, results in a significant reduction of MGMT activity in glioblastoma by preventing its transcription, and thus patients are more responsive to treatment (41). Previous clinical trials have shown tumour response to TMZ is significantly ameliorated when expression of MGMT is low due to promoter methylation (41, 42).

Chemoresistance has been shown to be mediated my multiple molecular events that are independent of MGMT expression. TMZ resistance mechanisms in glioblastoma

can be broadly classified into epigenetic, cellular, and tumour microenvironmental-related mechanisms (Figure 3.1). Epigenetic mechanisms can be further categorised into processes associated with DNA repair (pre-transcriptional), microRNAs (post-translational), or histone modification (post-translational). Cellular mechanisms are largely related to transmembrane protein expression and therefore are intrinsic in nature, including growth factor receptor signalling and drug efflux protein expression. Conversely, the intrinsic activity of cellular apoptosis and autophagy pathways can be altered in response to exposure to TMZ. Whilst extracellular factors including microenvironmental mechanisms can influence TMZ sensitivity. Typical tumour microenvironmental factors include hypoxia-driven resistance and intercellular GCSC interactions (325). A more in-depth analysis of these mechanisms of resistance are discussed previously in Chapter 1 Introduction (1.1.6.2).

As glioblastomas show significant heterogeneity between patients, identifying key proteins involved in TMZ resistance provides an important basis for biomarker identification and individualised treatment according to multiple resistance mechanisms.

3.1.2 Notch in Glioblastoma

Notch signalling regulates a number of processes during embryonic and adult development, including NSC biology (326). Deregulation of the Notch pathway has been associated with the development of several diseases through both germline and somatic mutations. Of the latter, mutations in components of Notch signalling lead to cancer and malignancy, of which the best-known example is T-ALL (205, 236). Over the years, the role of aberrant Notch signalling in oncogenesis has been well documented

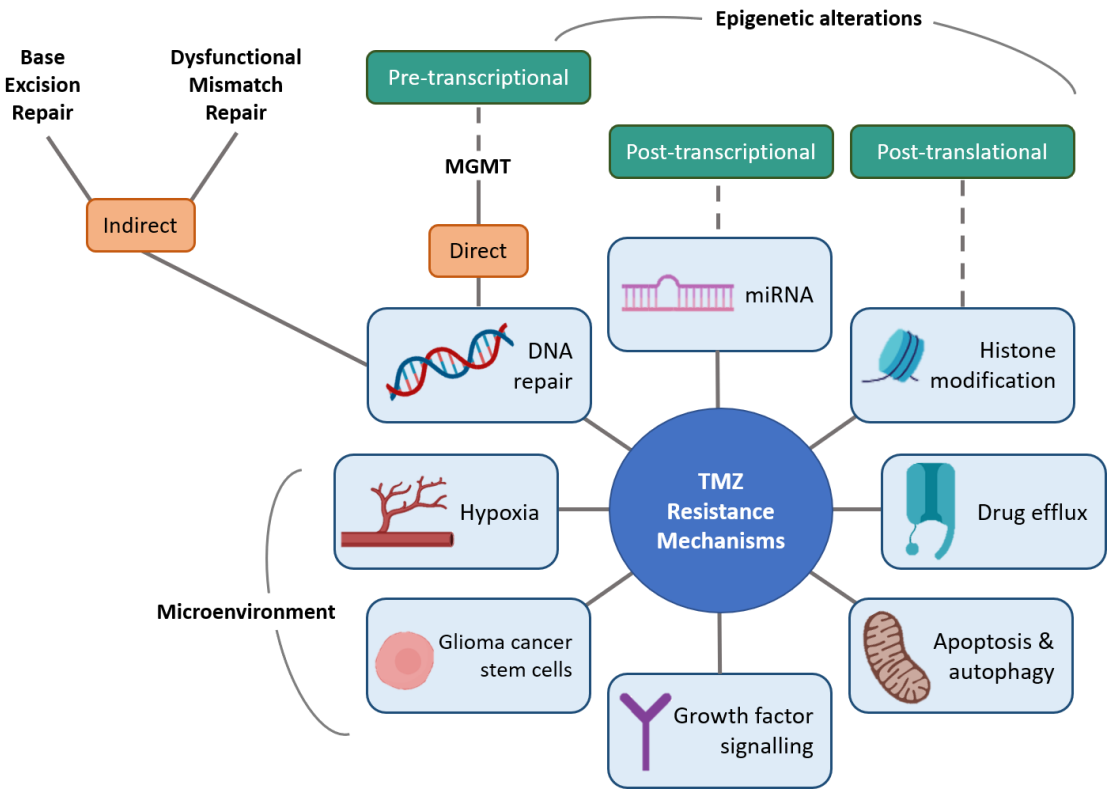

Figure 3.1: Mechanisms of resistance to TMZ chemotherapy in glioblastoma.

Resistance mechanisms can be broadly classified into epigenetic, cellular, and microenvironmental-related mechanisms. Epigenetic mechanisms can be further divided into processes associated with DNA repair (pre-transcriptional), microRNAs (post-translational), or histone modifications (post-translational). Cellular mechanisms include active TMZ efflux by ATP-binding cassette transporters, alterations in apoptosis-autophagy processes, and the activation of receptor tyrosine kinase growth factor signalling such as EGFR and IGFR. Microenvironmental adaptations include overexpression of hypoxia-inducible factor-1 in response to rapid tumour growth promoting cell survival, and the presence of glioma cancer stem cells that are intrinsically resistant to TMZ treatment and promote tumour recurrence. MGMT: O6-methylguanine-DNA methyltransferase; miRNA: microRNA. Diagram adapted from (325).

in numerous solid tumours outside the brain as well as in glioblastoma, although its components are rarely mutated (327).

Several studies have reported abnormal expression of various components of the Notch signalling pathway in brain tumours. For example, increased expression in mRNA and protein levels of Notch1, Notch4, DLL1, DLL4, JAG1, RBPJ, Hey1, Hey2, and Hes1 are increased in brain tumour cells compared to normal brain (238-240). Increased expression of Notch pathway components is correlated with a higher glioma grade and a worse prognosis for patients (238). This therefore indicates that increased activation of Notch signalling promotes a more undifferentiated and aggressive tumour phenotype.

Notch pathway activation is considered to be a key characteristic of glioblastoma pathogenesis. A number of studies have shown increased Notch pathway activation in primary glioblastoma compared with low-grade gliomas (243), secondary glioblastomas (244), and normal brain tissue (238-240). Increased Notch signalling is associated with a number of the so-called "hallmarks of cancer" defied by Hanahan *et al*. including self-sufficiency in growth signals, insensitivity to anti-growth signals, evasion of apoptosis, limitless replicative potential, sustained angiogenesis, and tissue invasion and metastasis (328). Given its role in tumour biology, *in vitro* Notch pathway modulation has been studied by knockdown and pharmacological targeting with a range of inhibitors including GSIs, other small molecule inhibitors, as well as target monoclonal antibodies (245, 246). These studies have shown that inhibition of Notch signalling can successfully reverse many of these hallmarks of cancer.

Both DLL4 and JAG1 are two key Notch ligands which have been previously implicated in tumour angiogenesis. In glioblastoma, both ligands are upregulated, however their

relative effects and interactions in tumour biology, particularly in tumour response to therapeutic intervention remains unclear. Oon *et al*. have recently shown both DLL4 and JAG1 promote tumour growth by modulating angiogenesis, and both mediate tumour resistance to anti-VEGF therapy with bevacizumab (306). In glioblastoma, DLL4 expression in endothelial cells correlates with peritumoural brain oedema and poor prognosis (307, 308). Similarly, JAG1 expression in tumour and endothelial cells is associated with reduced time to progression and OS in primary glioblastoma patients (309). There is growing evidence to suggest Notch signalling regulates the self-renewal of GCSCs in glioblastoma (303, 310), and GCSCs are generally believed to mediate tumour recurrence and resistance to treatment (197). However, whether DLL4 and/or JAG1 are involved in the regulation of GCSCs, tumour recurrence, or TMZ chemoresistance remains to be elucidated.

This chapter looks at the roles DLL4 and JAG1 play on glioblastoma resistance to TMZ chemotherapy, and if this can be overcome by inhibition of DLL4- and JAG1- induced Notch signalling.

3.2 Methods

The methods employed in this chapter involve the general culture of two glioblastoma cell lines (U87 and U251; Methods 2.2). Both these cell lines were transduced with mDLL4 and mJAG1 encoded retroviruses as described in Methods 2.4. Validation of DLL4 and JAG1 overexpression alongside analysis of Notch signalling target expression was confirmed by qPCR (Methods 2.6), Western Blotting (Methods 2.7), and IF analysis (Methods 2.8.1).

The TMZ IC50 for both U87 and U251 cell lines overexpressing DLL4 and JAG1 was performed at three timepoints: 72 h, 96 h, and 120 h post-TMZ treatment as described in Methods 2.3.1. The effect of 25 nM DBZ pre-treatment on TMZ IC50 was also assessed.

Both U87 and U251 cell lines were cultured in 2D and growth response to single 25 nM DBZ/25 µM TMZ and combination 25 nM DBZ and 25 µM TMZ treatment was determined by both MTT assay (Methods 2.3) and Ki67 IF staining (Methods 2.8.1).

Spheroids were generated for each cell line (Methods 2.2.6) and response to single 25 nM DBZ/25 µM TMZ and combination 25 nM DBZ and 25 µM TMZ treatment was determined by 3D spheroid growth. The TMZ IC50 for both U87 and U251 spheroids overexpressing DLL4 and JAG1 was performed at three timepoints: day 4, day 7, and day 10 post-TMZ treatment as described in Methods 2.2.6. The effect of 25 nM DBZ pre-treatment on spheroid TMZ IC50 was also assessed.

Tables listing primers (Table 3.1) and antibodies (Table 3.2) used in this chapter are given below.

All data were presented as mean ± SD (unless otherwise stated) and analysed using GraphPad Prism (version 6.01, GraphPad Software Inc., San Diego, USA). The statistical test employed are described in the figure legend of each experiment.

Table 3.1: List of primers used in Chapter 3

Gene		**Primer Sequence (5' →3')**	**Product size (bp)**
mDLL4	Forward	AGGTGCCACTTCGGTTACAC	62
	Reverse	GGGAGAGCAAATGGCTGATA	
mJAG1	Forward	TCTCTGACCCCTGCCATAAC	169
	Reverse	TTGAATCCATTCACCAGATCC	
HES1	Forward	AGTGAAGCACCTCCGGAAC	107
	Reverse	CGTTCATGCACTCGCTGA	
HEY1	Forward	CGAGCTGGACGAGACCAT	76
	Reverse	GGAACCTAGAGCCGAACTCA	
HEY2	Forward	GTACCATCCAGCAGTGCATC	65
	Reverse	AGAGAATTCAGTCAGGGCATTT	
GAPDH	Forward	GACCCCTTCATTGACCTCAAC	134
	Reverse	TGGACTGTGGTCATGAGTCC	

Table 3.2: List of primary and secondary antibodies used for Western Blotting and Immunofluorescence in Chapter 3

Primary Antibodies						
Name	**Species**	**Molecular Weight (kDa)**	**Supplier**	**Product Code**	**Western Blot dilution**	**IF dilution**
Anti-β-tubulin	Mouse	51	ThermoFisher Scientific	MA5-16308	1:2000	N/A
Anti-Cleaved Notch-1 (NICD)	Rabbit	120	Cell Signalling Technology	4147	1:1000	N/A
Anti-DLL4	Rabbit	74	Abcam	AB7280	1:1000	1:1000
Anti-GAPDH (GA1R)	Mouse	37	ThermoFisher Scientific	MA5-15738	1:2000	N/A
Anti-HES1	Rabbit	30	Cell Signalling Technology	11988	1:1000	N/A
Anti-JAG1 (28H8)	Rabbit	180	Cell Signalling Technology	2620	1:1000	1:1000
Anti-Ki67	Rabbit	319	Abcam	AB15580	N/A	1:2000

Secondary Antibodies					
Name	**Species**	**Supplier**	**Product Code**	**Western blot dilution**	**IF dilution**
Anti-rabbit IgG HRP conjugate	Goat	ThermoFisher Scientific	65-6120	1:5000	N/A
Anti-mouse IgG HRP conjugate	Goat	ThermoFisher Scientific	31430	1:5000	N/A
Anti-rabbit IgG Alexa Fluor 647	Goat	ThermoFisher Scientific	A21245	N/A	1:1000

3.3 Results

3.3.1 DLL4 and JAG1 induce Notch Signalling in Glioblastoma Cell Lines

3.3.1.1 Characterisation of U87 Cell Line

The U87 glioblastoma cell lines over-expressing mDLL4 (U87-mDLL4), mJAG1 (U87-mJAG1) and empty vector control (U87-EV) were previously established by Professor Ji-Liang Li (University of Plymouth) by retroviral transduction. These cells were initially characterised to ensure successful transduction and ligand expression by qPCR, Western blot, and IF. mDLL4 and mJAG1 gene expression was significantly increased in the overexpression cells by qPCR compared to U87-EV control (Figure 3.2A). Both Western blotting (Figure 3.2C) and IF (Figure 3.3) revealed DLL4 and JAG1 are abundantly overexpressed in U87-mDLL4 and U87-mJAG1 cells, respectively, compared to U87-EV. The DLL4 antibody utilised for IF corresponded to an extracellular region (amino acids 121 to 134) of DLL4, whilst the JAG1 antibody binds to residues surrounding the Glu1140 intracellular region of human JAG1. However, IF analysis shows DLL4 and JAG1 both display predominantly cytoplasmic expression (Figure 3.3).

3.3.1.2 Characterisation of U251 Cell Line

The U251 cell line was transduced with empty vector control-, mDLL4- and mJAG1-encoded retroviruses. The cell line was initially characterised to ensure successful transduction and ligand expression of DLL4 and JAG1 by qPCR, Western blot, and IF. *mDLL4* and *mJAG1* gene expression was increased significantly in U251-mDLL4 and U251-mJAG1, respectively (Figure 3.2B). In addition, both Western blotting (Figure 3.2C) and IF (Figure 3.4) revealed DLL4 and JAG1 protein expression is significantly increased in U251-mDLL4 and U251-mJAG1, respectively, compared to U251-EV. IF analysis shows both DLL4 and JAG1 display cytoplasmic expression in U251 cells.

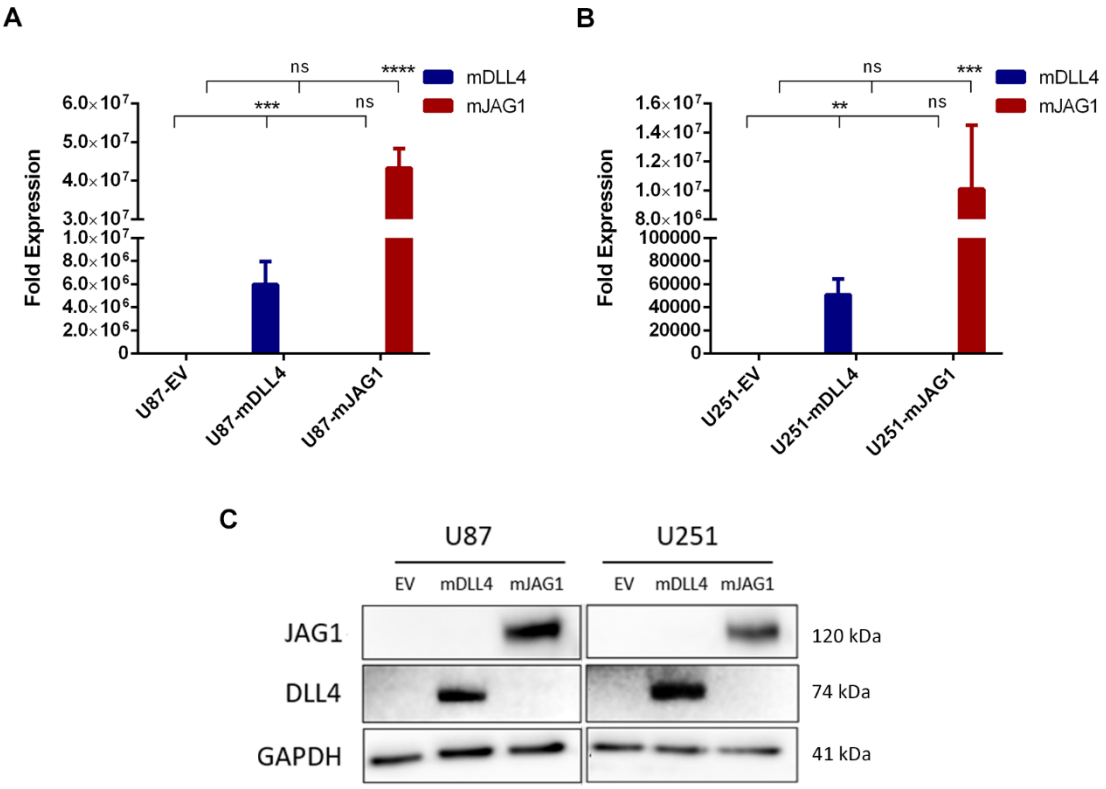

Figure 3.2: Expression of DLL4 and JAG1 in U87 and U251 cells transduced with mDLL4 and mJAG1.

U87 and U251 cell lines overexpressing DLL4, JAG1, and EV control were established by retroviral transduction. RNA was extracted and mRNA expression of m*DLL4* and m*JAG1* in **(A)** U87 and **(B)** U251 cell lines was determined by qPCR normalised to *GAPDH*. **(C)** Protein expression of DLL4 and JAG1 in U87 and U251 cell lines confirmed successful retroviral transduction. Protein was extracted from cells and separated (20 µg) by SDS-PAGE (10% SDS gel). Membranes were probed with rabbit anti-DLL4 (1:1000; Abcam #AB7280), rabbit anti-JAG1 (1:1000; Cell Signalling Technology #2626), and mouse anti-GAPDH (1:2000; ThermoFisher Scientific #MA5-15738) in 5% milk in PBS-T overnight at 4 °C. Membranes were washed and probed with anti-rabbit IgG HRP conjugate (1:5000, ThermoFisher Scientific #65-6120) and anti-mouse IgG HRP conjugate (1:5000; ThermoFisher Scientific #31430) secondary antibodies in 5% milk in PBS-T at RT for 1 h. ECL. (Mean ± SD, n = 3, two-way ANOVA with Dunnett's post-hoc test, ** $p < 0.01$, *** $p < 0.001$, **** $p < 0.0001$, and ns denotes not significant).

`

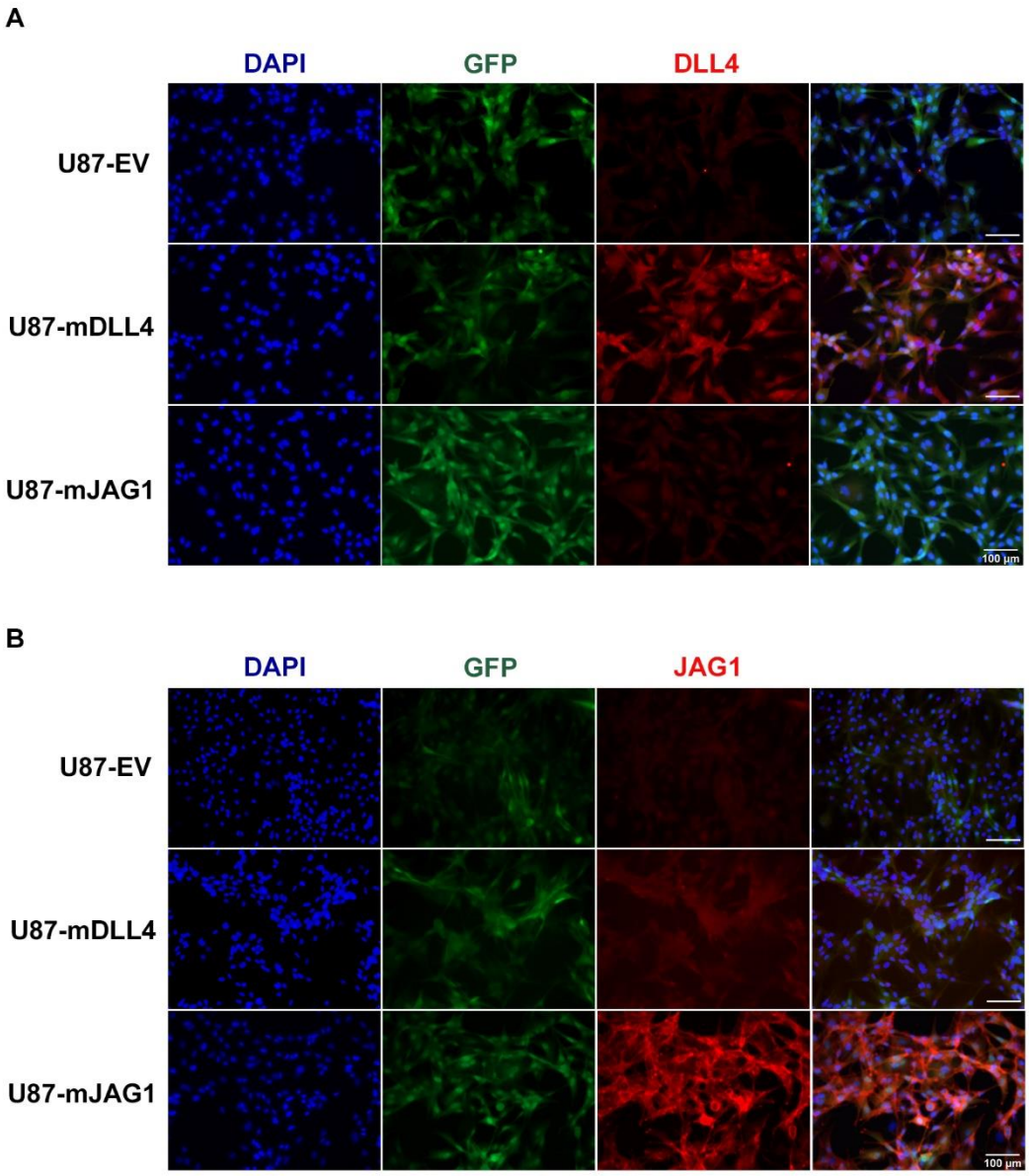

Figure 3.3: DLL4 and JAG1 expression in U87 cells following mDLL4 and mJAG1 retroviral transduction.

Representative Immunofluorescence staining of **(A)** DLL4 and **(B)** JAG1 in U87 cells. Cells were seeded in 96-well plates at 2000 cells per well and grown for 48 h. Cells were fixed in 4% PFA and immunostained for rabbit anti-DLL4 (1:1000; Abcam #AB7280) and rabbit anti-JAG1 (1:1000; Cell Signalling Technology #2626) followed by goat anti-rabbit IgG Alexa Fluor 647 (1:1000; ThermoFisher Scientific #A21245) and counterstaining with 2 µg/mL DAPI. Images were taken at 20X magnification. Scale bar = 100 µm.

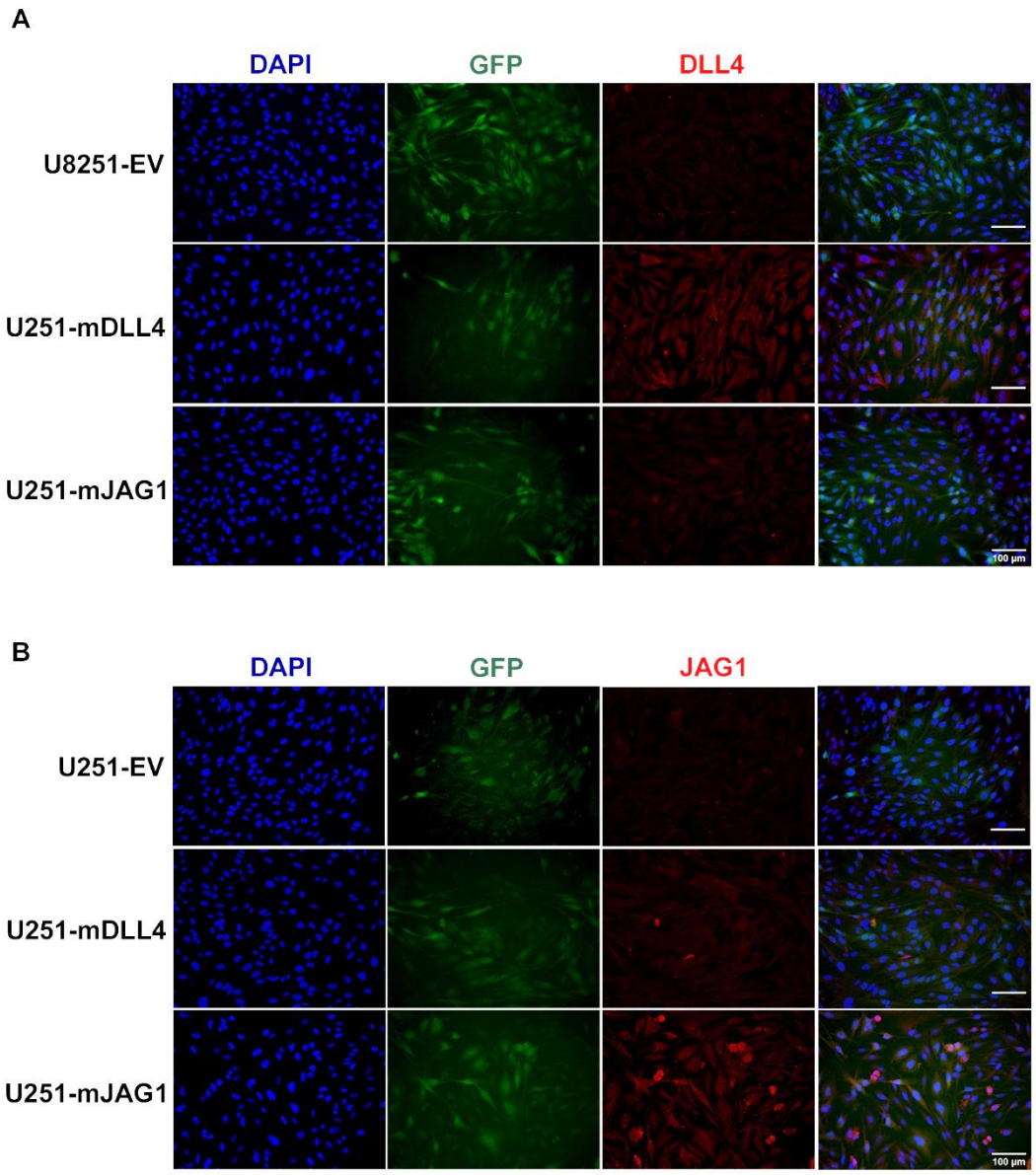

Figure 3.4: DLL4 and JAG1 expression in U251 cells following mDLL4 and mJAG1 retroviral transduction.

Representative Immunofluorescence staining of **(A)** DLL4 and **(B)** JAG1 in U251 cells. Cells were seeded in 96-well plates at 2000 cells per well and grown for 48 h. Cells were fixed in 4% PFA and immunostained for rabbit anti-DLL4 (1:1000; Abcam #AB7280) and rabbit anti-JAG1 (1:1000; Cell Signalling Technology #2626) followed by goat anti-rabbit IgG Alexa Fluor 647 (1:1000; ThermoFisher Scientific #A21245) and counterstaining with 2 µg/mL DAPI. Images were taken at 20X magnification. Scale bar = 100 µm.

3.3.1.3 *Induction of Notch Signalling in U87 and U251 Cells Following DLL4 and JAG1 Overexpression*

Analysis was performed to assess the ability of the DLL4 and JAG1 ligands to activate Notch signalling by binding to Notch receptors of neighbouring cells in both the U87 and U251 cell line. qPCR analysis showed U87 cells expressing mDLL4 and mJAG1 upregulated the expression of the Notch downstream target genes *HES1, HEY1* and *HEY2* (Figure 3.5A). Protein expression of cleaved activated Notch1 (NICD) and Hes1 was also increased following DLL4 and JAG1 overexpression in the U87 cell line as detected by Western blot analysis (Figure 3.5C).

Similarly, qPCR analysing showed mDLL4 and mJAG1 overexpression in the U251 cell line increased the mRNA expression of the Notch downstream target genes *HES1*, *HEY1* and *HEY2* (Figure 3.5B). Alongside increased protein expression of NICD and Hes1 (Figure 3.5C).

3.3.2 Increased Glioblastoma Resistance to Temozolomide by DLL4 and JAG1 in 2D Culture

We initially determined the IC50 for TMZ in the U87 and U251 cell lines at three separate time points: 72 h, 96 h and 120 h post-TMZ treatment. Cells were treated with TMZ concentrations ranging from 0 to 2 mM, and at the experimental endpoints, cell viability was determined using the MTT assay. Cell viability was calculated as a percentage of matched untreated control and the IC50 determined by non-linear regression analysis.

3.3.2.1 *U87 Cell Line*

Seventy-two h post-treatment, the TMZ IC50 for U87-mDLL4 and U87-mJAG1 was significantly higher compared to U87-EV control (1267.7 µM ± 171.4 µM and 927.5 µM

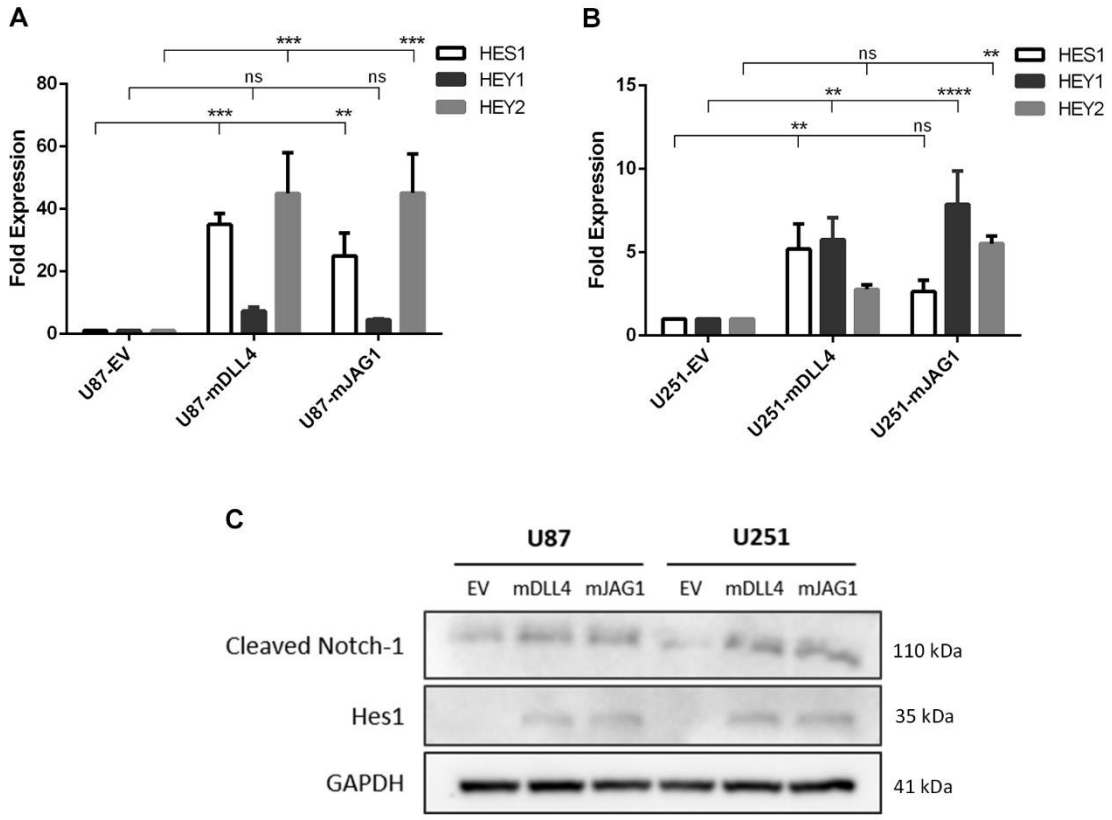

Figure 3.5: DLL4 and JAG1 induce Notch signalling in the U87 and U251 glioblastoma cell lines.

U87 and U251 cell lines overexpressing DLL4, JAG1, and EV control were established by retroviral transduction. RNA was extracted and mRNA expression of the Notch target genes *HES1*, *HEY1*, and *HEY2* in **(A)** U87 and **(B)** U251 cell lines was determined by qPCR normalised to *GAPDH*. **(C)** Protein expression of cleaved Notch1 and Hes1 in U87 and U251 cell lines confirmed successful induction of Notch signalling. Protein was extracted from cells and separated (20 µg) by SDS-PAGE (10% SDS gel). Membranes were probed with rabbit anti-cleaved Notch1 (1:1000), rabbit anti-Hes1 (1:1000; Cell Signalling Technology #11988), and mouse anti-GAPDH (1:2000; ThermoFisher Scientific #MA5-15738) in 5% milk in PBS-T overnight at 4 ^{o}C. Membranes were washed and probed with anti-rabbit IgG HRP conjugate (1:5000, ThermoFisher Scientific #65-6120) and anti-mouse IgG HRP conjugate (1:5000; ThermoFisher Scientific #31430) secondary antibodies in 5% milk in PBS-T at RT for 1 h. ECL. (Mean ± SD, n = 3, two-way ANOVA with Dunnett's post-hoc test, ** $p < 0.01$, *** $p < 0.001$, **** $p < 0.0001$, and ns denotes not significant).

± 22.1 µM respectively, vs 663 µM ± 32.6 µM, Figure 3.6A-B). Again at 96 h post-treatment, the TMZ IC50 was significantly increased for U87-mDLL4 and U87-mJAG1 (968.7 µM ± 100.5 µM, and 729.4 µM ± 35.4 µM, respectively) compared to U87-EV (644.4 µM ± 50.7 µM; Figure 3.6C-D). Finally, at 120 h post-treatment the TMZ IC50 for U87-mDLL4 and U87-mJAG1 were both significantly higher than U87-EV (952.2 µM ± 91.3 µM and 762.0 µM ± 10.9 µM respectively, vs 493.4 µM ± 28.4 µM, Figure 3.6E-F).

3.3.2.2 U251 Cell Line

In the U251 cell line, following 72 h TMZ treatment the TMZ IC50 is significantly increased in U251-mDLL4 and U251-mJAG1 compared to U251-EV control (2320.0µM ± 18.4µM and 2114.0µM ± 86.3µM respectively, vs 1509µM ± 145.6µM, Figure 3.7A-B). Again at 96 h post-treatment, the TMZ IC50 was significantly increased for U251-mDLL4 and U251-mJAG1 (1206 µM ± 84.6 µM, and 958.3 µM ± 70.17 µM, respectively) compared to U87-EV (751.1 µM ± 41.9 µM; Figure 3.7C-D). Finally, at 120 h post-treatment the TMZ IC50 for U251-mDLL4 and U251-mJAG1 were both significantly higher than U251-EV control (1026.6 µM ± 79.1 µM, and 807.2 µM ± 70.6 µM respectively, vs 568.1 µM ± 44.4 µM, Figure 3.7E-F).

Taken together, the results for the U87 and U251 cell line suggests induction of Notch signalling by DLL4 and JAG1 confers resistance to TMZ in glioblastoma cell lines.

3.3.3 Glioblastoma Resistance to Temozolomide by DLL4 and JAG1 is Reversed by Notch Inhibition by Dibenzazepine

DBZ is a GSI which has previously been shown to effectively inhibit activation of Notch signalling by preventing the release of the NICD by γ-secretase (246).

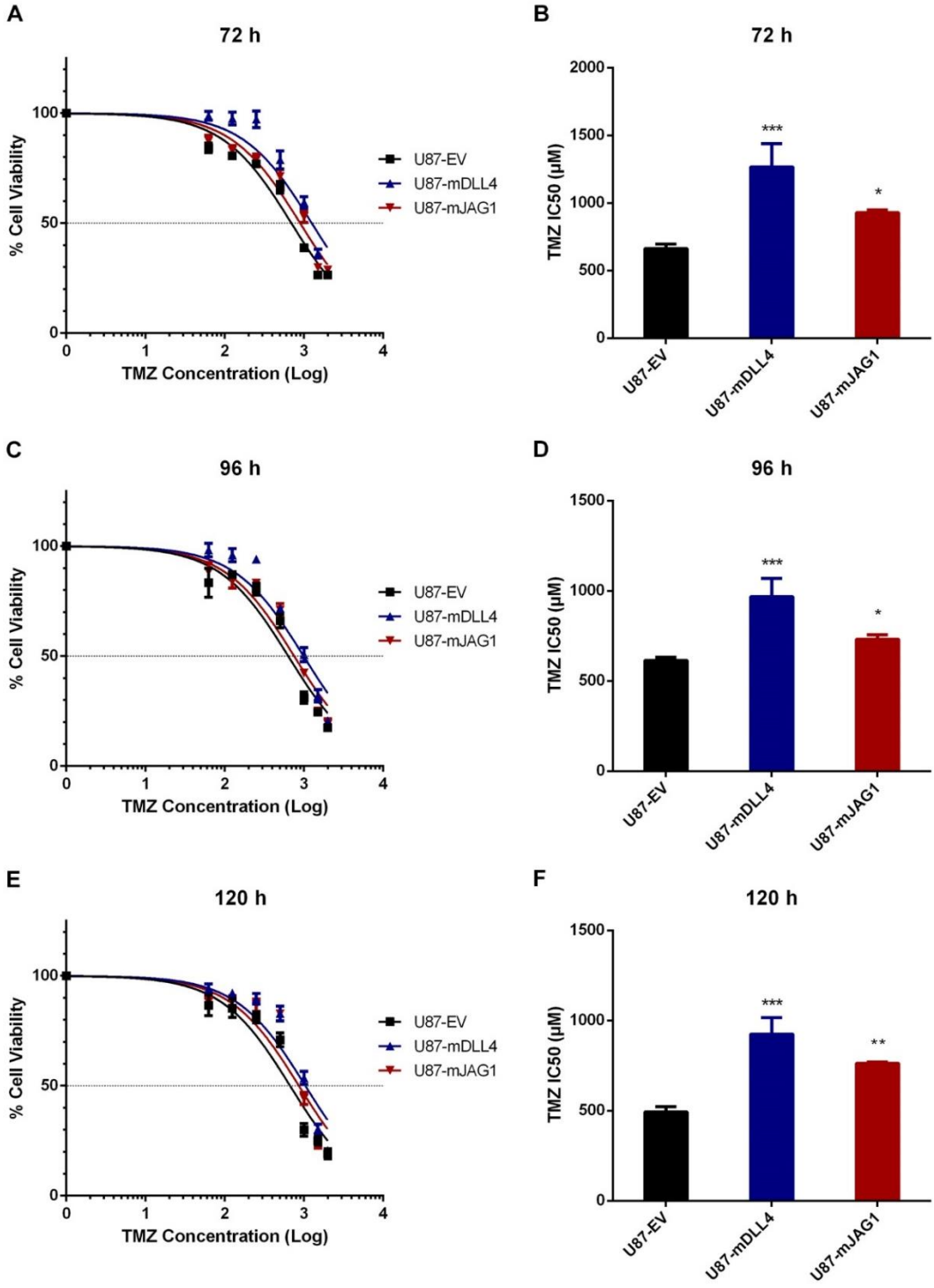

Figure 3.6: DLL4 and JAG1 confer U87 glioblastoma resistance to TMZ.

U87 cells were seeded at 4000 cells per well and 24 h later, subjected to 0 to 2 mM TMZ treatment. Cell viability was determined by MTT assay at 72, 96, and 120 h post-treatment. IC50 was assessed by non-linear regression analysis using GraphPad Prism. **(A)** Cell viability and **(B)** IC50 of U87 cells following 72 h TMZ treatment. **(C)** Cell viability and **(D)** IC50 of U87 cells following 96 h TMZ treatment. **(E)** Cell viability and **(F)** IC50 of U87 cells following 120 h TMZ treatment. (Mean ± SD, n = 3, ordinary one-way ANOVA with Dunnett's post-hoc test, * $p < 0.05$, ** $p < 0.01$, *** $p < 0.001$, and ns denotes not significant).

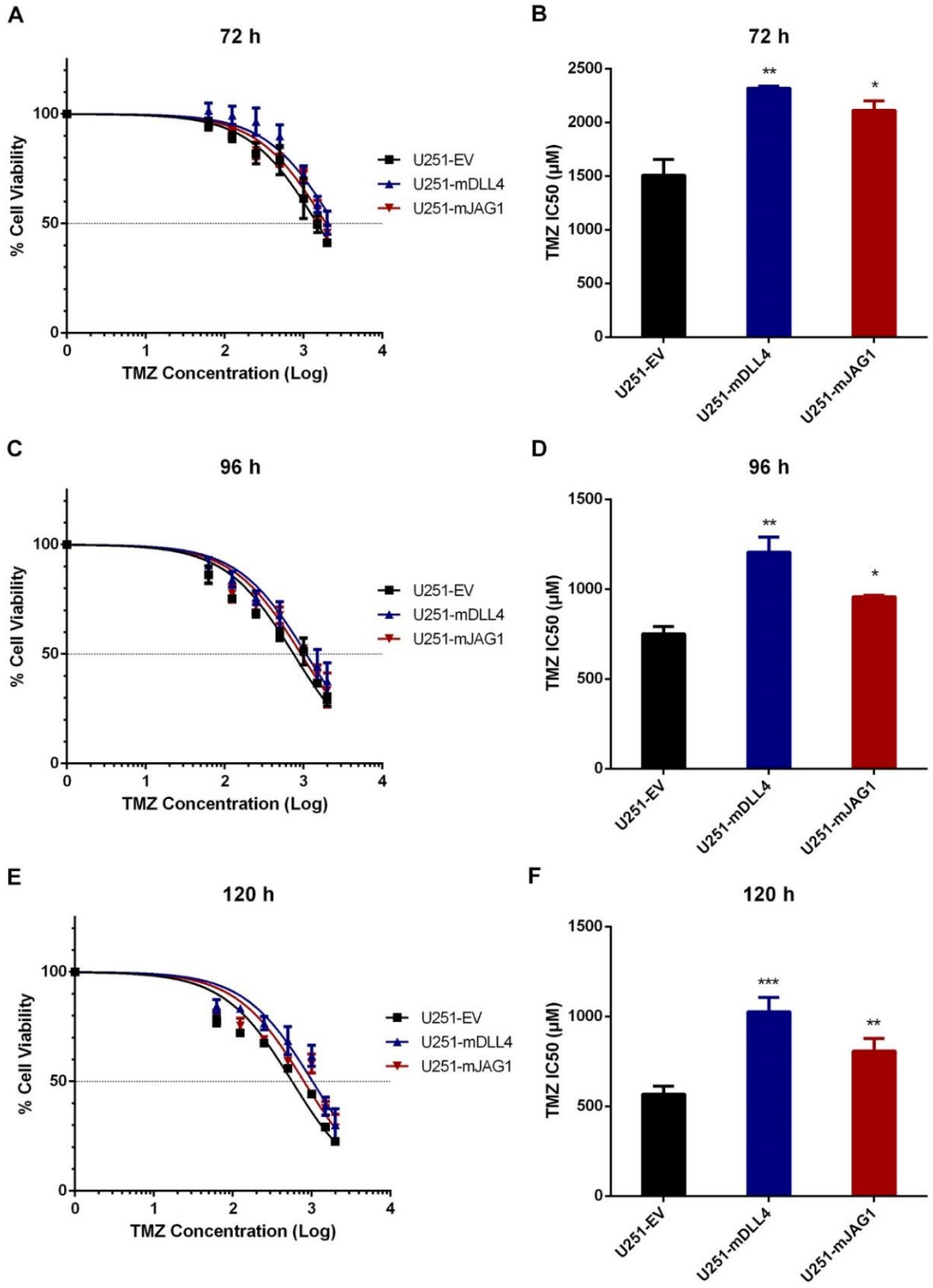

Figure 3.7: DLL4 and JAG1 confer U251 glioblastoma resistance to TMZ.

U251 cells were seeded at 2000 cells per well and 24 h later, subjected to 0 to 2 mM TMZ treatment. Cell viability was determined by MTT assay at 72, 96, and 120 h post-treatment. IC50 was assessed by non-linear regression analysis using GraphPad Prism. **(A)** Cell viability and **(B)** IC50 of U87 cells following 72 h TMZ treatment. **(C)** Cell viability and **(D)** IC50 of U87 cells following 96 h TMZ treatment. **(E)** Cell viability and **(F)** IC50 of U87 cells following 120 h TMZ treatment. (Mean ± SD, n = 3, ordinary one-way ANOVA with Dunnett's post-hoc test, * $p < 0.05$, ** $p < 0.01$, *** $p < 0.001$, and ns denotes not significant).

3.3.3.1 Dibenzazepine Reduces the Expression of Notch Downstream Target Genes

DBZ exhibits modest selectivity in blocking Notch intramembrane proteolysis. Previous studies have identified DBZ can be utilised to inhibit Notch signalling from concentrations ranging from < 2 nM to 50 nM (329, 330). We initially tested the concentration of DBZ required to effectively inhibit Notch signalling in the U87 and U251 cell lines overexpressing DLL4 and JAG1. U87 and U251 cells were treated with DMSO control (0 nM), 10 nM, 25 nM, and 50 nM DBZ.

In U87 cells, *HES1, HEY1*, and *HEY2* mRNA expression was most significantly reduced following 25 nM and 50 nM DBZ treatment (Figure 3.8A-C). Protein expression of Hes1 was also reduced following 25 nM and 50 nM DBZ treatment in U87-EV, U87-mDLL4 and U87-JAG1 cells compared to DMSO control (Figure 3.8D).

Similarly in U251 cells, 25nM and 50 nM DBZ significantly reduced *HES1, HEY1*, and *HEY2* mRNA expression compared to control (Figure 3.9A-C). Protein expression of Hes1 was also decreased following 25 nM and 50 nM DBZ treatment in U251-EV, U251-mDLL4 and U251-mJAG1 cells compared to DMSO control (Figure 3.9D). As a result, 25 nM DBZ was used for subsequent experiments whereby inhibition of Notch signalling was required.

3.3.3.2 Dibenzazepine Pre-treatment Reverses Glioblastoma Resistance to Temozolomide

As we have shown, DLL4 and JAG1 increase the TMZ IC50 in both the U87 and U251 glioblastoma cell lines. We next assessed if DBZ pre-treatment is able to reverse this increase in IC50. U87 and U251 cells were subjected to 24 h treatment with 25 nM DBZ before being treated with TMZ concentrations ranging from 0 to 2 mM. At the experimental endpoints (72 h, 96 h and 120 h post-TMZ treatment), cell viability was

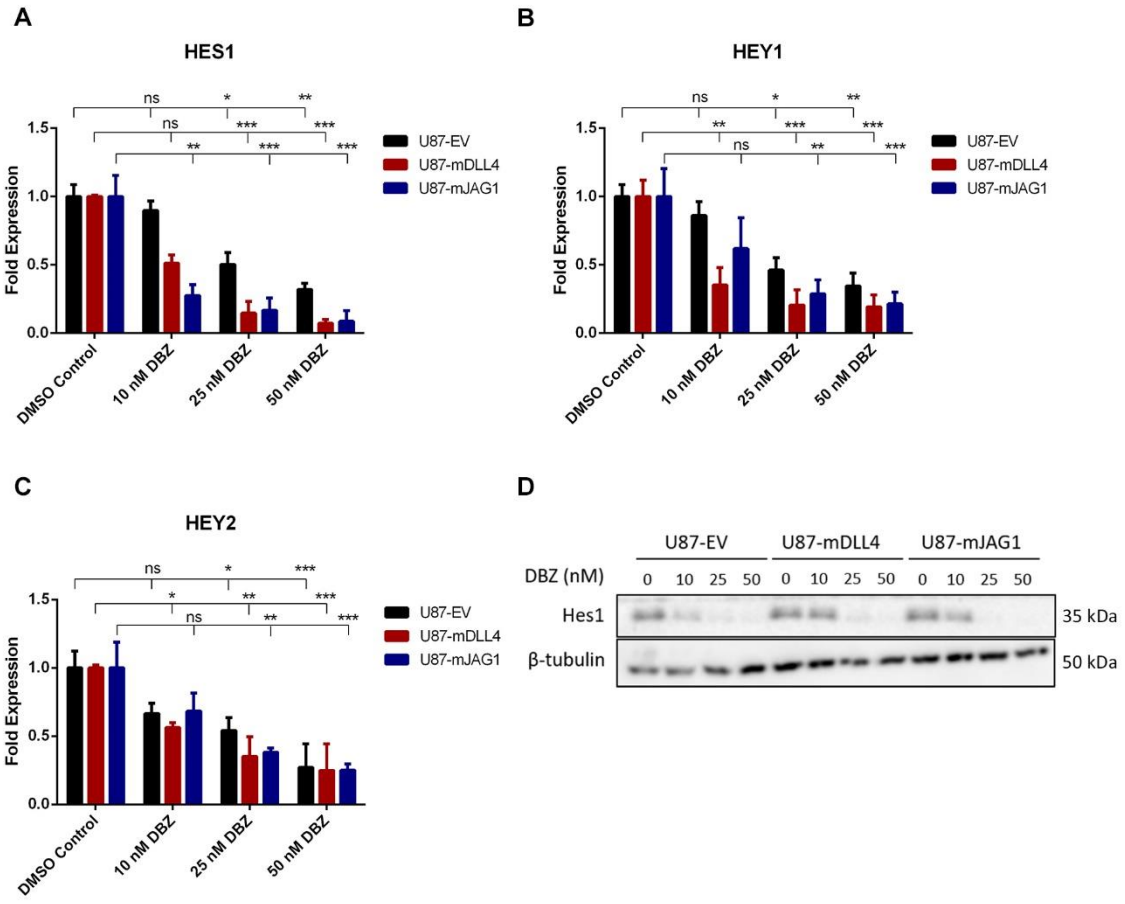

Figure 3.8: Expression of the Notch downstream target genes HES1, HEY1 and HEY2 in U87 cells following DBZ treatment.

U87 cells were treated with 0 to 50 nM DBZ and 48 h later collected for qPCR and Western Blotting analysis. RNA was extracted and mRNA expression of the Notch target genes **(A)** *HES1*, **(B)** *HEY1*, and **(C)** *HEY2* was determined by qPCR normalised to *GAPDH*. **(D)** Western blotting of Hes1 confirmed successful inhibition of Notch signalling following 25 and 50 nM DBZ treatment. Protein was extracted from cells and separated (20 µg) by SDS-PAGE (10% SDS gel). Membranes were probed with rabbit anti-Hes1 (1:1000; Cell Signalling Technology #11988) and mouse anti-β-tubulin (1:2000; ThermoFisher Scientific #MA5-16308) in 5% milk in PBS-T overnight at 4 ^{o}C. Membranes were washed and probed with anti-rabbit IgG HRP conjugate (1:5000, ThermoFisher Scientific #65-6120) and anti-mouse IgG HRP conjugate (1:5000; ThermoFisher Scientific #31430) secondary antibodies in 5% milk in PBS-T at RT for 1 h. ECL. (Mean ± SD, n = 3, two-way ANOVA with Dunnett's post-hoc test, * $p < 0.05$, ** $p < 0.01$, *** $p < 0.001$, and ns denotes not significant).

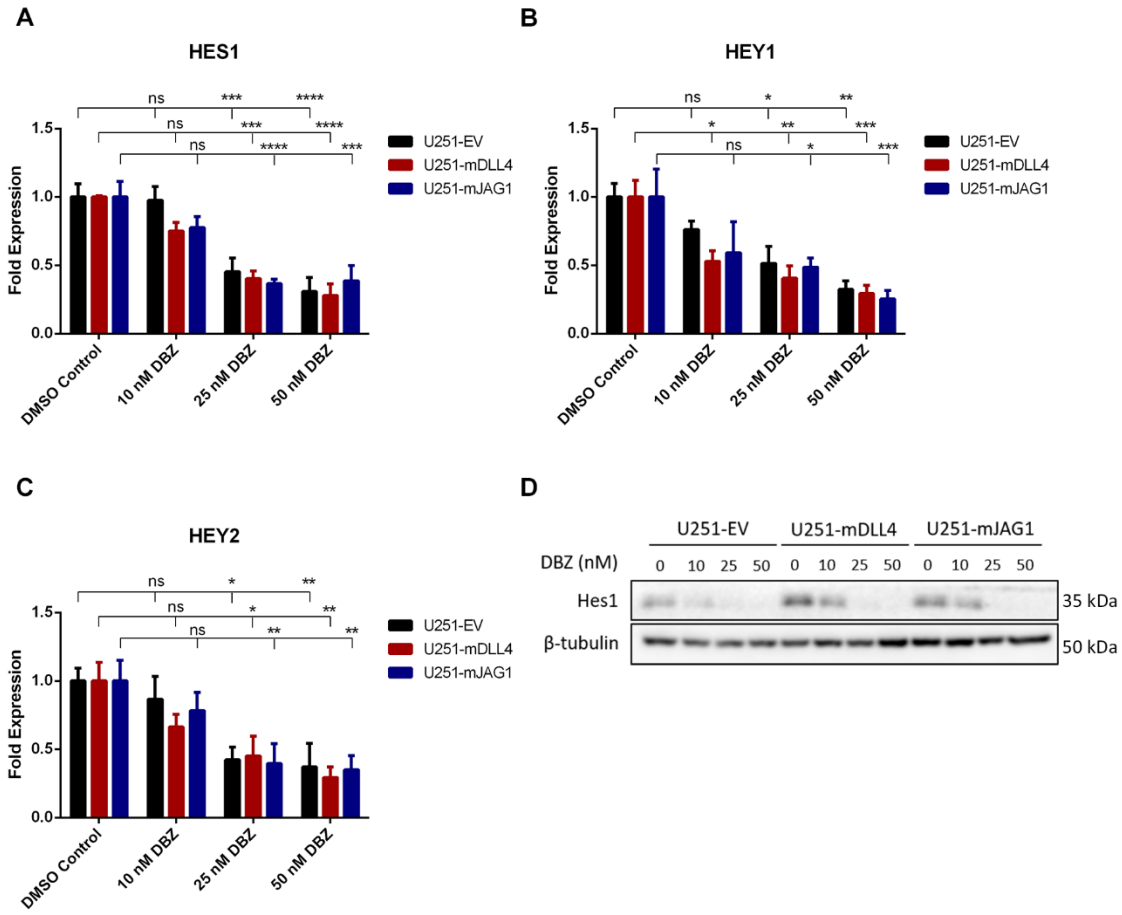

Figure 3.9: Expression of the Notch downstream target genes HES1, HEY1 and HEY2 in U251 cells following DBZ treatment.

U251 cells were treated with 0 to 50 nM DBZ and 48 h later collected for qPCR and Western Blotting analysis. RNA was extracted and mRNA expression of the Notch target genes **(A)** *HES1*, **(B)** *HEY1*, and **(C)** *HEY2* was determined by qPCR normalised to *GAPDH*. **(D)** Western blotting of Hes1 confirmed successful inhibition of Notch signalling following 25 and 50 nM DBZ treatment. Protein was extracted from cells and separated (20 µg) by SDS-PAGE (10% SDS gel). Membranes were probed with rabbit anti-Hes1 (1:1000; Cell Signalling Technology #11988) and mouse anti-β-tubulin (1:2000; ThermoFisher Scientific #MA5-16308) in 5% milk in PBS-T overnight at 4 °C. Membranes were washed and probed with anti-rabbit IgG HRP conjugate (1:5000, ThermoFisher Scientific #65-6120) and anti-mouse IgG HRP conjugate (1:5000; ThermoFisher Scientific #31430) secondary antibodies in 5% milk in PBS-T at RT for 1 h. ECL. (Mean ± SD, n = 3, two-way ANOVA with Dunnett's post-hoc test, * $p < 0.05$, ** $p < 0.01$, *** $p < 0.001$, **** $p < 0.0001$, and ns denotes not significant).

determined by MTT assay. Cell viability was calculated as a percentage of matched untreated control and the IC50 determined by non-linear regression analysis.

3.3.3.2.1 U87 Cell Line

In the U87 cell line at 72 h post-TMZ treatment, the TMZ IC50 is significantly reduced in U87-EV, U87-mDLL4 and U87-mJAG1 cells pre-treated with DBZ compared to TMZ only (Figure 3.10A-B). Significant reductions in TMZ IC50 are also observed at both 96 h (Figure 3.10C-D) and 120 h (Figure 3.10E-F) post-TMZ treatment for cells pre-treated with 25 nM DBZ compared to TMZ only.

3.3.3.2.2 U251 Cell Line

In the U251 cell line at 72 h post-TMZ treatment, the TMZ IC50 is also significantly reduced in U251-EV, U251-mDLL4, and U251-mJAG1 cells pre-treated with DBZ compared to TMZ only (Figure 3.11A-B). Significant reductions in TMZ IC50 are also observed at both 96 h (Figure 3.11C-D) and 120 h (Figure 3.11E-F) post-TMZ treatment for cells pre-treated with 25 nM DBZ compared to TMZ only.

Taken together, these results suggest DLL4 and JAG1-induced Notch signalling plays a significant role in mediating TMZ resistance and can be reversed by inhibiting Notch signalling with the GSI DBZ.

3.3.4 DLL4 and JAG1 Have No Effect on Glioblastoma Cell Line Proliferation

We assessed proliferation of the U87 and U251 cell lines over a total of 7 days by MTT assay. Both DLL4 and JAG1 had no effect on proliferation in either the U87 or U251 cell lines compared to EV control (Figure 3.12).

We also utilised Ki67 staining to determine differences in cell proliferation following DLL4 and JAG1 overexpression. In both the U87 (Figure 3.13) and U251 (Figure 3.14).

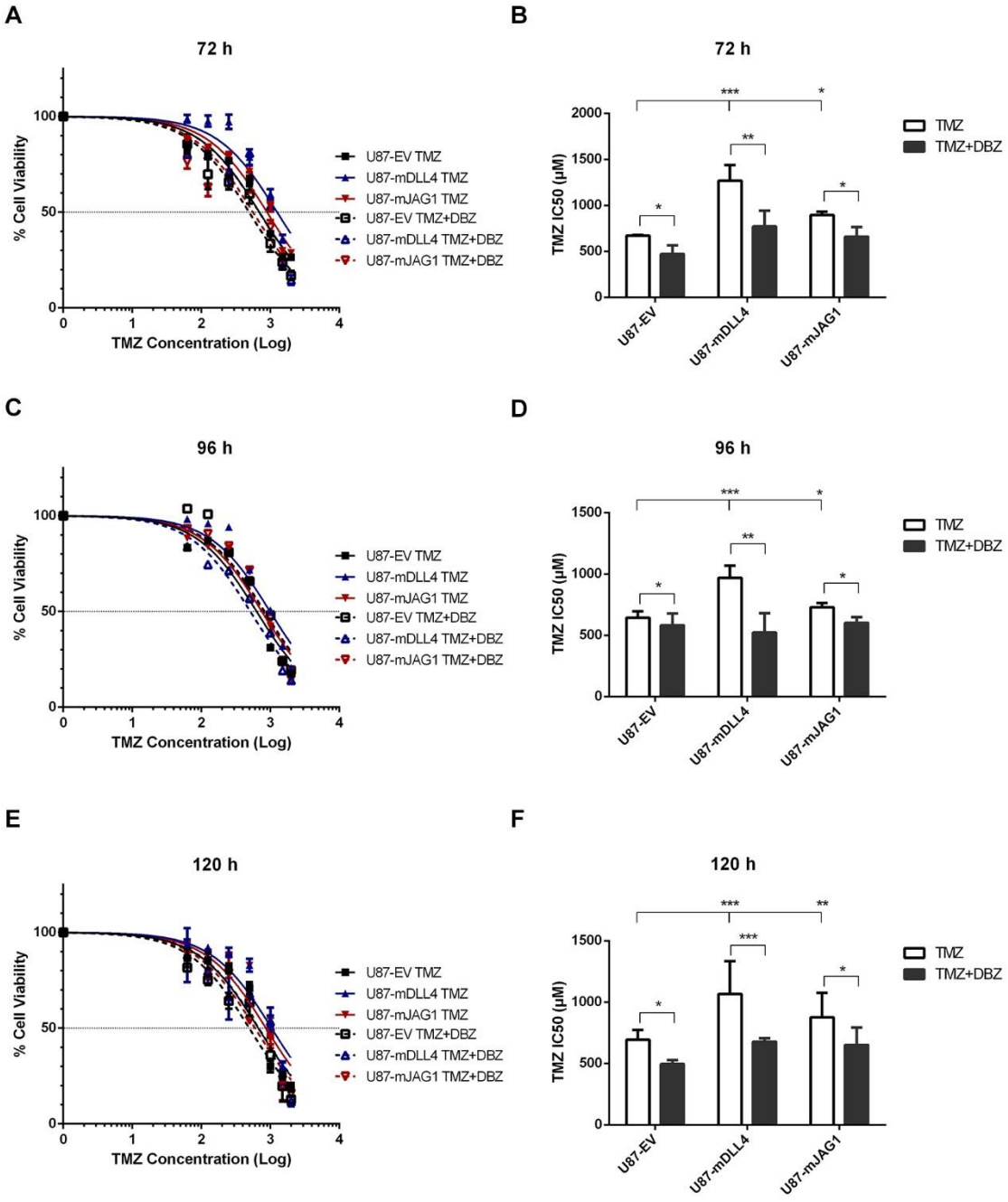

Figure 3.10: DBZ pre-treatment reduces TMZ IC50 in U87 cells.

U87 cells were seeded at 4000 cells per well and treated with 25 nM DBZ. Twenty-four h later cells were subjected to 0 to 2 mM TMZ treatment. Cell viability was determined by MTT assay at 72, 96, and 120 h post-TMZ treatment. IC50 was assessed by non-linear regression analysis using GraphPad Prism. **(A)** Cell viability and **(B)** IC50 of U87 cells following 72 h TMZ treatment. **(C)** Cell viability and **(D)** IC50 of U87 cells following 96 h TMZ treatment. **(E)** Cell viability and **(F)** IC50 of U87 cells following 120 h TMZ treatment. (Mean ± SD, n = 3, two-way ANOVA with Sidak's post-hoc test, * $p < 0.05$, ** $p < 0.01$, *** $p < 0.001$, and ns denotes not significant).

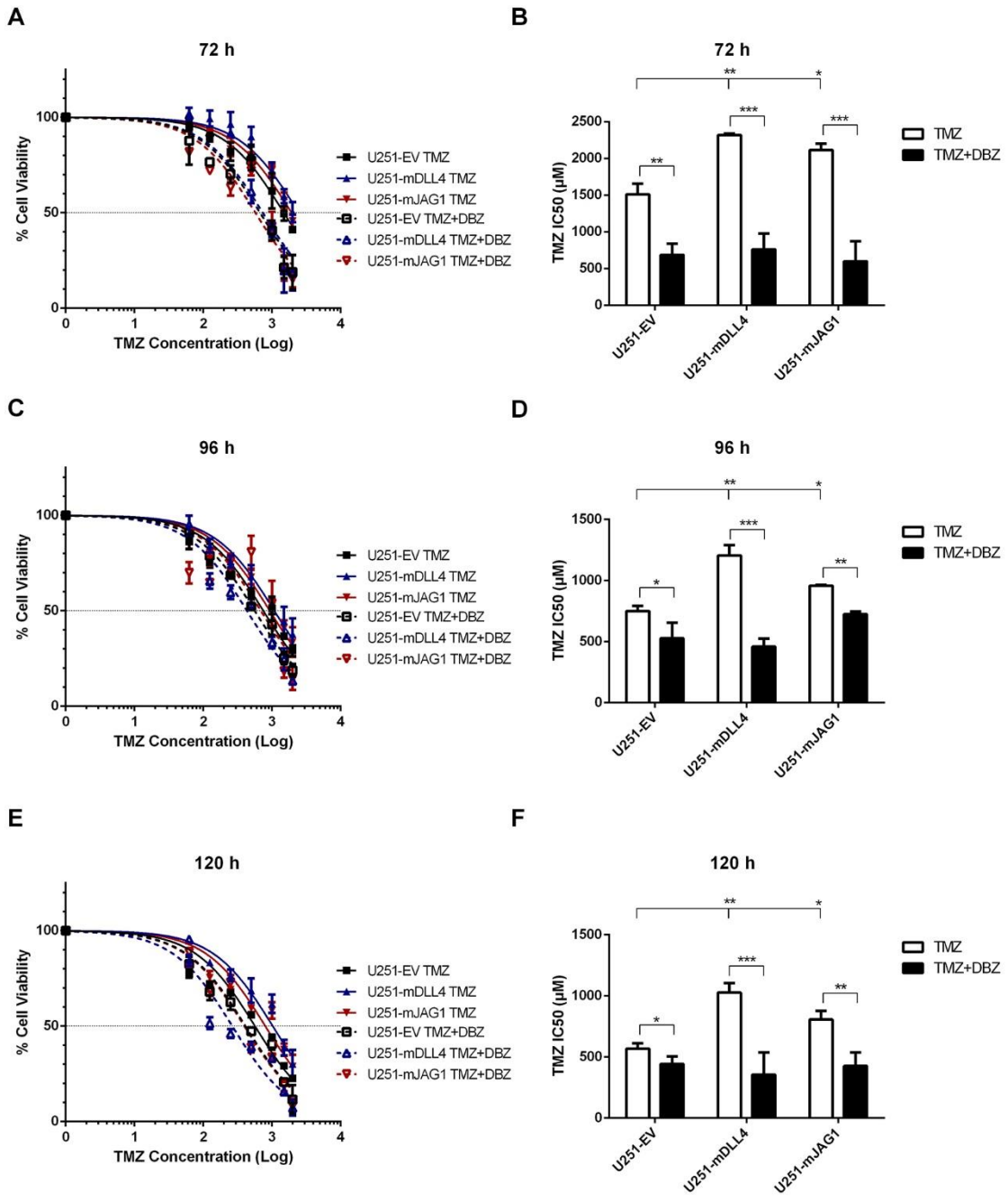

Figure 3.11: DBZ pre-treatment reduces TMZ IC50 in U251 cells.

U251 cells were seeded at 2000 cells per well and treated with 25 nM DBZ. Twenty-four h later cells were subjected to 0 to 2 mM TMZ treatment. Cell viability was determined by MTT assay at 72, 96, and 120 h post-TMZ treatment. IC50 was assessed by non-linear regression analysis using GraphPad Prism. **(A)** Cell viability and **(B)** IC50 of U87 cells following 72 h TMZ treatment. **(C)** Cell viability and **(D)** IC50 of U87 cells following 96 h TMZ treatment. **(E)** Cell viability and **(F)** IC50 of U87 cells following 120 h TMZ treatment. (Mean ± SD, n = 3, two-way ANOVA with Sidaks's post-hoc test, * $p < 0.05$, ** $p < 0.01$, *** $p < 0.001$, and ns denotes not significant).

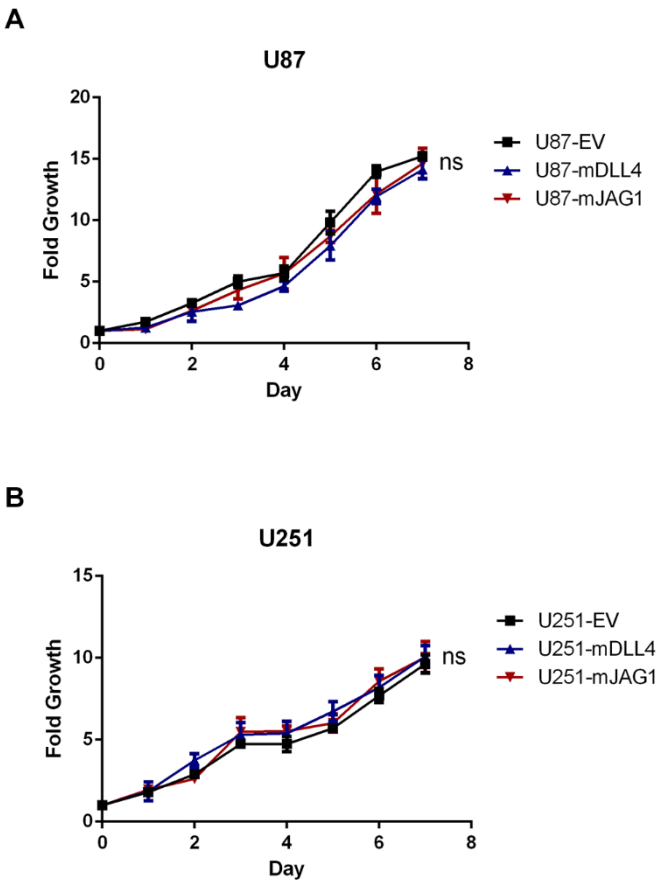

Figure 3.12: DLL4 and JAG1 have no effect on U87 and U251 cell proliferation.

Cellular proliferation of the **(A)** U87 and **(B)** U251 cell lines. Cells were seeded at 1000 cells per well and cellular proliferation was determined over 7 days by MTT assay. (Mean ± SD, n = 3, ordinary one-way ANOVA with Dunnett's post-hoc test, ns denotes not significant).

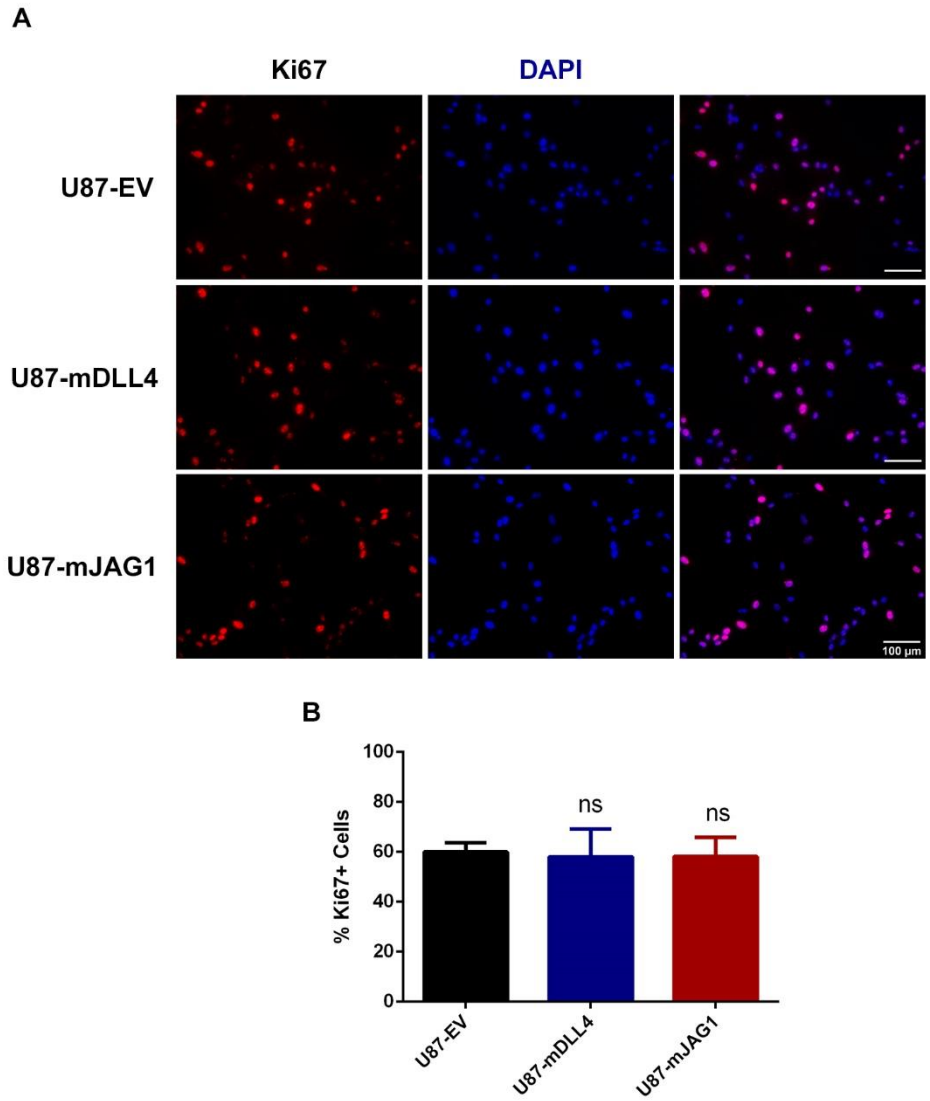

Figure 3.13: DLL4 and JAG1 have no effect on U87 cell proliferation.

(A) Representative Ki67 immunofluorescence staining of U87 cells. Cells were seeded in 96-well plates at 2000 cells per well and grown for 48 h. Cells were then fixed in 4% PFA and immunostained for rabbit anti-Ki67 (1:2000; Abcam #AB15580) followed by goat anti-rabbit IgG Alexa Fluor 647 (1:1000, ThermoFisher Scientific #A21245) secondary antibody and counterstaining with 2 µg/mL DAPI. **(B)** Percentage of positive Ki67 cells. Images were taken at 20X magnification. Scale bar = 100 µm. (Mean ± SD, n = 3, ordinary one-way ANOVA with Dunnett's post-hoc test, ns denotes not significant).

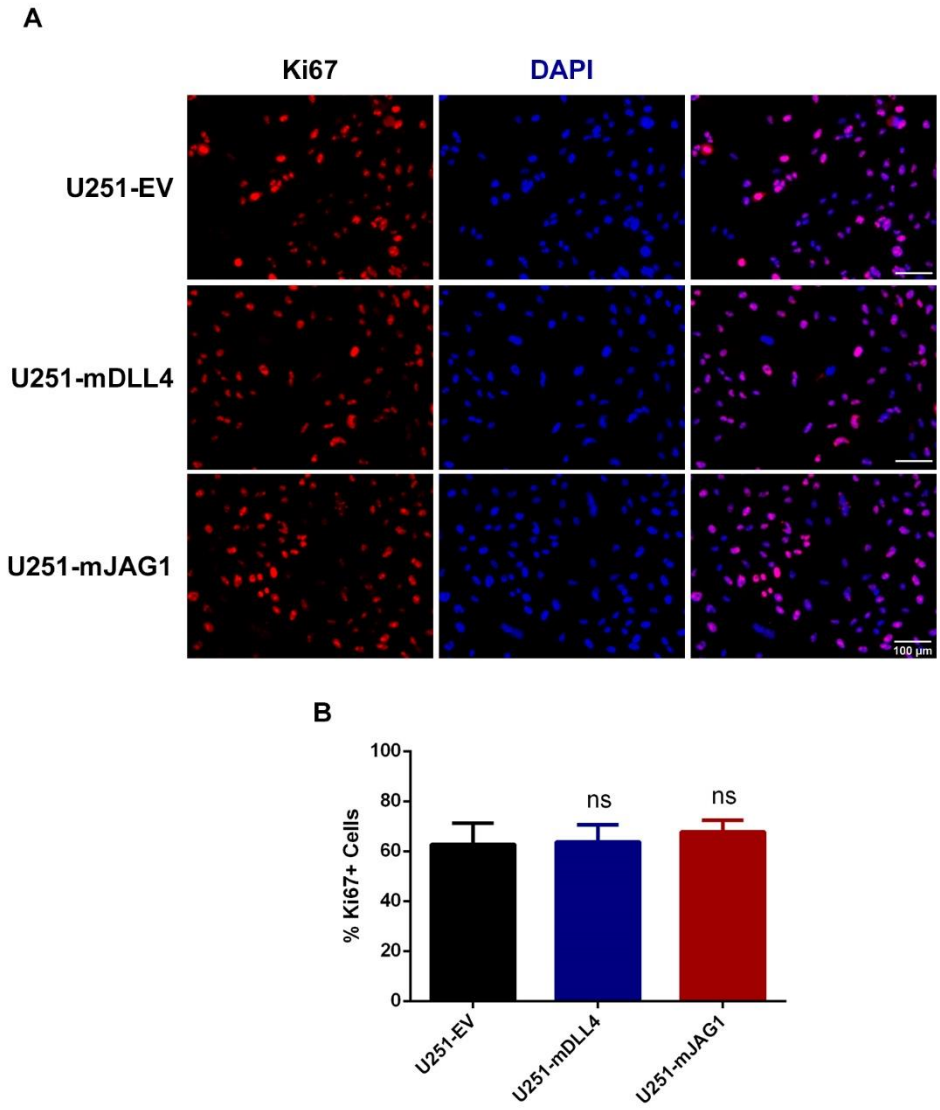

Figure 3.14: DLL4 and JAG1 have no effect on U251 cell proliferation.

(A) Representative Ki67 immunofluorescence staining of U251 cells. Cells were seeded in 96-well plates at 2000 cells per well and grown for 48 h. Cells were then fixed in 4% PFA and immunostained for rabbit anti-Ki67 (1:2000; Abcam #AB15580) followed by goat anti-rabbit IgG Alexa Fluor 647 (1:1000, ThermoFisher Scientific #A21245) secondary antibody and counterstaining with 2 µg/mL DAPI. **(B)** Percentage of positive Ki67 cells. Images were taken at 20X magnification. Scale bar = 100 µm. (Mean ± SD, n = 3, ordinary one-way ANOVA with Dunnett's post-hoc test, ns denotes not significant).

cell lines, DLL4 and JAG1 have no effect on the percentage of Ki67 positive cells, confirming DLL4 and JAG1 has no effect on cell proliferation.

3.3.5 Temozolomide and Dibenzazepine Co-treatment Significantly Reduces Glioblastoma Cell Line Proliferation

Proliferation of the U87 and U251 cell lines was assessed following single DBZ/TMZ and combination DBZ and TMZ treatment over a total of 7 days by MTT assay. Ki67 staining was also utilised to determine differences in cell proliferation following single and combination treatments.

3.3.5.1 U87 Cell Line

In U87-EV cells, proliferation was reduced following single DBZ and single TMZ treatment compared to DMSO control and was most significantly reduced by combination DBZ and TMZ treatment (Figure 3.15A). Conversely, in both U87-mDLL4 and U87-mJAG1 cells (Figure 3.15B-C), single TMZ treatment had no effect in reducing cellular proliferation. However, single DBZ treatment resulted in reduced cellular proliferation compared to DMSO control, and proliferation was most significantly reduced by combination DBZ and TMZ treatment.

In addition, Ki67 staining showed in U87-EV cells, single TMZ treatment has no effect on Ki67 staining compared to DMSO control (60.7% ± 4.5% vs 63.5% ±.5.1%) However, single DBZ (51.7% ± 3.4%) and combination DBZ and TMZ treatment (46.0% ± 3.9%) resulted in significantly reduced KI67 staining compared to control (Figure 3.16). In both U87-mDLL4 and U87-mJAG1, both single DBZ and combination DBZ and TMZ treatment resulted in a significant reduction in the percentage of KI67 positive cells compared to DMSO control. However, single TMZ treatment resulted in increased KI67 staining (Figure 3.16).

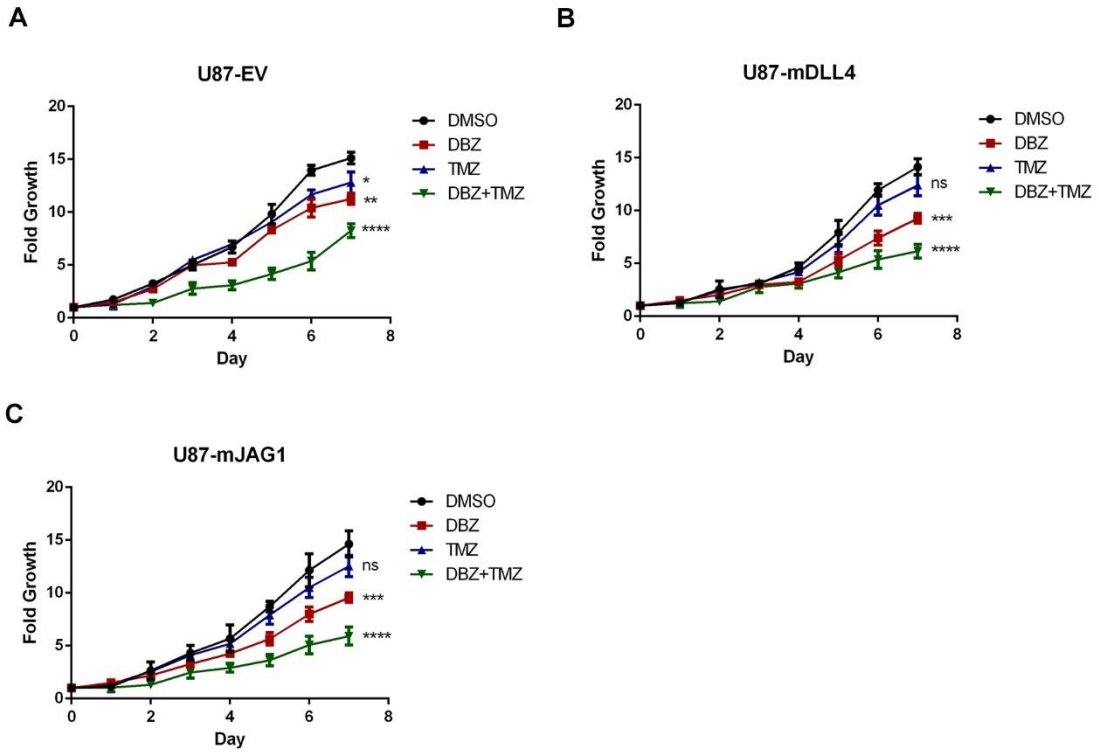

Figure 3.15: U87 cell proliferation following single 25 nM DBZ/25 µM TMZ and combination 25 nM DBZ and 25 µM TMZ treatment.

Cellular proliferation of **(A)** U87-EV, **(B)** U87-mDLL4, and **(C)** U87-mJAG1 cells following single and combination treatment. Cells were seeded at 1000 cells per well and 24 h later, treated with single 25 nM DBZ/25 µM TMZ and combination 25 nM DBZ and 25 µM TMZ treatment. Cellular proliferation was determined over 7 days by MTT assay. (Mean ± SD, n = 3, ordinary one-way ANOVA with Dunnett's post-hoc test, * $p < 0.05$, ** $p < 0.01$, **** $p < 0.001$, **** $p < 0.0001$, and ns denotes not significant).

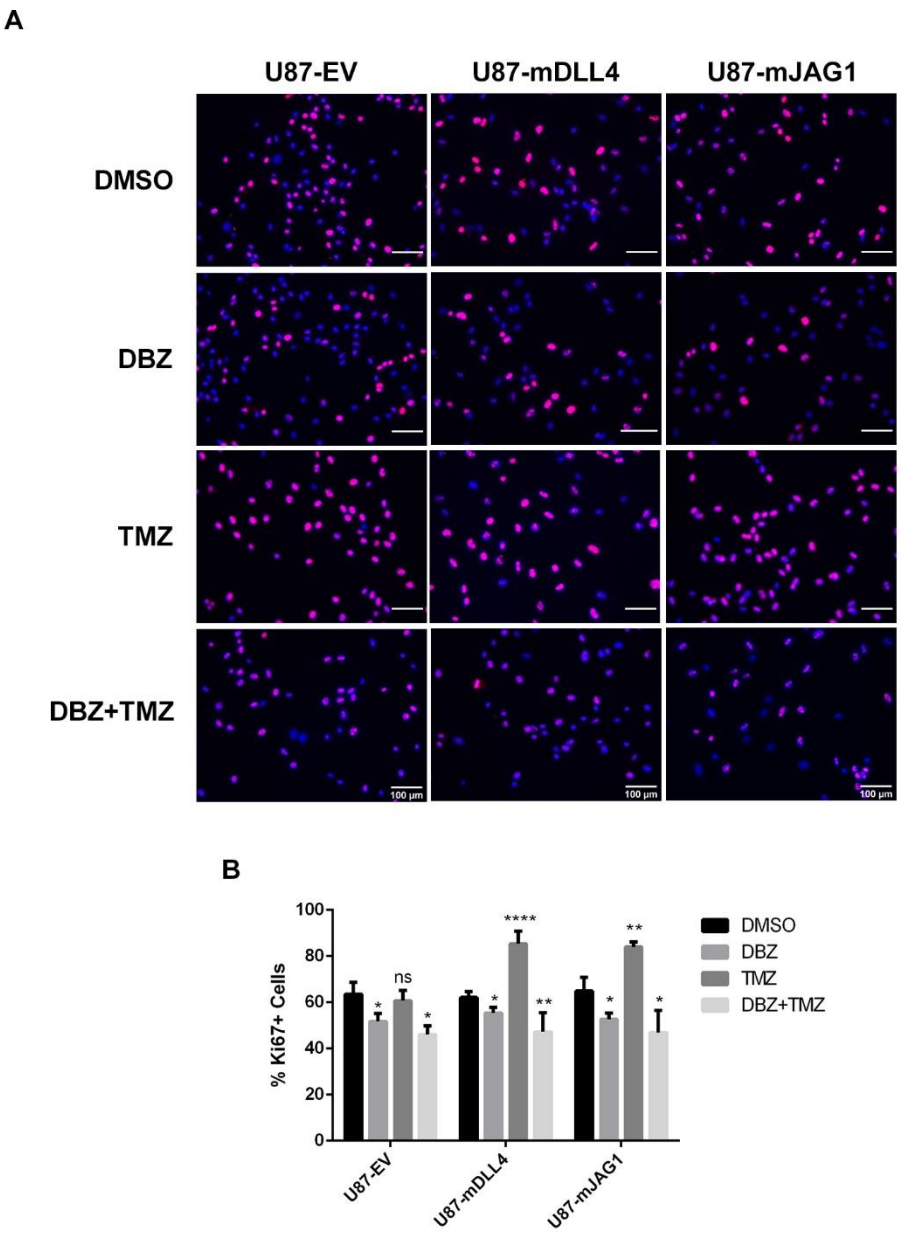

Figure 3.16: The effect of single 25 nM DBZ/25 µM TMZ and combination 25nM DBZ and 25 µM TMZ treatment on Ki67 staining of U87 cells.

Representative Ki67 immunofluorescence staining of **(A)** U87-EV, U87-mDLL4 and U87-mJAG1 cells following single and combination treatments. Cells were seeded in 96-well plates at 1000 cells per well and 24 h later, treated with single 25 nM DBZ/25 µM TMZ and combination 25 nM DBZ and 25 µM TMZ treatment. Following 48 h in culture, cells were fixed in 4% PFA and immunostained for rabbit anti-Ki67 (1:2000; Abcam #AB15580) followed by goat anti-rabbit IgG Alexa Fluor 647 (1:1000, ThermoFisher Scientific #A21245) secondary antibody and counterstaining with 2 µg/mL DAPI. **(B)** Percentage of positive Ki67 U87 cells following single and combination treatments. Images were taken at 20X magnification. Scale bar = 100 µm. (Mean ± SD, n = 3, two-way ANOVA with Dunnett's post-hoc test, * $p < 0.05$, ** $p < 0.01$, **** $p < 0.0001$, and ns denotes not significant).

3.3.5.2 U251 Cell Line

Similar results were observed in the U251 cell line. In U251-EV cells proliferation was reduced following single DBZ and TMZ treatment compared to DMSO control, and growth was most significantly reduced following combination DBZ and TMZ treatment (Figure 3.17A). On the other hand, in both U251-mDLL4 and U251-mJAG1 cells, single TMZ had no effect in reducing proliferation. However, single DBZ treatment reduced cellular proliferation compared to DMSO control, and proliferation was most significantly reduced by combination DBZ and TMZ treatment (Figure 3.17B-C).

Additionally, Ki67 staining showed in U251-EV cells, single TMZ treatment has no effect on Ki67 staining compared to DMSO control (65.0% ± 2.3% vs 66.7% ± 3.3%). However, single DBZ (52.3% ± 4.2%) and combination DBZ and TMZ treatment (46.9% ± 7.0%) resulted in significantly reduced Ki67 staining (Figure 3.18). In both U251-mDLL4 and U251-mJAG1, both single DBZ and combination DBZ and TMZ treatment resulted in a significant reduction in the percentage of KI67 positive cells compared to DMSO control. Whilst single TMZ treatment resulted in significantly increased Ki67 staining (Figure 3.18).

Taken together, these results suggest DLL4 and JAG1 induced Notch signalling results in resistance to TMZ treatment by increasing proliferation in glioblastoma cells, which can be reversed upon combination DBZ and TMZ treatment.

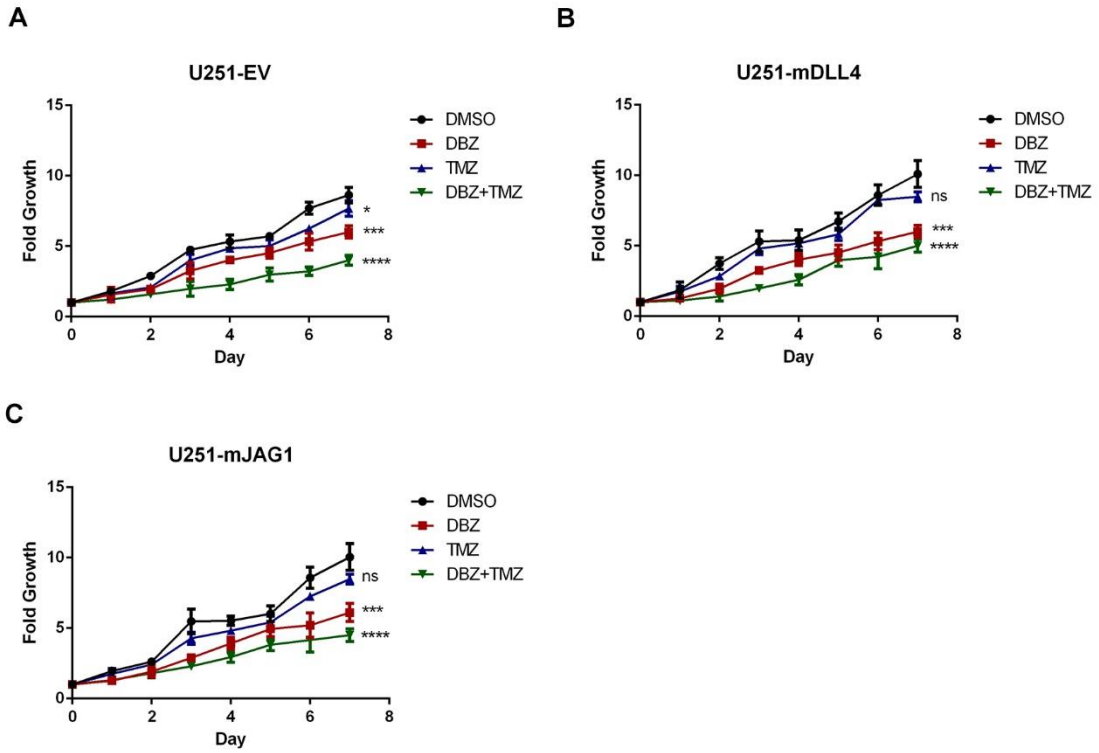

Figure 3.17: U251 cell proliferation following single 25 nM DBZ/25 µM TMZ and combination 25 nM DBZ and 25 µM TMZ treatment.

Cellular proliferation of **(A)** U251-EV, **(B)** U251-mDLL4, and **(C)** U251-mJAG1 cells following single and combination treatment. Cells were seeded at 1000 cells per well and 24 h later, treated with single 25 nM DBZ/25 µM TMZ and combination 25 nM DBZ and 25 µM TMZ treatment. Cellular proliferation was determined over 7 days by MTT assay. (Mean ± SD, n = 3, ordinary one-way ANOVA with Dunnett's post-hoc test, * $p < 0.05$, ** $p < 0.01$, *** $p < 0.001$, **** $p < 0.0001$, and ns denotes not significant).

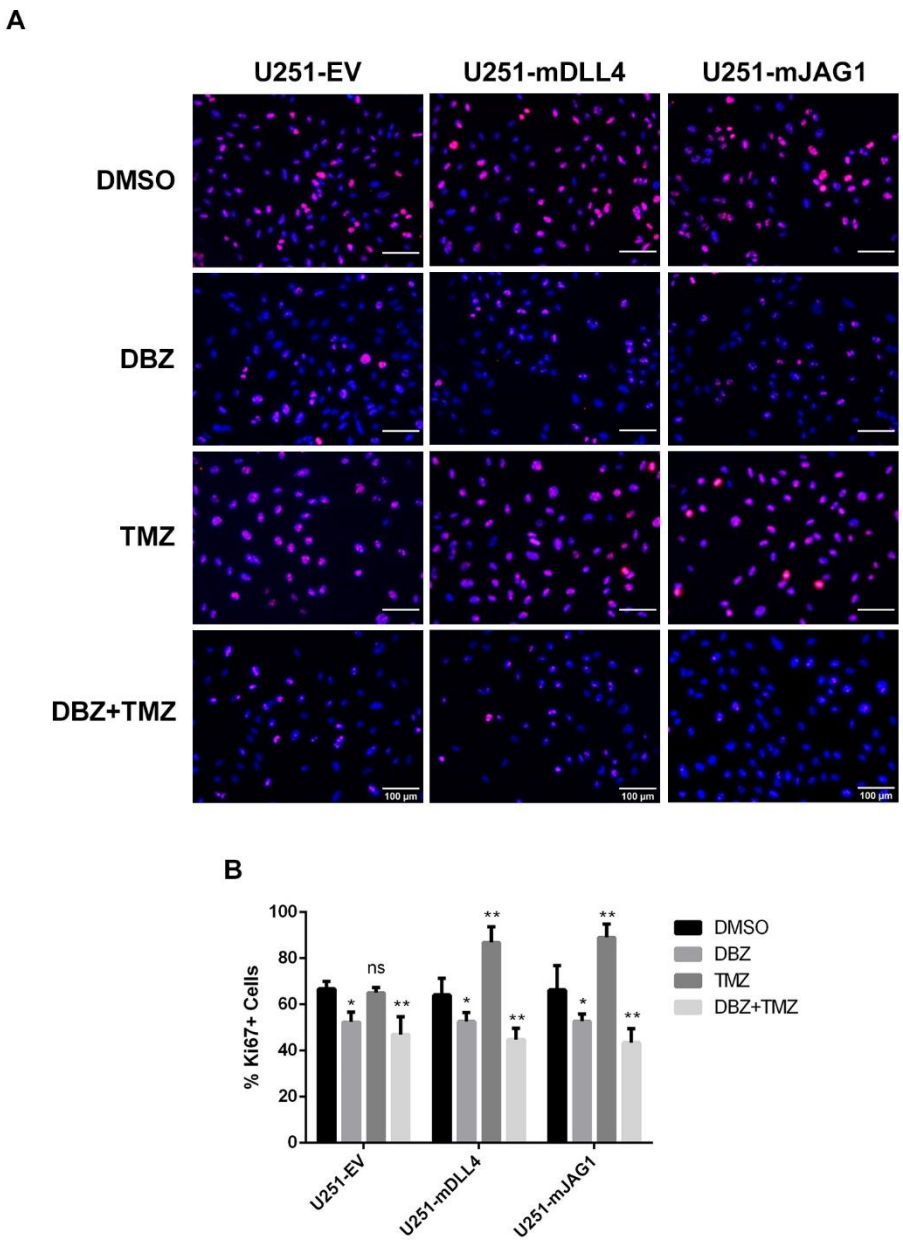

Figure 3.18: The effect of single 25nM DBZ/25 µM TMZ and combination 25nM DBZ and 25µM TMZ treatment on KI67 staining of U251 cells.

Representative Ki67 immunofluorescence staining of **(A)** U251-EV, U251-mDLL4 and U251-mJAG1 cells following single and combination treatments. Cells were seeded in 96-well plates at 1000 cells per well and 24 h later, treated with single 25 nM DBZ/25 µM TMZ and combination 25 nM DBZ and 25 µM TMZ treatment. Following 48 h in culture, cells were fixed in 4% PFA and immunostained for rabbit anti-Ki67 (1:2000; Abcam #AB15580) followed by goat anti-rabbit IgG Alexa Fluor 647 (1:1000, ThermoFisher Scientific #A21245) secondary antibody and counterstaining with 2 µg/mL DAPI. **(B)** Percentage of positive Ki67 U87 cells following single and combination treatments. Images were taken at 20X magnification. Scale bar = 100 µm. (Mean ± SD, n = 3, two-way ANOVA with Dunnett's post-hoc test, * $p < 0.05$, ** $p < 0.01$, and ns denotes not significant).

3.3.6 Combination Dibenzazepine and Temozolomide Treatment Reduces Growth in a 3D Spheroid Model

3.3.6.1 Development of the 3D Spheroid Model

In order to culture spheroids using the glioblastoma cell lines, we utilised Ultra-Low Attachment 96-well plates. Cells were seeded at a pre-determined concentration in culture media and the plate centrifuged in order for the cells to initially form an aggregate at the bottom of the well, before establishing a spheroid morphology following 48 h in culture (Methods 2.2.6: 3D Spheroid Culture).

3.3.6.1.1 U87 Spheroids

Following the methodology described above, we successfully performed spheroid culture of U87 glioblastoma cells. Spheroid culture was initiated and 48 h later, the first phase contrast images were taken (Day 0). Spheroids were then imaged every 2 days, and media changed every 2/3 days (Figure 3.19A).

For the U87 cell line we observed for U87-JAG1, spheroid growth at day 21 is significantly increased compared to U87-EV control (21.3 ± 2.3 fold vs 17.5 ± 2.3 fold). Conversely, U87-mDLL4 spheroid growth at day 21 is significantly reduced compared to U87-EV (12.4 ± 1.8 fold vs 17.5 ± 2.3 fold; Figure 3.19B). Representative images of U87 spheroids are shown in Figure 3.19C.

3.3.6.1.2 U251 Spheroids

For U251 spheroid culture, initially spheres were cultured in DMEM. However, we found the spheroids only slightly increased in size over the 21 days in culture (Figure 3.20A). As a result, U251 spheroids were then cultured in DMEM containing 2.5% Matrigel to act as an extracellular matrix. Culturing the spheroids in Matrigel resulted in increased U251 spheroid growth up to day 14, however, there was no further

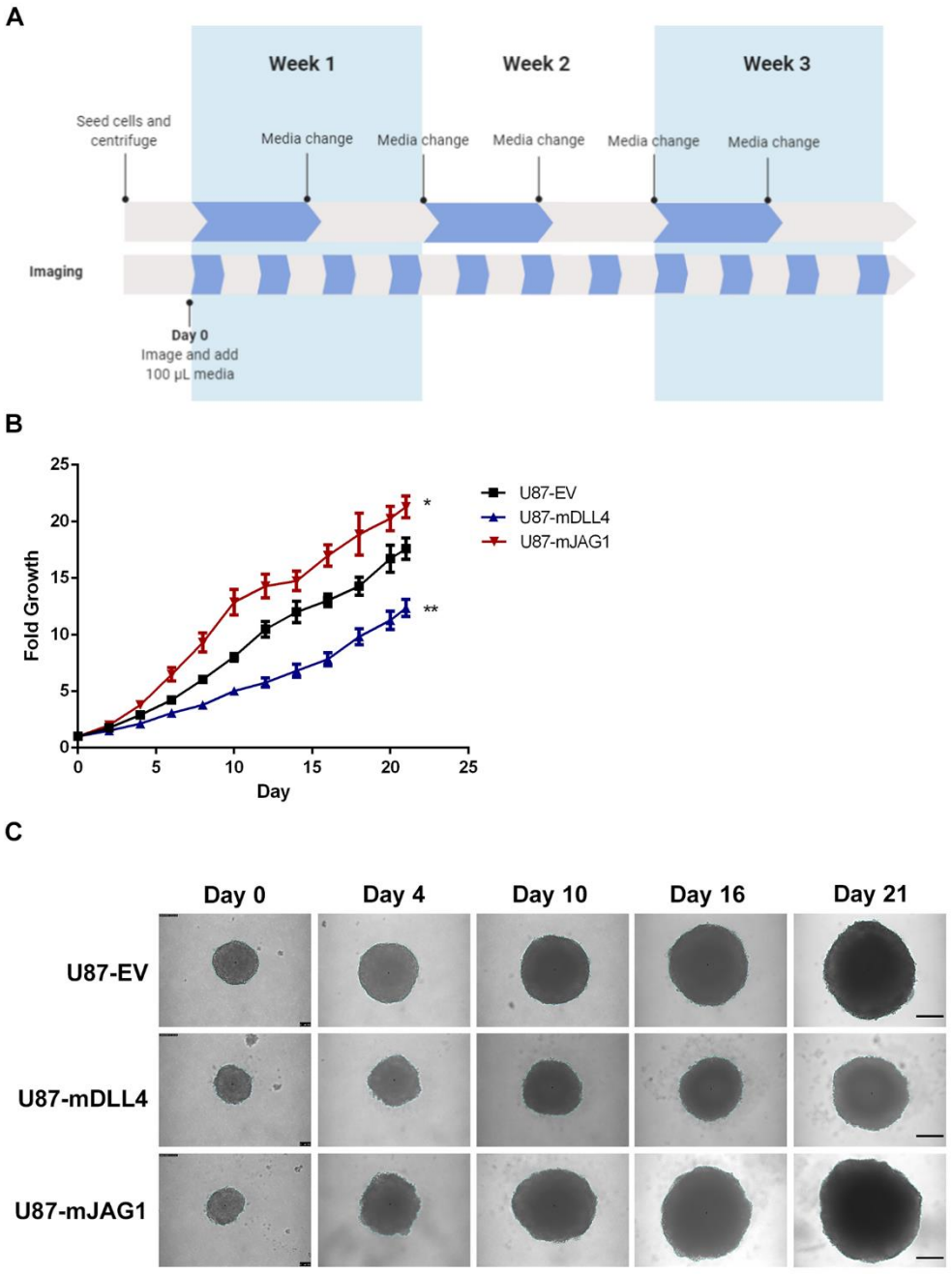

Figure 3.19: Development of the U87 3D spheroid model.

(A) Experimental overview of the 3D spheroid model. **(B)** U87 spheroid growth over 21 days. Cells were seeded at 8000 cells per well in a Corning Costar 96-well Ultra-Low Attachment Plate and subjected to centrifugation at 1400 x g for 10 minutes. Spheroids were allowed to recover for 48 h, before the first phase contrast images were taken (Day 0). Images were taken every 2/3 days and spheroid volume was analysed using ImageJ software and an accompanying macro. **(C)** Representative images of U87 spheroids over 21 days. Images were taken at 5X magnification. Scale bar = 200 µm. (Mean ± SD, n = 3, ordinary one-way ANOVA with Dunnett's post-hoc test, * $p < 0.05$, ** $p < 0.01$).

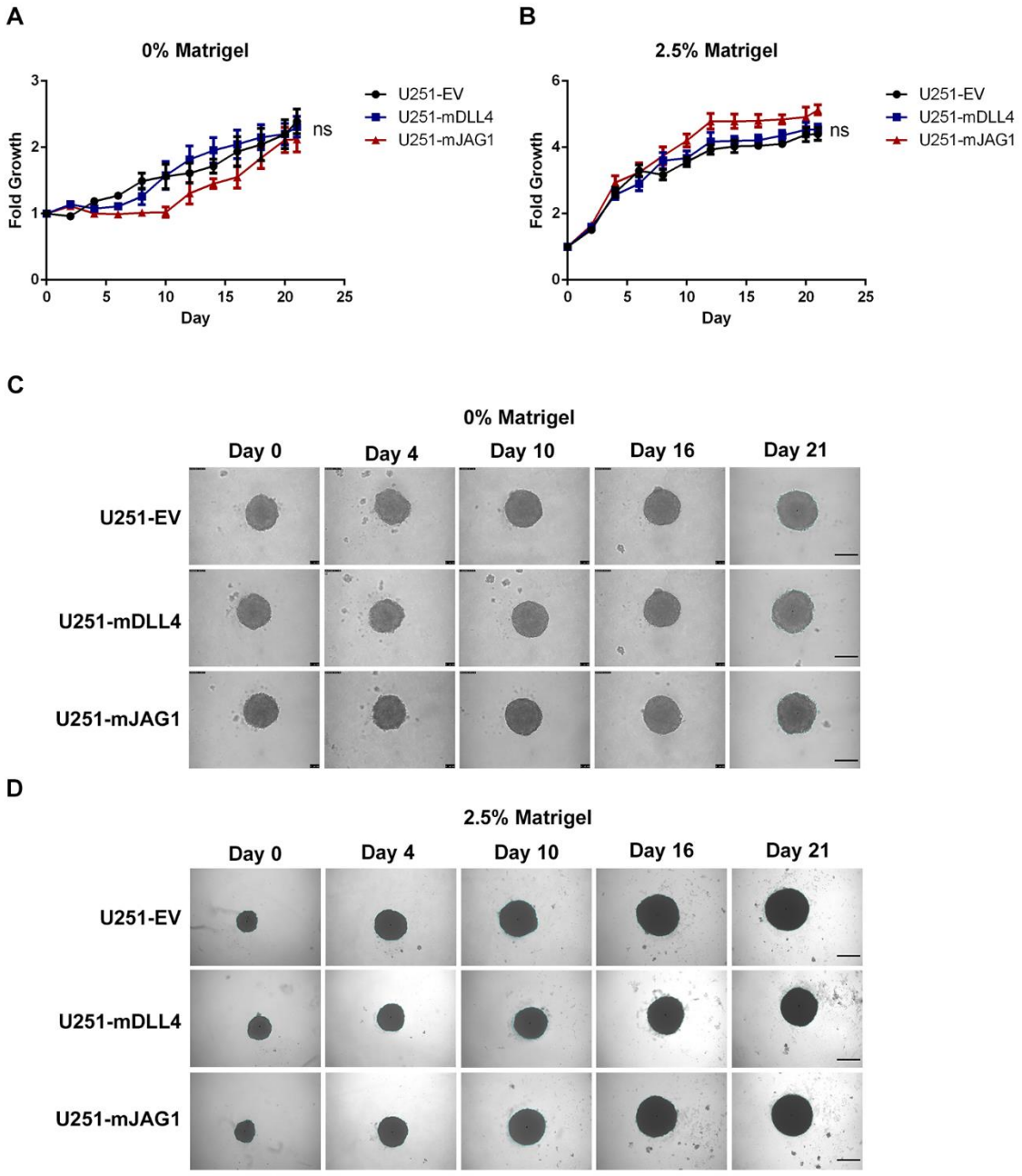

Figure 3.20: Development of the U251 3D spheroid model.

U251 spheroid growth over 21 days following culture in **(A)** DMEM containing 0% Matrigel and **(B)** DMEM containing 2.5% Matrigel. Cells were seeded at 8000 cells per well in a Corning Costar 96-well Ultra-Low Attachment Plate and subjected to centrifugation at 1400 x g for 10 minutes. Spheroids were allowed to recover for 48 h, before the first phase contrast images were taken (Day 0). Images were taken every 2/3 days and spheroid volume was analysed using ImageJ software and an accompanying macro. Representative images of U251 spheroids cultured in **(C)** 0% Matrigel and **(D)** 2.5% Matrigel over 21 days. Images were taken at 5X magnification. Scale bar = 200 µm. (Mean ± SD, n = 3, ordinary one-way ANOVA with Dunnett's post-hoc test, ns denotes not significant).

increase in spheroid growth after this point (Figure 3.20B). No difference in fold growth between the U251-mDLL4 and U251-mJAG1 spheroids compared to U251-EV control was observed. As a result, we did not use the U251 spheroids to assess growth following single and combination treatments but used them for TMZ IC50 analysis. Representative images of U251 spheroids cultured in DMEM containing 0% and 2.5% Matrigel are shown in (Figure 3.20C-D).

3.3.6.2 Combination Dibenzazepine and Temozolomide Treatment Significantly Reduced U87 3D Spheroid Growth

Utilising the method developed for U87 3D spheroid culture, we assessed the effect of U87 spheroid growth following single 25 nM DBZ/25 µM TMZ, and combination 25 nM DBZ and 25 µM TMZ treatment. In the U87-EV spheroids, growth was reduced following single DBZ and TMZ treatment compared to DMSO control and was most significantly reduced by combination DBZ and TMZ treatment (Figure 3.21A). Conversely, in both U87-mDLL4 and U87-mJAG1 spheroids (Figure 3.21B-C), single TMZ treatment had no effect in reducing spheroid growth compared to control. However, single DBZ treatment resulted in reduced growth compared to DMSO control, and growth was most significantly reduced following combination DBZ and TMZ treatment. Representative images of single and combination treated spheroids at day 21 are given in Figure 3.21D.

3.3.7 Increased Glioblastoma Resistance to Temozolomide by DLL4 and JAG1 in a 3D Spheroid Model

Utilising the 3D spheroid model, we assessed the TMZ IC50 in U87 and U251 spheroids at three separate time points: 4 days, 7 days, and 10 days post-TMZ treatment.

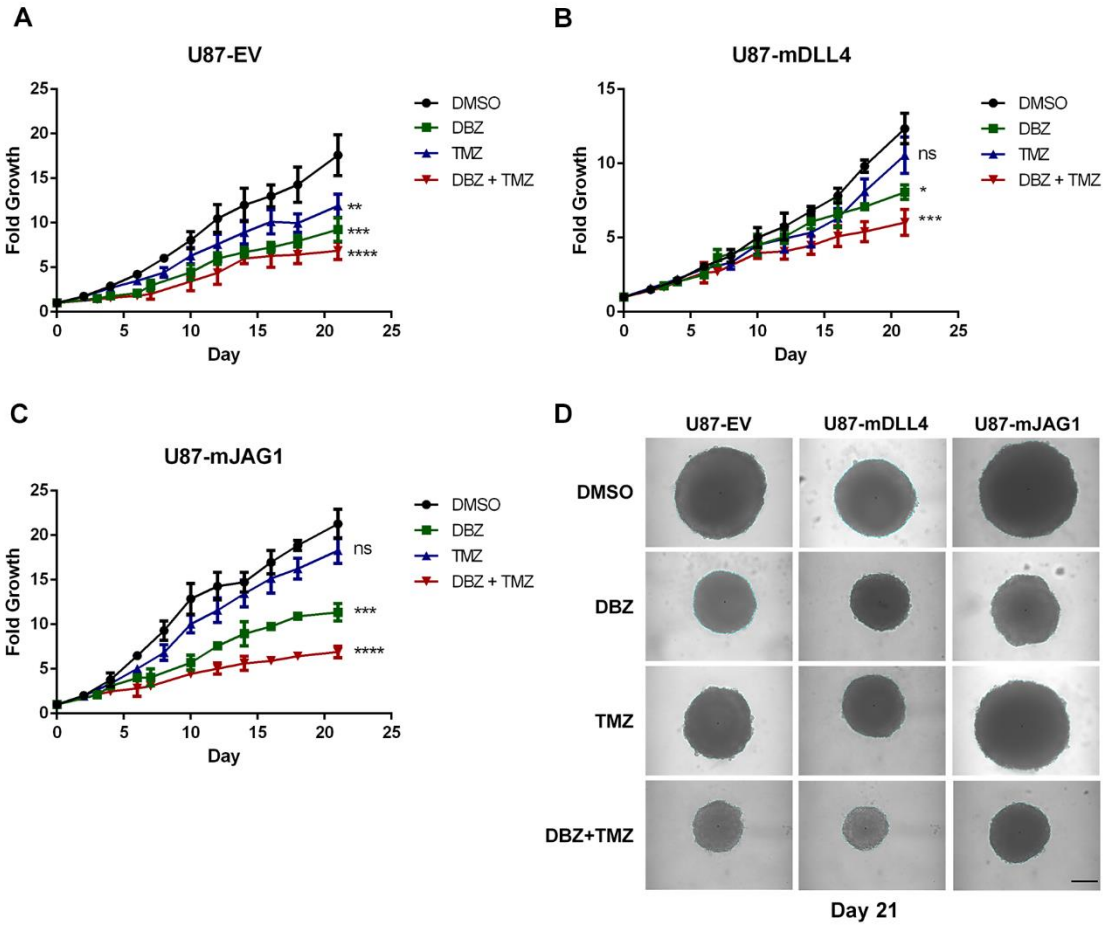

Figure 3.21: Combination DBZ and TMZ treatment significantly reduces U87 spheroid growth.

Growth of **(A)** U87-EV, **(B)** U87-mDLL4, and **(C)** U87-mJAG1 spheroids following single DBZ/TMZ, and combination DBZ and TMZ treatment over 21 days. Cells were seeded at 8000 cells per well in a Corning Costar 96-well Ultra-Low Attachment Plate and subjected to centrifugation at 1400 x g for 10 minutes. Spheroids were allowed to recover for 48 h, before the spheroids were treated with single 25 nM DBZ/25 µM TMZ and combination 25 nM DBZ and 25 µM TMZ treatment and first phase contrast images were taken (Day 0). Images were taken every 2/3 days and spheroid volume was analysed using ImageJ software and an accompanying macro. **(D)** Representative images of U87 spheroids at day 21 following treatments. Images were taken at 5X magnification. Scale bar = 200 µm. (Mean ± SD, n = 3, ordinary one-way ANOVA with Dunnett's post-hoc test, * $p < 0.05$, ** $p < 0.01$, *** $p < 0.001$, **** $p < 0.0001$, and ns denotes not significant).

Spheroid culture was initiated prior to 0 to 2 mM TMZ treatment, and at the experimental endpoints, spheroid size was determined and calculated as percentage compared to untreated control, and the IC50 determined by non-linear regression analysis.

3.3.7.1 U87 Spheroids

Four days post treatment, the TMZ IC50 for U87-mDLL4 and U87-mJAG1 spheroids was significantly higher compared to EV control (1239.0 µM ± 23.0 µM and 1070.5 µM ± 13.4 µM respectively, vs 866.9 µM ± 125.6 µM; Figure 3.22A-B). Again at 7 days post-treatment, the TMZ IC50 was significantly increased for U87-mDLL4 and U87-mJAG1 spheroids (347.0 µM ± 17.8 µM and 241.4 µM ± 15.3 µM, respectively) compared to U87-EV (195.8 µM ± 14.5 µM; Figure 3.22C-D). Finally, at 10 days post-treatment the TMZ IC50 for U87-mDLL4 and U87-mJAG1 spheroids was both significantly higher than that for U87-EV control (229.8 µM ± 15.8 µM and 164.8 µM ± 20.1 µM respectively, vs 104.2 µM ± 10.2 µM; Figure 3.22E-F).

3.3.7.2 U251 Spheroids

In the U251 spheroids, following 4 days TMZ treatment, the TMZ IC50 is significantly increased in the U251-mDLL4 and U251-mJAG1 spheroids compared to U251-EV control spheroids (1155.6 µM ± 92.0 µM, and 930.4 µM ± 53.0 µM respectively, vs 661.1 µM ± 118.0 µM; Figure 3.23A-B). Again at 7 days post-treatment, the TMZ IC50 was significantly increased for U251-mDLL4 and U251-mJAG1 spheroids (622.9 µM ± 47.4 µM and 448.8 µM ±25.3 µM, respectively) compared to U251-EV spheroids (359.8 µM ± 32.7 µM; Figure 3.23C-D). Finally, at 10 days post-treatment the TMZ IC50 for U251-mDLL4 and U251-mJAG1 spheroids were both significantly higher than U251-EV control (576.4 µM ± 45.7 µM and 519.8 µM ± 53.1 µM respectively, vs 353.3 µM ± 34.7

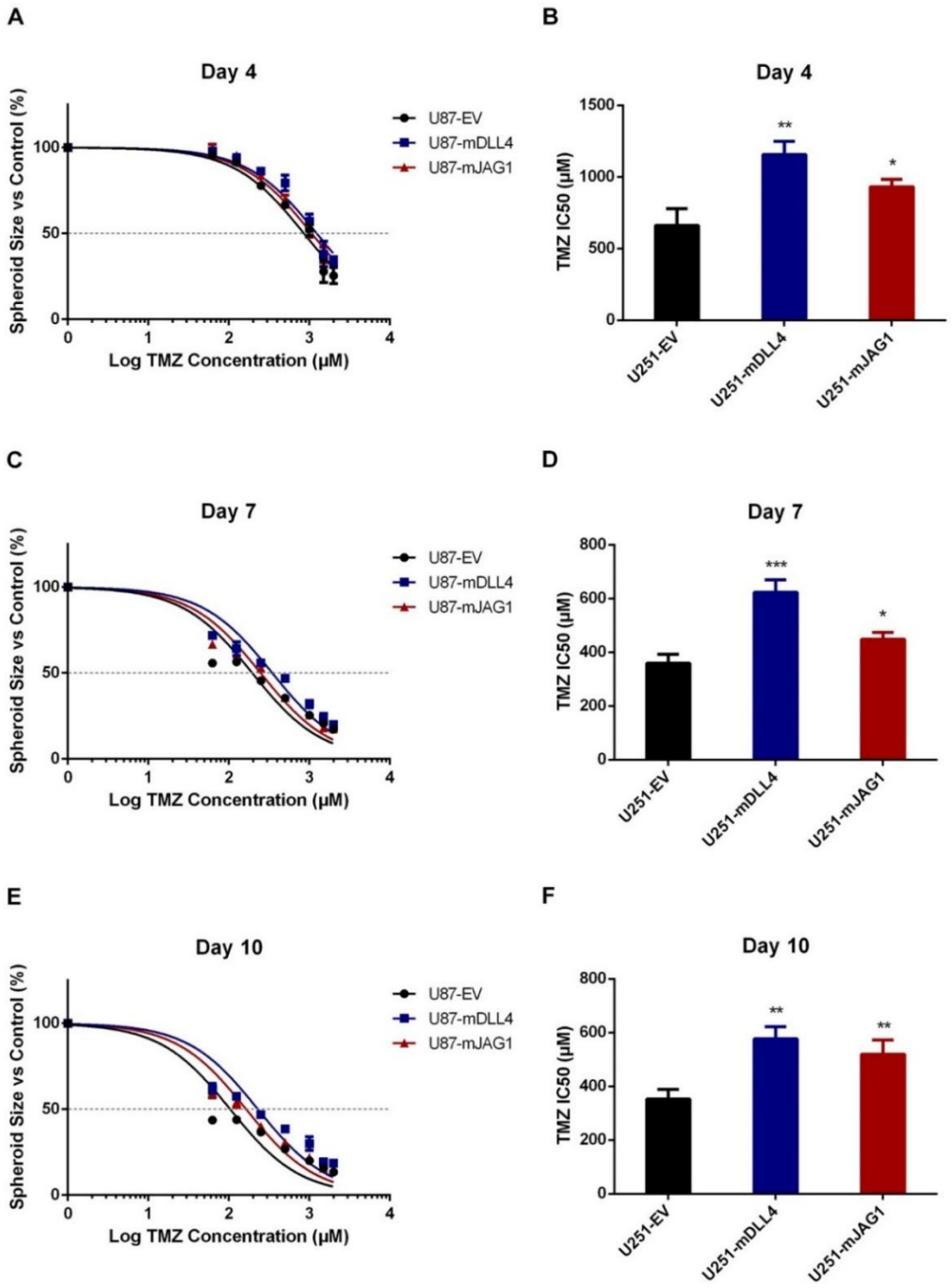

Figure 3.22: DLL4 and JAG1 confer TMZ resistance in a U87 3D spheroid model.

U87 cells were seeded at 8000 cells per well in a Corning Costar 96-well Ultra-Low Attachment Plate and subjected to centrifugation at 1400 x g for 10 minutes. Spheroids were allowed to recover for 48 h, before being treated with 0 to 2 mM TMZ. Images were taken at day 4, 7, and 10 post-TMZ treatment and spheroid volume was analysed using ImageJ software and an accompanying macro. **(A)** Percentage spheroid size compared to DMSO control and **(B)** IC50 of U87 spheroids following 4 days TMZ treatment. **(C)** Percentage spheroid size compared to DMSO control and **(D)** IC50 of U87 spheroids following 7 days TMZ treatment. **(E)** Percentage spheroid size compared to DMSO control and **(F)** IC50 of U87 spheroids following 10 days TMZ treatment. (Mean ± SD, n = 3, ordinary one-way ANOVA with Dunnett's post-hoc test, * $p < 0.05$, ** $p < 0.01$, *** $p < 0.001$, and ns denotes not significant).

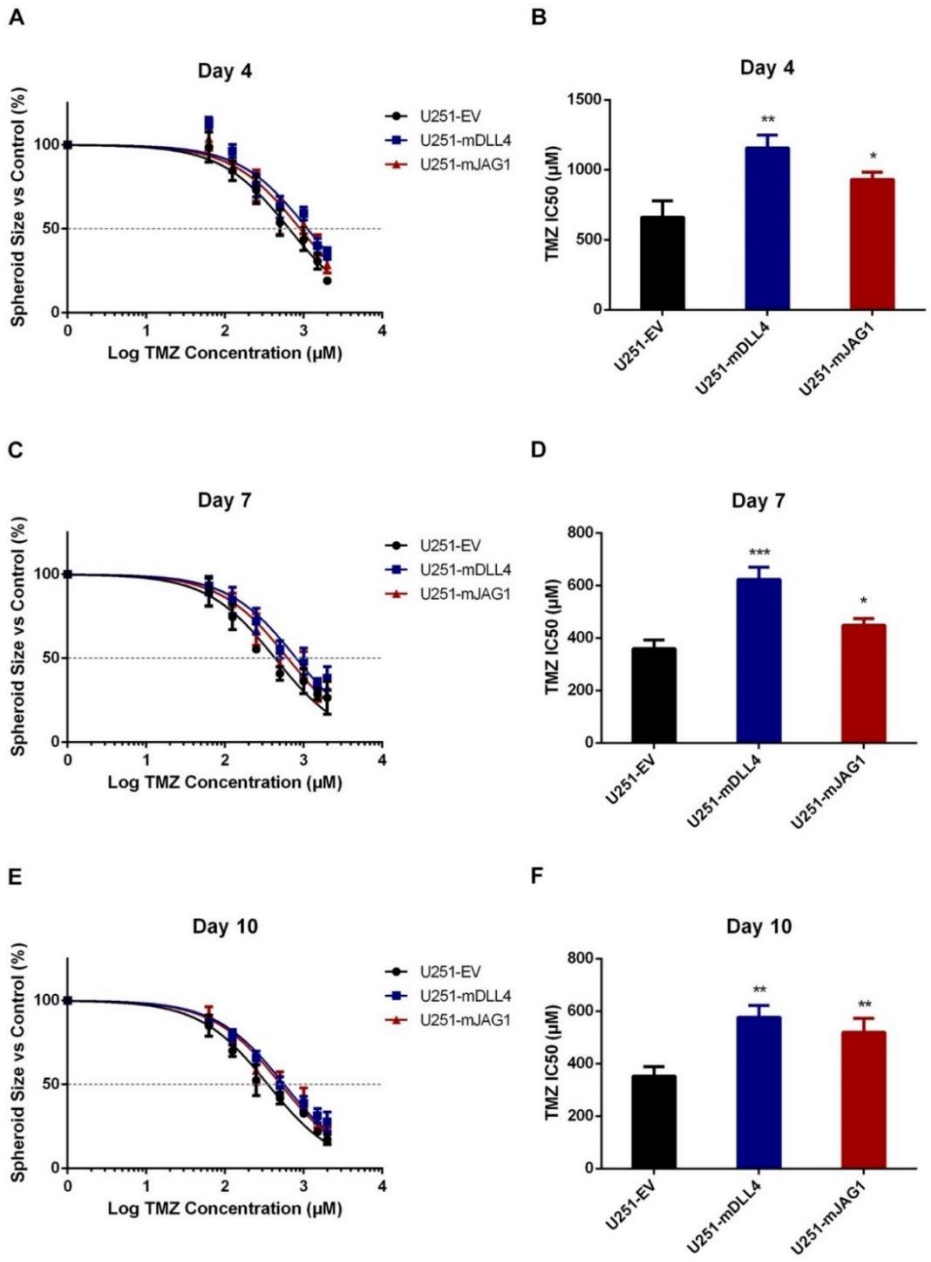

Figure 3.23: DLL4 and JAG1 confer TMZ resistance in a U251 3D spheroid model.

U251 cells were seeded at 8000 cells per well in a Corning Costar 96-well Ultra-Low Attachment Plate and subjected to centrifugation at 1400 x g for 10 minutes. Spheroids were allowed to recover for 48 h, before being treated with 0 to 2 mM TMZ. Images were taken at day 4, 7, and 10 post-TMZ treatment and spheroid volume was analysed using ImageJ software and an accompanying macro. **(A)** Percentage spheroid size compared to DMSO control and **(B)** IC50 of U251 spheroids following 4 days TMZ treatment. **(C)** Percentage spheroid size compared to DMSO control and **(D)** IC50 of U251 spheroids following 7 days TMZ treatment. **(E)** Percentage spheroid size compared to DMSO control and **(F)** IC50 of U251 spheroids following 10 days TMZ treatment. (Mean ± SD, n = 3, ordinary one-way ANOVA with Dunnett's post-hoc test, * $p < 0.05$, ** $p < 0.01$, *** $p < 0.001$, and ns denotes not significant).

µM; Figure 3.23E-F).

3.3.7.3 Dibenzazepine Pre-treatment Reverses Glioblastoma Resistance to Temozolomide in a 3D Spheroid Model

As we have shown, DLL4 and JAG1 increase the TMZ IC50 in both U87 and U251 3D spheroid culture. We next assessed if DBZ pre-treatment is able to reverse this effect. U87 and U251 spheroids were subjected to 24 h treatment with 25 nM DBZ before being treated with TMZ concentrations ranging from 0 to 2 mM. At the experimental endpoints (4 days, 7 days, and 10 days post-TMZ treatment), spheroid size was determined and calculated as percentage compared to untreated control, and the IC50 determined by non-linear regression analysis.

3.3.7.3.1 U87 Spheroids

In U87 spheroids at 4 days post-TMZ treatment, the TMZ IC50 is significantly reduced in U87-EV, U87-mDLL4 and U87-mJAG1 spheroids pre-treated with DBZ compared to TMZ only (Figure 3.24A-B). Significant reductions in TMZ IC50 are also observed at both 7 days (Figure 3.24C-D) and 10 days (Figure 3.24E-F) post-TMZ treatment for spheroids pre-treated with 25 nM DBZ compared to TMZ only.

3.3.7.3.2 U251 Spheroids

In U251 spheroids at 4 days post-TMZ treatment, the TMZ IC50 is also significantly reduced in U251-EV, U251-mDLL4, and U251-mJAG1 spheroids pre-treated with DBZ compared to TMZ only (Figure 3.25A-B). Significant reductions in TMZ IC50 are also observed at both 7 days (Figure 3.25C-D) and 10 days (Figure 3.25E-F) post-TMZ treatment for spheroids pre-treated with 25 nM DBZ compared to TMZ only.

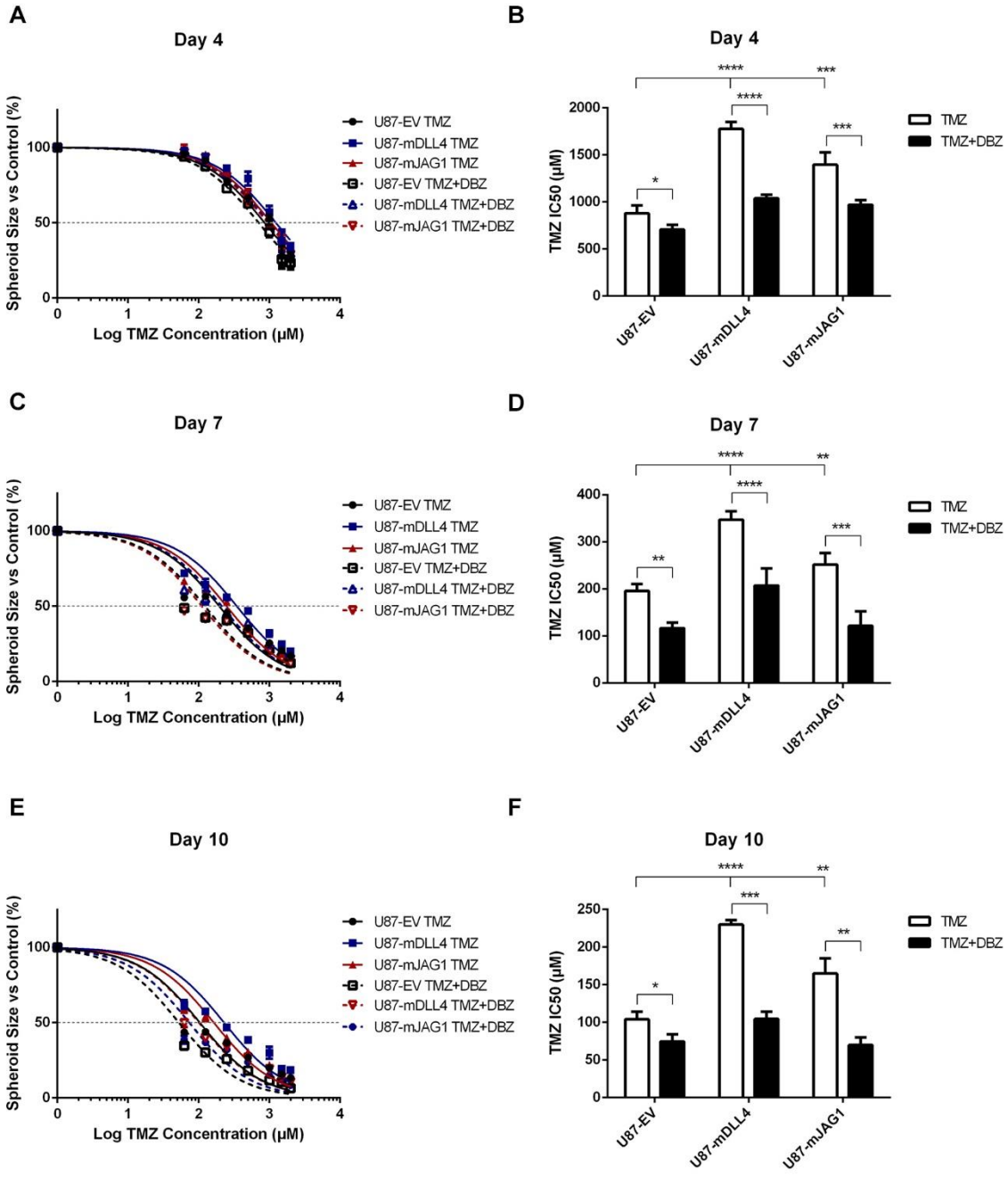

Figure 3.24: DBZ pre-treatment reduces TMZ IC50 in U87 spheroids.

U87 cells were seeded at 8000 cells per well in a Corning Costar 96-well Ultra-Low Attachment Plate and subjected to centrifugation at 1400 x g for 10 minutes. Spheroids were allowed to recover for 48 h prior to pre-treatment with 25 nM DBZ for 24 h followed by 0 to 2 mM TMZ treatment. Images were taken at day 4, 7, and 10 post-TMZ treatment and spheroid volume was analysed using ImageJ software and an accompanying macro. **(A)** Percentage spheroid size compared to DMSO control and **(B)** IC50 of U87 spheroids following 4 days TMZ treatment. **(C)** Percentage spheroid size compared to DMSO control and **(D)** IC50 of U87 spheroids following 7 days TMZ treatment. **(E)** Percentage spheroid size compared to DMSO control and **(F)** IC50 of U87 spheroids following 10 days TMZ treatment. (Mean ± SD, n = 3, two-way ANOVA with Sidak's post-hoc test, * $p < 0.05$, ** $p < 0.01$, *** $p < 0.001$, **** $p < 0.0001$, and ns denotes not significant).

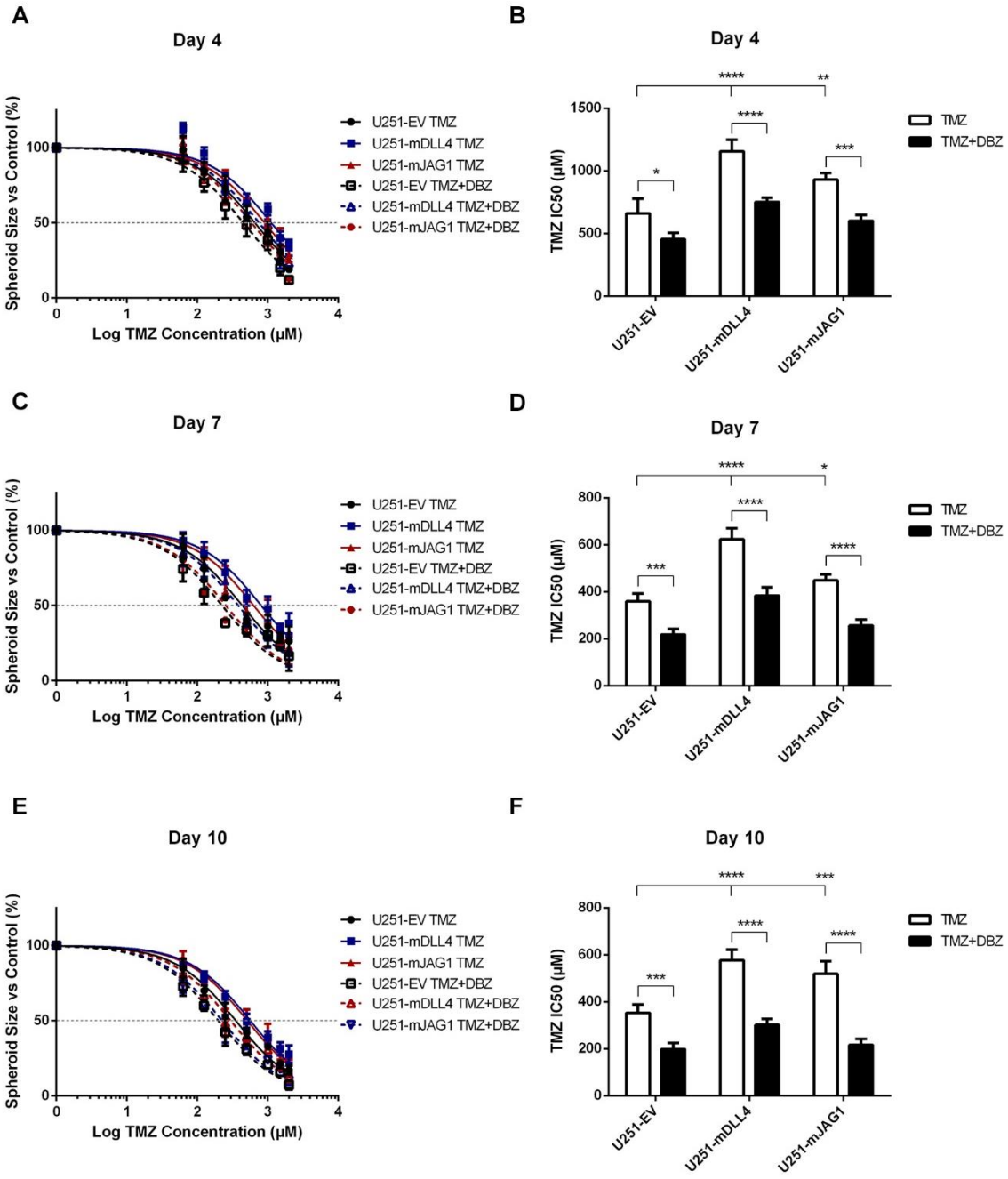

Figure 3.25: DBZ pre-treatment reduces TMZ IC50 in U251 spheroids.

U251 cells were seeded at 8000 cells per well in a Corning Costar 96-well Ultra-Low Attachment Plate and subjected to centrifugation at 1400 x g for 10 minutes. Spheroids were allowed to recover for 48 h prior to pre-treatment with 25 nM DBZ for 24 h followed by 0 to 2 mM TMZ treatment. Images were taken at day 4, 7, and 10 post-TMZ treatment and spheroid volume was analysed using ImageJ software and an accompanying macro. **(A)** Percentage spheroid size compared to DMSO control and **(B)** IC50 of U251 spheroids following 4 days TMZ treatment. **(C)** Percentage spheroid size compared to DMSO control and **(D)** IC50 of U251 spheroids following 7 days TMZ treatment. **(E)** Percentage spheroid size compared to DMSO control and **(F)** IC50 of U251 spheroids following 10 days TMZ treatment. (Mean ± SD, n = 3, two-way ANOVA with Sidak's post-hoc test, * $p < 0.05$, ** $p < 0.01$, *** $p < 0.001$, **** $p < 0.0001$, and ns denotes not significant).

Taken together, these results from 3D spheroid culture confirm those obtained for 2D culture: DLL4 and JAG1-induced Notch signalling plays a significant role in mediating TMZ resistance and can be reversed by inhibiting Notch signalling with the GSI DBZ.

3.4 Discussion

Glioblastoma is the most commonly diagnosed primary malignant brain tumour in adults, with a median survival of just 14.6 months. The existing gold standard treatment is palliative, and despite multimodal aggressive therapy, glioblastoma Is uniformly fatal with survival over 3 years being considered long-term. Due to the poor survival rate of glioblastoma patients, it is therefore vital that novel avenues for therapy are explored to improve patient prognosis. In this chapter we examined the role of DLL4 and JAG1 on glioblastoma resistance to TMZ chemotherapy. We investigated the effect both these ligands have on 2D growth, 3D spheroid growth, and TMZ IC50.

We have shown that overexpression of DLL4 and JAG1 has no effect on 2D growth of U87 and U251 cells compared to control. However, In our 3D spheroid model, DLL4 significantly inhibited spheroid growth, whereas JAG1 overexpression promoted spheroid growth. This is similar to results seen in tumour models of angiogenesis whereby DLL4-Notch signalling reduces tumour angiogenesis, whilst induction of Notch signalling by JAG1 promotes angiogenesis (331, 332). Notch signalling is reliant on the interaction between Notch receptors and ligands at the boundary between neighbouring cells. It is known to mediate cell-cell communication through a number of contact morphologies, ranging from relatively broad adherens junctions (333, 334) to submicron filopodial contacts (335, 336). It has been shown that signalling between pairs of cells correlates with their contact area (337), and in the context of Notch signalling, is important for directing cell fate by lateral inhibition (338). As such, this spheroid model may be more representative of glioblastoma growth *in vivo*, as the cells are within a 3D structure unlike 2D which results in fewer cell-cell contact points.

Unlike 2D monolayer culture, spheroid cultures are of intermediate complexity and containing many elements found in solid tumours such as regions of chronic hypoxia, extracellular matrix, cell-cell and cell-extracellular matrix interactions, metabolite and catabolite gradients, regions of necrosis, and pH gradients (313). Reduced drug penetration has also been identified in spheroids, which in combination with other modelled factors give spheroids intrinsic resistance to chemotherapy similar to tumours *in vivo* which show limited drug penetration and distribution (313, 339). Previously, several research groups have shown the rationale for using a 3D spheroid system to model the clinical efficacy of combination treatments in glioblastoma. This model system has been shown to be a robust methodology to identify novel therapies for glioblastoma which reflect the *in vivo* response. However, this model still lacks important factors from the tumour microenvironment known to contribute to tumour response to treatment including tumour vasculature, fibroblasts, and immune cells.

Following single and combination treatments, our results in 2D and 3D spheroid culture show treatment of DLL4 and JAG1 overexpressing spheroids with TMZ resulted in no significant reduction of spheroid growth compared to DMSO control. However, single DBZ and combination DBZ and TMZ treatment significantly reduces spheroid growth, suggesting DLL4- and JAG1-induced Notch signalling plays a role in TMZ resistance.

This is the first study to show overexpression of the Notch ligands DLL4 and JAG1 significantly increase the TMZ IC50, and this is consistent for both 2D and 3D culture. By pre-treating the cells with the GSI DBZ we have shown that this increase can be reversed, again suggesting DLL4- and JAG1- induced Notch signalling plays a role in TMZ resistance *in vitro.* In the literature there are vast differences in TMZ IC50 values

obtained for both the U87 and U251 cell lines. A study by Haas *et al.* found the TMZ IC50 at 72 h post-treatment was 1309 µM for U87 cells and 1008 µM for U251 cells, which are similar to the results obtained in this study (340). Conversely, a study by Kanzawa *et al.* showed the TMZ IC50 for U87 and U251 cells was approximately 100 µM following 48 h treatment (341). These significant differences in TMZ IC50 between studies could be due to a number of variables such as differences in the purity of TMZ used, the quality of the cells cultured, and the culture media used. Some studies have noted vast differences in in IC50 values between low and high passage cell lines (342), however during this study all experiments were performed with the cell lines at a low passage number (< 20) to ensure the results obtained remained consistent.

Interestingly, we observed a general trend whereby TMZ IC50 is increased in U87 and U251 3D cultured spheroids compared to U87 and U251 cells cultured in 2D at the same timepoint (day 4 post-TMZ treatment). *In vitro* 3D tumour spheroids are believed to mimic *in vivo* solid tumours and show increased resistance to anti-cancer drugs compared to 2D cultured cell lines (343). This is because 3D *in vitro* cultures are recognised for recapitulating the physiological microenvironment and exhibiting high concordance with *in vivo* conditions such as the structural organisation, growth kinetics, hypoxia, and nutrient gradients observed in solid tumours (313). Drug penetration to the spheroid core is also limited due to cell-cell and cell-ECM interactions that form a physical barrier limiting drug distribution (339). These key properties imprint to the spheroid a resistance profile comparable to solid tumours and supports the idea that 3D culture is a better model for the cytotoxic evaluation of these drugs *in vitro* compared to 2D cultured cell lines (343).

Numerous mechanisms have been suggested to play a role in TMZ resistance in glioblastoma (as previously discussed in Introduction 1.1.6.2). One such mechanism is the epigenetic silencing of the DNA repair protein MGMT. MGMT is silenced by promoter methylation in approximately half of all glioblastomas (42). Both the U87 and U251 cell lines utilised in this study exhibit MGMT promoter methylation (158), therefore MGMT has little effect on TMZ resistance in our cell lines since lack of methylation is associated with resistance. Both cell lines also exhibit wild-type *IDH1* status (340), another key biomarker which determines patient prognosis. Glioblastomas with wild-type *IDH1* have a median OS of 1 year, whilst *IDH1*-mutated glioblastomas have a median OS of over 2 years (344).

Similar to the results presented in this study, previous research by Hiddingh *et al*. demonstrated expression of the extracellular matrix protein EFEMP1, which acts via γ-secretase activation of the Notch pathway, is associated with TMZ resistance. Inhibition of signalling by a GSI resulted in sensitisation of glioblastoma to TMZ both *in vitro* and *in vivo* (345). In addition, a study by Yahyanejad *et al.* has shown Notch inhibition in combination with both TMZ and radiotherapy enhances 3D spheroid growth delay *in vitro* and prolongs the survival of mice bearing orthotopic glioblastoma (255). These results alongside those presented in this thesis are encouraging in developing new combination therapies for glioblastoma in order to overcome TMZ resistance.

To date, several classes of Notch inhibitors have been developed. In this study we utilised DBZ, a GSI. As γ-secretase is involved in the intramembrane proteolysis of type I membrane proteins, it cleaves a number of other functionally important proteins including amyloid precursor protein (346), E-cadherin (347), receptor tyrosine-protein

kinase erbB-4 (348), CD44 (349), tyrosinase (350), and Alcadein (247, 351), suggesting γ-secretase plays a role in numerous biological activities. Being pan-Notch inhibitors, *in vivo,* GSIs cause intestinal toxicity via goblet cell metaplasia of the small intestine (329). In order to limit toxicity, a preclinical study using antibodies for specific Notch receptor inhibitors showed inhibition of the Notch1 receptor alone induces mild goblet cell metaplasia, whereas inhibition of the Notch2 receptor only is able to abolish this effect (352). Therefore, this emphasises the value of paralogue-specific antagonists in targeting specific Notch receptors and ligands *in vivo* to minimise side effects during clinical trials.

A Phase I clinical trial conducted by Krop *et al*. assessed both the pharmacology and pharmacodynamics of the GSI MK-0752 in patients with solid tumours who had failed to respond to standard therapies. Dose-dependent inhibition of Notch signalling by MK-0752 was observed. A complete response was seen in a patient with anaplastic astrocytoma, and stable disease in 10 patients with glioblastoma. The study observed MK-0752 has a modest level of activity in patients with gliomas, and provides the first clinical evidence validating Notch as a therapeutic target in gliomas (305). Another Phase 0/I trial assessed the molecular and clinical effects of Notch inhibition in glioma patients using the GSI RO4929097 alongside the current standard of care. The addition of RO4929097 to TMZ and radiotherapy was well tolerated, and evidence of target modulation was observed (252). These clinical studies alongside the data presented in this chapter provide support for further study of Notch pathway inhibitors in patients with gliomas, potentially selecting patients with evidence of overexpression and/or activation of Notch pathway components, particularly DLL4 and/or JAG1.

Chapter 4

4 DLL4 and JAG1 Increase Glioblastoma Resistance to Temozolomide Chemotherapy by Regulation of Glioma Cancer Stem Cells

4.1 Introduction

4.1.1 Glioma Cancer Stem Cells

CSCs in brain tumours were initially identified by the discovery of tumourigenic cells expressing the marker CD133 exhibiting stem cell properties both *in vitro* and *in vivo*. (175). This observation was further extended by a study which demonstrated stem-like neural precursor cells in glioblastoma can initiate growth and tumour recurrence following multiple serial transplantations (3). GCSCs divide asymmetrically giving rise to identical, highly tumourigenic CSCs, and non-tumourigenic cancer cells which form the bulk of the tumour contributing to intertumoural heterogeneity. Quiescent GCSCs have the capacity for continued self-renewal and proliferation supported by factors of the tumour microenvironment including hypoxia and TGF-β promoting tumour recurrence, providing an explanation for resistance to conventional treatment (353). This ability for self-renewal is maintained by key pathways involved in NSC maintenance including the Notch, Wnt, and Hedgehog signalling pathways (354). The aggressive nature of glioblastoma is attributed to the presence of GCSCs and the effective targeting of these cells may result in a paradigm shift in the treatment of glioblastoma.

4.1.1.1 Cancer Stem Cell Hypothesis

The CSC hypothesis posits that cellular heterogeneity within a tumour is organised in a hierarchical manner whereby CSCs have an enhanced capacity for self-renewal and the

ability to seed new tumours upon implantation in an experimental host. CSCs serve as critical drivers of tumour heterogeneity and malignancy in numerous solid tumours including glioblastoma. Functionally, CSCs are defined by their ability to self-renew and differentiate, recapitulating the heterogeneity found within a tumour. CSCs also demonstrate an enhanced capacity for invasion, metastasis, immune evasion, and therapeutic resistance.

A fundamental trait of the hierarchical model is CSCs sustain and fuel tumour growth and that their eradication is crucial to effective therapy. Several aspects of the CSC model remain intensely debated including the cell of origin, cell surface markers, and the relative frequencies of CSCs in tumours. However, several lineage-tracing studies have provided significant support of a hierarchical model in glioblastoma. These studies demonstrate the majority of tumour cells have very limited proliferative potential, and are derived from a population of cells that exhibit stem cell-like features (355). Chen *et al*. crossed a strain of mice genetically engineered to develop gliomas with another strain expressing green fluorescent protein under the control of the Nestin, a NSC marker. In the resulting tumours, the fraction of glioma cells expressing GFP were relatively quiescent and displayed key stem cell features. Following TMZ treatment, the recurrent tumours demonstrated a cellular hierarchy originating with the Nestin-GFP population. Selective depletion of the GFP-positive cell population considerably reduced tumour growth, and when combined with TMZ, significantly impeded tumour development (195). Another key study by Peter Dirks and colleagues studied the clonal evolution of barcoded glioblastoma cells following serial xenotransplantation to define their individual fate behaviours. They identified that the growth of glioblastoma clones *in vivo* is consistent with a conserved proliferative

hierarchy with the root being GCSCs. The model identified slow-cycling stem-like cells give rise to rapidly cycling progenitor cells with an extensive cell maintenance capacity, which in turn generates non-proliferative cells. It was also identified that chemotherapy with TMZ facilitates the expansion of pre-existing treatment resistant GCSCs (356). Both studies show the importance of GCSCs in tumour maintenance and identify GCSCs as the drivers of recurrence following treatment.

A significant contributor to the poor prognosis of glioblastoma patients include a high degree of intratumoural heterogeneity and plasticity, the infiltrative and migratory nature of tumour cells, and a high rate of recurrence. Recurrent tumours in glioblastoma are frequently evolutionary different to the original tumour, with both distinct drivers and sensitivities, which limits the informative capacity of initial tumour biopsies when treating recurrence (357). A significant number of these features can be modelled in the context of the CSC hypothesis. GCSCs are believed to play a significant role in mediating therapeutic resistance by supporting radioresistance (177), chemoresistance (179, 195), angiogenesis (358), invasion (359), and recurrence (195). Both *in vivo* and *in vitro* observations support the existence of GCSCs that express stemness related markers, are capable of initiating tumours, and recapitulate tumour heterogeneity and histopathology when injected orthotopically in mice (4, 299).

4.1.2 Glioblastoma Cell of Origin

Although glioblastoma represents the first and one of the most highly characterised cancers by The Cancer Genome Atlas (TCGA) at the genomic level (360, 361), significant controversy remains with respect to its precise cell of origin (Figure 4.1). Whilst some believe glioblastomas arise from a subpopulation of NSCs, others argue the “de-differentiation” of more differentiated astrocytes may give rise to

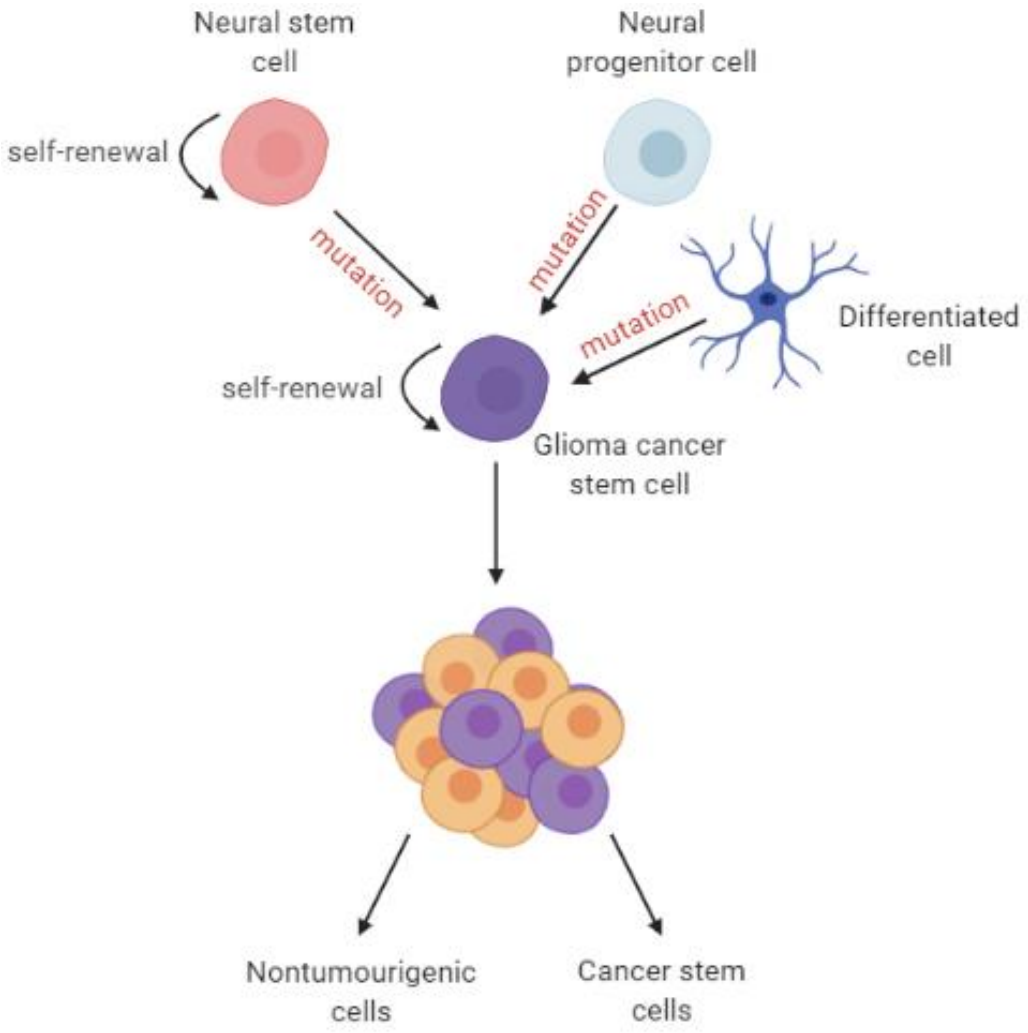

Figure 4.1: Glioblastoma cell of origin.

The origin of cancer stem cells in glioblastoma is intensely debated within the field. Glioma cancer stem cells (GCSCs) are thought to derive from mutated neural stem/progenitor cells or differentiated cells that have undergone de-differentiation to GCSCs. The tumour mass is composed of a heterogeneous cell population, only a small percentage of which comprise GCSCs. Diagram adapted from (362).

glioblastoma. In murine models, overexpression of active Ras and Akt, or inactivation of p53 and NF1 tumour suppressors in neural progenitor cells, but not differentiated astrocytes, was sufficient to induce the formation of glioblastoma-like lesions (363-365). However, others show genetic alterations in either neural stem cells or differentiated astrocytes can give rise to glioblastoma (366). More recently, a study by Llaguno *et al*. systematically assessed the tumour-initiating potential of adult neural populations at various stages of lineage differentiation. Using cell type-specific tamoxifen-inducible Cre recombinase transgenes targeting glioblastoma-relevant tumour suppressors (NF1, p53, and Pten) in late-stage neuronal progenitors, neuroblasts, and differentiated neurons. Mutant mice showed both cellular and molecular defects highlighting the impact of tumour suppressor loss, with mutant neurons being the most resistant to the early changes associated with tumour development. However, no evidence of gliomagenesis was observed, showing increasing lineage restriction is associated with reduced susceptibility to tumourigenesis. The study identified a glioblastoma cell of origin hierarchy whereby stem cells sit at the apex and differentiated cell types are least susceptible to malignant transformation (367).

4.1.3 Markers of Glioma Cancer Stem Cells

GCSCs are characterised by long-term self-renewal *in vitro*, the expression of NSC markers, and the ability to differentiate into cells that form the bulk of the tumour, recapitulating the parental tumour in orthotopic xenografts. CD133 (also known as Prominin-1) was originally identified as a surface antigen expressed on hematopoietic stem cells (368), as used to isolate NSCs from human foetal brain (369). Cell sorting for CD133 has since been utilised to enrich for cells with tumorigenic potential in glioma,

has been identified as being essential for GCSC maintenance, and high expression is associated with poor survival in glioblastoma patients (3, 370). However, the use of CD133 as a CSC marker in glioblastoma remains controversial. During the seminal studies, 100 CD133+ glioblastoma cells were sufficient to develop xenografted tumours that recapitulated the heterogeneity observed in the parental tumour. Conversely, CD133- tumour cells were effectively depleted for tumorigenic potential (4, 175). However, several studies have since identified tumourigenic CD133- GCSCs which show differential growth characteristics and molecular profiles compared to CD133+ GCSCs (371).

In addition to CD133, a variety of other markers have been described for GCSCs. CSC markers in glioblastoma are categorised according to their cellular localisation and include cell surface markers (e.g. CD15, CD133, A2B5, L1CAM), cytoskeletal proteins (e.g. Nestin), transcription factors (e.g. SOX2, OCT4, NANOG), post-transcriptional factors (e.g. Musashi1), and polycomb transcriptional suppressors (e.g. Bmi1, Ezh2) (372). The transcription factors SOX2 and OCT4 play a critical role in the perpetual self-renewal of GCSCs. SOX2, which is highly expressed in glioblastoma, is considered a master transcription factor crucial for maintaining stem cell pluripotency and its expression is correlated with CD133 (299). Both of which have been identified as being markers of poor prognosis in glioblastoma patients (373, 374).

4.1.4 Glioma Cancer Stem Cells and Treatment Resistance

Chemoresistance is considered a hallmark of recurrent glioblastoma, and as previously discussed, there is significant evidence connecting chemoresistance and tumour recurrence in glioblastoma. The hierarchical stem cell theory postulates only stem cells are able to replenish the tumour as they give rise to a proliferating transient

subpopulation which then differentiate into non-stem cells which form the tumour bulk. With this concept in mind, the observation of intertumoral molecular heterogeneity indicates clonal development from genetically distinct GCSCs (375). This is believed by many to explain treatment failures through the propagation of recurrent tumours from pre-existing GCSCs with endogenous therapeutic resistance to treatment. It has been observed that MGMT protein expression, MGMT promoter methylation, and response to TMZ treatment differ in distinct clones derived from the same tumour suggesting that chemoresistance is pre-existing at a clonal level within the primary tumour (376).

As previously discussed in Chapter 1 Introduction (1.1.6.2), a number of mechanisms have been identified to mediate the therapeutic resistance of GCSCs to TMZ and include the upregulation of anti-apoptotic proteins (e.g. Bcl-2), inhibitors of apoptosis, and drug efflux transporters (176), the enhanced expression of DNA damage checkpoint response kinases (e.g. Chk1 and Chk2) (177), increased EGFR expression and activity (178), and increased MGMT expression (179). There is also significant evidence to suggest pathways involved in neural development (including Notch (197), BMP (198), NF-κB (199), and Wnt signalling) are deregulated in glioblastoma and play a prominent role in mediating TMZ resistance in GCSCs.

4.1.5 Glioma Cancer Stem Cells and Notch Signalling

The Notch signalling pathway is evolutionary conserved in all metazoans and plays a critical role in embryonic development and organogenesis. The pathway is commonly known for the maintenance and proliferation of adult NSCs within the neurogenic niche of the subventricular zone, and Notch signalling is also implicated in the proliferation of GCSCs (377). The pathway suppresses both neurogenesis and

gliogenesis by targeting the expression of basic helix-loop-helix (bHLH) transcription repressor proteins Hes1-7 and Hey1, 2, and L, which in turn, maintain the self-renewal of adult NSCs and GCSCs by suppressing the transcription of genes promoting differentiation (378). Conversely, other proteins of the Notch signalling pathway (e.g. Notch1, RBPJ/CSL, NICD1, γ-secretase complex etc.) are observed to be overexpressed in differentiated astrocytes and glioblastoma tumour cells (238-240). Many studies have shown Notch signalling promotes the self-renewal and survival of neural stem and progenitor cells, and blocks differentiation (296, 297). Conversely, withdrawal of Notch signalling leads to diminished progenitor cell pools and increased neuronal differentiation (296, 297).

The role of Notch signalling and GCSCs in glioblastoma treatment resistance and recurrence was examined by Gilbert *et al.* showing inhibition of Notch signalling with a GSI enhanced glioma treatment by inhibiting neurosphere repopulation of culture patient samples and xenograft recurrence in mice (197). Using a murine orthotopic mouse model, Chu *et al*. examined the effects of Notch inhibition on glioblastoma xenografts. Weekly treatment with the GIS MRK003 resulted in a significant inhibition of Notch signalling, tumour growth, CSC marker expression, and clonogenicity (304). A more recent study has shown Notch inhibition combined with the current standard of care (radiotherapy plus TMZ chemotherapy) has an anti-GCSC effect, providing an improved survival benefit in a glioblastoma orthotopic mouse model (255). A phase I clinical trial has recently assessed both the pharmacology and pharmacodynamics of the GSI MK-0752 in patients with solid tumours who had failed to respond to conventional therapy. Dose-dependent inhibition of Notch signalling by the GSI was observed. A complete response was seen in a patient with anaplastic astrocytoma, and

stable disease in 10 patients with glioblastoma. The study showed MK-0752 has a modest level of activity in glioma patients, and provides the first clinical evidence validating Notch signalling as a therapeutic target in glioblastomas (305).

Within a tumour, the numerous cellular components provide both physical and chemical cues which aid the maintenance of the GCSC population, induce cancer cell proliferation, and promote tumour heterogeneity (302). It has been identified that the fate of GCSCs is determined by paracrine or juxtacrine signalling from neighbouring cells (301). In malignant gliomas, GCSCs are often reported as being located in regions of hypoxia and perivascular areas. Zhu *et al* identified that, in perivascular areas, Notch ligands can increase the GCSC phenotype in neighbouring cancer cells, whilst also enhancing their capacity for self-renewal (303).

Both canonical and non-canonical Notch signalling have been implicated in shaping tumour-stromal interactions and regulating GCSC maintenance. Notch ligands expressed by endothelial cells have been known to influence Notch signalling and cell fate determination in neighbouring cancer cells by juxtacrine signalling (379). However, the exact mechanism this occurs remains to be elucidated. A recent study by Man *et al*. identified a novel mechanism by which Notch signalling regulates the fate of GCSCs. The study demonstrates how hypoxia induces the expression of Vasorin in GCSCs by the activation of a HIF-1α/STAT2 coactivator complex and Vasorin, in turn, stabilised Notch in the plasma membrane preventing it from ubiquitylation and lysosomal degradation by Numb. Therefore, Vasorin acts as a switch to augment Notch signalling under conditions of hypoxia (380).

Taken together, these studies highlight the importance of Notch signalling in GCSCs and response to treatment, however little is known about the importance of specific

Notch ligands in this setting. This chapter looks at the role DLL4- and JAG1-induced Notch signalling plays in GCSC self-renewal, GCSC resistance to TMZ chemotherapy, and if this resistance can be overcome by inhibition of Notch signalling.

4.2 Methods

The methods employed in this chapter involve the general culture of two glioblastoma cell lines (U87 and U251) and the CSC-5 glioma cancer stem cell line (Methods 2.2). The U87 and U251 cell lines were converted to neurosphere culture as described in Methods 2.2.7.2. These converted cultures were utilised in the neurosphere recovery assay developed by Gilbert *et al.* which measures neurosphere formation at three time points to assess the ability of the culture to repopulate following treatment (Methods 2.2.7.3). In brief, we assess the number of neurospheres formed shortly after single 25 nM DBZ/25 µM TMZ, and combination 25 nM DBZ and 25 µM TMZ treatment (7 days). Second, the number of neurospheres that form during a one-week recovery period are counted (day 14). Finally, the neurospheres are dissociated and the number of secondary neurospheres that form are counted as a measure of self-renewal (day 21). We also determined the expression of the GCSC markers CD133, SOX2, and Nestin, alongside the expression of the neural lineage markers glial fibrillary acidic protein (GFAP), β-III-tubulin (TUBB3), and oligodendrocyte transcription factor 1 (OLIG1) by qPCR (Methods 2.6) at the three timepoints of the neurosphere recovery assay.

The CSC-5 glioma cancer stem line was transduced with mDLL4 and mJAG1 encoded retroviruses as described in Methods 2.4. Validation of DLL4 and JAG1 overexpression alongside analysis of Notch signalling target expression was confirmed by qPCR (Methods 2.6), Western Blotting (Methods 2.7), and IF analysis (Methods 2.8.2). The CSC-5 cell line overexpressing DLL4 and JAG1 was utilised in the neurosphere recovery assay and neurosphere recovery was assessed following single 25 nM DBZ/25 µM TMZ, and combination 25 nM DBZ and 25 µM TMZ treatment (Methods 2.2.7.3). We also determined the expression of the GCSC markers CD133, SOX2, and Nestin, alongside

the neural lineage markers GFAP, β-III-tubulin, and OLIG1 by both qPCR (Methods 2.6) and whole mount IF staining (Methods 2.8.2) at the three timepoints of the neurosphere recovery assay.

The CSC-5 cell line was subjected to shRNA knockdown of DLL4 and JAG1 as described in Methods 2.5. Validation of DLL4 and JAG1 shRNA knockdown alongside analysis of Notch signalling target expression was confirmed by qPCR (Methods 2.6) and Western Blotting (Methods 2.7). The CSC-5 DLL4 and JAG1 shRNA knockdown lines were utilised in the neurosphere recovery assay and neurosphere recovery was assessed following single 25 nM DBZ/25 μM TMZ, and combination 25 nM DBZ and 25 μM TMZ treatment (Methods 2.2.7.3).

Tables listing primers (Table 4.1), antibodies for Western Blotting (Table 4.2), and antibodies for IF (Table 4.3) used in this chapter are given below.

All data were presented as mean ± SD (unless otherwise stated) and analysed using GraphPad Prism (version 6.01, GraphPad Software Inc., San Diego, USA). The statistical test employed are described in the figure legend of each experiment.

Table 4.1: List of primers used in Chapter 4

Gene		Primer Sequence (5' →3')	Product size (bp)
CD133	Forward	CCTCTGGTGGGGTATTTCTT	210
	Reverse	CAGTTTCCGACTCCTTTTGA	
DLL4	Forward	ACAACTTGTCGGACTTCCAG	77
	Reverse	CAGCTCCTTCTTCTGGTTTG	
GAPDH	Forward	GACCCCTTCATTGACCTCAAC	134
	Reverse	TGGACTGTGGTCATGAGTCC	
GFAP	Forward	GAGCAGGAGGAGCGGCAC	164
	Reverse	TAGGTGGCGATCTCGATGTCC	
HES1	Forward	AGTGAAGCACCTCCGGAAC	107
	Reverse	CGTTCATGCACTCGCTGA	
HEY1	Forward	CGAGCTGGACGAGACCAT	76
	Reverse	GGAACCTAGAGCCGAACTCA	
HEY2	Forward	GTACCATCCAGCAGTGCATC	65
	Reverse	GGAACCTAGAGCCGAACTCA	
JAG1	Forward	TGGGCTTTGAGTGTGAGTGT	93
	Reverse	CCCCGTGGGAACAGTTATTA	
mDLL4	Forward	AGGTGCCACTTCGGTTACAC	62
	Reverse	GGGAGAGCAAATGGCTGATA	
mJAG1	Forward	TCTCTGACCCCTGCCATAAC	169
	Reverse	TTGAATCCATTCACCAGATCC	
NES	Forward	ATAGAGGGCAAAGTGGTAAGCAG	177
	Reverse	TTCTAGTGTCTCATGGCTCTGGTT	
OLIG1	Forward	GTCATCCTGCCCTACTCAGC	107
	Reverse	CTGCCCAGCAGTAGGATGTAG	
SOX2	Forward	GGGAAATGGGAGGGGTGCAAAAGAGG	151
	Reverse	TTGCGTGAGTGTGGATGGGATTGGTG	
TUBB3	Forward	CCAAGGGTCACTACACGGAG	187
	Reverse	ATGATGCGGTCGGGATACTC	

Table 4.2: List of primary and secondary antibodies used for Western Blotting in Chapter 4.

Primary Antibodies					
Name	**Species**	**Molecular Weight (kDa)**	**Supplier**	**Product Code**	**Dilution**
Anti-β-tubulin	Mouse	51	ThermoFisher Scientific	MA5-16308	1:2000
Anti-Cleaved Notch-1 (NICD)	Rabbit	120	Cell Signalling Technology	4147	1:1000
Anti-DLL4	Rabbit	74	Abcam	AB7280	1:1000
Anti-GAPDH (GA1R)	Mouse	37	ThermoFisher Scientific	MA5-15738	1:2000
Anti-HES1	Rabbit	30	Cell Signalling Technology	11988	1:1000
Anti-JAG1 (28H8)	Rabbit	180	Cell Signalling Technology	2620	1:1000

Secondary Antibodies				
Name	**Species**	**Supplier**	**Product Code**	**Dilution**
Anti-rabbit IgG HRP conjugate	Goat	ThermoFisher Scientific	65-6120	1:5000
Anti-mouse IgG HRP conjugate	Goat	ThermoFisher Scientific	31430	1:5000

Table 4.3: List of primary and secondary antibodies used for Immunofluorescence in Chapter 4.

Primary Antibodies					
Name	**Species**	**Supplier**	**Product Code**	**Dilution**	**Whole Mount Staining Dilution**
Anti-β-III-tubulin	Mouse	R&D Systems	MAB1195	N/A	1:250
Anti-CD133 (W6B3C1)	Mouse	Miltenyi Biotec	130-092-395	N/A	1:50
Anti-DLL4	Rabbit	Abcam	AB7280	1:1000	1:250
Anti-GFAP (28H8)	Mouse	Sigma Aldrich	G3893	N/A	1:250
Anti-JAG1	Rabbit	Cell Signalling Technology	2620S	1:1000	1:250
Anti-Ki67	Rabbit	Abcam	AB15580	1:2000	1:1000
Anti-Nestin	Rabbit	Sigma Aldrich	N5413	N/A	1:250
Anti-SOX2	Rabbit	Abcam	AB97959	N/A	1:250
Anti-SOX10	Mouse	R&D Systems	MAB2864	N/A	1:250

Secondary Antibodies				
Name	**Species**	**Supplier**	**Product Code**	**Dilution**
Anti-mouse IgG Alexa Fluor 568	Donkey	ThermoFisher Scientific	A10037	1:5000
Anti-rabbit IgG Alexa Fluor 647	Goat	ThermoFisher Scientific	A21245	1:1000

4.3 Results

4.3.1 DLL4 and JAG1-induced Notch signalling regulates the self-renewal of U87 and U251 glioblastoma neurospheres *in vitro*

In order to assess the effect of DLL4 and JAG1 on GCSC self-renewal, U87 and U251 glioblastoma cell lines were converted to neurosphere culture by culturing in CSC medium containing N2 supplement, EGF, and FGF. These converted cultures were then utilised in a neurosphere recovery assay to assess the capacity of tumour cells to repopulate following treatment at three time points. First, we assessed the ability of the cells to form neurospheres one week after treatment (primary neurosphere formation). Second, we counted the number of neurospheres that formed during a one-week recovery period (neurosphere recovery). Finally, we dissociated the neurospheres to single cells and counted the number of neurospheres that formed as a measure of self-renewal (secondary neurosphere formation). This assay provides a quantitative way to assess culture repopulation following drug treatment (See Figure 2.2, Chapter 2: Materials and Methods).

4.3.1.1 Primary Neurosphere Formation

4.3.1.1.1 U87 Cell Line

In the U87 cell line, overexpression of both DLL4 and JAG1 increased the number of neurospheres formed compared to U87-EV control (Figure 4.2). Administration of the Notch inhibitor DBZ resulted in a significant decrease in the number of neurospheres formed by 31.2%, 59.6% and 53.5% respectively for U87-EV, U87-mDLL4, and U87-mJAG1 compared to DMSO control. Similarly, TMZ treatment also reduced the number of neurosphere formed by 27.6%, 21.0%, and 35.3% respectively, for U87-EV, U87-

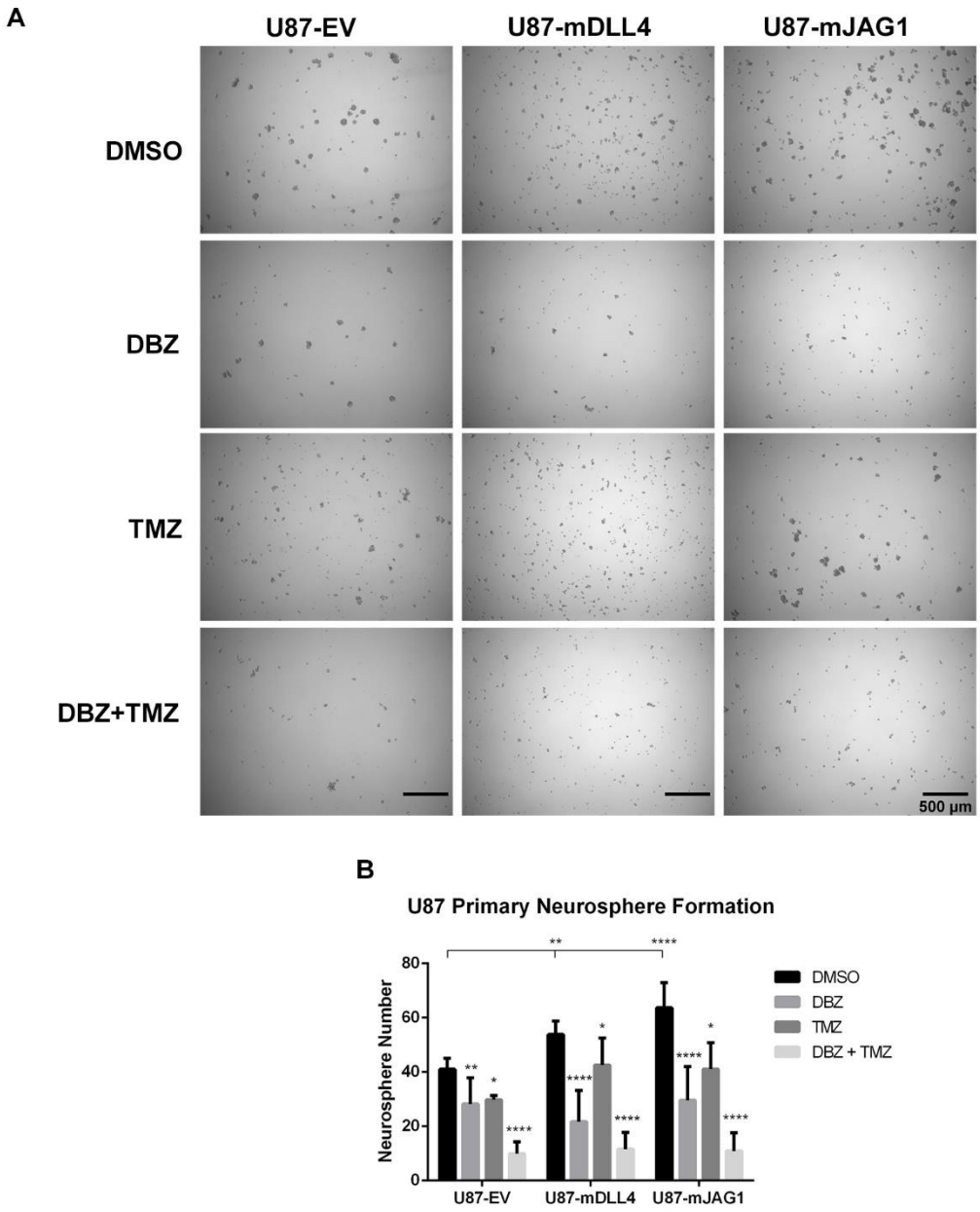

Figure 4.2: DLL4- and JAG1-induced Notch signalling regulates U87 primary neurosphere formation.

U87 cells (12,000 per well in a 6-well plate) were cultured in CSC medium and immediately treated with single 25 nM DBZ/25 µM TMZ, combination 25 nM DBZ and 25 µM TMZ, or DMSO control treatment. Primary neurosphere formation was assessed 7 days after seeding. **(A)** Images showing U87 primary neurosphere formation following single (DBZ/TMZ) and combination (DBZ and TMZ) treatment. **(B)** Quantification of the number of U87 primary neurospheres formed following 7 days treatment. Scale bar = 500 µm. (Mean ± SD, n = 3, two-way ANOVA with Dunnett's post-hoc test, * $p < 0.05$, ** $p < 0.01$, and **** $p < 0.0001$).

mDLL4, and U87-JAG1 compared to DMSO control. However, combination TMZ and DBZ treatment resulted in the most significant decrease in primary neurosphere formation: 75.9%, 78.6%, and 82.9% respectively for U87-EV. U87-mDLL4, and U87-mJAG1 compared to DMSO control.

4.3.1.1.2 U251 Cell Line

Like the U87 cell line, overexpression of both DLL4 and JAG1 in U251 cells resulted in an increase in the number of neurospheres formed compared to U251-EV control (Figure 4.3). DBZ treatment resulted in a significant decrease in the number of neurospheres formed by 36.6%, 56.6%, and 55.6% respectively for U251-EV, U251-mDLL4, and U251-mJAG1 compared to DMSO control. However, TMZ treatment only slightly reduced the number of neurosphere formed by 2.0%, 23.7%, and 18.5% respectively, for U251-EV, U251-mDLL4, and U251-JAG1 compared to DMSO control. However, combination TMZ and DBZ treatment resulted in the most significant decrease in primary neurosphere formation: 79.8%, 86.8%, and 89.2% respectively for U87-EV. U87-mDLL4, and U87-mJAG1 compared to DMSO control.

4.3.1.2 Neurosphere Recovery

4.3.1.2.1 U87 Cell Line

To determine if DBZ enhances TMZ therapy, we examined the effect of combined treatment on neurosphere recovery following treatment. In the U87 cell line, overexpression of both DLL4 and JAG1 again increased the neurosphere number compared to U87-EV control (Figure 4.4). Recovery following DBZ treatment resulted in a significant decrease in the number of neurospheres recovered by 41.3%, 45.1%, and 53.0% respectively for U87-EV, U87-mDLL4, and U87-mJAG1 compared to DMSO

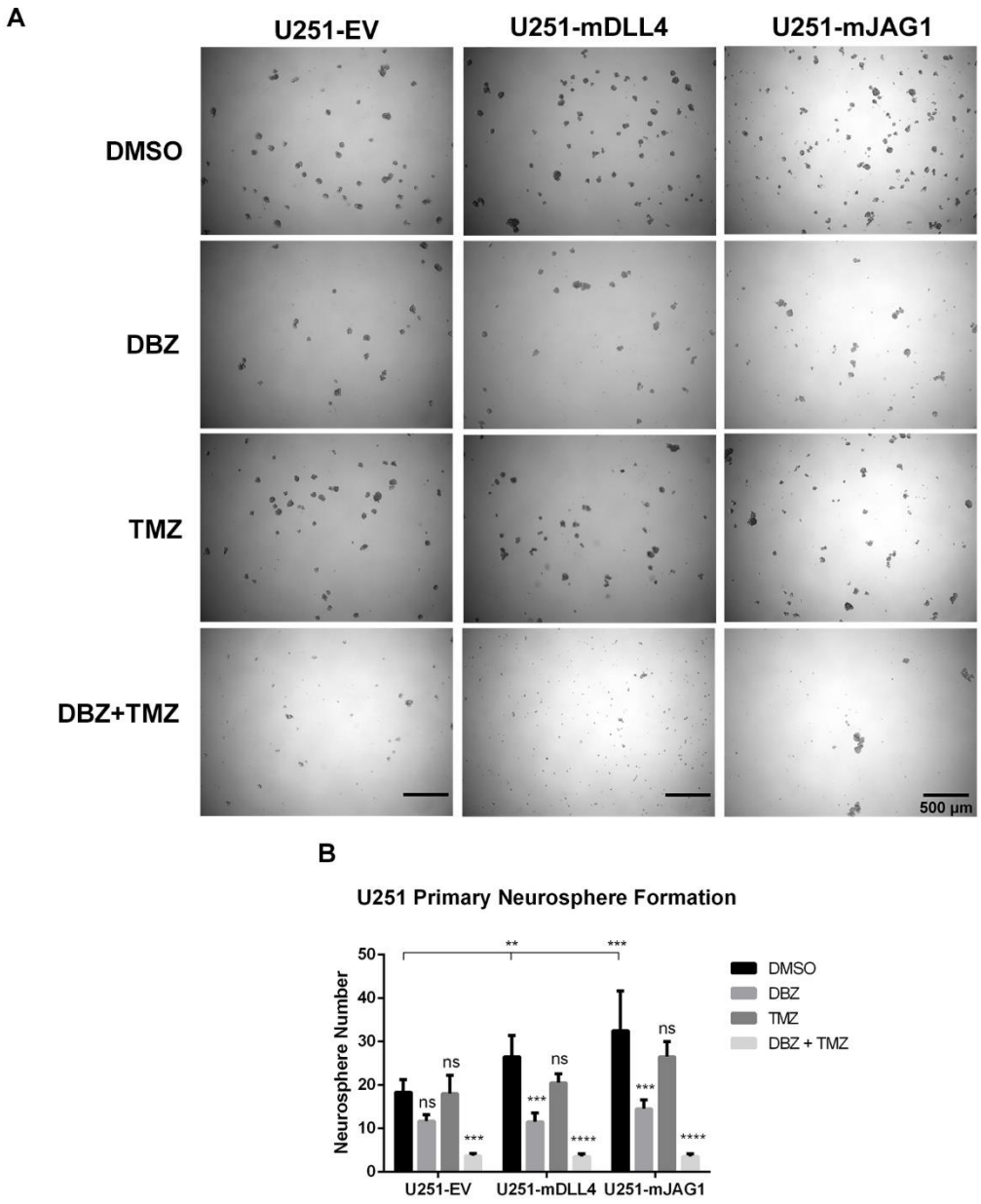

Figure 4.3: DLL4- and JAG1-induced Notch signalling regulates U251 primary neurosphere formation.

U251 cells (12,000 per well in a 6-well plate) were cultured in CSC medium and immediately treated with single 25 nM DBZ/25 µM TMZ, combination 25 nM DBZ and 25 µM TMZ, or DMSO control treatment. Primary neurosphere formation was assessed 7 days after seeding. **(A)** Images showing U251 primary neurosphere formation following single (DBZ/TMZ) and combination (DBZ and TMZ) treatment. **(B)** Quantification of the number of U251 primary neurospheres formed following 7 days treatment. Scale bar = 500 µm. (Mean ± SD, n = 3, two-way ANOVA with Dunnett's post-hoc test, ** $p < 0.01$, *** $p < 0.001$, **** $p < 0.0001$, and ns denotes not significant).

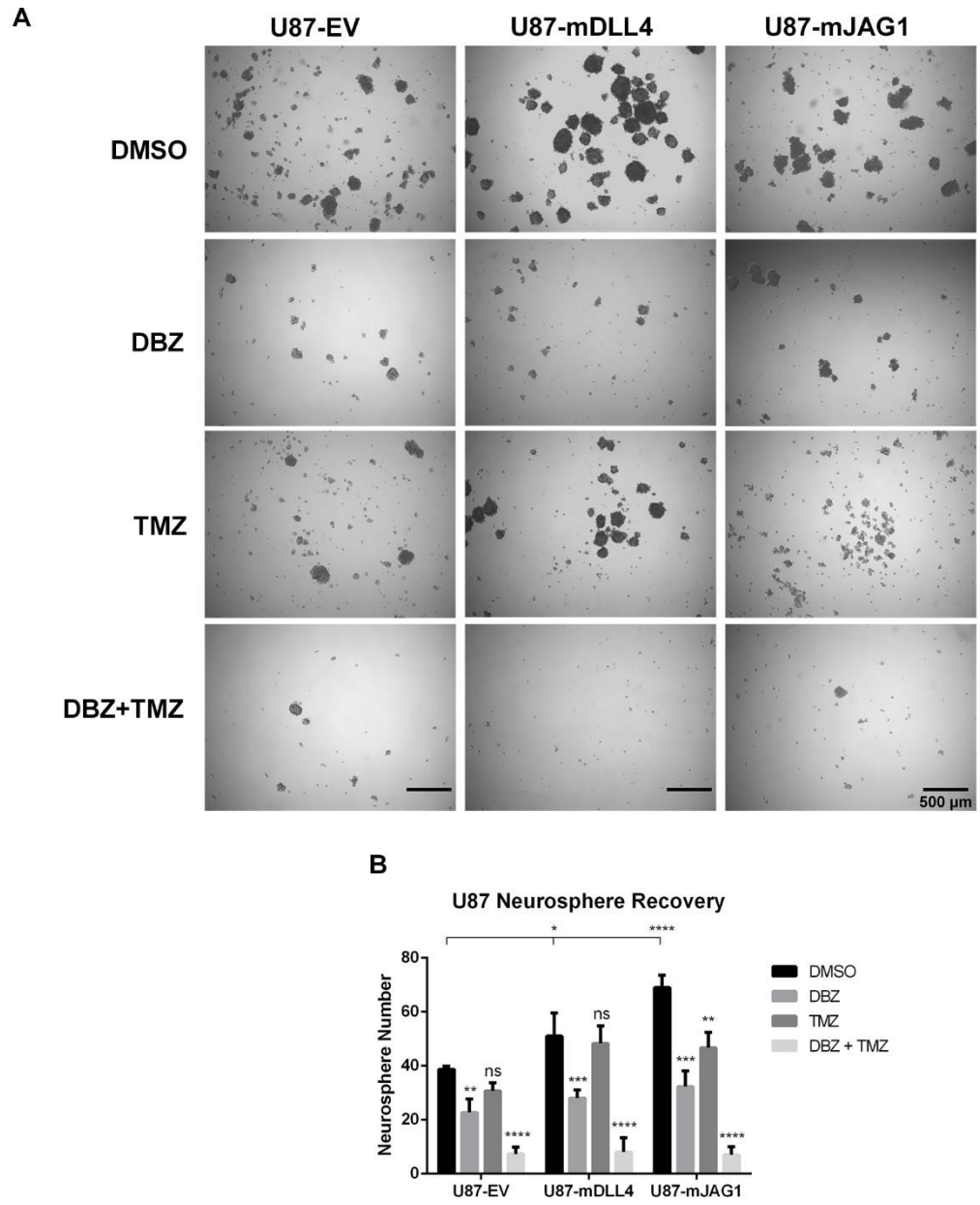

Figure 4.4: DBZ and TMZ combination treatment significantly reduces U87 neurosphere recovery.

U87 cells (12,000 per well in a 6-well plate) were cultured in CSC medium and immediately treated with single 25 nM DBZ/25 µM TMZ, combination 25 nM DBZ and 25 µM TMZ, or DMSO control treatment. Primary neurosphere formation was assessed 7 days after seeding. Following addition of fresh CSC media and a further week in culture, neurosphere recovery was assessed at day 14. **(A)** Images showing U87 neurosphere recovery following single (DBZ/TMZ) and combination (DBZ and TMZ) treatment. **(B)** Quantification of U87 neurosphere recovery. Scale bar = 500 µm. (Mean ± SD, n = 3, two-way ANOVA with Dunnett's post-hoc test, * $p < 0.05$, ** $p < 0.01$, *** $p < 0.001$, **** $p < 0.0001$, and ns denotes not significant).

control. However, combination DBZ and TMZ treatment resulted in the most significant decrease in neurosphere recovery, reducing recovery by 81.1%, 84.3%, and 89.9% respectively, for U87-EV, U87-mDLL4, and U87-JAG1 compared to DMSO control.

4.3.1.2.2 U251 Cell Line

Similar to the U87 cell line, overexpression of both DLL4 and JAG1 increased the neurosphere number compared to U87-EV control (Figure 4.5). Recovery following DBZ treatment resulted in a significant decrease is neurosphere recovery by 41.3%, 45.1%, and 53.0% respectively U87-EV, U87-mDLL4, and U87-mJAG1 compared to DMSO control. TMZ treatment also slightly reduced neurosphere recovery by 26.6%, 38.3%, and 40.0% respectively, for U87-EV, U87-mDLL4, and U87-JAG1 compared to DMSO control. Combination DBZ and TMZ resulted in the largest decrease in neurosphere recovery, reducing the neurosphere number by 84.9%, 92.9%, and 80.5%, respectively, for U87-EV, U87-mDLL4, and U87-JAG1 compared to DMSO control.

4.3.1.3 Secondary Neurosphere Formation

4.3.1.3.1 U87 Cell Line

The final part of the neurosphere assay assesses secondary neurosphere formation following dissociation to single cells as a measure of self-renewal. Overexpression of DLL4 and JAG1 in the U87 cell line resulted in increased U87 secondary neurosphere formation compared to U87-EV control (Figure 4.6). Treatment with DBZ significantly reduced U87 neurosphere recovery, reducing the neurosphere number by 22.4%, 47.4%, and 47.0%, respectively, for U87-EV, U87-mDLL4, and U87-JAG1 compared to DMSO control. TMZ treatment had little effect on secondary neurosphere formation, reducing the number of neurospheres by 24.6%, 10.2%, and 7.8% respectively for U87-

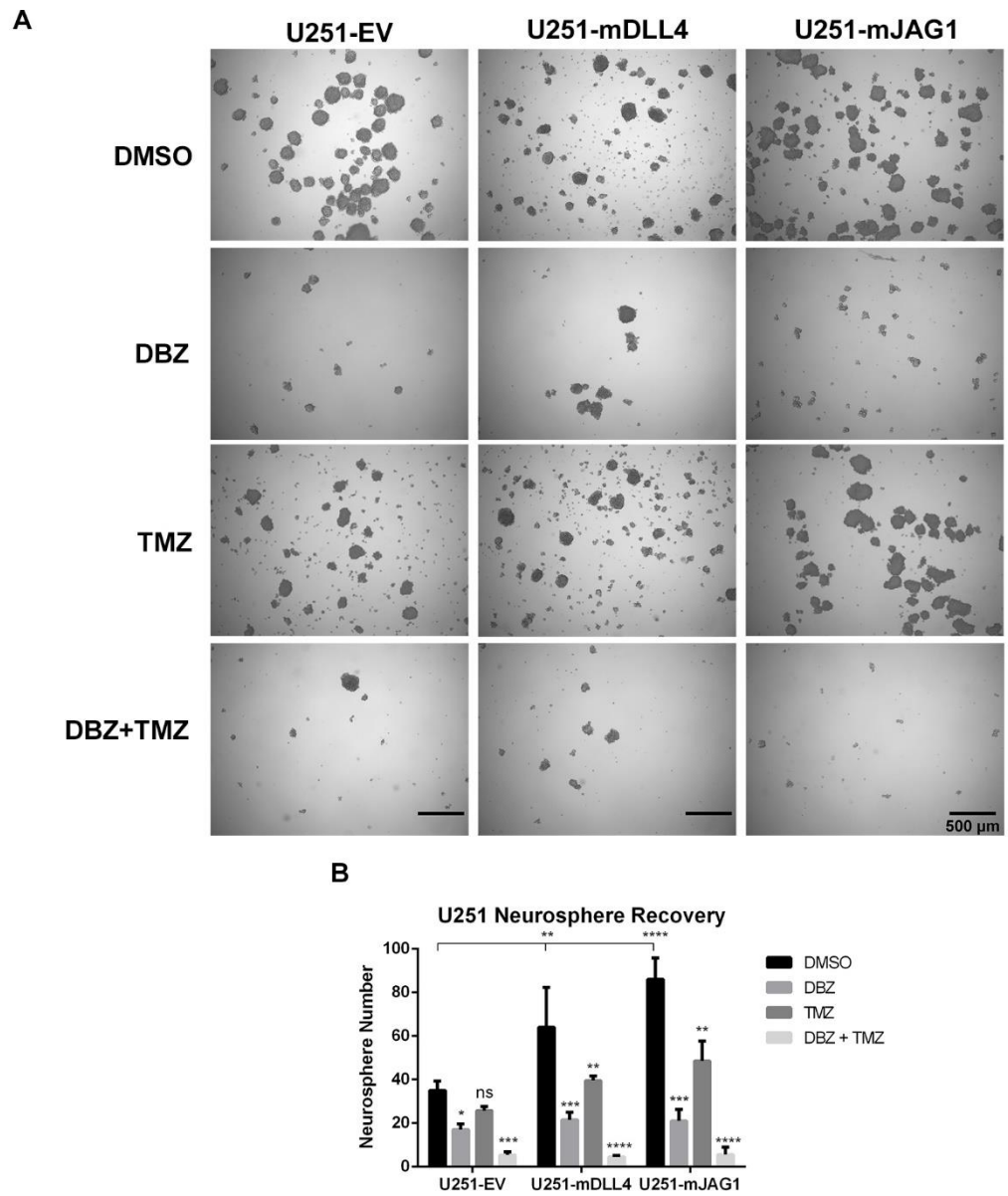

Figure 4.5: DBZ and TMZ combination treatment significantly reduces U251 neurosphere recovery.

U251 cells (12,000 per well in a 6-well plate) were cultured in CSC medium and immediately treated with single 25 nM DBZ/25 µM TMZ, combination 25 nM DBZ and 25 µM TMZ, or DMSO control treatment. Primary neurosphere formation was assessed 7 days after seeding. Following addition of fresh CSC media and a further week in culture, neurosphere recovery was assessed at day 14. **(A)** Images showing U251 neurosphere recovery following single (DBZ/TMZ) and combination (DBZ and TMZ) treatment. **(B)** Quantification of U251 neurosphere recovery. Scale bar = 500 µm. (Mean ± SD, n = 3, two-way ANOVA with Dunnett's post-hoc test, * $p < 0.05$, ** $p < 0.01$, *** $p < 0.001$, **** $p < 0.0001$, and ns denotes not significant).

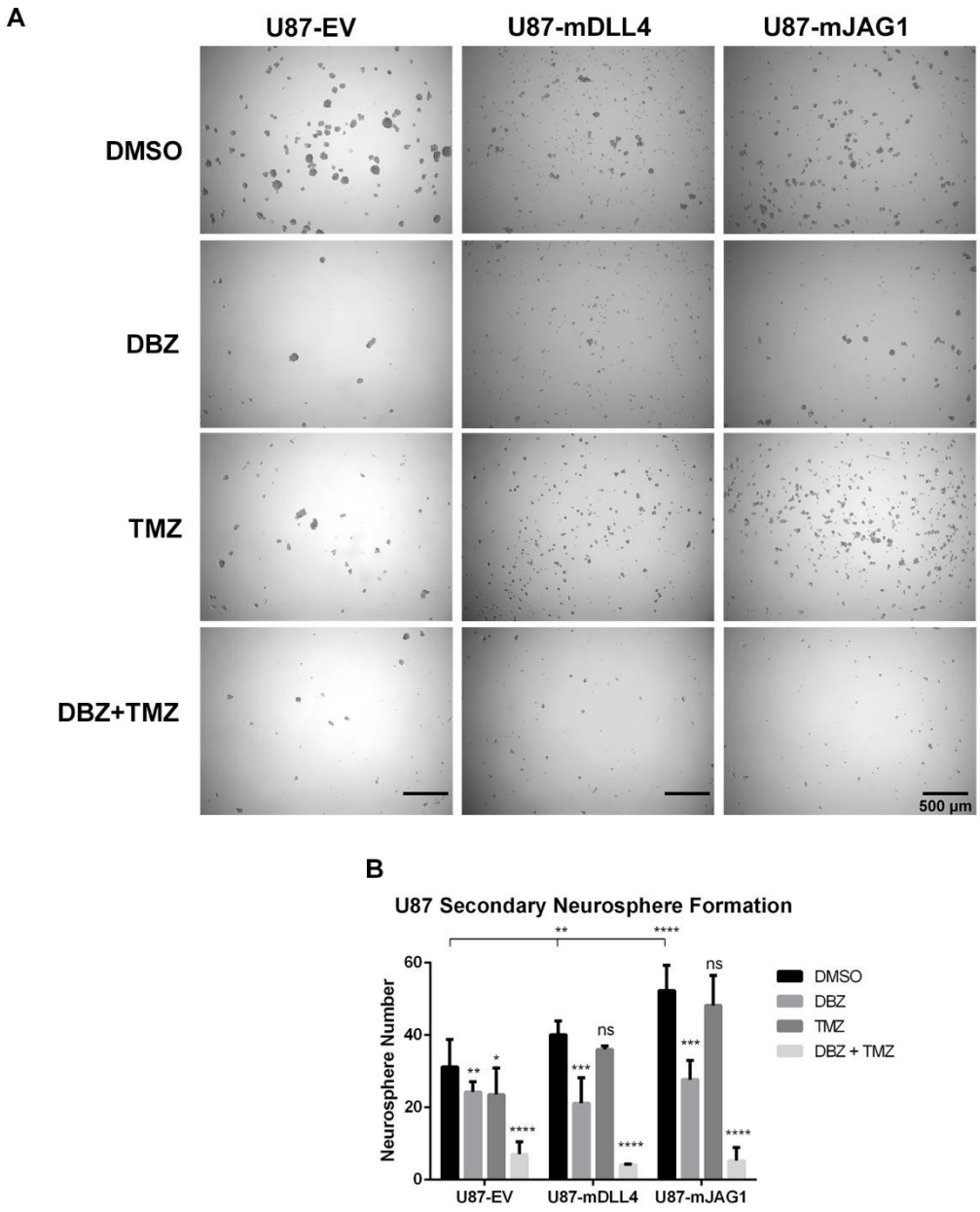

Figure 4.6: DBZ and TMZ combination treatment significantly reduces U87 secondary neurosphere formation.

U87 cells (12,000 per well in a 6-well plate) were cultured in CSC medium and immediately treated with single 25 nM DBZ/25 µM TMZ, combination 25 nM DBZ and 25 µM TMZ, or DMSO control treatment. Primary neurosphere formation was assessed 7 days after seeding. Following addition of fresh CSC media and a further week in culture, neurosphere recovery was assessed at day 14. Neurospheres were then dissociated to single cells and re-seeded (12,000 cells per well in a 6-well plate). At day 21, the number of secondary neurospheres formed were counted as a measure of self-renewal. **(A)** Images showing U87 secondary neurosphere formation following single (DBZ/TMZ) and combination (DBZ and TMZ) treatment and dissociation to single cells. **(B)** Quantification of U87 secondary neurosphere formation. Scale bar = 500 µm. (Mean ± SD, n = 3, two-way ANOVA with Dunnett's post-hoc test, * $p < 0.05$, ** $p < 0.01$, *** $p < 0.001$, **** $p < 0.0001$, and ns denotes not significant).

-EV, U87-mDLL4, and U87-JAG1 compared to DMSO control. Of note, TMZ had no significant effect in reducing secondary neurosphere formation for the U87 neurospheres overexpressing DLL4 and JAG1, suggesting DLL4- and JAG1-induced Notch signalling plays a role in mediating TMZ resistance. Combination DBZ and TMZ treatment resulted in a significant reduction in secondary neurosphere formation, reducing the neurosphere number by 77.6%, 89.8%, and 90.0% respectively, U87-EV, U87-mDLL4, and U87-JAG1 compared to DMSO control.

4.3.1.3.2 U251 Cell Line

Like the U87 cell line, overexpression of both DLL4 and JAG1 increased the neurosphere number compared to U87-EV control (Figure 4.7). Secondary neurosphere formation following DBZ treatment resulted in a significant decrease is neurosphere number by 55.6%, 80%, and 78% respectively U251-EV, U251-mDLL4, and U251-mJAG1 compared to DMSO control. TMZ treatment also slightly reduced secondary neurosphere formation by 33.3%, 40.0%, and 40.0% respectively, for U251-EV, U251-mDLL4, and U251-JAG1 compared to DMSO control. However, combination DBZ and TMZ treatment resulted in the most significant decrease in secondary neurosphere formation, reducing the neurosphere number by 88.8%, 93.5%, and 90.0%, respectively, for U251-EV, U251-mDLL4, and U251-JAG1 compared to DMSO control. Taken together these results suggest combination DBZ and TMZ treatment significantly inhibits neurosphere self-renewal compared to DBZ/TMZ treatment alone in neurospheres overexpressing DLL4 and JAG1.

4.3.2 DLL4 and JAG1 Increase Glioma Cancer Stem Cell Marker Expression

In order to assess the effect of DLL4 and JAG1 overexpression alongside single and combination treatments on cellular differentiation, we determined the expression of

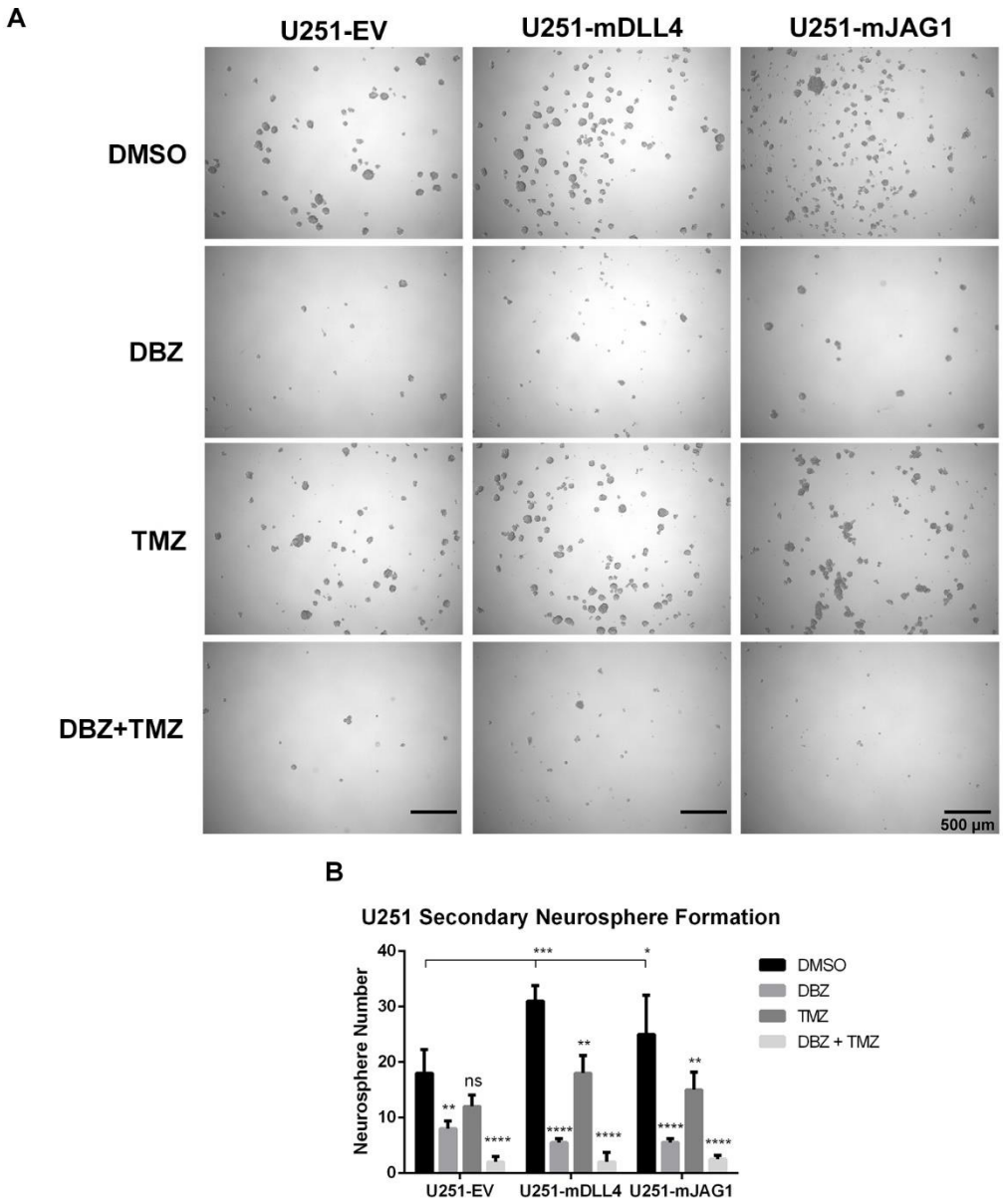

Figure 4.7: DBZ and TMZ combination treatment significantly reduces U251 secondary neurosphere formation.

U251 cells (12,000 per well in a 6-well plate) were cultured in CSC medium and immediately treated with single 25 nM DBZ/25 µM TMZ, combination 25 nM DBZ and 25 µM TMZ, or DMSO control treatment. Primary neurosphere formation was assessed 7 days after seeding. Following addition of fresh CSC media and a further week in culture, neurosphere recovery was assessed at day 14. Neurospheres were then dissociated to single cells and re-seeded (12,000 cells per well in a 6-well plate). At day 21, the number of secondary neurospheres formed were counted as a measure of self-renewal. **(A)** Images showing U251 secondary neurosphere formation following single (DBZ/TMZ) and combination (DBZ and TMZ) treatment and dissociation to single cells. **(B)** Quantification of U251 secondary neurosphere formation. Scale bar = 500 µm. (Mean ± SD, n = 3, two-way ANOVA with Dunnett's post-hoc test, * $p < 0.05$, ** $p < 0.01$, *** $p < 0.001$, **** $p < 0.0001$, and ns denotes not significant).

key GCSC markers and neural lineage markers by qPCR at the three timepoints of the neurosphere recovery assay. CD133, SOX2, and Nestin are three common markers used to define GCSCs, whilst GFAP (astrocytes) (381), TUBB3 (neurons) (382), and OLIG1 (oligodendrocytes) (383) are markers of neural differentiation.

4.3.2.1 Primary Neurosphere Formation

Overexpression of DLL4 and JAG1 resulted in increased mRNA expression of all three GCSC markers (*CD133, SOX2*, and *NES*) following U87 primary neurosphere formation, and the expression of these markers is further increased upon TMZ treatment. GCSC marker expression is significantly reduced upon single DBZ and combination DBZ and TMZ treatment (Figure 4.8A-C). Conversely, expression of the neural lineage markers *GFAP*, *TUBB3*, and *OLIG1* are increased following DBZ treatment of U87 neurospheres, and may be the result of GCSC differentiation (Figure 4.8D-F).

Results for U251 primary neurosphere formation also show overexpression of DLL4 and JAG1 results in increased expression of all three GCSC markers, and the expression of these markers is further increased following TMZ treatment. Like the U87 cell line, mRNA expression of GCSC markers is significantly reduced upon single DBZ and combination DBZ and TMZ treatment (Figure 4.9A-C). mRNA expression of the neural lineage markers *GFAP*, *TUBB3*, and *OLIG1* are unaltered following DLL4 and JAG1 overexpression, however their expression are increased following DBZ treatment of U251 neurospheres (Figure 4.9D-F), suggesting inhibition of Notch signalling results in differentiation of GCSCs and DLL4 and JAG1 play a role in maintaining the GCSC phenotype in both U87 and U251 neurospheres.

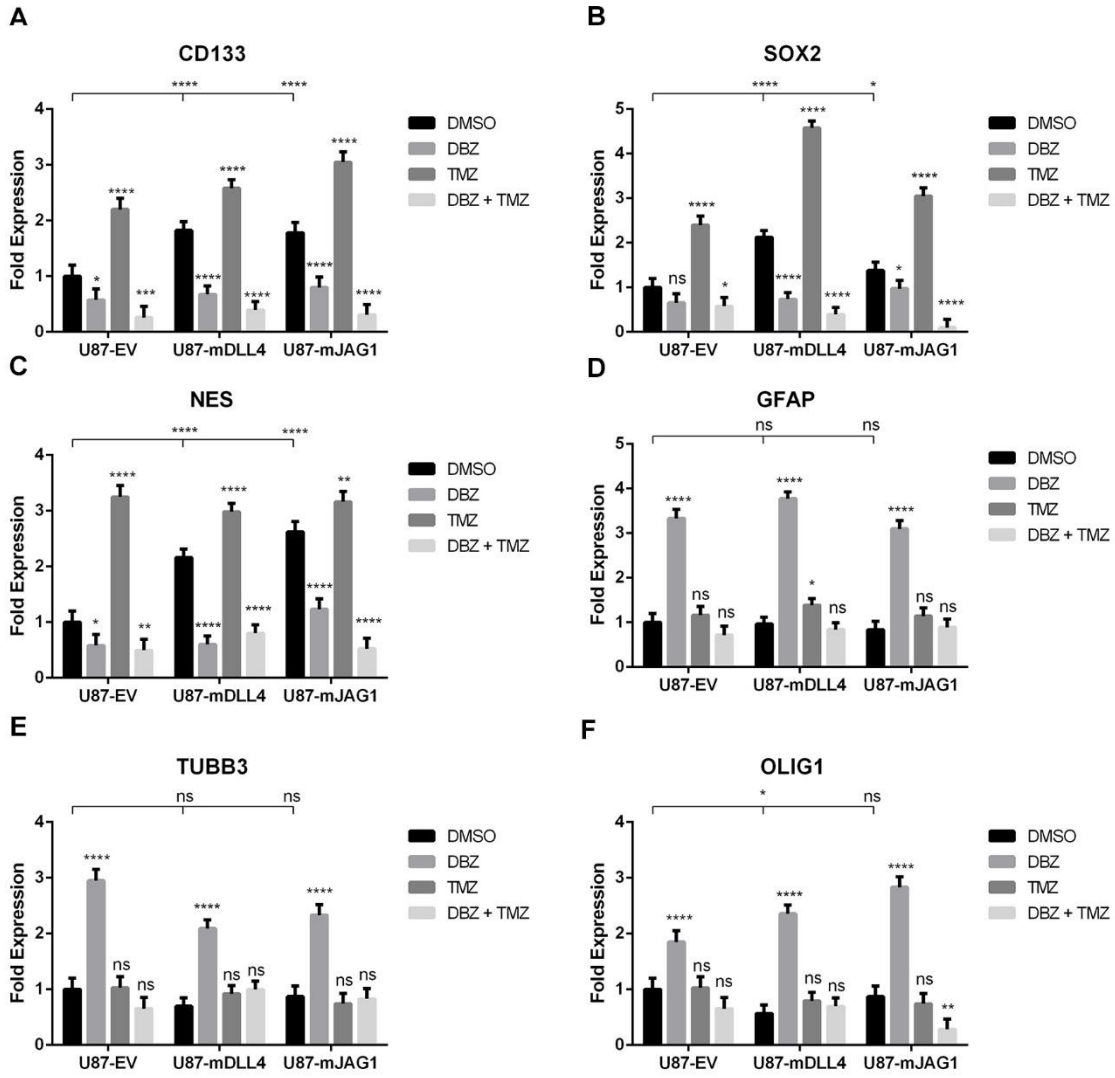

Figure 4.8: DLL4 and JAG1 increase GCSC marker expression in U87 primary neurospheres which is reversed upon combination DBZ and TMZ treatment.

U87 cells (12,000 per well in a 6-well plate) were cultured in CSC medium and immediately treated with single 25 nM DBZ/25 µM TMZ, combination 25 nM DBZ and 25 µM TMZ, or DMSO control treatment. RNA was extracted 7 days after seeding following primary neurosphere formation. mRNA expression of the GCSC markers **(A)** *CD133*, **(B)** *SOX2*, and **(C)** *NES*, and the neural lineage markers **(D)** *GFAP*, **(E)** *TUBB3*, and **(F)** *OLIG1* was determined by qPCR normalised to *GAPDH*. (Mean ± SEM, n = 3, two-way ANOVA with Dunnett's post-hoc test, * $p < 0.05$, ** $p < 0.01$, *** $p < 0.001$, **** $p < 0.0001$, and ns denotes not significant).

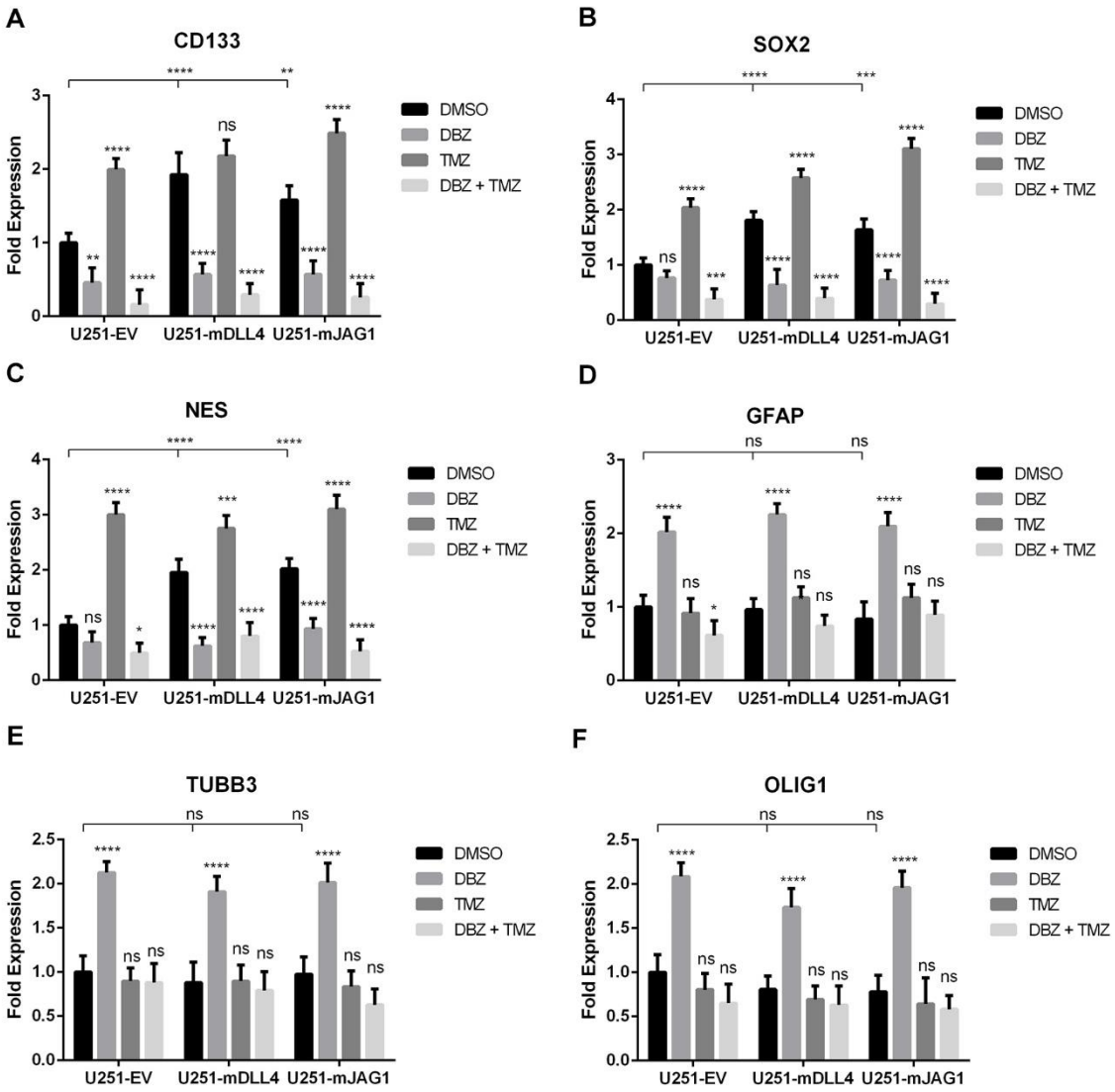

Figure 4.9: DLL4 and JAG1 increase GCSC marker expression in U251 primary neurospheres which is reversed upon combination DBZ and TMZ treatment.

U251 cells (12,000 per well in a 6-well plate) were cultured in CSC medium and immediately treated with single 25 nM DBZ/25 µM TMZ, combination 25nM DBZ and 25 µM TMZ, or DMSO control treatment. RNA was extracted 7 days after seeding following primary neurosphere formation. mRNA expression of the GCSC markers **(A)** *CD133*, **(B)** *SOX2*, and **(C)** *NES*, and the neural lineage markers **(D)** *GFAP*, **(E)** *TUBB3*, and **(F)** *OLIG1* was determined by qPCR normalised to *GAPDH*. (Mean ± SEM, n = 3, two-way ANOVA with Dunnett's post-hoc test, * $p < 0.05$, ** $p < 0.01$, *** $p < 0.001$, **** $p < 0.0001$, and ns denotes not significant).

4.3.2.2 Neurosphere Recovery

Similar results were obtained following U87 neurosphere recovery. DLL4 and JAG1 increased GCSC marker mRNA expression, and this expression is further increased upon TMZ treatment. However, single DBZ and combination DBZ and TMZ treatment significantly reduces GCSC marker expression (Figure 4.10A-C). mRNA expression of the neural lineage markers *GFAP*, *TUBB3*, and *OLIG1* are unaltered following DLL4 and JAG1 overexpression, however their expression are significantly increased following DBZ treatment whilst single TMZ and combination DBZ and TMZ treatment has no effect (Figure 4.10D-F).

Results for U251 neurosphere recovery again suggest overexpression of DLL4 and JAG1 increases the mRNA expression of all three GCSC markers, and the expression of these markers is increased following TMZ treatment. Similar to the U87 cell line, mRNA expression of GCSC markers is significantly reduced upon single DBZ and combination DBZ and TMZ treatment (Figure 4.11A-C). mRNA expression of the neural lineage markers *GFAP*, *TUBB3*, and *OLIG1* are unaltered following DLL4 and JAG1 overexpression, however their expression are increased in U251 DBZ-treated recovered neurospheres (Figure 4.11D-F).

4.3.2.3 Secondary Neurosphere Formation

Following the dissociation of neurospheres to single cells and subsequent secondary neurosphere formation, similar results were obtained as above. Overexpression of DLL4 and JAG1 resulted in increased expression of all three GCSC markers following U87 secondary neurosphere formation, and the expression of these markers is further increased following TMZ treatment. GCSC marker mRNA expression is significantly reduced in neurospheres treated with single DBZ and combination DBZ and TMZ

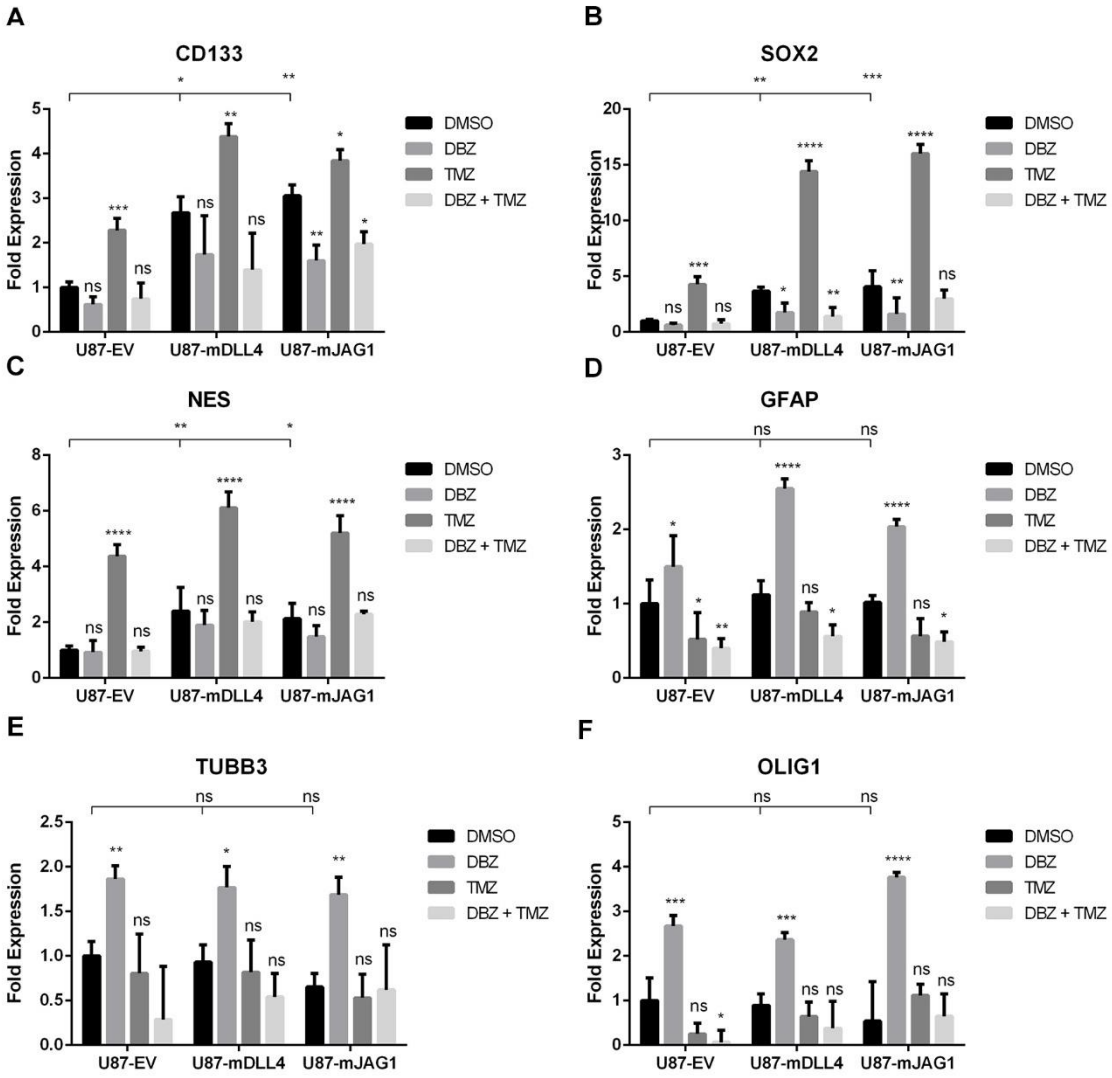

Figure 4.10: DLL4 and JAG1 increase GCSC marker expression in recovered U87 neurospheres which is reversed upon combination DBZ and TMZ treatment.

U87 cells (12,000 per well in a 6-well plate) were cultured in CSC medium and immediately treated with single 25 nM DBZ/25 µM TMZ, combination 25 nM DBZ and 25 µM TMZ, or DMSO control treatment. Primary neurosphere formation was assessed 7 days after seeding. Following addition of fresh CSC media and a further week in culture, neurosphere recovery was assessed at day 14 and RNA was extracted. mRNA expression of the GCSC markers **(A)** *CD133*, **(B)** *SOX2*, and **(C)** *NES*, and the neural lineage markers **(D)** *GFAP*, **(E)** *TUBB3*, and **(F)** *OLIG1* was determined by qPCR normalised to *GAPDH*. (Mean ± SEM, n = 3, two-way ANOVA with Dunnett's post-hoc test, * $p < 0.05$, ** $p < 0.01$, *** $p < 0.001$, **** $p < 0.0001$, and ns denotes not significant).

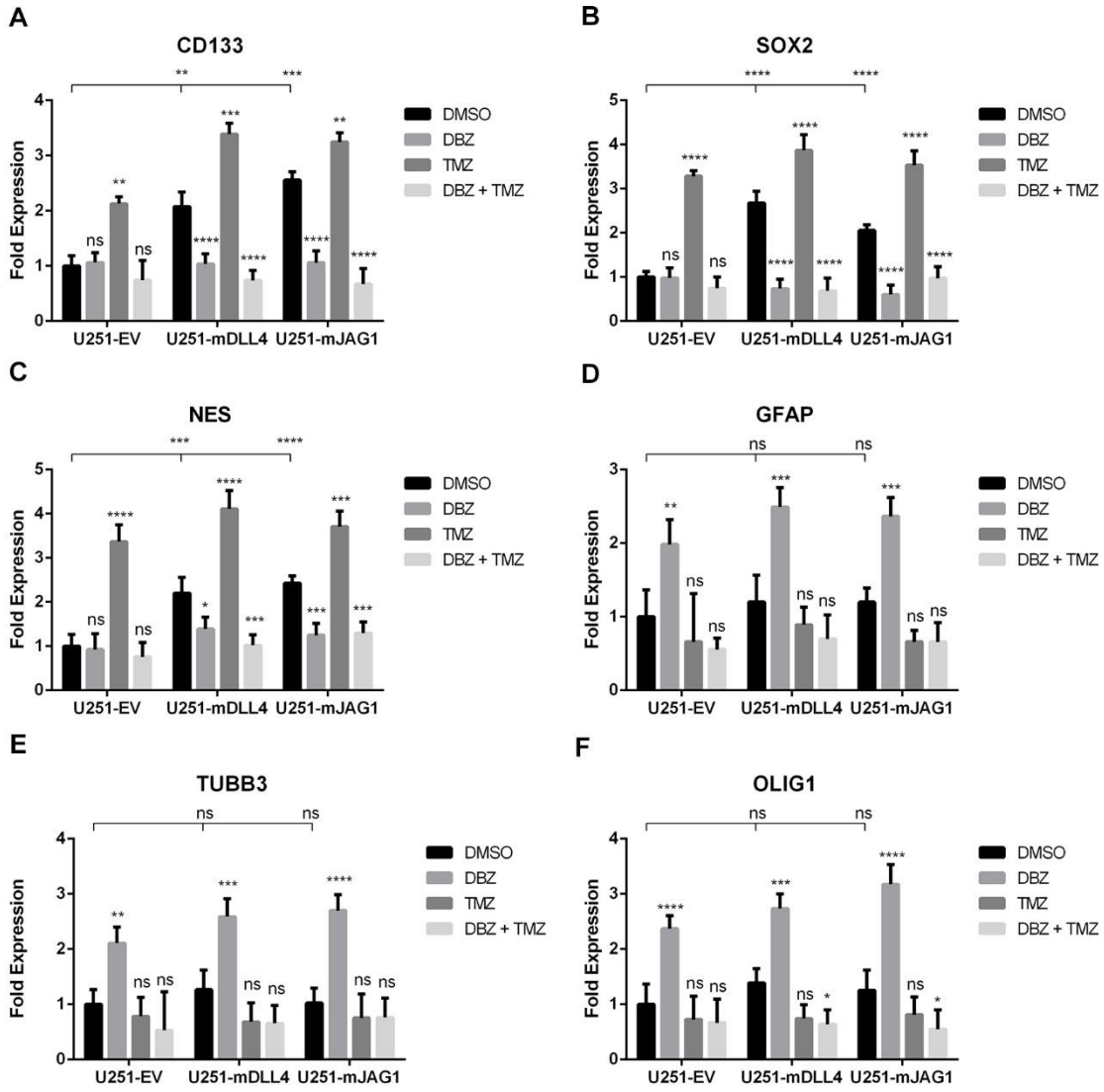

Figure 4.11: DLL4 and JAG1 increase GCSC marker expression in recovered U251 neurospheres which is reversed upon combination DBZ and TMZ treatment.

U251 cells (12,000 per well in a 6-well plate) were cultured in CSC medium and immediately treated with single 25 nM DBZ/25 µM TMZ, combination 25 nM DBZ and 25 µM TMZ, or DMSO control treatment. Primary neurosphere formation was assessed 7 days after seeding. Following addition of fresh CSC media and a further week in culture, neurosphere recovery was assessed at day 14 and RNA was extracted. mRNA expression of the GCSC markers **(A)** *CD133*, **(B)** *SOX2*, and **(C)** *NES*, and the neural lineage markers **(D)** *GFAP*, **(E)** *TUBB3*, and **(F)** *OLIG1* was determined by qPCR normalised to *GAPDH*. (Mean ± SEM, n = 3, two-way ANOVA with Dunnett's post-hoc test, * $p < 0.05$, ** $p < 0.01$, *** $p < 0.001$, **** $p < 0.0001$, and ns denotes not significant).

treatment (Figure 4.12A-C). Conversely, expression of the neural lineage markers *GFAP, TUBB3*, and *OLIG1* are increased following DBZ treatment of neurospheres (Figure 4.12D-F).

Results for U251 secondary neurosphere formation also show overexpression of DLL4 and JAG1 results in increased expression of all three GCSC markers, and the expression of these markers is significantly increased following TMZ treatment. Like the U87 cell line, mRNA expression of GCSC markers is also reduced upon single DBZ and combination DBZ and TMZ treatment (Figure 4.13A-C). mRNA expression of the neural lineage markers *GFAP*, *TUBB3*, and *OLIG1* are unaffected following DLL4 and JAG1 overexpression, however their expression are increased in DBZ treated U251 neurospheres (Figure 4.13D-F) suggesting inhibition of Notch signalling results in differentiation of GCSCs and DLL4 and JAG1 play a role in maintaining the GCSC phenotype. These results cement the key role played by the Notch signalling pathway in GCSCs.

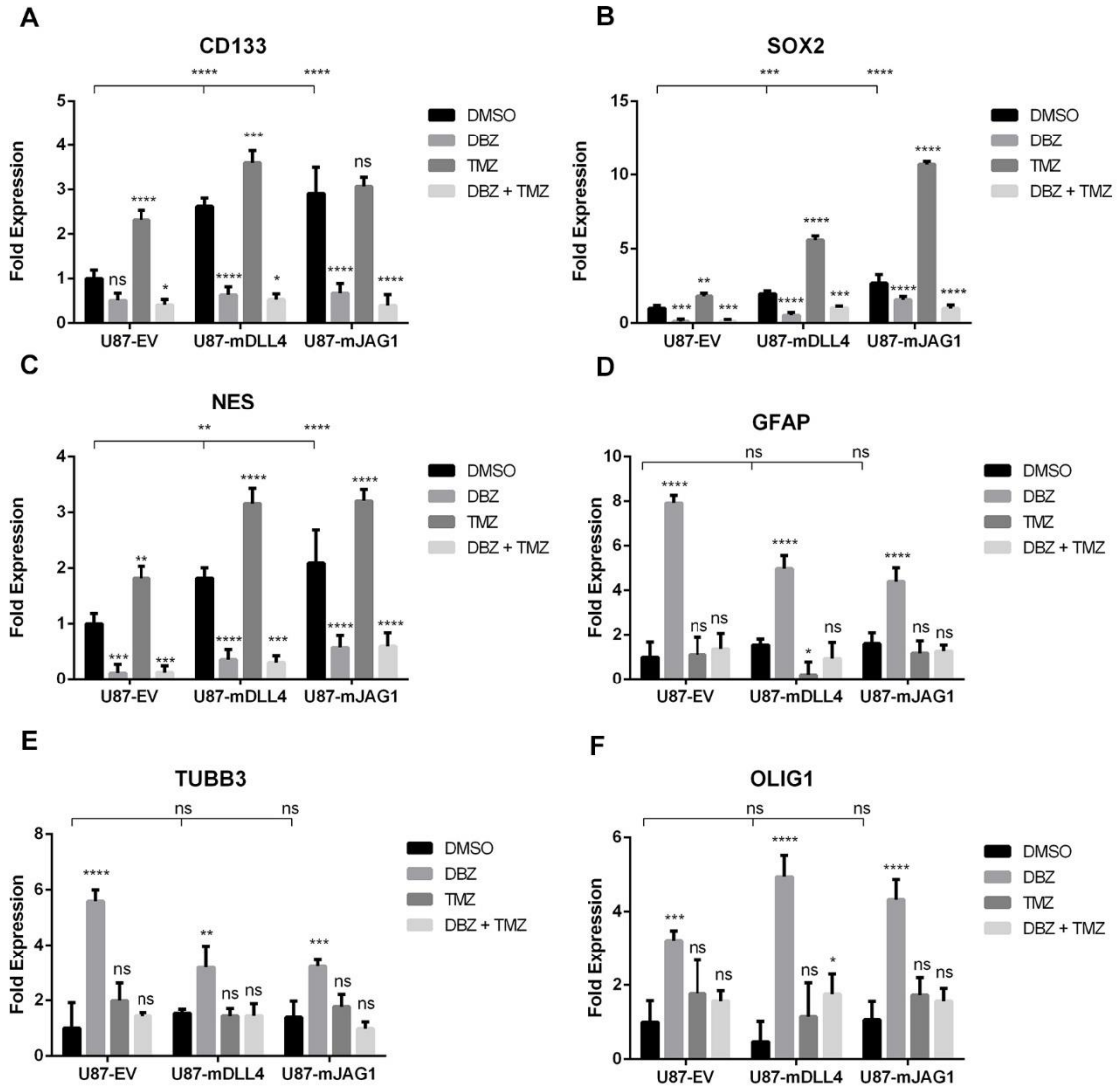

Figure 4.12: DLL4 and JAG1 increase GCSC marker expression in U87 secondary neurospheres which is reversed upon combination DBZ and TMZ treatment.

U87 cells (12,000 per well in a 6-well plate) were cultured in CSC medium and immediately treated with single 25 nM DBZ/25 µM TMZ, combination 25 nM DBZ and 25 µM TMZ, or DMSO control treatment. Primary neurosphere formation was assessed 7 days after seeding. Following addition of fresh CSC media and a further week in culture, neurosphere recovery was assessed at day 14. Neurospheres were then dissociated to single cells and re-seeded (12,000 cells per well in a 6-well plate). At day 21, the number of secondary neurospheres formed were counted as a measure of self-renewal and RNA was extracted. mRNA expression of the GCSC markers **(A)** *CD133*, **(B)** *SOX2*, and **(C)** *NES*, and the neural lineage markers **(D)** *GFAP*, **(E)** *TUBB3*, and **(F)** *OLIG1* was determined by qPCR normalised to *GAPDH*. (Mean ± SEM, n = 3, two-way ANOVA with Dunnett's post-hoc test, * $p < 0.05$, ** $p < 0.01$, *** $p < 0.001$, **** $p < 0.0001$, and ns denotes not significant).

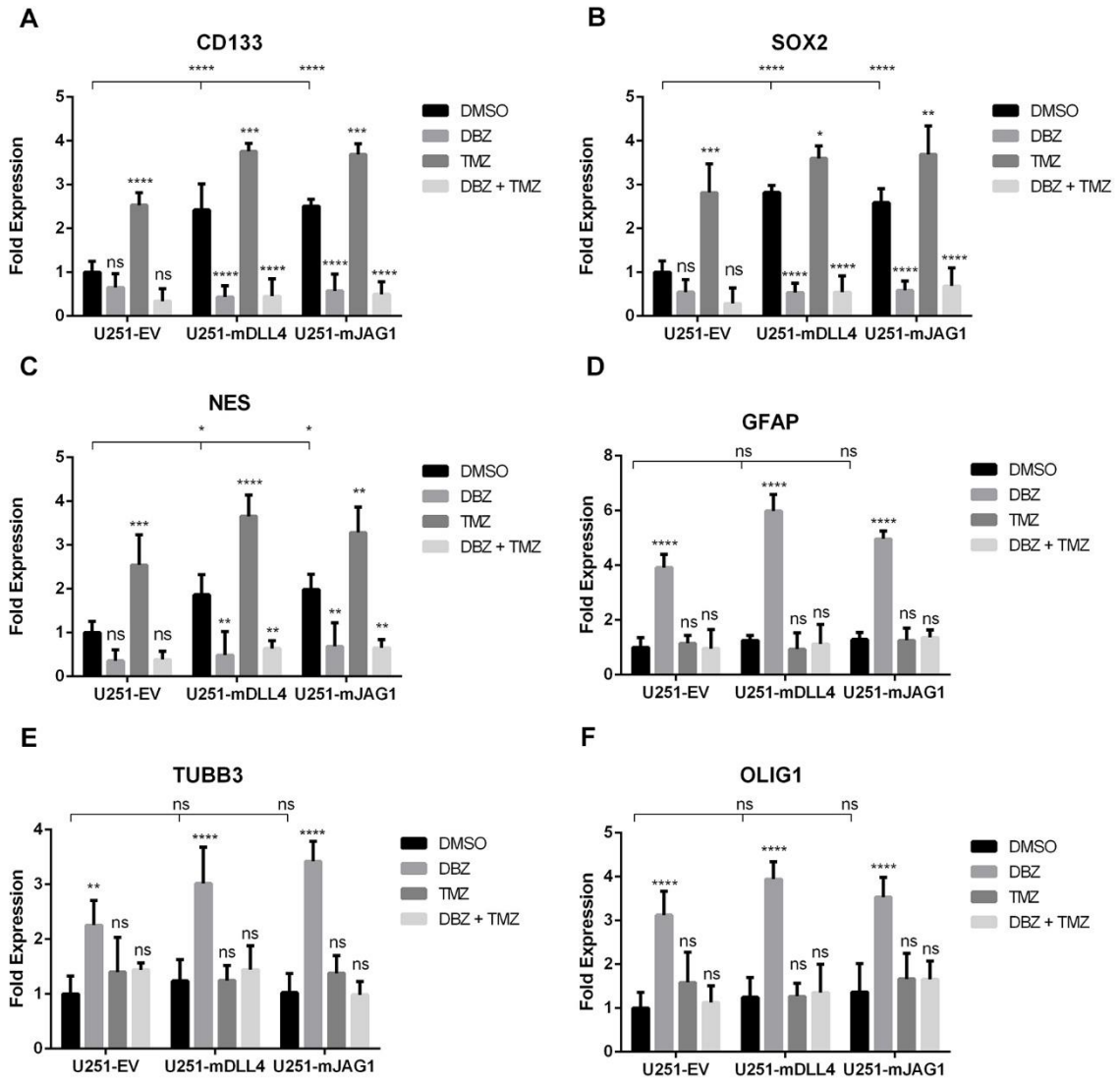

Figure 4.13: DLL4 and JAG1 increase GCSC marker expression in U251 secondary neurospheres which is reversed upon combination DBZ and TMZ treatment.

U251 cells (12,000 per well in a 6-well plate) were cultured in CSC medium and immediately treated with single 25 nM DBZ/25 µM TMZ, combination 25 nM DBZ and 25 µM TMZ, or DMSO control treatment. Primary neurosphere formation was assessed 7 days after seeding. Following addition of fresh CSC media and a further week in culture, neurosphere recovery was assessed at day 14. Neurospheres were then dissociated to single cells and re-seeded (12,000 cells per well in a 6-well plate). At day 21, the number of secondary neurospheres formed were counted as a measure of self-renewal and RNA was extracted. mRNA expression of the GCSC markers **(A)** *CD133*, **(B)** *SOX2*, and **(C)** *NES*, and the neural lineage markers **(D)** *GFAP*, **(E)** *TUBB3*, and **(F)** *OLIG1* was determined by qPCR normalised to *GAPDH*. (Mean ± SEM, n = 3, two-way ANOVA with Dunnett's post-hoc test, * $p < 0.05$, ** $p < 0.01$, *** $p < 0.001$, **** $p < 0.0001$, and ns denotes not significant).

4.3.3 DLL4 and JAG1 induce Notch signalling in a Glioma cancer stem cell line, CSC-5.

4.3.3.1 Characterisation of CSC-5 glioma cancer stem cell line following DLL4 and JAG1 overexpression

The patient-derived GCSC line CSC-5 was transduced with empty vector control-, mDLL4- and mJAG1-encoded retroviruses. The cell line was initially characterised to ensure successful transduction and ligand expression of DLL4 and JAG1 by qPCR, western blot, and IF. mDLL4 and mJAG1 gene expression was significantly increased in CSC-5 -mDLL4 and CSC-5 -mJAG1, respectively (Figure 4.14A). In addition, both Western blotting (Figure 4.14B) and IF (Figure 4.15) revealed DLL4 and JAG1 protein expression is significantly increased in CSC-5 -mDLL4 and CSC-5 -mJAG1, respectively, compared to CSC-5 -EV.

4.3.3.2 Induction of Notch Signalling in CSC-5 Cells Following DLL4 and JAG1 Overexpression

Analysis was performed to assess the ability of the DLL4 and JAG1 ligands to activate Notch signalling by binding to Notch receptors of neighbouring cells in the CSC-5 cell line. qPCR analysis showed CSC-5 cells expressing mDLL4 and mJAG1 upregulated the expression of the Notch downstream target genes *HES1, HEY1,* and *HEY2* (Figure 4.16A). Protein expression of cleaved activated Notch1 and Hes1 was also increased following DLL4 and JAG1 overexpression in CSC-5 GCSCs as detected by Western blot analysis (Figure 4.16B).

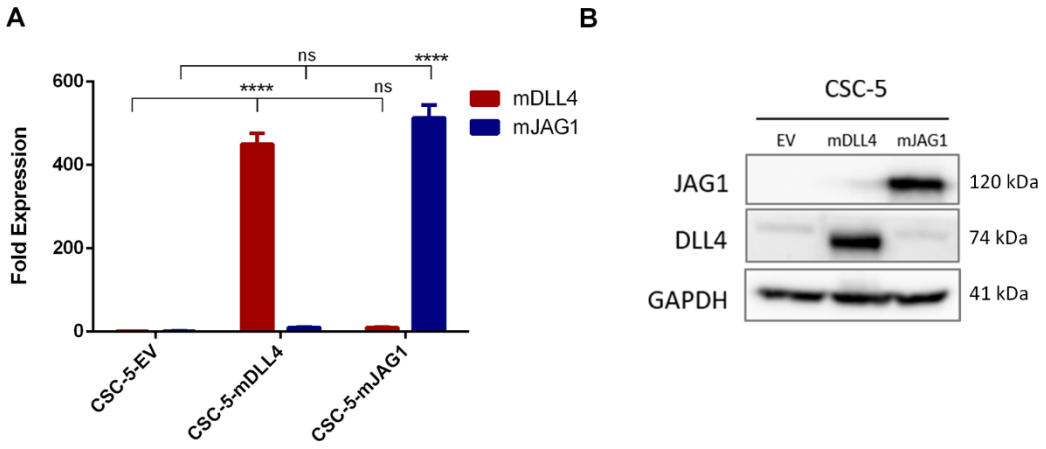

Figure 4.14: Expression of DLL4 and JAG1 in CSC-5 glioma cancer stem cells transduced with mDLL4 and mJAG1.

The CSC-5 cell line overexpressing DLL4, JAG1, and EV control was established by retroviral transduction. RNA was extracted and **(A)** mRNA expression of *mDLL4* and *mJAG1* was determined by qPCR normalised to *GAPDH*. **(B)** Protein expression of DLL4 and JAG1 in the CSC-5 cell line confirmed successful retroviral transduction. Protein was extracted from cells and separated (20 µg) by SDS-PAGE (10% SDS gel). Membranes were probed with rabbit anti-DLL4 (1:1000; Abcam #AB7280), rabbit anti-JAG1 (1:1000; Cell Signalling Technology #2626), and mouse anti-GAPDH (1:2000; ThermoFisher Scientific #MA5-15738) in 5% milk in PBS-T overnight at 4 °C. Membranes were washed and probed with anti-rabbit IgG HRP conjugate (1:5000, ThermoFisher Scientific #65-6120) and anti-mouse IgG HRP conjugate (1:5000; ThermoFisher Scientific #31430) secondary antibodies in 5% milk in PBS-T at RT for 1 h. ECL. (Mean ± SEM, n = 3, two-way ANOVA with Dunnett's post-hoc test, **** $p < 0.0001$, ns denotes not significant).

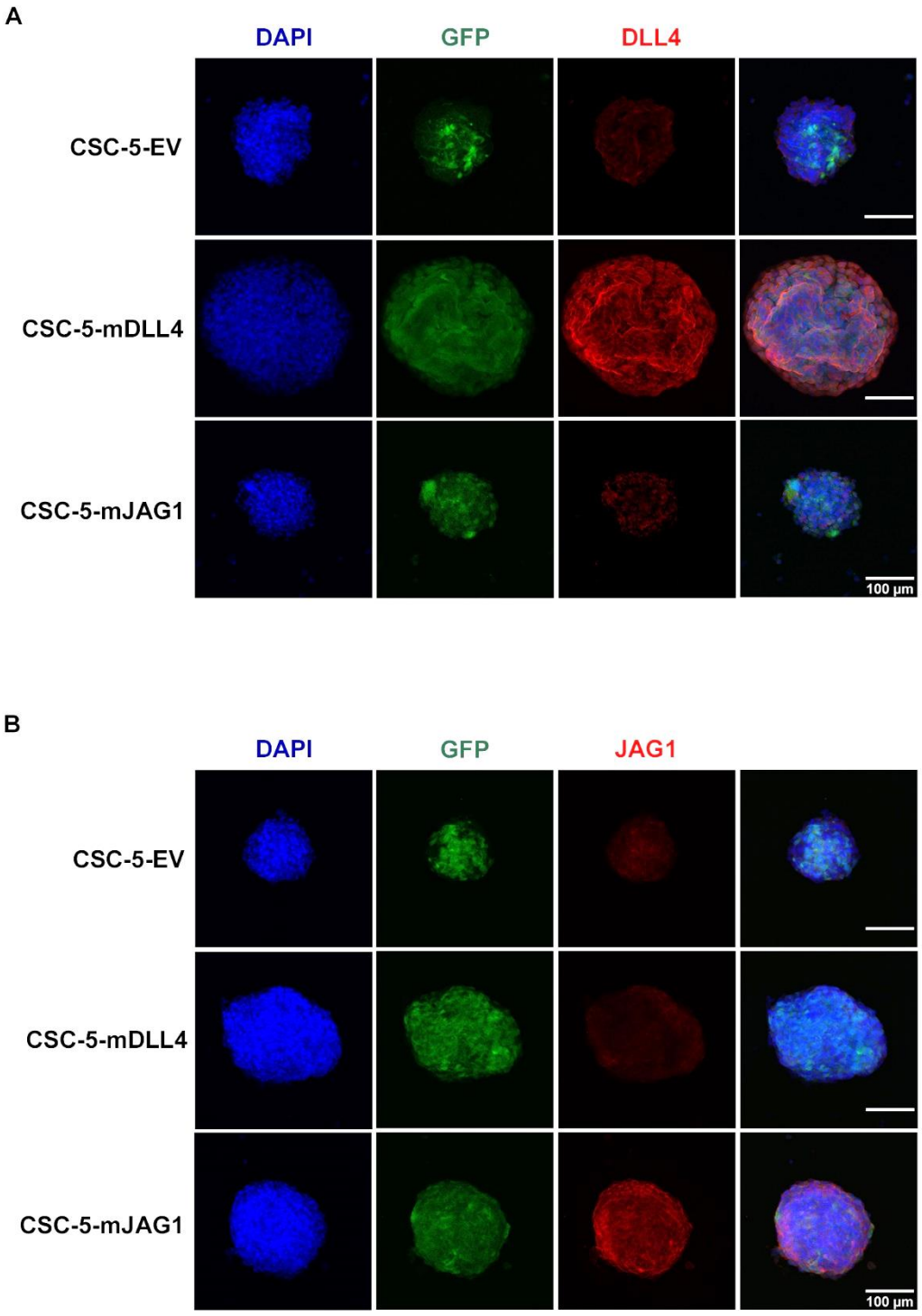

Figure 4.15: DLL4 and JAG1 expression in CSC-5 glioma cancer stem cells following mDLL4 and mJAG1 retroviral transduction.

Representative Immunofluorescence staining of **(A)** DLL4 and **(B)** JAG1 in CSC-5 cells. Cells were seeded in 6-well plates at 12,000 cells per well and grown for 7 days. Cells were then fixed in 4% PFA and immunostained for rabbit anti-DLL4 (1:1000; Abcam #AB7280) and rabbit anti-JAG1 (1:1000; Cell Signalling Technology #2626) followed by goat anti-rabbit IgG Alexa Fluor 647 (1:1000; ThermoFisher Scientific #A21245) and counterstaining with 2 µg/mL DAPI. Images were taken at 20X magnification. Scale bar = 100 µm.

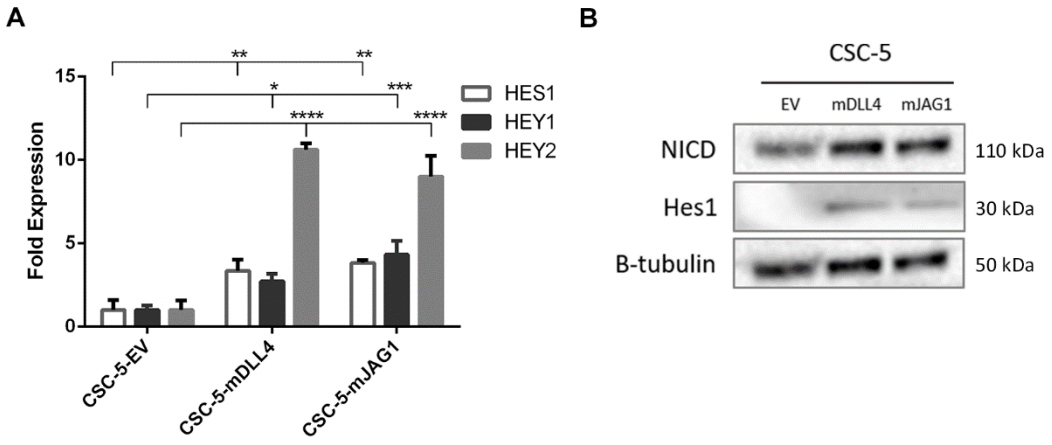

Figure 4.16: DLL4 and JAG1 induce Notch signalling in CSC-5 glioma cancer stem cells.

The CSC-5 cell line overexpressing DLL4, JAG1 and EV control was established by retroviral transduction. RNA was extracted and **(A)** mRNA expression of the Notch target genes *HES1*, *HEY1*, and *HEY2* was determined by qPCR normalised to *GAPDH*. **(B)** Protein expression of cleaved Notch1 and Hes1 in the CSC-5 cell lines confirmed successful induction of Notch signalling following DLL4 and JAG1 overexpression. Protein was extracted from cells and separated (20 µg) by SDS-PAGE (10% SDS gel). Membranes were probed with rabbit anti-cleaved Notch1 (1:1000), rabbit anti-Hes1 (1:1000; Cell Signalling Technology #11988), and mouse anti-GAPDH (1:2000; ThermoFisher Scientific #MA5-15738) in 5% milk in PBS-T overnight at 4 °C. Membranes were washed and probed with anti-rabbit IgG HRP conjugate (1:5000, ThermoFisher Scientific #65-6120) and anti-mouse IgG HRP conjugate (1:5000; ThermoFisher Scientific #31430) secondary antibodies in 5% milk in PBS-T at RT for 1 h. ECL. (Mean ± SEM, n = 3, two-way ANOVA with Dunnett's post-hoc test, * $p < 0.05$, ** $p < 0.01$, *** $p < 0.001$, **** $p < 0.0001$, ns denotes not significant).

4.3.4 DLL4 and JAG1 increase self-renewal in CSC-5 gliomas cancer stem cells

Utilising the CSC-5 cells overexpressing DLL4 and JAG1 we next performed the neurosphere recovery assay to assess CSC-5 primary neurosphere formation, neurosphere recovery and secondary neurosphere formation following single (DBZ/TMZ) and combination (DBZ and TMZ) treatment.

4.3.4.1 CSC-5 Primary Neurosphere Formation

Overexpression of both DLL4 and JAG1 increased the number of CSC-5 neurospheres formed compared to CSC-5-EV control (Figure 4.17A-B). Treatment with the Notch inhibitor DBZ resulted in a significant decrease in the number of CSC-5 neurospheres formed by 39.7%, 50.0% and 44.4% respectively for CSC-5-EV, CSC-5-mDLL4, and CSC-5-mJAG1 compared to DMSO control. TMZ treatment also reduced the number of neurosphere formed, but to less of an extent compared to DBZ, by 15.1%, 25.0%, and 29.3% respectively, for CSC-5-EV, CSC-5-mDLL4, and CSC-5-mJAG1 compared to DMSO control. However, combination TMZ and DBZ treatment resulted in the most significant decrease in primary neurosphere formation, resulting in a reduction of the number of neurospheres by 77.4%, 73.8%, and 81.8% respectively for CSC-5-EV, CSC-5-mDLL4, and CSC-5-JAG1 compared to DMSO control.

As the CSC-5 neurospheres are much more uniform compared to those formed by the U87 and U251 cell lines, CSC-5 neurosphere size was also assessed. Following DLL4 and JAG1 overexpression, CSC-5 neurosphere volume was markedly increased compared to EV control (Figure 4.17C). CSC-5's treated with DBZ had a significantly smaller volume compared to DMSO control. However, TMZ treatment had no significant effect in reducing neurosphere volume. Combination DBZ and TMZ treatment resulted in the

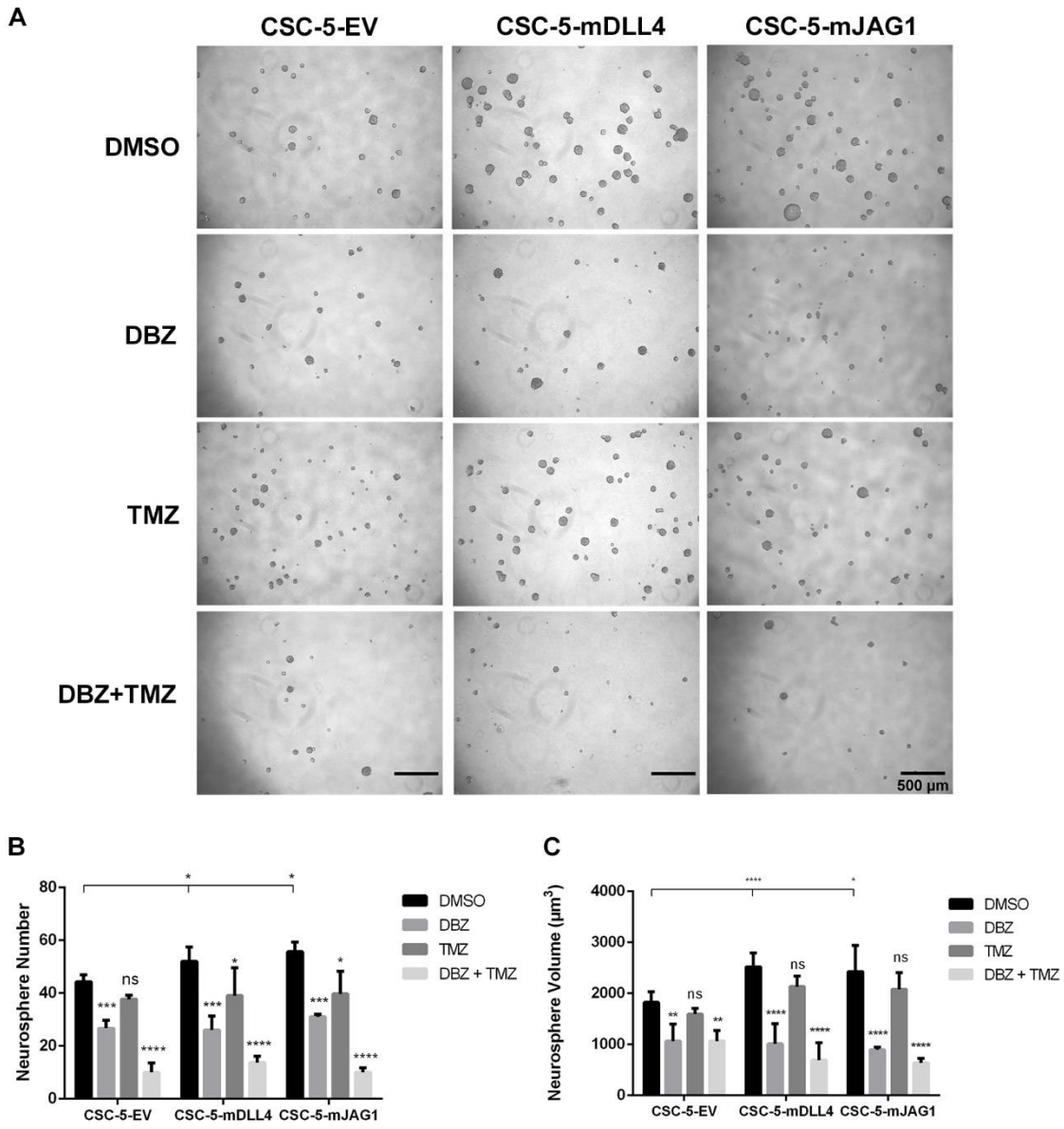

Figure 4.17: DBZ and TMZ combination treatment significantly reduces CSC-5 primary neurosphere formation.

CSC-5 cells (12,000 per well in a 6-well plate) were cultured in CSC medium and immediately treated with single 25 nM DBZ/25 µM TMZ, combination 25 nM DBZ and 25 µM TMZ, or DMSO control treatment. Primary neurosphere formation was assessed 7 days after seeding. **(A)** Images showing CSC-5 primary neurosphere formation following single (DBZ/TMZ) and combination (DBZ and TMZ) treatment. **(B)** Quantification of the number of CSC-5 primary neurospheres formed following 7 days treatment. **(C)** Quantification of CSC-5 primary neurosphere volume. Scale bar = 500 µm. (Mean ± SD, n = 3, two-way ANOVA with Dunnett's post-hoc test, * $p < 0.05$, ** $p < 0.01$, *** $p < 0.001$, **** $p < 0.0001$, and ns denotes not significant).

most significant reduction of neurosphere volume, suggesting the combination treatment is synergistically effective in reducing both neurosphere number and size.

4.3.4.2 CSC-5 Neurosphere Recovery

The next stage of the neurosphere recovery assay assesses the ability of the culture to repopulate following treatment. Once again, the number of CSC-5 neurospheres is significantly increased following overexpression of DLL4 and JAG1 compared to CSC-5-EV control (Figure 4.18A-B). Single DBZ treatment resulted in a slight decrease in the number of CSC-5 neurospheres recovered by 20.3%, 55.1% and 29.5% respectively for CSC-5-EV, CSC-5-mDLL4, and CSC-5-mJAG1 compared to DMSO control. TMZ treatment had little effect the number of neurospheres formed, conversely increasing the neurosphere number by 6.7% for CSC-5-EV, but reducing the number by 20.1% and 21.8% respectively for CSC-5-DLL4 and CSC-5-JAG1 compared to DMSO control. However, combination TMZ and DBZ treatment resulted in a highly significant decrease in neurosphere recovery, resulting in a reduction of the number of neurospheres by 74.7%, 85.5%, and 85.9% respectively for CSC-5-EV, CSC-5-mDLL4, and CSC-5-JAG1 compared to DMSO control.

The volume of the recovered neurospheres was also assessed. There was no difference in neurosphere volume for the CSC-5 neurospheres overexpressing DLL4 and JAG compared to EV control (Figure 4.18C). CSC-5's treated with DBZ had a markedly reduced volume compared to DMSO control, however, TMZ treatment had no effect in reducing neurosphere volume following recovery. Combination DBZ and TMZ treatment resulted in the most significant reduction of neurosphere volume, again suggesting the combination treatment is effective in reducing both neurosphere number and size following the recovery period after treatment.

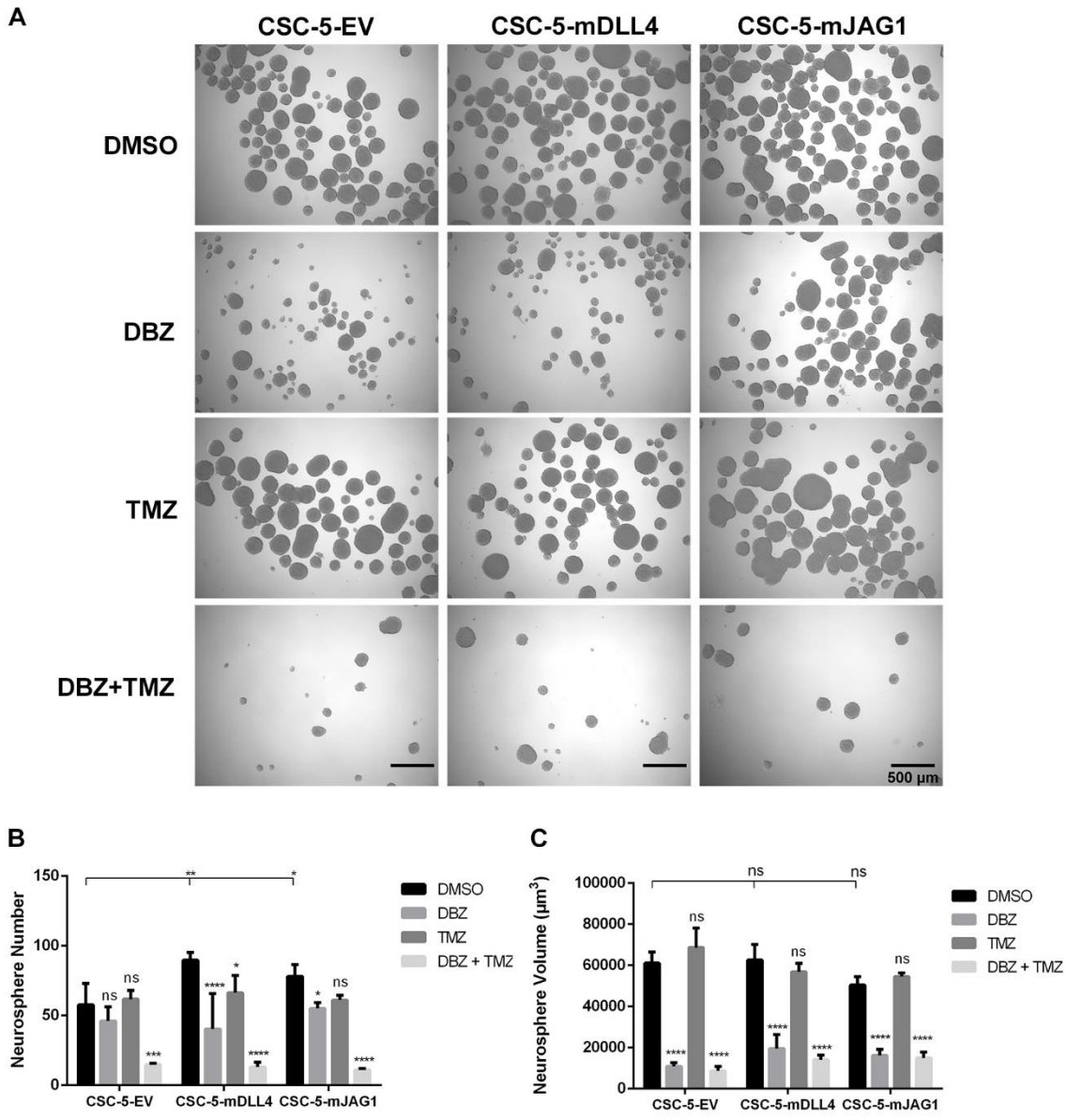

Figure 4.18: DBZ and TMZ combination treatment significantly reduces CSC-5 neurosphere recovery following treatment.

CSC-5 cells (12,000 per well in a 6-well plate) were cultured in CSC medium and immediately treated with single 25 nM DBZ/25 µM TMZ, combination 25 nM DBZ and 25 µM TMZ, or DMSO control treatment. Primary neurosphere formation was assessed 7 days after seeding. Following addition of fresh CSC media and a further week in culture, neurosphere recovery was assessed at day 14. **(A)** Images showing CSC-5 neurosphere recovery following single (DBZ/TMZ) and combination (DBZ and TMZ) treatment. **(B)** Quantification of CSC-5 neurosphere recovery. **(C)** Quantification of CSC-5 neurosphere volume following recovery after treatment. Scale bar = 500 µm. (Mean ± SD, n = 3, two-way ANOVA with Dunnett's post-hoc test, * $p < 0.05$, ** $p < 0.01$, *** $p < 0.001$, **** $p < 0.0001$, and ns denotes not significant).

4.3.4.3 CSC-5 Secondary Neurosphere Formation

The final part of the assay assesses the ability of neurospheres to form following dissociation to single cells. Overexpression of both DLL4 and JAG1 had no effect on the number of secondary neurospheres formed compared to control (Figure 4.19A-B). DBZ only and TMZ only treatment also had no effect of the number of neurospheres formed compared to DMSO control. However, combination DBZ and TMZ treatment resulted in a significant reduction of neurosphere number, reducing secondary neurosphere formation by 67.1%, 67.2%, and 78.5%, respectively, for CSC-5-EV, CSC-5-mDLL4, and CSC-5-mJAG1 compared to DMSO control. Similarly, it was only combination treatment which had a significant effect in reducing the volume of the secondary neurospheres formed (Figure 4.19C).

Overall, these results show DLL4- and JAG1-induced Notch signalling in CSC-5 cells increase neurosphere formation and size, and inhibition of Notch signalling by DBZ treatment alongside TMZ significantly reduces both neurosphere number and size. This suggests DLL4- and JAG1-induced Notch signalling plays a key role in GCSC self-renewal and maintenance.

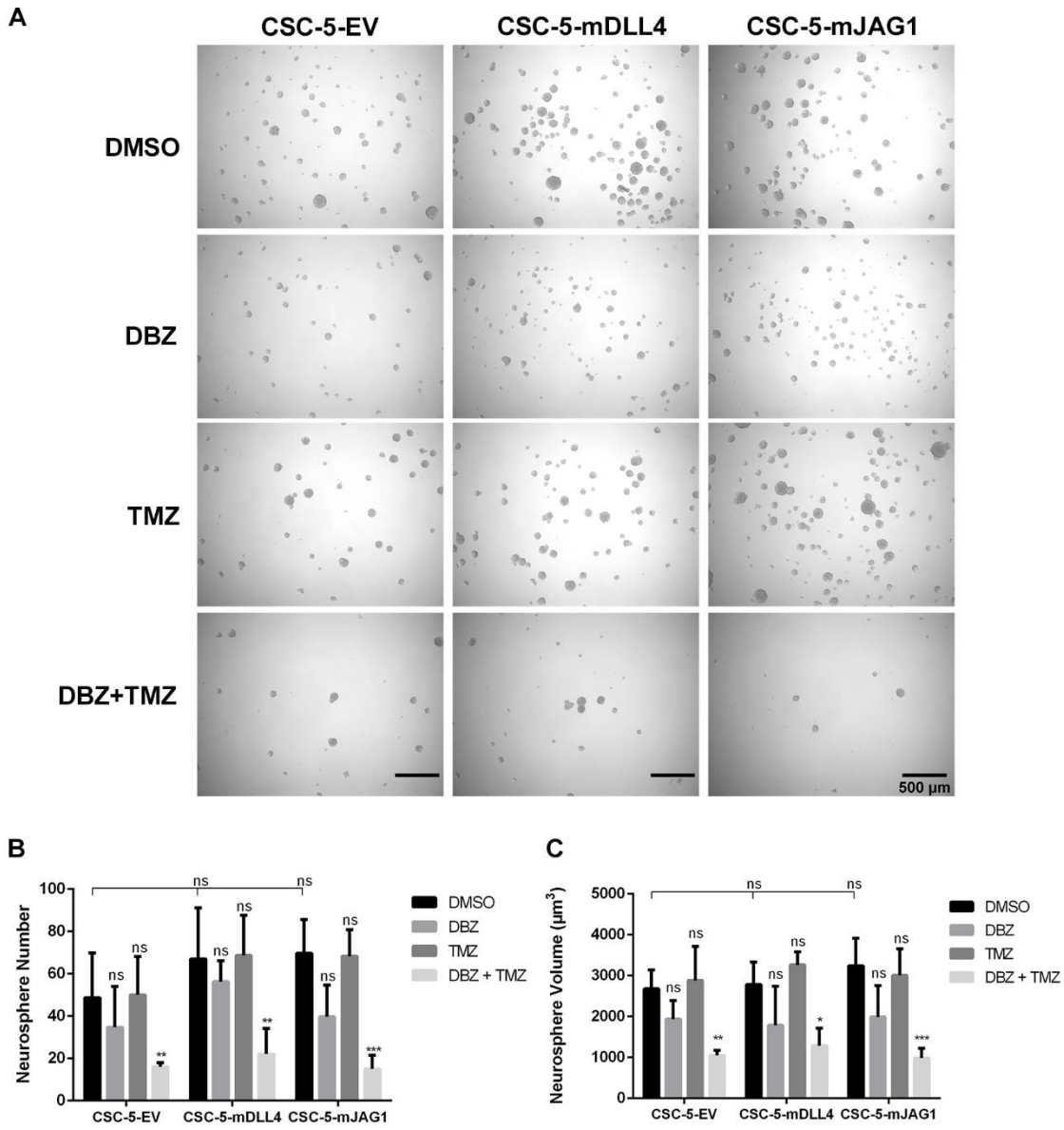

Figure 4.19: DBZ and TMZ combination treatment significantly reduces CSC-5 secondary neurosphere formation following treatment.

CSC-5 cells (12,000 per well in a 6-well plate) were cultured in CSC medium and immediately treated with single 25 nM DBZ/25 µM TMZ, combination 25 nM DBZ and 25 µM TMZ, or DMSO control treatment. Primary neurosphere formation was assessed 7 days after seeding. Following addition of fresh CSC media and a further week in culture, neurosphere recovery was assessed at day 14. Neurospheres were then dissociated to single cells and re-seeded (12,000 cells per well in a 6-well plate). At day 21, the number of secondary neurospheres formed were counted as a measure of self-renewal. **(A)** Images showing CSC-5 secondary neurosphere formation following single (DBZ/TMZ) and combination (DBZ and TMZ) treatment and dissociation to single cells. **(B)** Quantification of CSC-5 secondary neurosphere formation. **(C)** Quantification of CSC-5 neurosphere volume following secondary neurosphere formation. Scale bar = 500 µm. (Mean ± SD, n = 3, two-way ANOVA with Dunnett's post-hoc test, * $p < 0.05$, ** $p < 0.01$, *** $p < 0.001$, **** $p < 0.0001$, and ns denotes not significant).

4.3.5 DLL4 and JAG1 Increase Glioma Cancer Stem Cell Marker Expression in the Patient-Derived GCSC Line CSC-5.

In order to assess the effect of DLL4 and JAG1 overexpression alongside single and combination treatments on GCSC differentiation, we determined the mRNA expression of key GCSC markers (*CD133, SOX2,* and *NES*) and markers of neuronal lineages (*GFAP, TUBB3,* and *OLIG1*) by qPCR at the three timepoints of the neurosphere recovery assay in the patient derived GCSC line CSC-5.

4.3.5.1 CSC-5 Primary Neurosphere Formation

Overexpression of DLL4 and JAG1 in the CSC-5 cell line resulted in increased expression of all three GCSC markers following primary neurosphere formation, and the expression of these markers is further increased upon TMZ treatment. GCSC marker expression is significantly reduced upon single DBZ and combination DBZ and TMZ treatment (Figure 4.20A-C). Conversely, expression of the neural lineage markers *GFAP* and *TUBB3* are increased following DBZ treatment of CSC neurospheres, however there is no significant change in *OLIG1* expression (Figure 4.20D-F) suggesting inhibition of Notch signalling in GCSCs resulting in GCSC differentiation into astrocytes or neurons, and DLL4 and JAG1 play a role in maintaining the GCSC phenotype.

4.3.5.2 Neurosphere Recovery

Similar results were obtained following recovery of CSC-5 neurospheres following treatment. Again, DLL4 and JAG1 increased GCSC marker expression, and this expression was further increased upon TMZ treatment. However, single DBZ and combination DBZ and TMZ treatment significantly reduced GCSC marker expression (Figure 4.21A-C). Expression of the neural lineage markers *GFAP* and *TUBB3*, but not *OLIG1*, are increased following DBZ treatment whilst single TMZ and combination

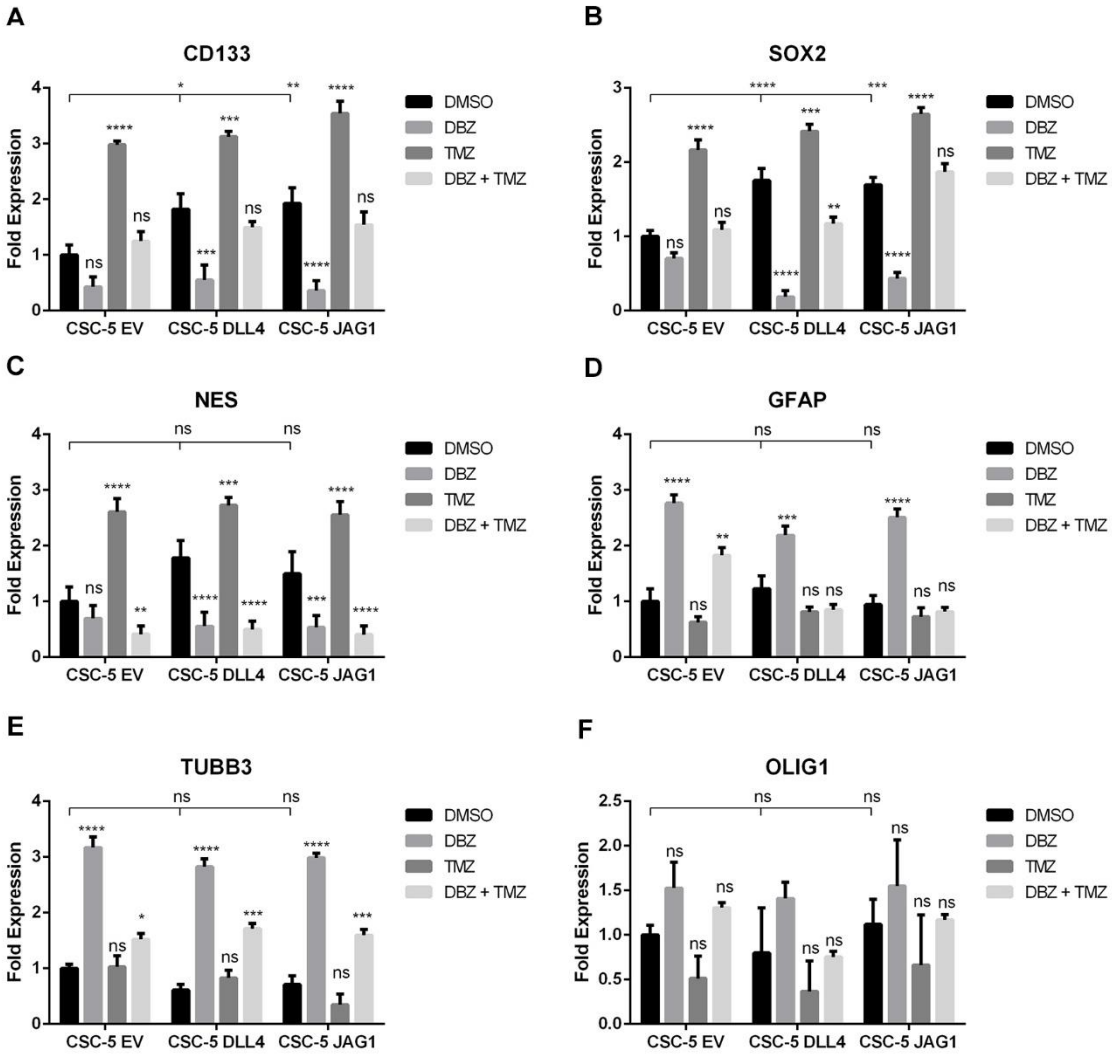

Figure 4.20: DLL4 and JAG1 increase GCSC marker expression in CSC-5 primary neurospheres.

CSC-5 cells (12,000 per well in a 6-well plate) were cultured in CSC medium and immediately treated with single 25 nM DBZ/25 µM TMZ, combination 25 nM DBZ and 25 µM TMZ, or DMSO control treatment. RNA was extracted 7 days after seeding following primary neurosphere formation. mRNA expression of the GCSC markers **(A)** *CD133*, **(B)** *SOX2*, and **(C)** *NES*, and the neural lineage markers **(D)** *GFAP*, **(E)** *TUBB3*, and **(F)** *OLIG1* was determined by qPCR normalised to *GAPDH*. (Mean ± SEM, n = 3, two-way ANOVA with Dunnett's post-hoc test, * $p < 0.05$, ** $p < 0.01$, *** $p < 0.001$, **** $p < 0.0001$, and ns denotes not significant).

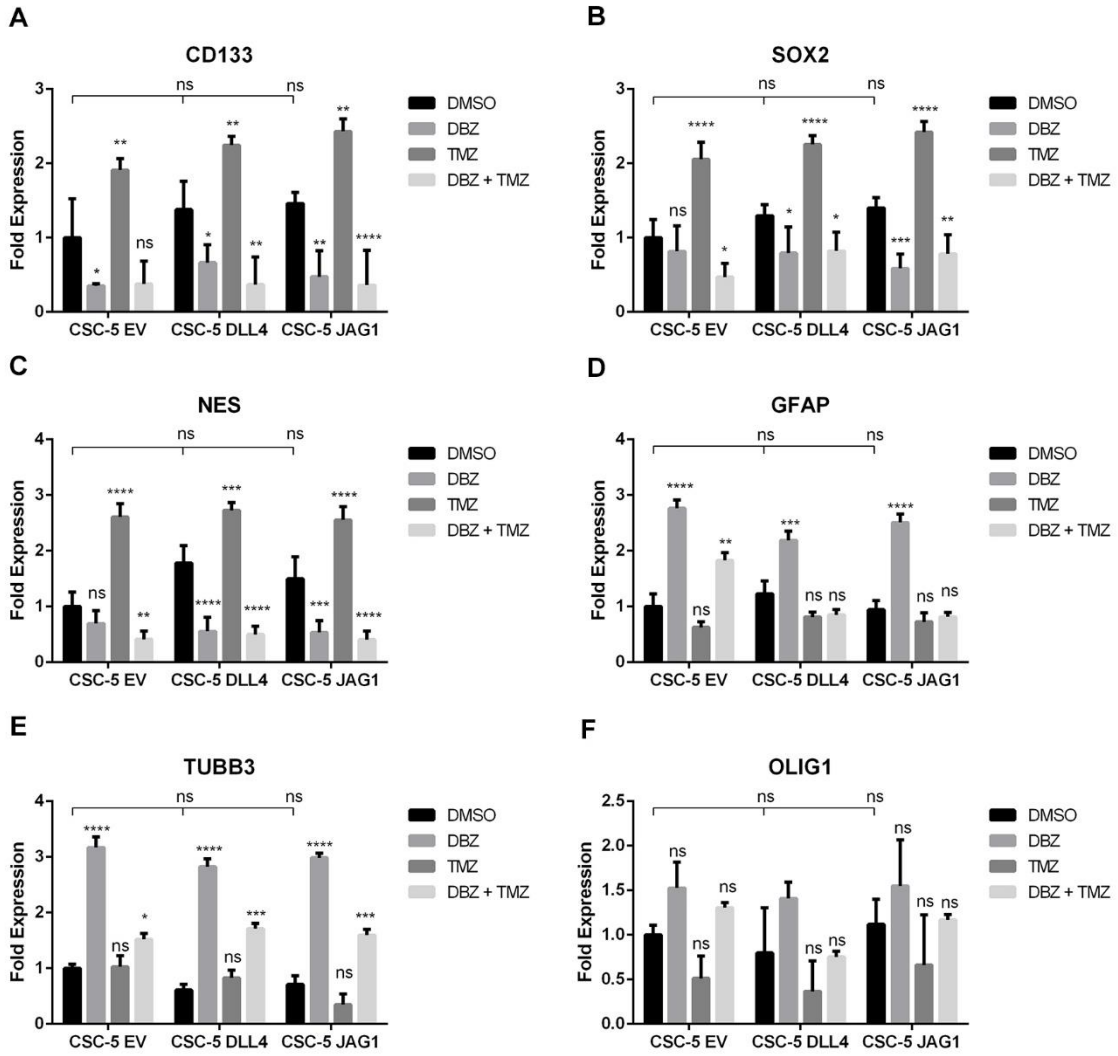

Figure 4.21: DLL4 and JAG1 increase GCSC marker expression in recovered CSC-5 neurospheres.

CSC-5 cells (12,000 per well in a 6-well plate) were cultured in CSC medium and immediately treated with single 25 nM DBZ/25 µM TMZ, combination 25 nM DBZ and 25 µM TMZ, or DMSO control treatment. Primary neurosphere formation was assessed 7 days after seeding. Following addition of fresh CSC media and a further week in culture, neurosphere recovery was assessed at day 14 and RNA was extracted. mRNA expression of the GCSC markers **(A)** *CD133*, **(B)** *SOX2*, and **(C)** *NES*, and the neural lineage markers **(D)** *GFAP*, **(E)** *TUBB3*, and **(F)** *OLIG1* was determined by qPCR normalised to *GAPDH*. (Mean ± SEM, n = 3, two-way ANOVA with Dunnett's post-hoc test, * $p < 0.05$, ** $p < 0.01$, *** $p < 0.001$, **** $p < 0.0001$, and ns denotes not significant).

DBZ and TMZ treatment has no effect (Figure 4.21D-F).

4.3.5.3 Secondary Neurosphere Formation

Following the dissociation of CSC-5 neurospheres to single cells and subsequent secondary neurosphere formation, similar results were obtained as above. Overexpression of DLL4 and JAG1 resulted in increased expression of all three GCSC markers following secondary neurosphere formation, and the expression of these markers is further increased following TMZ treatment. GCSC marker expression is however reduced in neurospheres treated with single DBZ and combination DBZ and TMZ treatment (Figure 4.22A-C). Conversely, expression of the astrocytic marker *GFAP* (but not *TUBB3* and *OLIG1*) is increased following DBZ treatment of neurospheres (Figure 4.22D-F) suggesting inhibition of Notch signalling in the CSC-5 cell line results in the differentiation of GCSCs to astrocytes. These results are similar those obtained in the U87 and U251 cell line, and reinforce the key role played by the Notch signalling pathway in GCSCs and treatment resistance to TMZ in glioblastoma.

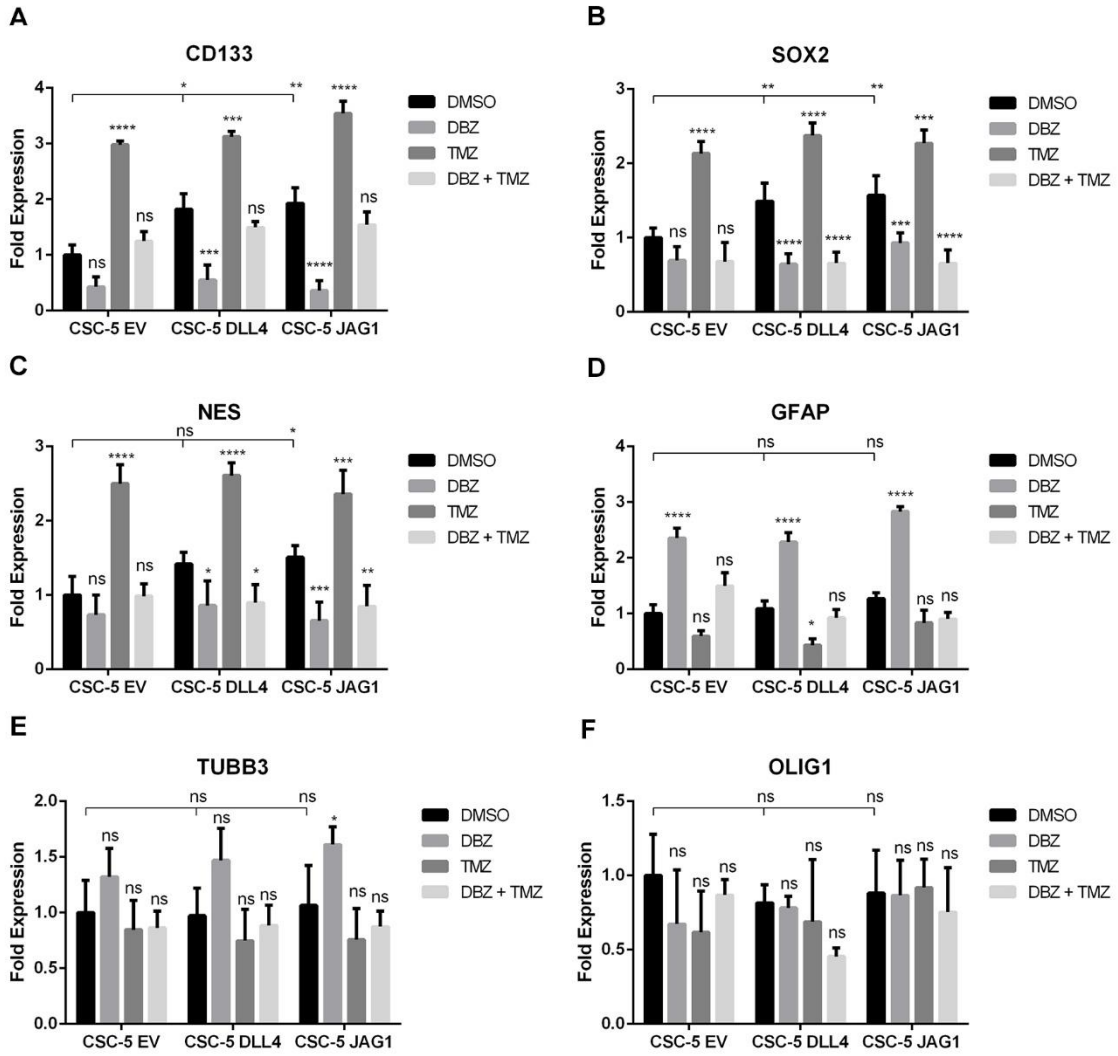

Figure 4.22: DLL4 and JAG1 increase GCSC marker expression in CSC-5 secondary neurospheres.

CSC-5 cells (12,000 per well in a 6-well plate) were cultured in CSC medium and immediately treated with single 25 nM DBZ/25 µM TMZ, combination 25 nM DBZ and 25 µM TMZ, or DMSO control treatment. Primary neurosphere formation was assessed 7 days after seeding. Following addition of fresh CSC media and a further week in culture, neurosphere recovery was assessed at day 14. Neurospheres were then dissociated to single cells and re-seeded (12,000 cells per well in a 6-well plate). At day 21, the number of secondary neurospheres formed were counted as a measure of self-renewal and RNA was extracted. mRNA expression of the GCSC markers **(A)** *CD133*, **(B)** *SOX2*, and **(C)** *NES*, and the neural lineage markers **(D)** *GFAP*, **(E)** *TUBB3*, and **(F)** *OLIG1* was determined by qPCR normalised to *GAPDH*. (Mean ± SEM, n = 3, two-way ANOVA with Dunnett's post-hoc test, * $p < 0.05$, ** $p < 0.01$, *** $p < 0.001$, **** $p < 0.0001$, and ns denotes not significant).

4.3.6 Single DBZ and Combination DBZ and TMZ treatment results in differentiation of CSC-5 glioma cancer stem cells

To confirm the results achieved by qPCR, we assessed the protein expression of the GCSC markers CD133, SOX2, and Nestin, alongside the expression of the neural differentiation markers GFAP (astrocytes) β-III-tubulin (neurons), and SOX10 (oligodendrocytes) by IF. Again, this was performed at all three timepoints during the neurosphere assay.

4.3.6.1 Primary Neurosphere Formation

4.3.6.1.1 GCSC and neural differentiation marker expression

For CSC-5-EV, CSC-5-mDLL4, and CSC-5-mJAG1 recovered neurospheres, IF staining shows combination DBZ and TMZ treatment shows increased expression of GFAP compared to DMSO control (Figure 4.23), however there is no apparent difference in CD133 staining or GFAP staining in single TMZ or single DBZ treatment compared to untreated control.

For CSC-5-EV, CSC-5-mDLL4, and CSC-5-mJAG1 primary neurospheres, IF staining shows increased levels of the neural differentiation marker β-III-tubulin following single DBZ treatment compared to untreated control. Conversely, single DBZ treatment shows increased levels of the GCSC marker Nestin. Combination DBZ and TMZ treatment shows an increase in the expression of β-III-tubulin compared to DMSO control, suggesting inhibition of Notch signalling by DBZ causes differentiation of GCSCs (Figure 4.24).

Finally, the expression of the GCSC marker SOX2 alongside the marker of oligodendrocyte differentiation SOX10 was assessed by IF. For CSC-5-EV, CSC-5-mDLL4,

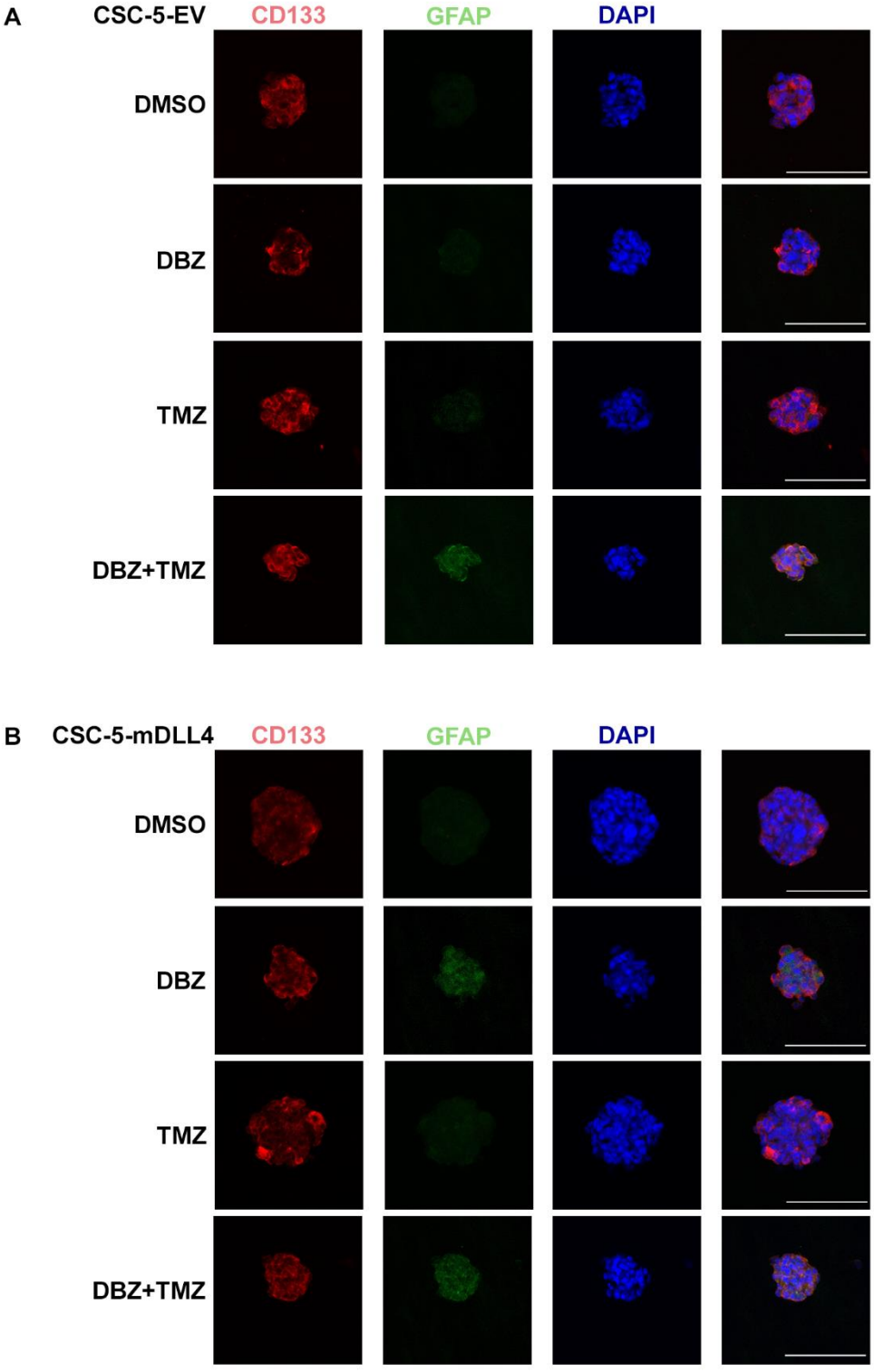
A
CSC-5-EV
CD133
GFAP
DAPI
DMSO
DBZ
TMZ
DBZ+TMZ
B
CSC-5-mDLL4
CD133
GFAP
DAPI
DMSO
DBZ
TMZ
DBZ+TMZ

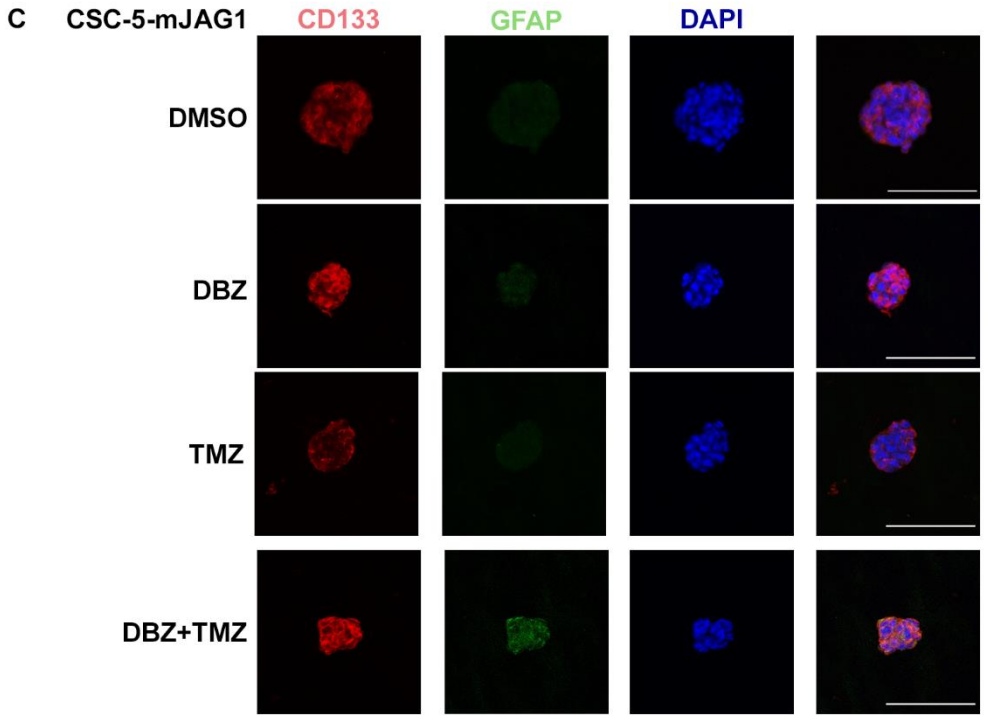

Figure 4.23: Immunofluorescent staining of CD133 and GFAP of primary CSC-5 neurosphere formation following single DBZ/TMZ and combination DBZ and TMZ treatment.

Representative confocal images of CD133 and GFAP staining in **(A)** CSC-5-EV, **(B)** CSC-5-mDLL4, and **(C)** CSC-5-mJAG1 neurospheres following single and combination treatments. CSC-5 cells (12,000 per well in a 6-well plate) were cultured in CSC medium and immediately treated with single 25 nM DBZ/25 µM TMZ, combination 25 nM DBZ and 25 µM TMZ, or DMSO control treatment. Primary neurosphere formation was assessed 7 days after seeding. Primary neurospheres were fixed in 4% PFA and immunostained for mouse anti-CD133 (W6B3C1; 1:50; Miltenyi Biotec #130-092-395) and rabbit anti-GFAP (1:250; Abcam #AB33922) followed by goat anti-rabbit IgG Alexa Fluor 647 (1:1000; ThermoFisher Scientific #A21245) and donkey anti-mouse IgG Alexa Fluor 568 (1:1000; ThermoFisher Scientific #A10037) secondary antibodies. Nuclei were counterstained with 2 µg/mL DAPI. Scale bar = 100 µm.

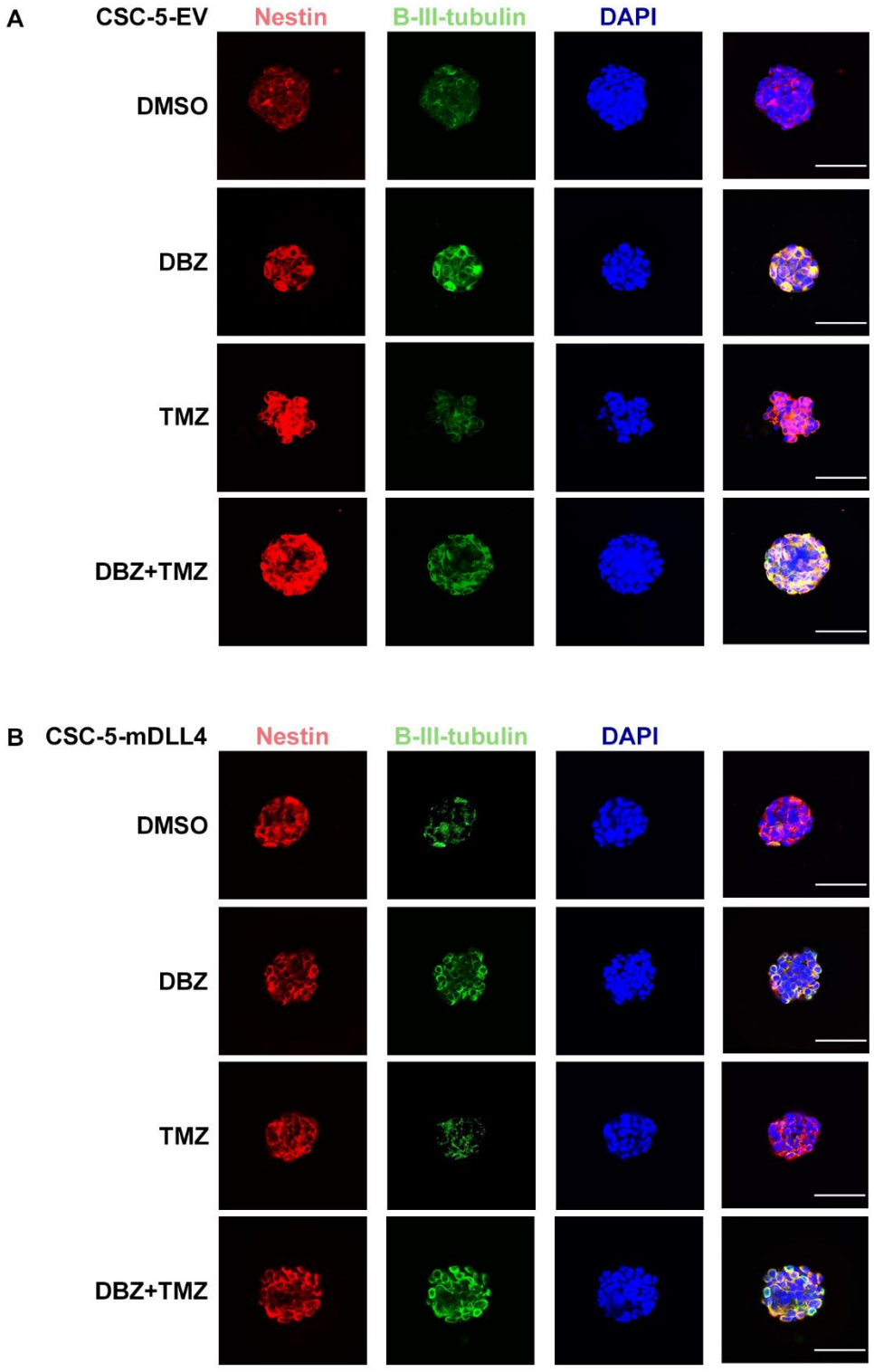
A
CSC-5-EV
Nestin
B-III-tubulin
DAPI
DMSO
DBZ
TMZ
DBZ+TMZ
B
CSC-5-mDLL4
Nestin
B-III-tubulin
DAPI
DMSO
DBZ
TMZ
DBZ+TMZ

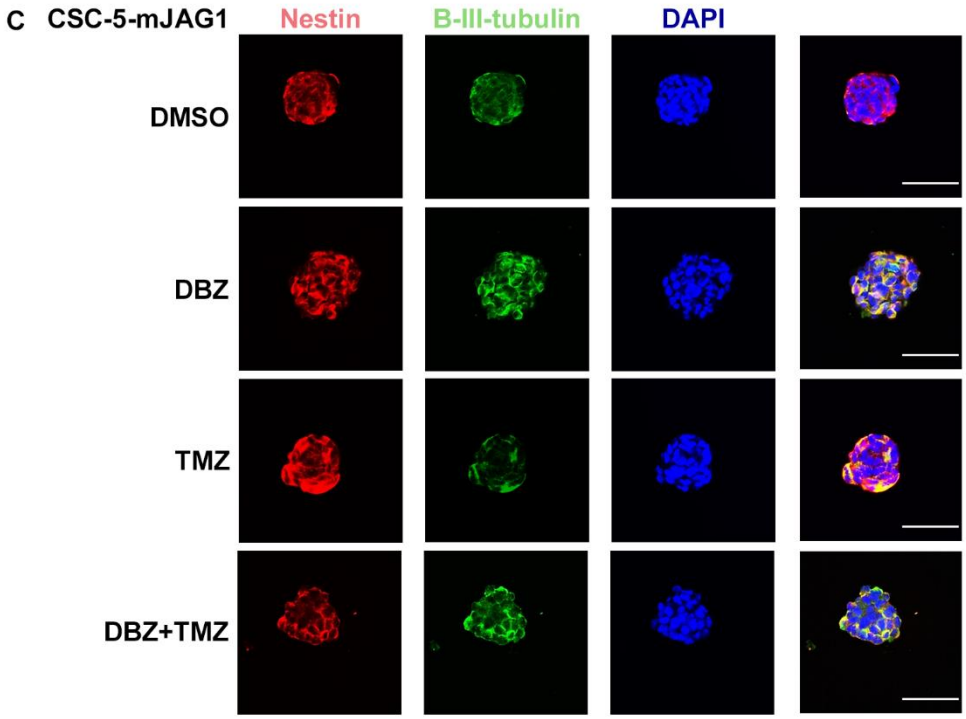

Figure 4.24: Immunofluorescent staining of Nestin and β-III-tubulin of primary CSC-5 neurosphere formation following single DBZ/TMZ and combination DBZ and TMZ treatment.

Representative confocal images of Nestin and β-III-tubulin staining in **(A)** CSC-5-EV, **(B)** CSC-5-mDLL4, and **(C)** CSC-5-mJAG1 neurospheres following single and combination treatments. CSC-5 cells (12,000 per well in a 6-well plate) were cultured in CSC medium and immediately treated with single 25 nM DBZ/25 µM TMZ, combination 25 nM DBZ and 25 µM TMZ, or DMSO control treatment. Primary neurosphere formation was assessed 7 days after seeding. Primary neurospheres were fixed in 4% PFA and immunostained for mouse anti-β-III-tubulin (1:250; R & D Systems #MAB1195) and rabbit anti-Nestin (1:250; Sigma Aldrich #N5413) followed by goat anti-rabbit IgG Alexa Fluor 647 (1:1000; ThermoFisher Scientific #A21245) and donkey anti-mouse IgG Alexa Fluor 568 (1:1000; ThermoFisher Scientific #A10037) secondary antibodies. Nuclei were counterstained with 2 µg/mL DAPI. Scale bar = 100 µm.

and CSC-5-mJAG1 primary neurospheres, IF staining shows increased levels SOX10 following single DBZ treatment compared to untreated control. Single TMZ treatment shows no/reduced SOX10 staining, whilst combination DBZ and TMZ treatment shows increased expression of SOX10 compared to DMSO control (Figure 4.25). Taken together, these results suggest Notch inhibition by DBZ results in GCSC differentiation.

4.3.6.1.2 Ki67 proliferation marker expression

IF staining was also used to assess the expression of the proliferation marker Ki67. We observed single TMZ treatment has no effect reducing Ki67 staining compared to DMSO control (Figure 4.26). However, single DBZ and combination DBZ and TMZ treatment shows reduced levels of Ki67 staining, suggesting inhibition of Notch signalling results in decreased proliferation of CSC-5 neurospheres.

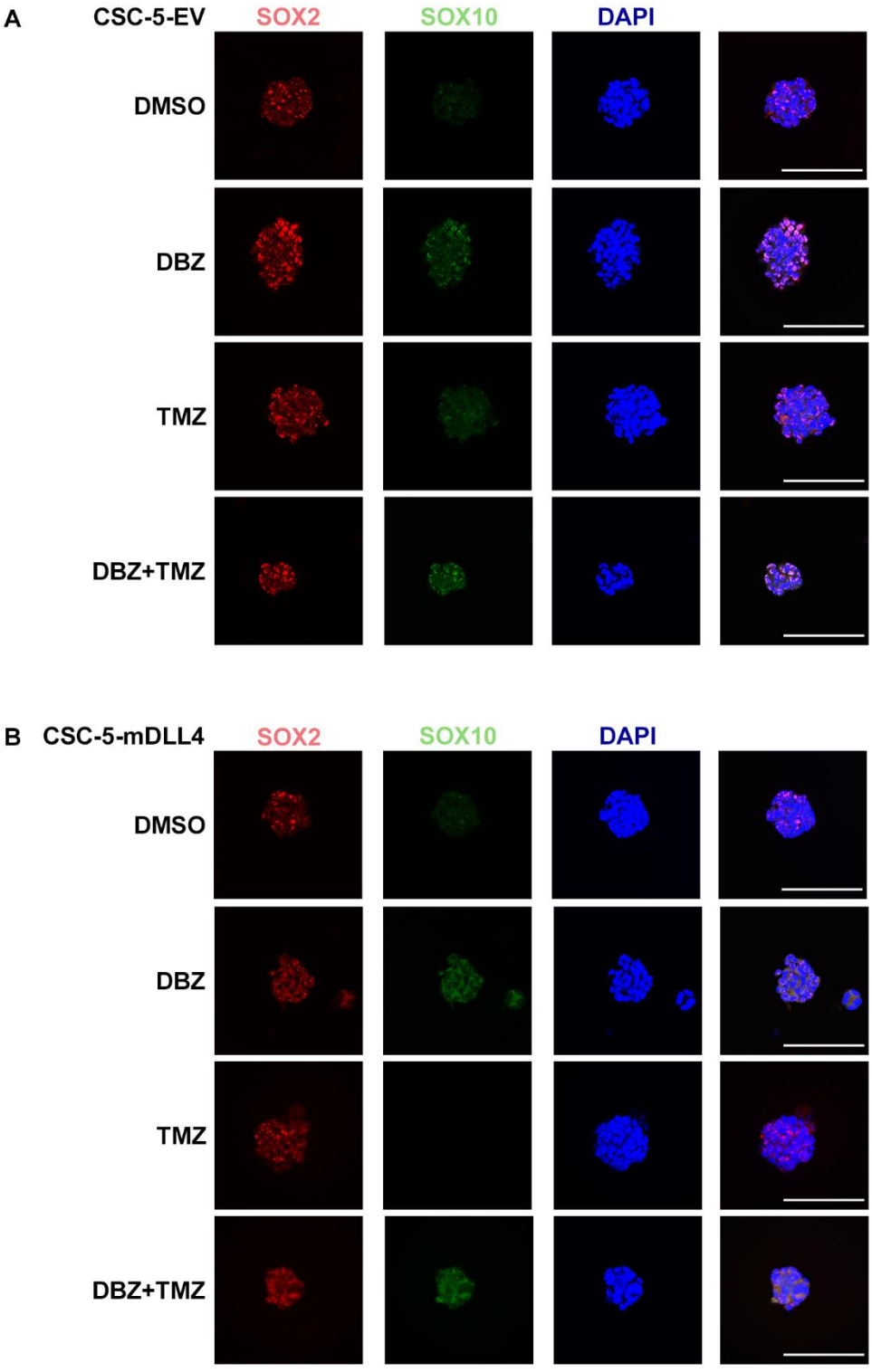
A
CSC-5-EV
SOX2
SOX10
DAPI
DMSO
DBZ
TMZ
DBZ+TMZ
B
CSC-5-mDLL4
SOX2
SOX10
DAPI
DMSO
DBZ
TMZ
DBZ+TMZ

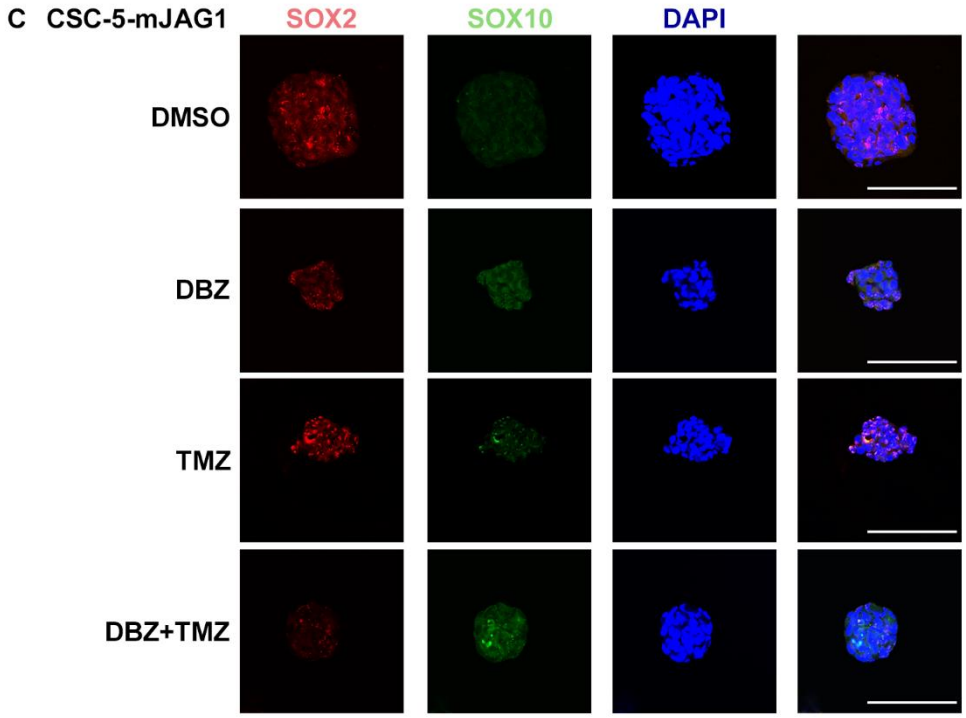

Figure 4.25: Immunofluorescent staining of SOX2 and SOX10 of primary CSC-5 neurosphere formation following single DBZ/TMZ and combination DBZ and TMZ treatment.

Representative confocal images of SOX2 and SOX10 staining in **(A)** CSC-5-EV, **(B)** CSC-5-mDLL4, and **(C)** CSC-5-mJAG1 neurospheres following single and combination treatments. CSC-5 cells (12,000 per well in a 6-well plate) were cultured in CSC medium and immediately treated with single 25 nM DBZ/25 µM TMZ, combination 25 nM DBZ and 25 µM TMZ, or DMSO control treatment. Primary neurosphere formation was assessed 7 days after seeding. Primary neurospheres were fixed in 4% PFA and immunostained for mouse anti-SOX10 (1:250; R & D Systems #MAB2864) and rabbit anti-SOX2 (1:250; Abcam #AB97959) followed by goat anti-rabbit IgG Alexa Fluor 647 (1:1000; ThermoFisher Scientific #A21245) and donkey anti-mouse IgG Alexa Fluor 568 (1:1000; ThermoFisher Scientific #A10037) secondary antibodies. Nuclei were counterstained with 2 µg/mL DAPI. Scale bar = 100 µm.

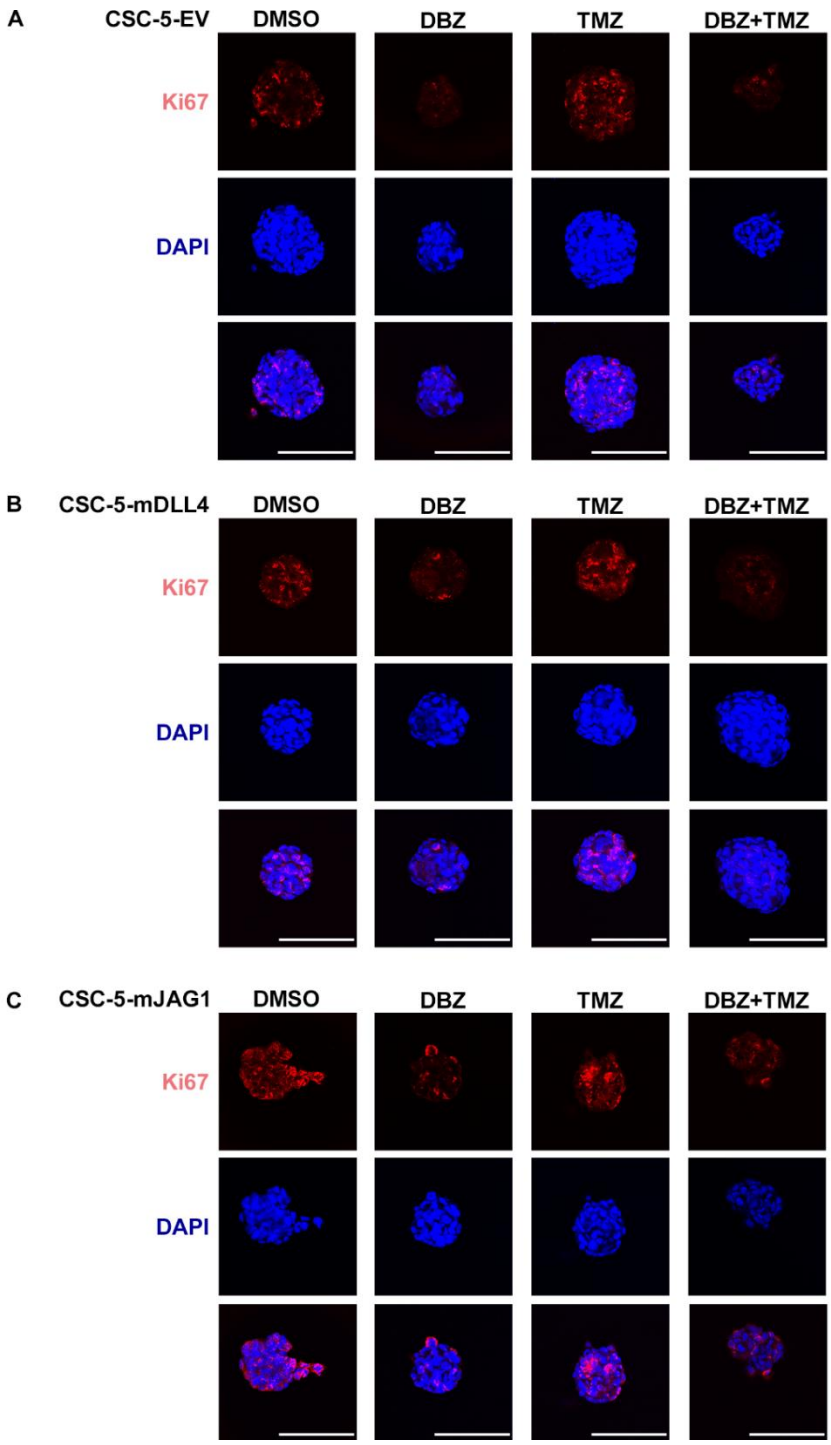

Figure 4.26: Immunofluorescent staining of the proliferation marker Ki67 following single DBZ/TMZ and combination DBZ and TMZ treatment.

Representative confocal images of Ki67 staining in **(A)** CSC-5-EV, **(B)** CSC-5-mDLL4, and **(C)** CSC-5-mJAG1 primary neurospheres following single and combination treatments. CSC-5 cells (12,000 per well in a 6-well plate) were cultured in CSC medium and immediately treated with single 25 nM DBZ/25 µM TMZ, combination 25 nM DBZ and 25 µM TMZ, or DMSO control. Primary neurosphere formation was assessed 7 days after seeding. Primary neurospheres were fixed in 4% PFA and immunostained for rabbit anti-Ki67 (1:1000; Abcam #AB15580) followed by goat anti-rabbit IgG Alexa Fluor 647 (1:1000; ThermoFisher Scientific #A21245) secondary antibody; nuclei were counterstained with 2 µg/mL DAPI. Scale bar = 100 µm.

4.3.6.2 Neurosphere Recovery

4.3.6.2.1 GCSC and neural differentiation marker expression

For CSC-5-EV, CSC-5-mDLL4, and CSC-5-mJAG1 recovered neurospheres, IF staining shows increased levels of the astrocytic marker GFAP following single DBZ treatment compared to untreated control. Single TMZ treatment shows increased staining for the GCSC marker CD133, whilst combination DBZ and TMZ treatment shows increased expression of GFAP compared to DMSO control (Figure 4.27).

Similar results were obtained when assessing Nestin and β-III-tubulin expression. Following single DBZ treatment and combination DBZ and TMZ treatment IF staining shows for CSC-5-EV, CSC-5-mDLL4 and CSC-5-mJAG1 neurospheres, expression of β-III-tubulin is increased compared to untreated control. However, there is no obvious difference in Nestin expression following single or combination treatments (Figure 4.28).

Finally, the expression of the GCSC marker SOX2 alongside the marker of oligodendrocyte differentiation SOX10 was assessed by IF. For CSC-5-EV, CSC-5-mDLL4, and CSC-5-mJAG1 recovered neurospheres, IF staining shows increased levels SOX10 following single DBZ treatment compared to untreated control. Single TMZ treatment shows increased staining for the GCSC marker SOX2, whilst combination DBZ and TMZ treatment shows increased expression of SOX10 compared to DMSO control (Figure 4.29). Taken together, the above results suggest Notch inhibition by the GSI DBZ results in the differentiation of GCSCs

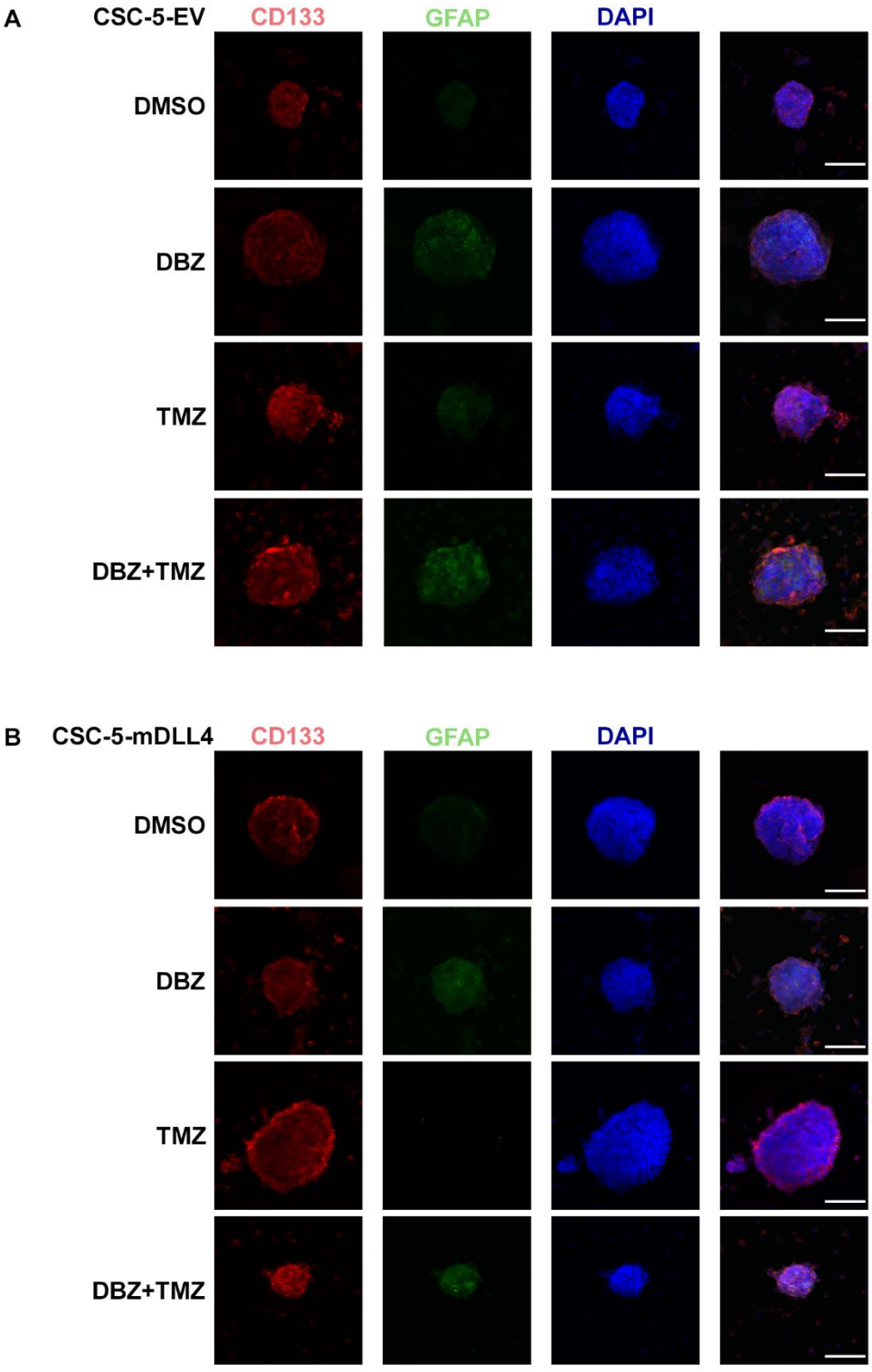
A
CSC-5-EV
CD133
GFAP
DAPI
DMSO
DBZ
TMZ
DBZ+TMZ
B
CSC-5-mDLL4
CD133
GFAP
DAPI
DMSO
DBZ
TMZ
DBZ+TMZ

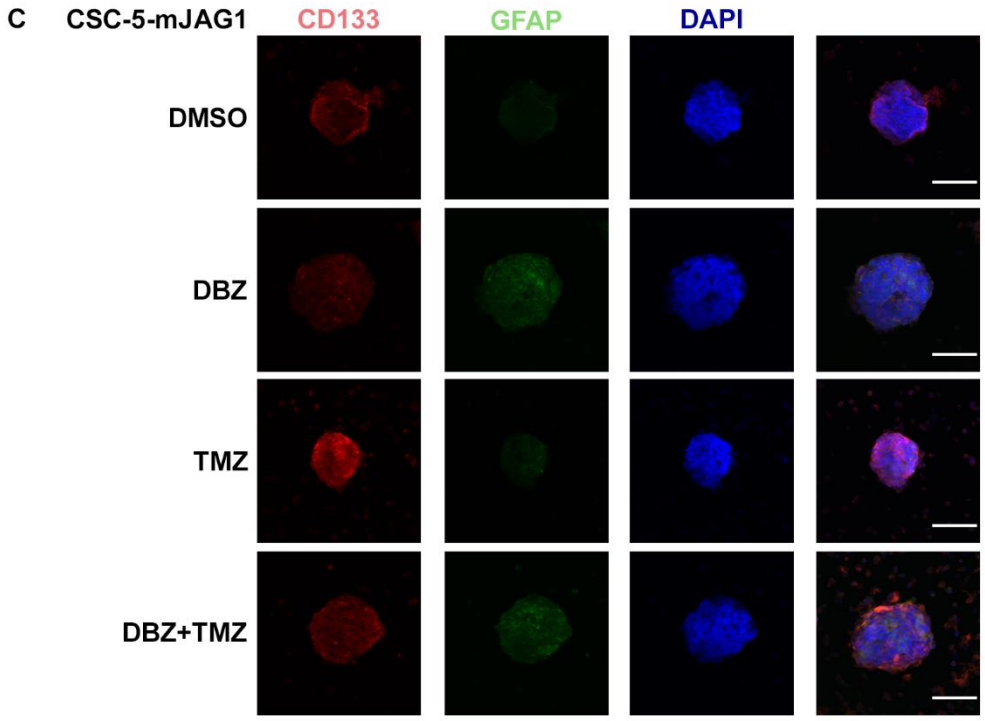

Figure 4.27: Immunofluorescent staining of CD133 and GFAP following CSC-5 neurosphere recovery following single DBZ/TMZ and combination DBZ and TMZ treatment.

Representative confocal images of CD133 and GFAP staining in **(A)** CSC-5-EV, **(B)** CSC-5-mDLL4, and **(C)** CSC-5-mJAG1 neurospheres following recovery from single and combination treatments. CSC-5 cells (12,000 per well in a 6-well plate) were cultured in CSC medium and immediately treated with single 25 nM DBZ/25 µM TMZ, combination 25 nM DBZ and 25 µM TMZ, or DMSO control treatment. Primary neurosphere formation was assessed 7 days after seeding. Following addition of fresh CSC media and a further week in culture, neurosphere recovery was assessed at day 14. Recovered neurospheres were fixed in 4% PFA and immunostained for mouse anti-β-III-tubulin (1:250; R & D Systems #MAB1195) and rabbit anti-Nestin (1:250; Sigma Aldrich #N5413) followed by goat anti-rabbit IgG Alexa Fluor 647 (1:1000; ThermoFisher Scientific #A21245) and donkey anti-mouse IgG Alexa Fluor 568 (1:1000; ThermoFisher Scientific #A10037) secondary antibodies. Nuclei were counterstained with 2 µg/mL DAPI. Scale bar = 100 µm.

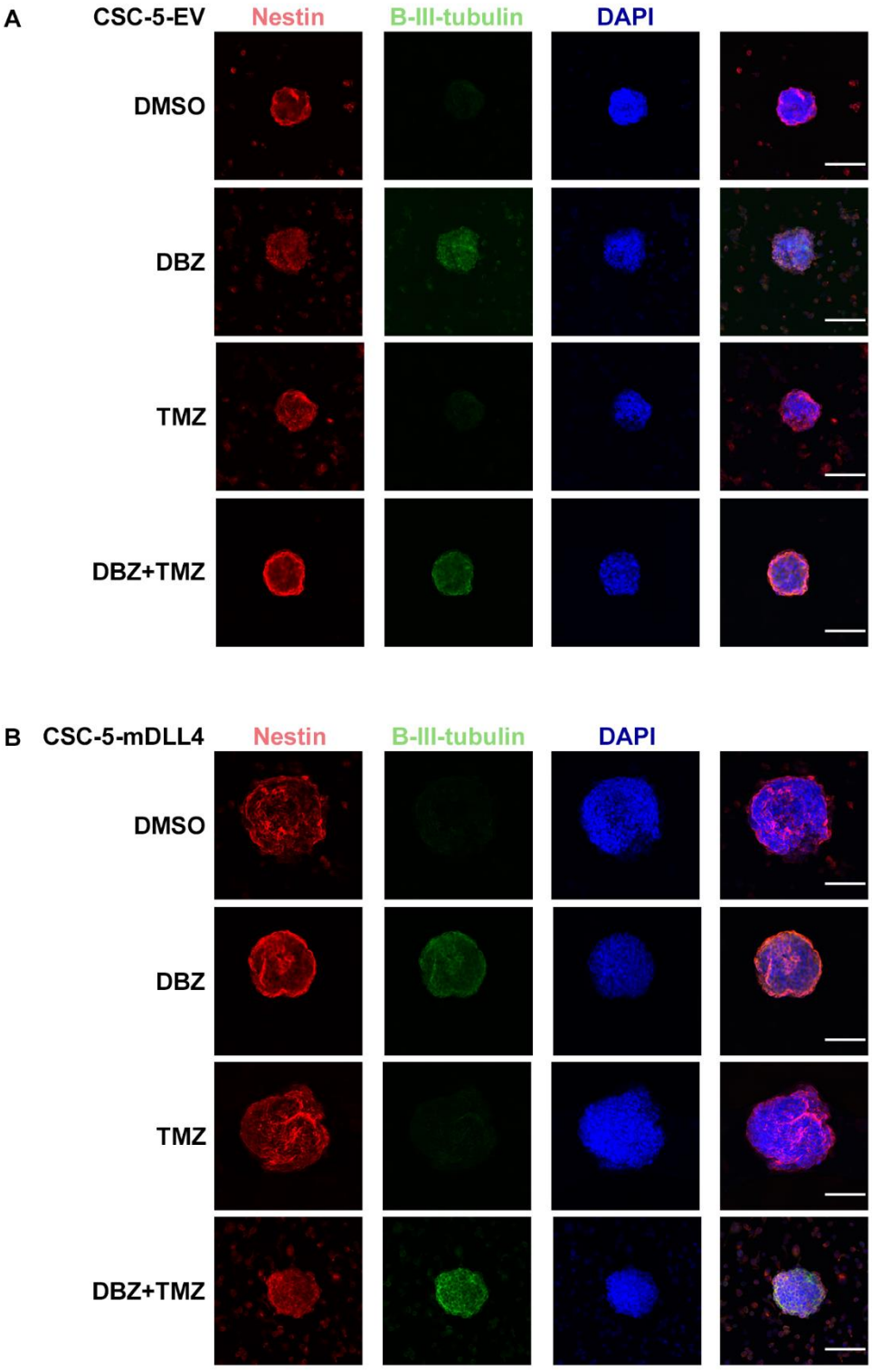
A
CSC-5-EV
Nestin
B-III-tubulin
DAPI
DMSO
DBZ
TMZ
DBZ+TMZ
B
CSC-5-mDLL4
Nestin
B-III-tubulin
DAPI
DMSO
DBZ
TMZ
DBZ+TMZ

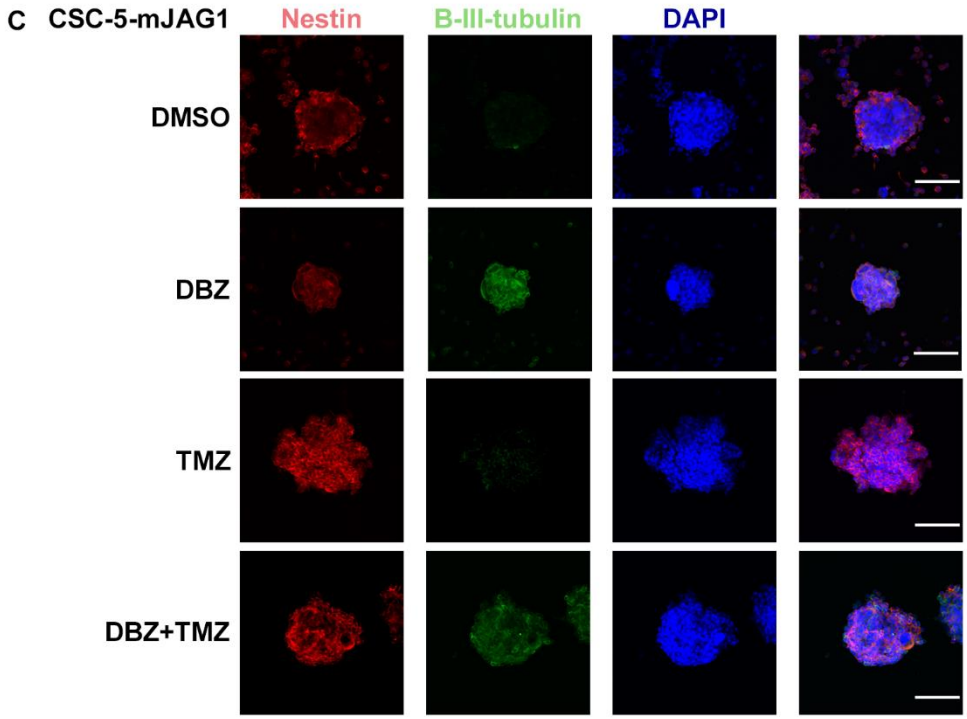

Figure 4.28: Immunofluorescent staining of Nestin and β-III-tubulin following CSC-5 neurosphere recovery following single DBZ/TMZ and combination DBZ and TMZ treatment.

Representative confocal images of Nestin and β-III-tubulin staining in **(A)** CSC-5-EV, **(B)** CSC-5-mDLL4, and **(C)** CSC-5-mJAG1 neurospheres following recovery from single and combination treatments. CSC-5 cells (12,000 per well in a 6-well plate) were cultured in CSC medium and immediately treated with single 25 nM DBZ/25 µM TMZ, combination 25 nM DBZ and 25 µM TMZ, or DMSO control treatment. Primary neurosphere formation was assessed 7 days after seeding. Following addition of fresh CSC media and a further week in culture, neurosphere recovery was assessed at day 14. Recovered neurospheres were fixed in 4% PFA and immunostained for mouse anti-β-III-tubulin (1:250; R & D Systems #MAB1195) and rabbit anti-Nestin (1:250; Sigma Aldrich #N5413) followed by goat anti-rabbit IgG Alexa Fluor 647 (1:1000; ThermoFisher Scientific #A21245) and donkey anti-mouse IgG Alexa Fluor 568 (1:1000; ThermoFisher Scientific #A10037) secondary antibodies. Nuclei were counterstained with 2 µg/mL DAPI. Scale bar = 100 µm.

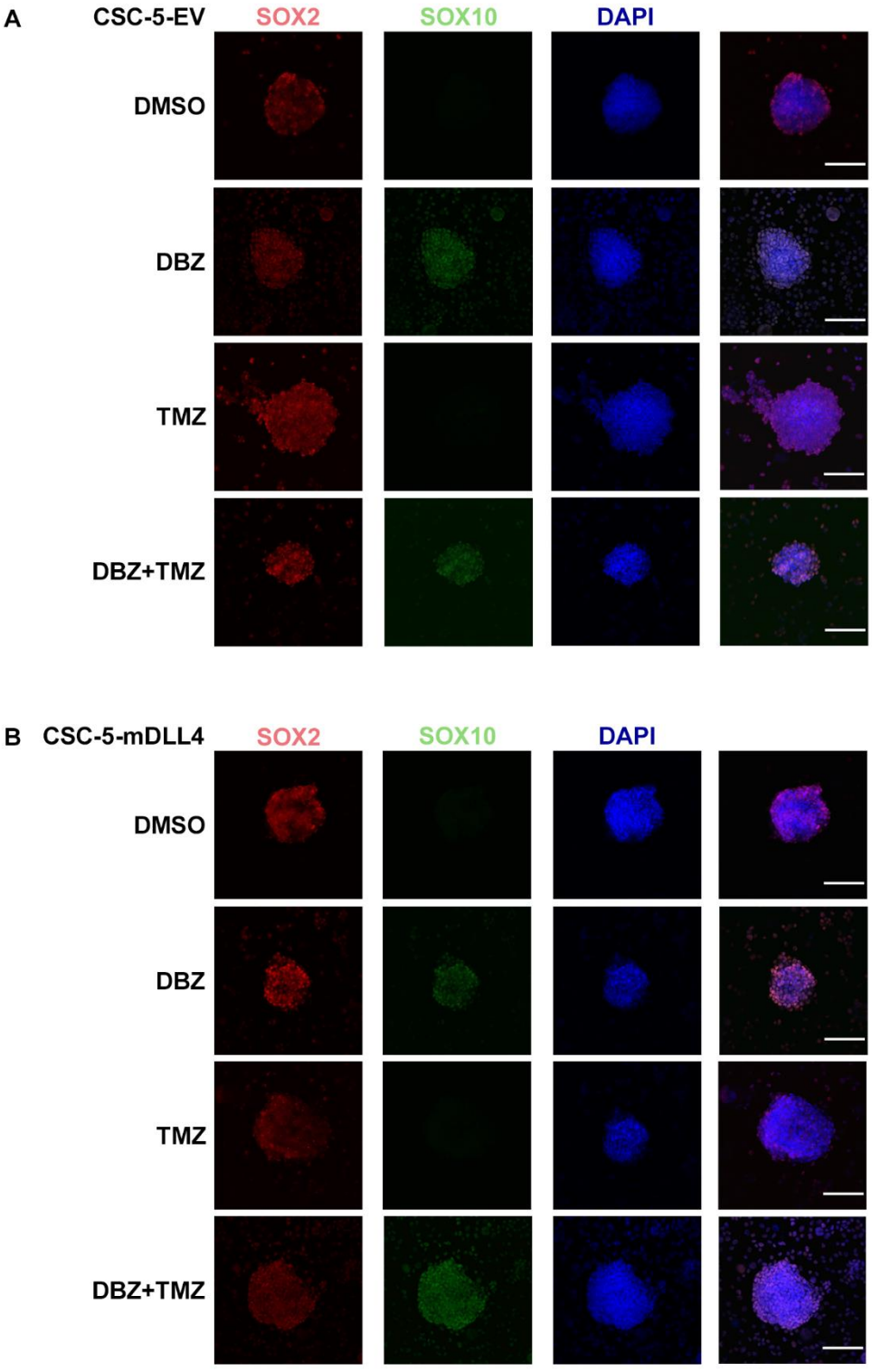
A
CSC-5-EV
SOX2
SOX10
DAPI
DMSO
DBZ
TMZ
DBZ+TMZ
B
CSC-5-mDLL4
SOX2
SOX10
DAPI
DMSO
DBZ
TMZ
DBZ+TMZ

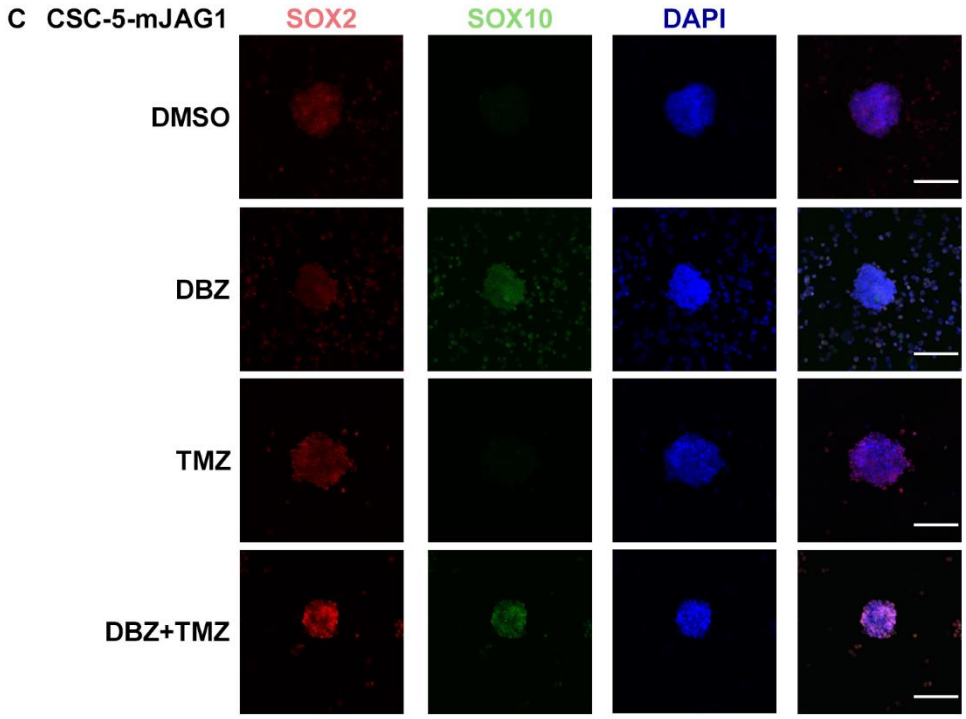

Figure 4.29: Immunofluorescent staining of SOX2 and SOX10 following CSC-5 neurosphere recovery following single DBZ/TMZ and combination DBZ and TMZ treatment.

Representative confocal images of SOX2 and SOX10 staining in **(A)** CSC-5-EV, **(B)** CSC-5-mDLL4, and **(C)** CSC-5-mJAG1 neurospheres following recovery from single and combination treatments. CSC-5 cells (12,000 per well in a 6-well plate) were cultured in CSC medium and immediately treated with single 25 nM DBZ/25 µM TMZ, combination 25 nM DBZ and 25 µM TMZ, or DMSO control treatment. Primary neurosphere formation was assessed 7 days after seeding. Following addition of fresh CSC media and a further week in culture, neurosphere recovery was assessed at day 14. Recovered neurospheres were fixed in 4% PFA and immunostained for mouse anti-SOX10 (1:250; R & D Systems #MAB2864) and rabbit anti-SOX2 (1:250; Abcam #AB97959) followed by goat anti-rabbit IgG Alexa Fluor 647 (1:1000; ThermoFisher Scientific #A21245) and donkey anti-mouse IgG Alexa Fluor 568 (1:1000; ThermoFisher Scientific #A10037) secondary antibodies. Nuclei were counterstained with 2 µg/mL DAPI. Scale bar = 100 µm.

4.3.6.2.2 Ki67 proliferation marker staining

IF staining was also used to assess the expression of the proliferation marker Ki67. We observed single TMZ treatment has no effect reducing Ki67 staining compared to DMSO control (Figure 4.30). However, single DBZ and combination DBZ and TMZ treatment shows reduced levels of Ki67 staining, suggesting inhibition of Notch signalling results in decreased proliferation of CSC-5 neurospheres.

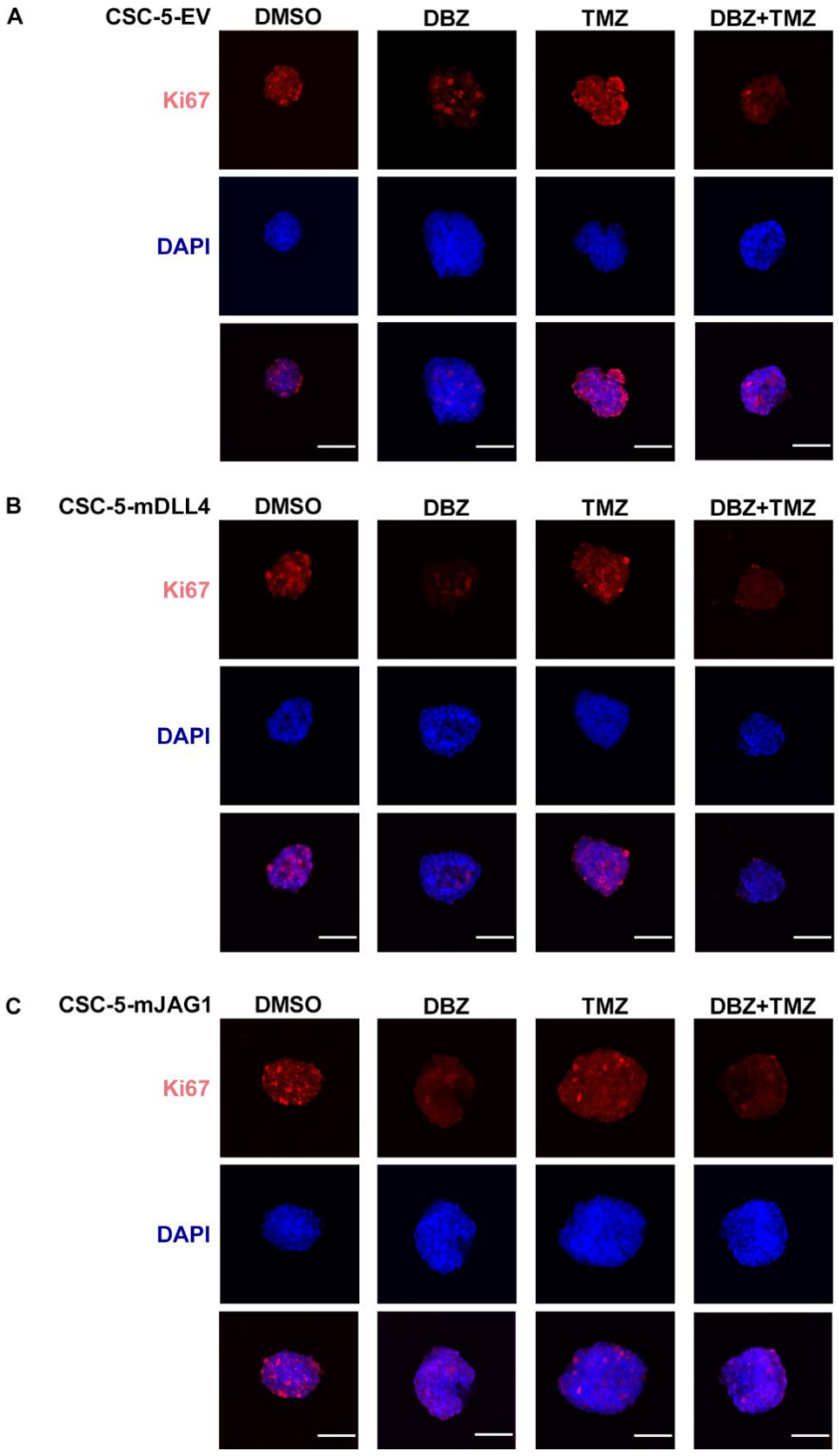

Figure 4.30: Immunofluorescent staining of the proliferation marker Ki67 following CSC-5 neurosphere recovery following single DBZ/TMZ and combination DBZ and TMZ treatment.

Representative confocal images of Ki67 staining in **(A)** CSC-5-EV, **(B)** CSC-5-mDLL4, and **(C)** CSC-5-mJAG1 neurospheres following recovery from single and combination treatments. CSC-5 cells (12,000 per well in a 6-well plate) were cultured in CSC medium and immediately treated with single 25 nM DBZ/25 µM TMZ, combination 25 nM DBZ and 25 µM TMZ, or DMSO control treatment. Primary neurosphere formation was assessed 7 days after seeding. Following

addition of fresh CSC media and a further week in culture, neurosphere recovery was assessed at day 14. Recovered neurospheres were fixed in 4% PFA and immunostained for rabbit anti-Ki67 (1:1000; Abcam #AB15580) followed by goat anti-rabbit IgG Alexa Fluor 647 (1:1000; ThermoFisher Scientific #A21245) secondary antibody; nuclei were counterstained with 2 µg/mL DAPI. Scale bar = 100 µm.

4.3.6.3 Secondary Neurosphere Formation

4.3.6.3.1 GCSC and neural differentiation marker expression

For CSC-5-EV, CSC-5-mDLL4, and CSC-5-mJAG1 secondary neurospheres, CD133 and GFAP expression was determined by IF. IF staining shows increased levels of the astrocytic marker GFAP following single DBZ treatment compared to untreated control. Single TMZ treatment shows increased staining for the GCSC marker CD133, whilst combination DBZ and TMZ treatment shows increased expression of GFAP compared to DMSO control (Figure 4.31).

Similar results were obtained when assessing Nestin and β-III-tubulin expression. Following single DBZ treatment and combination DBZ and TMZ treatment IF staining suggest expression of β-III-tubulin is increased compared to untreated control. However, there is no obvious difference in the expression of Nestin following single or combination treatments (Figure 4.32).

Finally, the expression of the GCSC marker SOX2 alongside the marker of oligodendrocyte differentiation SOX10 was assessed by IF. For CSC-5-EV, CSC-5-mDLL4, and CSC-5-mJAG1 secondary neurospheres, IF staining shows increased levels SOX10 following single DBZ treatment compared to untreated control. Single TMZ treatment shows increased staining for the GCSC marker SOX2, whilst combination DBZ and TMZ treatment shows increased expression of SOX10 compared to DMSO control (Figure 4.33). Taken together, these results suggest Notch inhibition by the GSI DBZ results in differentiation of GCSCs

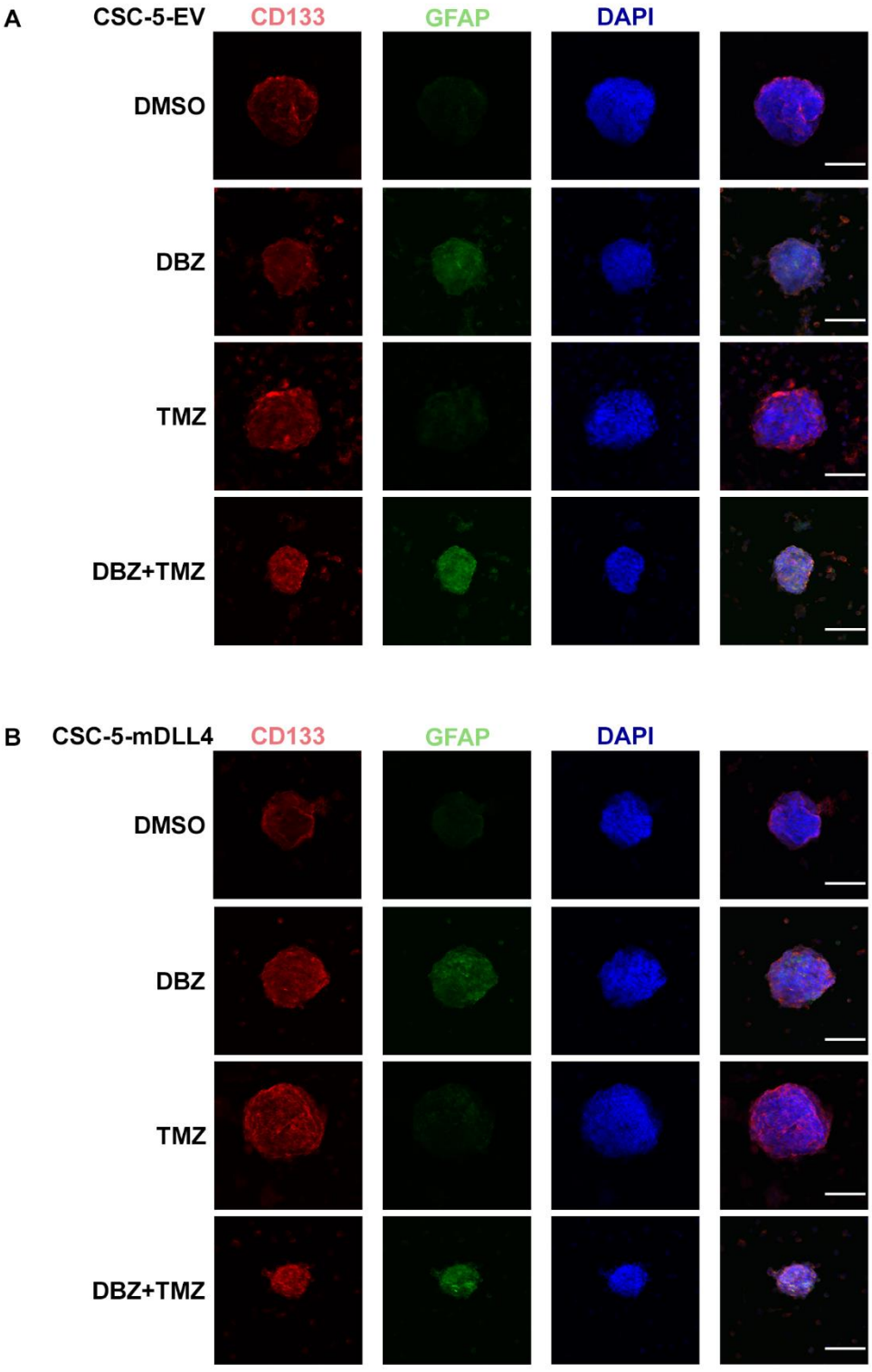
A
CSC-5-EV
CD133
GFAP
DAPI
DMSO
DBZ
TMZ
DBZ+TMZ
B
CSC-5-mDLL4
CD133
GFAP
DAPI
DMSO
DBZ
TMZ
DBZ+TMZ

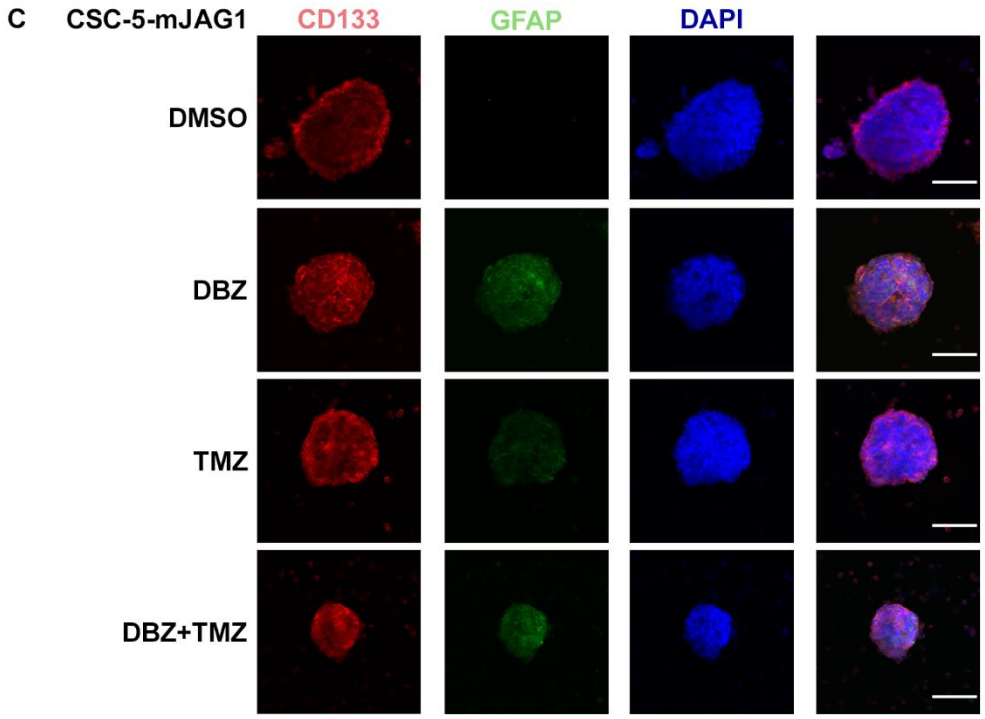

Figure 4.31: Immunofluorescent staining of CD133 and GFAP following CSC-5 secondary neurosphere formation following single DBZ/TMZ and combination DBZ and TMZ treatment.

Representative confocal images of CD133 and GFAP staining in **(A)** CSC-5-EV, **(B)** CSC-5-mDLL4, and **(C)** CSC-5-mJAG1 neurospheres following secondary neurosphere formation. CSC-5 cells (12,000 per well in a 6-well plate) were cultured in CSC medium and immediately treated with single 25 nM DBZ/25 µM TMZ, combination 25 nM DBZ and 25 µM TMZ, or DMSO control treatment. Primary neurosphere formation was assessed 7 days after seeding. Following addition of fresh CSC media and a further week in culture, neurosphere recovery was assessed at day 14. Neurospheres were then dissociated to single cells and re-seeded (12,000 cells per well in a 6-well plate). At day 21, the number of secondary neurospheres formed were assessed. Secondary neurospheres were fixed in 4% PFA and immunostained for mouse anti-β-III-tubulin (1:250; R & D Systems #MAB1195) and rabbit anti-Nestin (1:250; Sigma Aldrich #N5413) followed by goat anti-rabbit IgG Alexa Fluor 647 (1:1000; ThermoFisher Scientific #A21245) and donkey anti-mouse IgG Alexa Fluor 568 (1:1000; ThermoFisher Scientific #A10037) secondary antibodies. Nuclei were counterstained with 2 µg/mL DAPI. Scale bar = 100 µm.

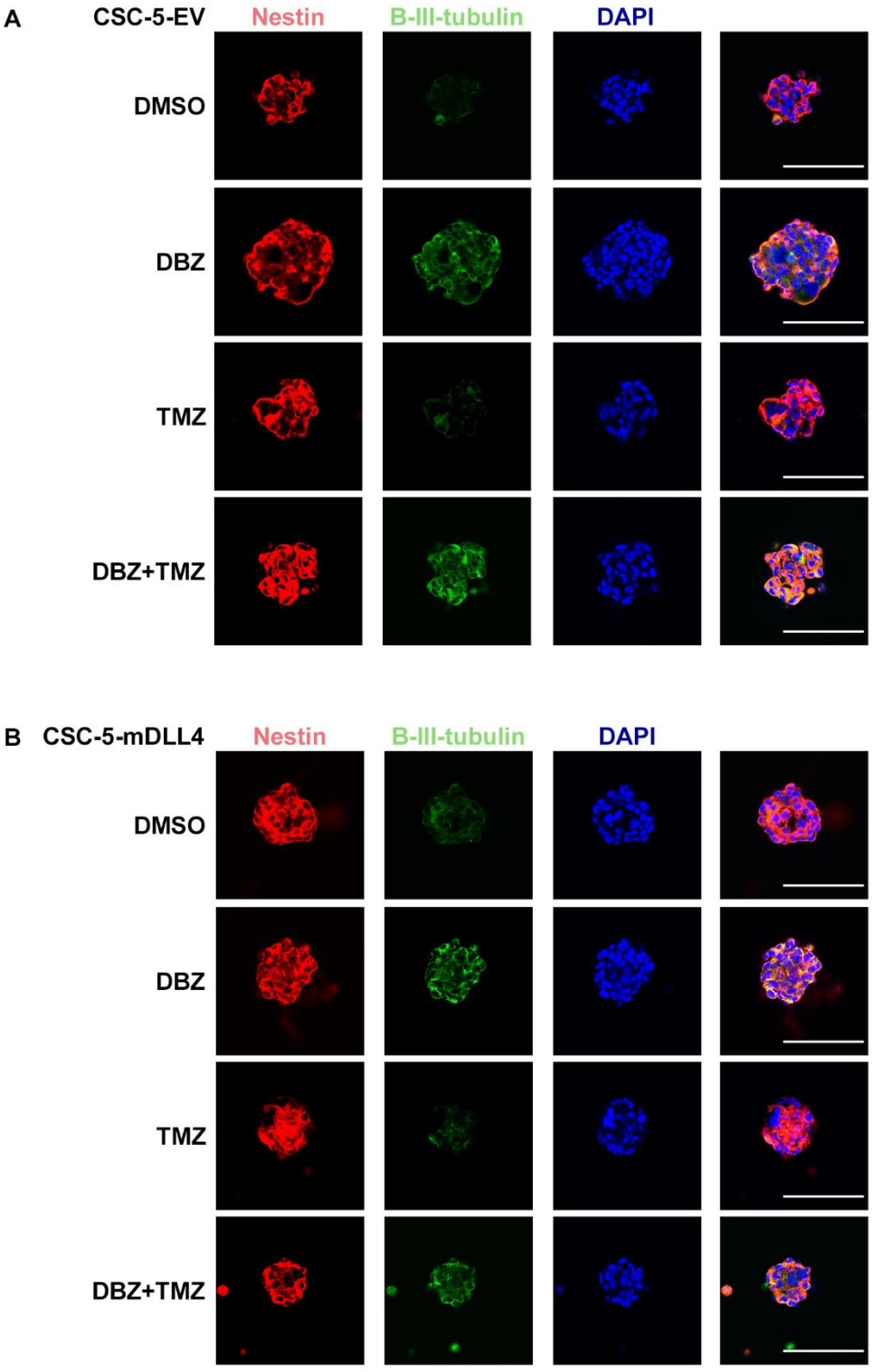
A
CSC-5-EV
Nestin
B-III-tubulin
DAPI
DMSO
DBZ
TMZ
DBZ+TMZ
B
CSC-5-mDLL4
Nestin
B-III-tubulin
DAPI
DMSO
DBZ
TMZ
DBZ+TMZ

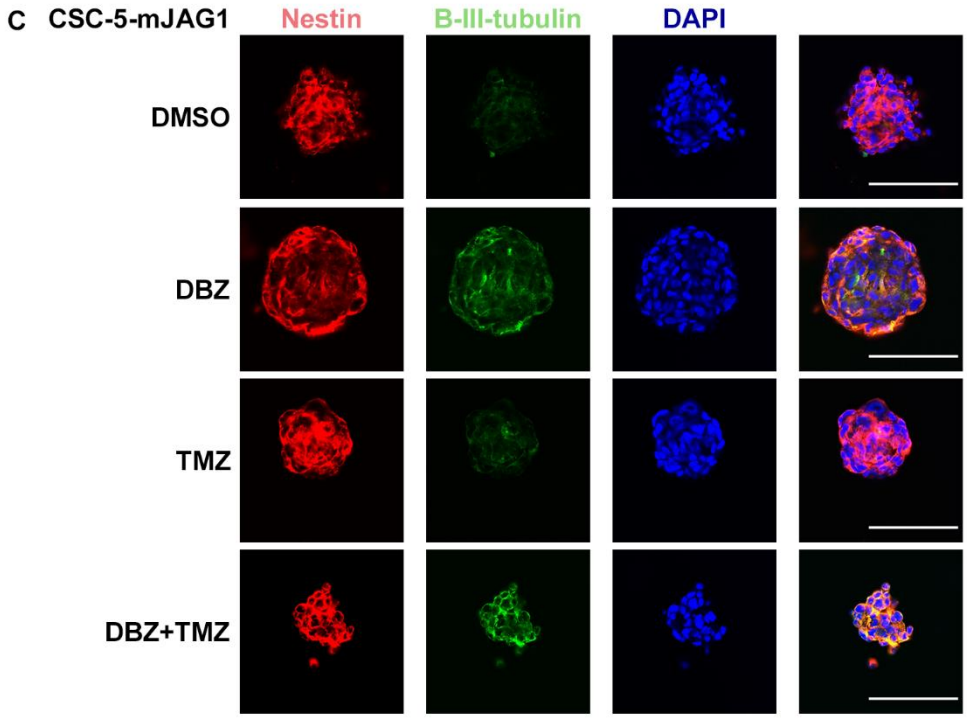

Figure 4.32: Immunofluorescent staining of Nestin and β-III-tubulin following CSC-5 secondary neurosphere formation following single DBZ/TMZ and combination DBZ and TMZ treatment.

Representative confocal images of Nestin and β-III-tubulin staining in **(A)** CSC-5-EV, **(B)** CSC-5-mDLL4, and **(C)** CSC-5-mJAG1 neurospheres following secondary neurosphere formation. CSC-5 cells (12,000 per well in a 6-well plate) were cultured in CSC medium and immediately treated with single 25 nM DBZ/25 µM TMZ, combination 25 nM DBZ and 25 µM TMZ, or DMSO control treatment. Primary neurosphere formation was assessed 7 days after seeding. Following addition of fresh CSC media and a further week in culture, neurosphere recovery was assessed at day 14. Neurospheres were then dissociated to single cells and re-seeded (12,000 cells per well in a 6-well plate). At day 21, the number of secondary neurospheres formed were assessed. Secondary neurospheres were fixed in 4% PFA and immunostained for mouse anti-β-III-tubulin (1:250; R & D Systems #MAB1195) and rabbit anti-Nestin (1:250; Sigma Aldrich #N5413) followed by goat anti-rabbit IgG Alexa Fluor 647 (1:1000; ThermoFisher Scientific #A21245) and donkey anti-mouse IgG Alexa Fluor 568 (1:1000; ThermoFisher Scientific #A10037) secondary antibodies. Nuclei were counterstained with 2 µg/mL DAPI. Scale bar = 100 µm.

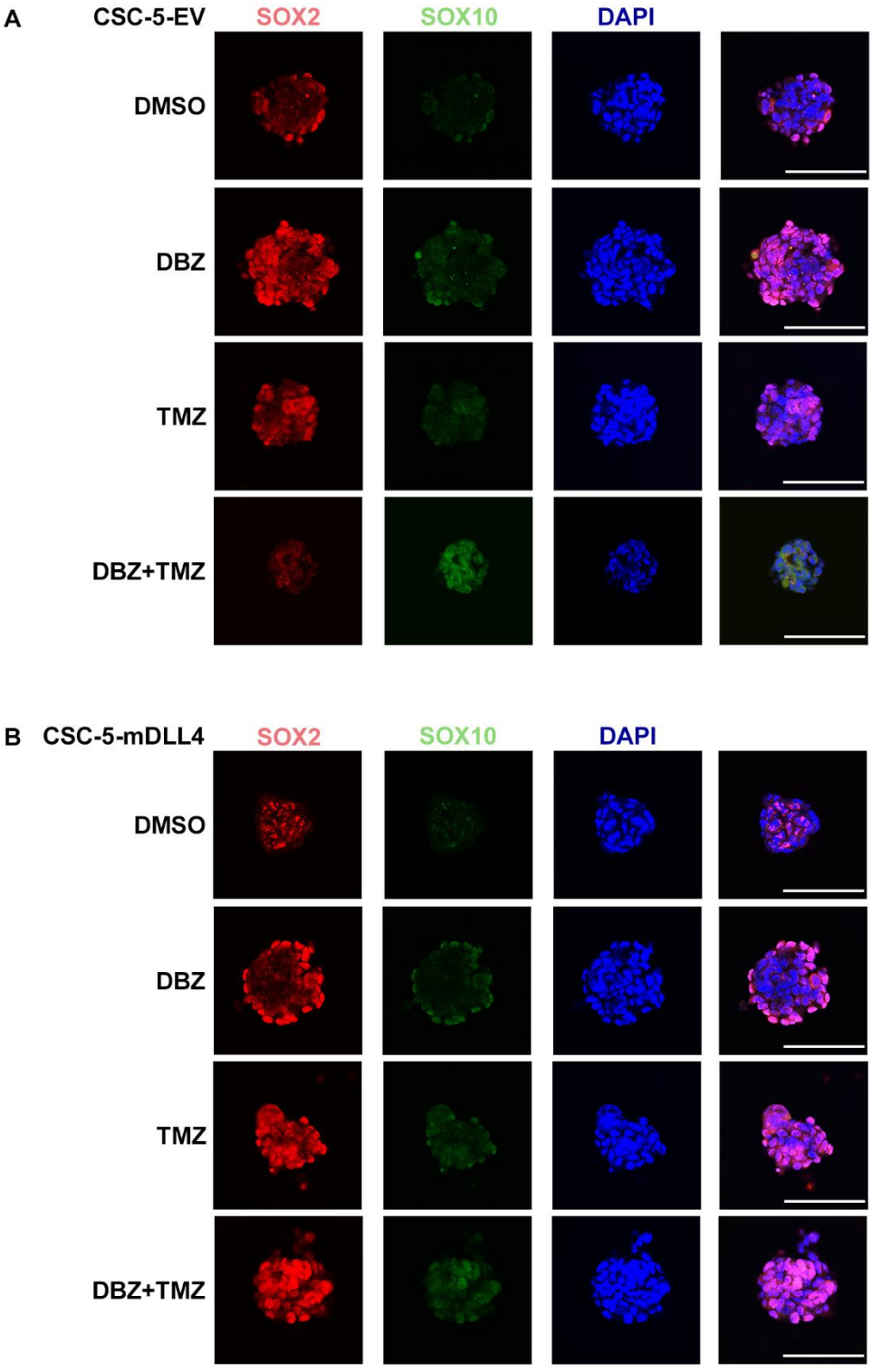
A
CSC-5-EV
SOX2
SOX10
DAPI
DMSO
DBZ
TMZ
DBZ+TMZ
B
CSC-5-mDLL4
SOX2
SOX10
DAPI
DMSO
DBZ
TMZ
DBZ+TMZ

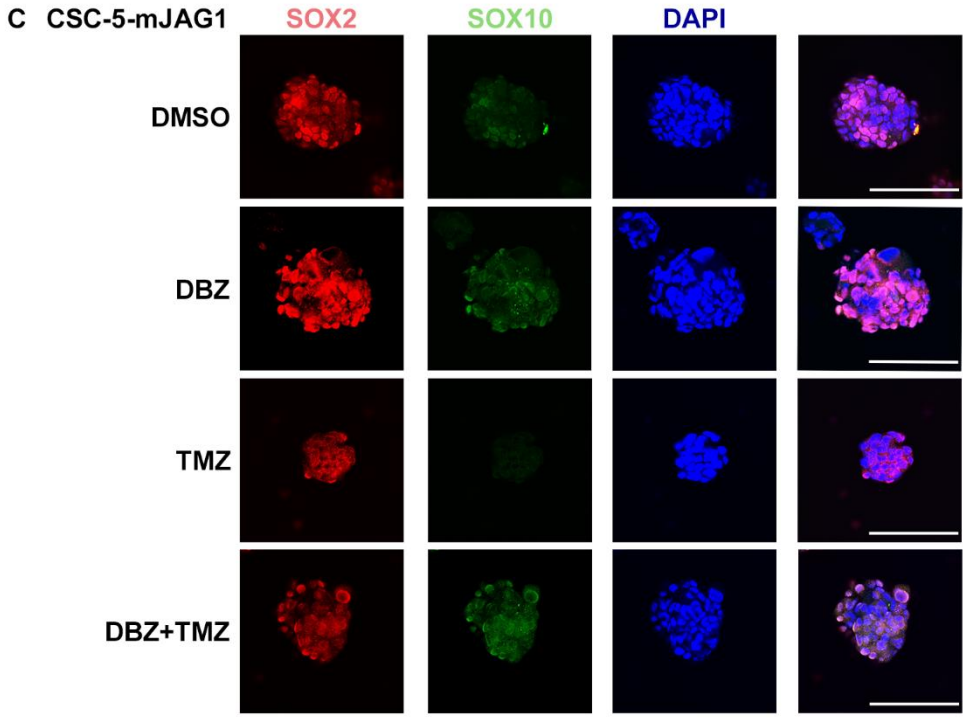

Figure 4.33: Immunofluorescent staining of SOX2 and SOX10 following CSC-5 secondary neurosphere formation following single DBZ/TMZ and combination DBZ and TMZ treatment.

Representative confocal images of SOX2 and SOX10 staining in **(A)** CSC-5-EV, **(B)** CSC-5-mDLL4, and **(C)** CSC-5-mJAG1 neurospheres following secondary neurosphere formation. CSC-5 cells (12,000 per well in a 6-well plate) were cultured in CSC medium and immediately treated with single 25 nM DBZ/25 µM TMZ, combination 25 nM DBZ and 25 µM TMZ, or DMSO control treatment. Primary neurosphere formation was assessed 7 days after seeding. Following addition of fresh CSC media and a further week in culture, neurosphere recovery was assessed at day 14. Neurospheres were then dissociated to single cells and re-seeded (12,000 cells per well in a 6-well plate). At day 21, the number of secondary neurospheres formed were assessed. Secondary neurospheres were fixed in 4% PFA and immunostained for mouse anti-SOX10 (1:250; R & D Systems #MAB2864) and rabbit anti-SOX2 (1:250; Abcam #AB97959) followed by goat anti-rabbit IgG Alexa Fluor 647 (1:1000; ThermoFisher Scientific #A21245) and donkey anti-mouse IgG Alexa Fluor 568 (1:1000; ThermoFisher Scientific #A10037) secondary antibodies. Nuclei were counterstained with 2 µg/mL DAPI. Scale bar = 100 µm.

4.3.6.3.2 Ki67 proliferation marker staining

IF staining was also used to assess Ki67 expression. We observed single TMZ treatment has no effect reducing Ki67 staining compared to DMSO control (Figure 4.34). However, single DBZ and combination DBZ and TMZ treatment shows reduced levels of Ki67 staining, suggesting inhibition of Notch signalling results in decreased proliferation of CSC-5 neurospheres.

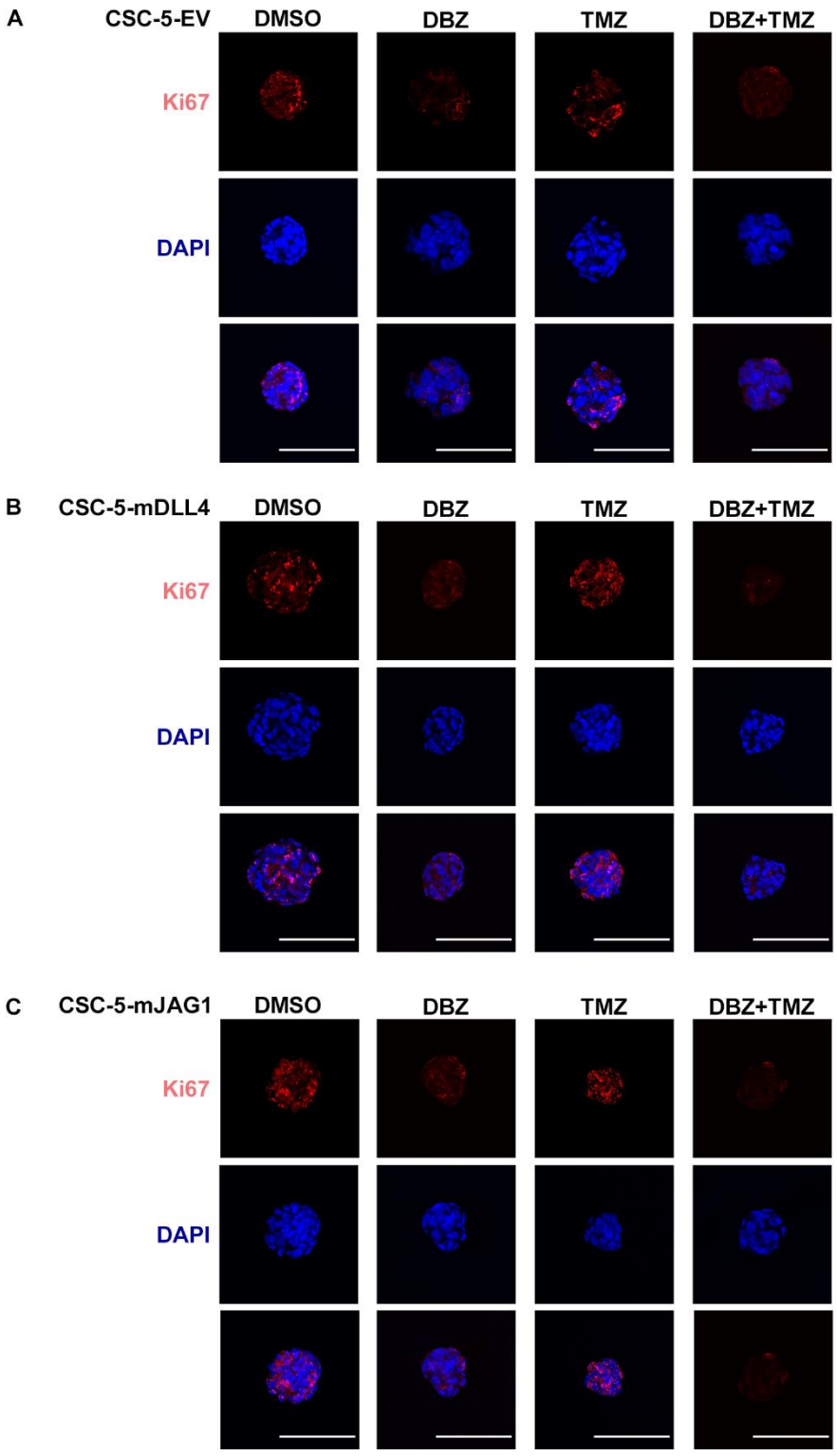

Figure 4.34: Immunofluorescent staining of the proliferation marker Ki67 following CSC-5 neurosphere secondary neurosphere formation.

Representative confocal images of Ki67 staining in **(A)** CSC-5-EV, **(B)** CSC-5-mDLL4, and **(C)** CSC-5-mJAG1 secondary neurospheres following single and combination treatments. CSC-5 cells (12,000 per well in a 6-well plate) were cultured in CSC medium and immediately treated with single 25 nM DBZ/25 µM TMZ, combination 25 nM DBZ and 25 µM TMZ, or DMSO control treatment. Primary neurosphere formation was assessed 7 days after seeding. Following addition of fresh CSC media and a further week in culture, neurosphere recovery was assessed

at day 14. Neurospheres were then dissociated to single cells and re-seeded (12,000 cells per well in a 6-well plate). At day 21, the number of secondary neurospheres formed were assessed. Secondary neurospheres were fixed in 4% PFA and immunostained for rabbit anti-Ki67 (1:1000; Abcam #AB15580) followed by goat anti-rabbit IgG Alexa Fluor 647 (1:1000; ThermoFisher Scientific #A21245) secondary antibody; nuclei were counterstained with 2 µg/mL DAPI. Scale bar = 100 µm.

4.3.7 DLL4 and JAG1 knockdown reduces Notch signalling in the glioma cancer stem cell line, CSC-5.

4.3.7.1 Characterisation of CSC-5 following DLL4 and JAG1 knockdown

The GCSC cell line CSC-5 was transduced with shRNA lentiviral particles targeting DLL4 and JAG1. Positively transduced cells were selected using puromycin, and the cell line was initially characterised to ensure successful knockdown of DLL4 and JAG1 expression by qPCR and Western blot analysis. *DLL4* and *JAG1* gene expression was significantly reduced in CSC-5-DLL4 shRNA and CSC-5-JAG1 shRNA, respectively (Figure 4.35A). In addition, Western blotting revealed DLL4 and JAG1 protein expression is significantly reduced in CSC-5-DLL4 shRNA and CSC-5-JAG1 shRNA, compared to CSC-5 shRNA control (Figure 4.35B).

4.3.7.2 Notch signalling is inhibited in CSC-5 cells following DLL4 and JAG1 knockdown

Analysis was performed to ensure shRNA knockdown of DLL4 and JAG1 reduced Notch signalling in CSC-5 cells. qPCR analysis revealed shRNA targeting of DLL4 and JAG1 significantly reduced the mRNA expression of the Notch downstream target genes *HES1, HEY1,* and *HEY2*, compared to CSC-5 shRNA control (Figure 4.36A). Protein expression of cleaved activated Notch1 and Hes1 was also reduced in CSC-5-DLL4 shRNA and CSC-5-JAG1 shRNA cells respectively, compared to CSC-5 shRNA control (Figure 4.36B).

4.3.8 DLL4 and JAG1 Knockdown Reduces CSC-5 Neurosphere Growth

Utilising the CSC-5 cells transduced with lentiviral particles targeting DLL4 and JAG1, we next performed the neurosphere recovery assay to assess CSC-5 primary neurosphere formation, neurosphere recovery and secondary neurosphere formation following single and combination treatment.

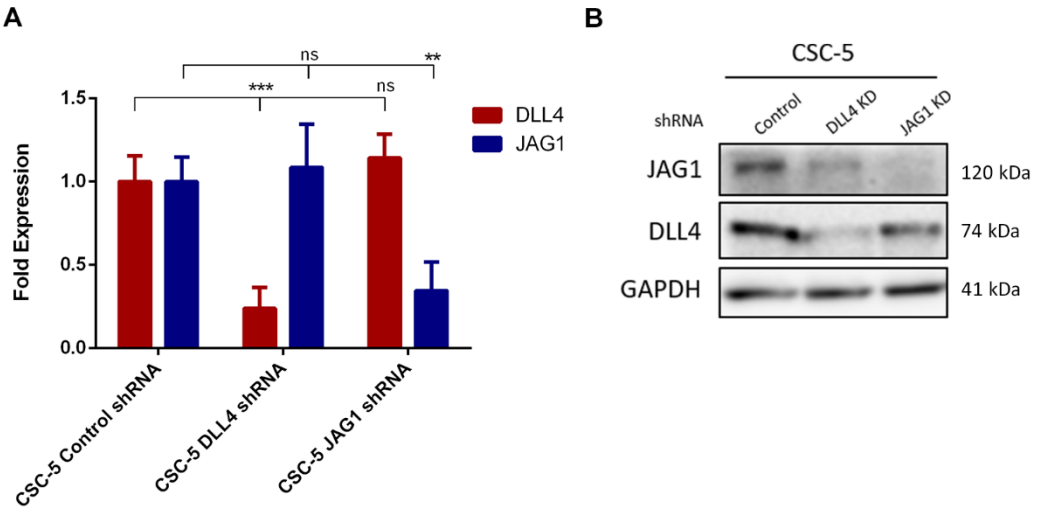

Figure 4.35: Expression of DLL4 and JAG1 in CSC-5 glioma cancer stem cells transduced with shRNA lentiviral particles targeting DLL4 and JAG1.

The CSC-5 cell line was transduced with shRNA lentiviral particles targeting DLL4 and JAG1. RNA was extracted and **(A)** mRNA expression of *DLL4* and *JAG1* was determined by qPCR normalised to *GAPDH*. **(B)** Protein expression of DLL4 and JAG1 in the CSC-5 cell line confirmed successful shRNA knockdown. Protein was extracted from cells and separated (20 µg) by SDS-PAGE (10% SDS gel). Membranes were probed with rabbit anti-DLL4 (1:1000; Abcam #AB7280), rabbit anti-JAG1 (1:1000; Cell Signalling Technology #2626), and mouse anti-GAPDH (1:2000; ThermoFisher Scientific #MA5-15738) in 5% milk in PBS-T overnight at 4 ^{o}C. Membranes were washed and probed with anti-rabbit IgG HRP conjugate (1:5000, ThermoFisher Scientific #65-6120) and anti-mouse IgG HRP conjugate (1:5000; ThermoFisher Scientific #31430) secondary antibodies in 5% milk in PBS-T at RT for 1 h. ECL. (Mean ± SEM, n = 3, two-way ANOVA with Dunnett's post-hoc test, ** $p < 0.01$, *** $p < 0.001$, and ns denotes not significant).

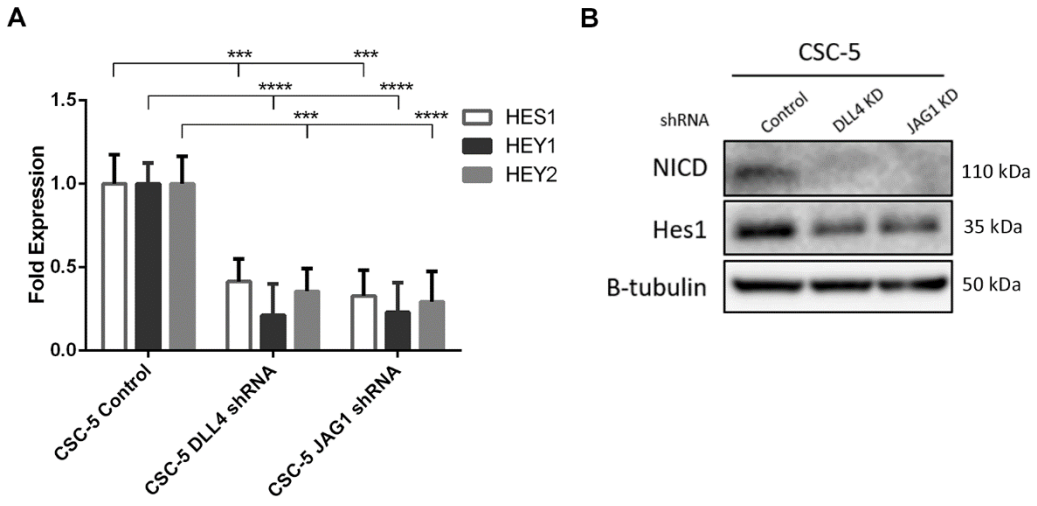

Figure 4.36: DLL4 and JAG1 shRNA knockdown reduces Notch signalling in CSC-5 glioma cancer stem cells.

The CSC-5 cell line was transduced with shRNA lentiviral particles targeting DLL4 and JAG1. RNA was extracted and **(A)** mRNA expression of the Notch target genes *HES1*, *HEY1*, and *HEY2* was determined by qPCR normalised to *GAPDH*. **(B)** Protein expression of cleaved Notch1 and Hes1 in the CSC-5 cell lines confirmed successful induction of Notch signalling following shRNA knockdown of DLL4 and JAG1. Protein was extracted from cells and separated (20 µg) by SDS-PAGE (10% SDS gel). Membranes were probed with rabbit anti-cleaved Notch1 (1:1000), rabbit anti-Hes1 (1:1000; Cell Signalling Technology #11988), and mouse anti-GAPDH (1:2000; ThermoFisher Scientific #MA5-15738) in 5% milk in PBS-T overnight at 4 °C. Membranes were washed and probed with anti-rabbit IgG HRP conjugate (1:5000, ThermoFisher Scientific #65-6120) and anti-mouse IgG HRP conjugate (1:5000; ThermoFisher Scientific #31430) secondary antibodies in 5% milk in PBS-T at RT for 1 h. ECL. (Mean ± SEM, n = 3, two-way ANOVA with Dunnett's post-hoc test, *** $p < 0.001$, **** $p < 0.0001$, and ns denotes not significant).

4.3.8.1 CSC-5 Primary Neurosphere Formation

shRNA knockdown of DLL4 and JAG1 resulted in a significant decrease in the number of CSC-5 neurospheres formed compared to CSC-5 control shRNA (Figure 4.37A-B). Treatment with the Notch inhibitor DBZ resulted in a significant decrease in the number of CSC-5 neurospheres formed by 67.6%, 58.1% and 47.5% respectively for CSC-5-control shRNA, CSC-5 DLL4 shRNA, and CSC-5-JAG1 shRNA compared to DMSO control. TMZ treatment also reduced the number of neurosphere formed by 13.6%, 45.6%, and 60.5% respectively, for CSC-5-control shRNA, CSC-5 DLL4 shRNA, and CSC-5-JAG1 shRNA compared to DMSO control. However, combination TMZ and DBZ treatment resulted in the most significant decrease in primary neurosphere formation, resulting in a reduction of the number of neurospheres by 83.3%, 81.25%, and 77.8% respectively for CSC-5-control shRNA, CSC-5 DLL4 shRNA, and CSC-5-JAG1 shRNA compared to DMSO control. The percentage reductions in neurosphere number for the CSC-5 DLL4 shRNA and CSC-5-JAG1 shRNA combination treated neurospheres are less than that of CSC-5 control shRNA due to the neurosphere number being significantly reduced as a result of DLL4 and JAG1 knockdown.

4.3.8.2 CSC-5 Neurosphere Recovery

Similar to the results above, the number of CSC-5 neurospheres is significantly reduced following shRNA knockdown of DLL4 and JAG1 compared to CSC-5-EV control (Figure 4.38A-B). Single DBZ treatment resulted in a decrease in the number of CSC-5 neurospheres recovered by 18.3%, 48.1% and 45.8% respectively for CSC-5-control shRNA, CSC-5 DLL4 shRNA, and CSC-5-JAG1 shRNA compared to DMSO control. TMZ treatment had little effect the number of neurosphere formed for CSC-5

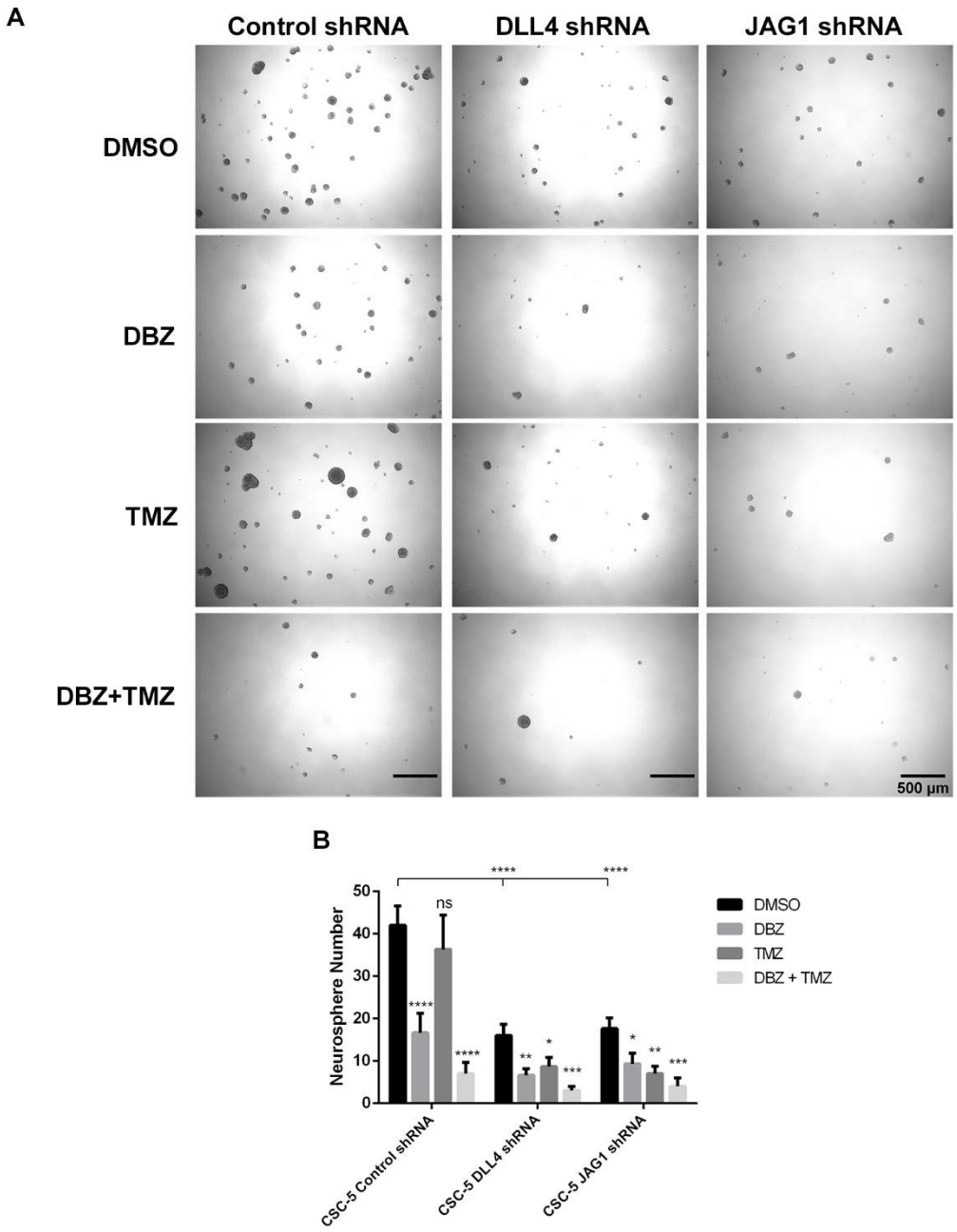

Figure 4.37: DLL4 and JAG1 shRNA knockdown significantly reduces CSC-5 primary neurosphere formation.

CSC-5 cells (12,000 per well in a 6-well plate) were cultured in CSC medium and immediately treated with single 25 nM DBZ/25 µM TMZ, combination 25 nM DBZ and 25 µM TMZ, or DMSO control treatment. Primary neurosphere formation was assessed 7 days after seeding. **(A)** Images showing CSC-5 primary neurosphere formation following single (DBZ/TMZ) and combination (DBZ and TMZ) treatment. **(B)** Quantification of the number of CSC-5 primary neurospheres formed following 7 days treatment. Scale bar = 500 µm. (Mean ± SD, n = 3, two-way ANOVA with Dunnett's post-hoc test, * $p < 0.05$, ** $p < 0.01$, *** $p < 0.001$, **** $p < 0.0001$, and ns denotes not significant).

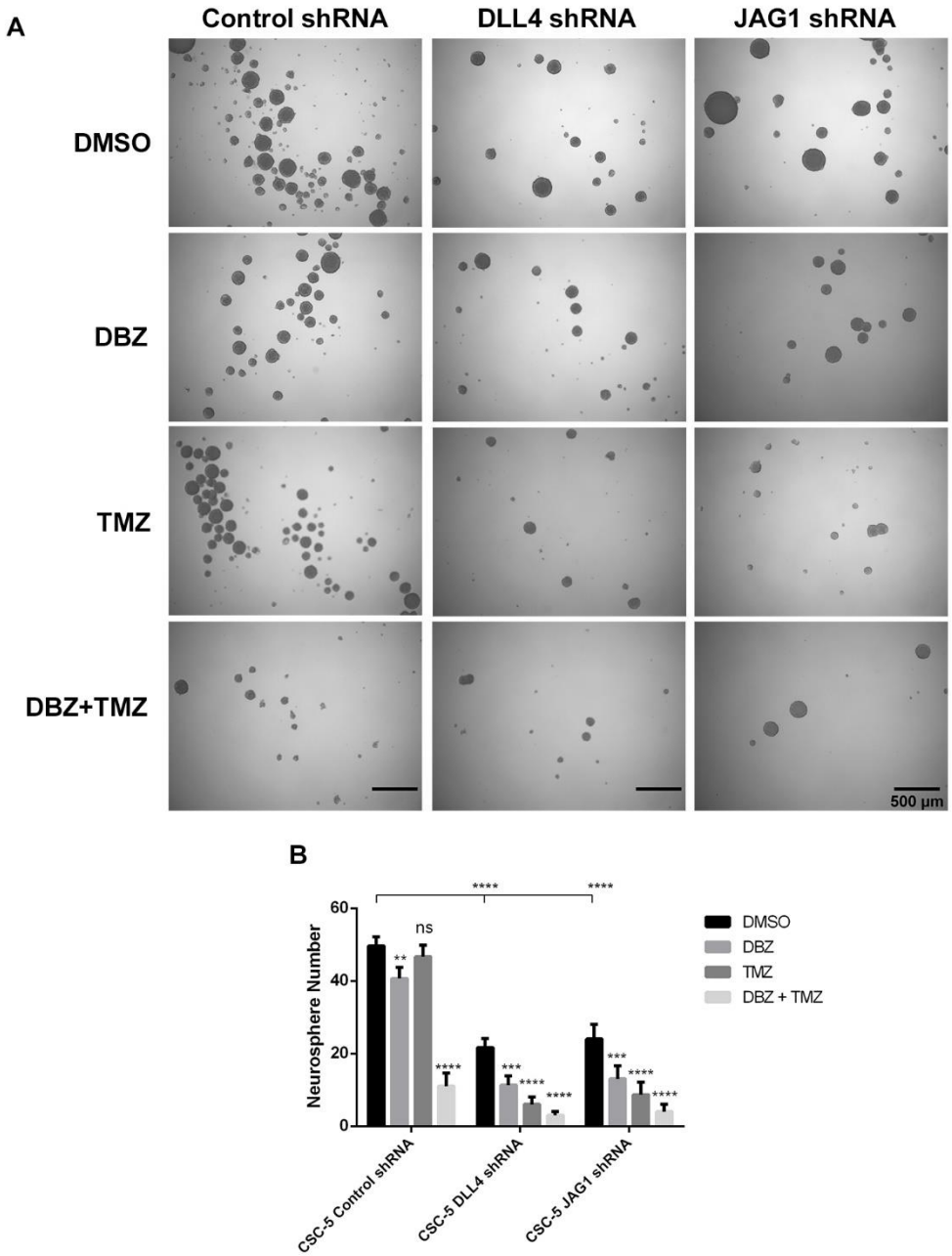

Figure 4.38: DLL4 and JAG1 shRNA knockdown significantly reduces CSC-5 neurosphere recovery.

CSC-5 cells (12,000 per well in a 6-well plate) were cultured in CSC medium and immediately treated with single 25 nM DBZ/25 µM TMZ, combination 25 nM DBZ and 25 µM TMZ, or DMSO control treatment. Primary neurosphere formation was assessed 7 days after seeding. Following addition of fresh CSC media and a further week in culture, neurosphere recovery was assessed at day 14. **(A)** Images showing CSC-5 neurosphere recovery following single (DBZ/TMZ) and combination (DBZ and TMZ) treatment. **(B)** Quantification of CSC-5 neurosphere recovery. Scale bar = 500 µm. (Mean ± SD, n = 3, two-way ANOVA with Dunnett's post-hoc test, ** $p < 0.01$, *** $p < 0.001$, **** $p < 0.0001$, and ns denotes not significant).

control shRNA treated neurospheres compared to untreated control, only reducing the number of neurospheres formed by 6%. Conversely for CSC-5 DLL4 shRNA and CSC-5 JAG1 shRNA knockdown neurospheres, neurosphere number was significantly reduced by 72.3% and 63.7% respectively compared to DMSO control. The combination effect of DLL4/JAG1 knockdown and TMZ treatment resulting in the reduction. Finally, combination TMZ and DBZ treatment resulted in a significant decrease in neurosphere recovery, resulting in a reduction of the number of neurospheres by 78.1%, 86.2%, and 83.3% respectively for CSC-5-control shRNA, CSC-5 DLL4 shRNA, and CSC-5-JAG1 shRNA compared to DMSO control.

4.3.8.3 CSC-5 Secondary Neurosphere Formation

shRNA knockdown of DLL4 and JAG1 had a significant effect in reducing the number of secondary neurospheres formed compared to CSC-5 control shRNA (Figure 4.39A-B). Single DBZ treatment resulted in a decrease in the number of CSC-5 secondary neurospheres by 16.1%, 18.4% and 11.9% respectively for CSC-5-control shRNA, CSC-5 DLL4 shRNA, and CSC-5-JAG1 shRNA compared to DMSO control. TMZ treatment had little effect the number of secondary neurospheres formed for CSC-5 control shRNA treated neurospheres compared to control, only reducing the number of neurospheres formed by 1.9%. Conversely for CSC-5 DLL4 shRNA and CSC-5 JAG1 shRNA knockdown neurospheres, neurosphere number was significantly reduced by 44.7% and 54.6% respectively compared to DMSO control. The combination effect of DLL4/JAG1 knockdown and TMZ treatment resulted in a significant reduction of neurosphere number. Combination DBZ and TMZ treatment resulted in a significant reduction of neurosphere number, reducing secondary neurosphere formation by 69.7%, 67.7%,

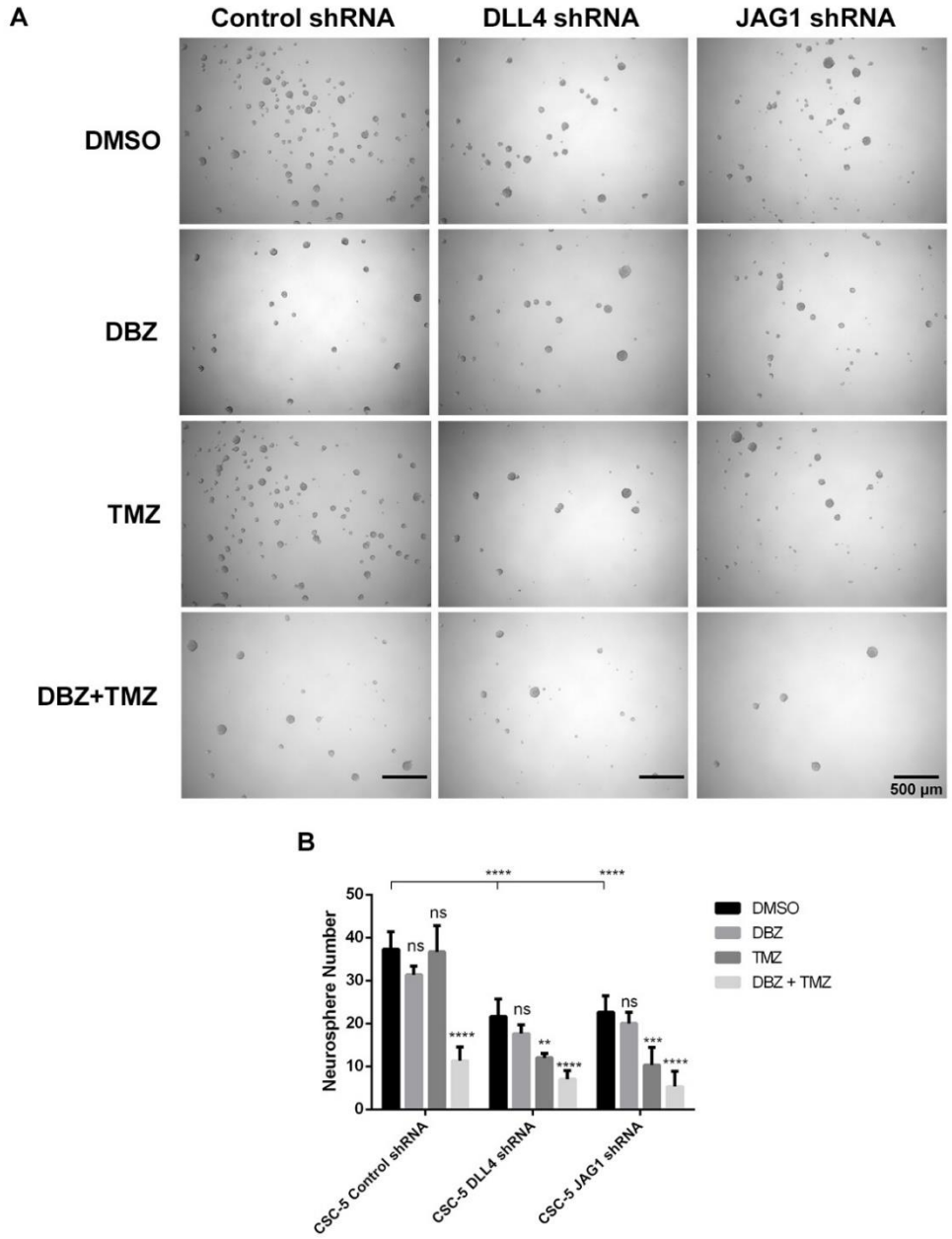

Figure 4.39: DLL4 and JAG1 shRNA knockdown significantly reduces CSC-5 secondary neurosphere formation.

CSC-5 cells (12,000 per well in a 6-well plate) were cultured in CSC medium and immediately treated with single 25 nM DBZ/25 µM TMZ, combination 25 nM DBZ and 25 µM TMZ, or DMSO control treatment. Primary neurosphere formation was assessed 7 days after seeding. Following addition of fresh CSC media and a further week in culture, neurosphere recovery was assessed at day 14. Neurospheres were then dissociated to single cells and re-seeded (12,000 cells per well in a 6-well plate). At day 21, the number of secondary neurospheres formed were counted as a measure of self-renewal. **(A)** Images showing CSC-5 secondary neurosphere formation following single (DBZ/TMZ) and combination (DBZ and TMZ) treatment and dissociation to single cells. **(B)** Quantification of CSC-5 neurosphere recovery. Scale bar = 500 µm. (Mean ± SD, n = 3, two-way ANOVA with Dunnett's post-hoc test, ** $p < 0.01$, *** $p < 0.001$, **** $p < 0.0001$, and ns denotes not significant).

and 76.7%, respectively, for CSC-5-control shRNA, CSC-5 DLL4 shRNA, and CSC-5-JAG1 shRNA compared to DMSO control.

Together, these results indicate the importance of DLL4 and JAG1 in the maintenance and proliferation of GCSCs as their knockdown significantly reduces neurosphere number. It also highlights inhibition of Notch signalling by DLL4 and JAG1 knockdown alongside TMZ treatment, as well as combination Notch inhibition and TMZ treatment significantly increase the sensitivity of glioblastoma to chemotherapy with TMZ by reducing GCSC turnover in the tumour.

4.4 Discussion

With the current standard of care, tumour recurrence in glioblastoma is highly likely due to the presence of GCSCs. These cells escape both radiotherapy- and chemotherapy-induced cell death and eventually re-enter the cell cycle contributing to tumour recurrence. Despite the advances in chemotherapy regimens, the median progression-free survival, which measures the time until tumour recurrence, is 6.9 months, with a median overall survival of 14.6 months with radiotherapy and TMZ (9). Therefore, there is a dire need to target the GCSC population that evades current treatment. Utilising conventional glioblastoma cell lines converted to neurosphere culture, and a patient derived GCSC line, CSC-5, we determined the role of DLL4- and JAG1-induced Notch signalling on GCSCs, and the effect TMZ and/or DBZ treatment has on neurosphere recovery.

The Notch signalling pathway is active in glioblastomas and GCSCs and can be inhibited with GSI treatment. As previously identified in Chapter 3, a 25 nM concentration of the GSI DBZ is sufficient to inhibit Notch signalling in glioblastoma cell lines. We successfully converted the adherent glioblastoma cell lines U87 and U251 to neurosphere culture by culturing these cells in CSC medium. This medium contains the mitogens EGF and FGF to promote the self-renewal of CSCs in culture (299).

We utilised the three timepoint neurosphere assay developed by Gilbert *et al.* (197), to assess the capacity of the cells cultured to repopulate following treatment with DBZ and/or TMZ. We utilised the *in vitro* neurosphere assay to study glioma response to drug treatments because neurospheres resemble the phenotypes and genotypes of the patients tumours more closely compared to 2D cultured cell lines (299, 315). In both the U87 and U251 cell line, it was identified that DLL4- and JAG1-induced Notch

signalling significantly increased primary neurosphere formation, neurosphere recovery, and secondary neurosphere formation compared to control. However, there was very little difference in neurosphere number between DLL4- and JAG1-induced Notch signalling. We have shown DLL4 and JAG1-induced Notch signalling regulates the self-renewal of U87 and U251 neurospheres, and this self-renewal is significantly inhibited upon combination DBZ and TMZ treatment. Similarly, in the patient derived GCSC cell line CSC-5, DLL4- and JAG1- induced Notch signalling significantly increased neurosphere number at the three timepoints of the neurosphere assay, and again this is significantly inhibited upon DBZ and TMZ combination treatment.

Conversely, we also performed shRNA knockdown of DLL4 and JAG1 in the CSC-5 cell line, which resulted in significantly reduced Notch signalling compared to control as show by decreased mRNA expression of the Notch target genes HES1, HEY1, and HEY2, alongside decreased protein expression of NCID and Hes1. In the DLL4 shRNA KD and JAG1 shRNA KD CSC-5 cells, neurosphere number was significantly reduced at the three timepoints of the neurosphere assay. Again, it was only the combination DBZ and TMZ treatment which resulted in a significant reduction of CSC-5 neurospheres compared to control. These results taken together with those in the U87 and U251 glioma cell lines cement the important role DLL4- and JAG1-induced Notch signalling in GCSC self-renewal.

The study by Gilbert *et al*. which developed the neurosphere assay also determined whether treatment scheduling of Notch inhibition and TMZ treatment affected neurosphere recovery. They tested whether Notch inhibition treatment administered before, during, or after TMZ treatment would have distinct effects. Interestingly it was identified that pre-treatment with the Notch inhibitor DAPT decreased the efficacy of

TMZ whilst post-treatment significantly inhibited secondary neurosphere formation (197). This was not something which was testing during our study; however, our combination treatment results are comparable with those of Gilbert *et al*. and shows a significant reduction in secondary neurosphere formation when DBZ and TMZ are administered concomitantly.

Whilst the exact mechanism by which the enhanced efficacy of the combination treatment has yet to be investigated, the marked reduction in neurosphere number upon combination treatment of the CSC-5 cell line suggests an anti-GCSC effect. This could be due to the differentiation of the GCSCs regulated by Notch inhibition, which then results in cellular apoptosis of the differentiated cells by TMZ.

In the U87 and U251 cell lines, we observed inhibition of DLL4- and JAG1-induced Notch signalling led to increased mRNA expression of the neural differentiation markers GFAP, β-III-tubulin and SOX10, whilst overexpression of DLL4 and JAG1 increased the expression of GCSC markers. Similarly, we observed inhibition of Notch signalling led to the differentiation of the CSC-5 GCSC cell line as observed by increased expression of the differentiation markers GFAP, β-III-tubulin, and SOX10 at both an mRNA and protein level. This is in line with the expected role of Notch signalling in the maintenance of GCSCs. Conversely, TMZ treatment and overexpression was shown to increase GCSC marker (CD133, SOX2, and Nestin) expression, confirming the role of Notch in CSC maintenance and the hypothesis that TMZ promotes increased GCSC self-renewal. The combination treatment of DBZ and TMZ enhanced expression of neural differentiation markers, and we hypothesise DBZ acts in synergy with TMZ to induce cell death in both the GCSC population and non-GCSC population.

2D cell lines are valuable reagents for generating important biological and mechanistic understanding of cancer targets, as well as for testing of anti-cancer agents. However, the caveat that all data are generated in 2D cell lines, which lack microenvironmental and the heterogeneity of tumour cells in vivo, must be remembered when interpreting drug responses. For this reason, we utilised the *in vitro* neurosphere assay to study glioma response to drug treatments because neurospheres resemble the phenotypes and genotypes of the patients tumours more closely (299, 315). Unfortunately, no preclinical model can fully recapitulate the complexity of tumours within patients or the physiological parameters determining intrinsic and acquired drug responses. Therefore, the best approach is to use a combination of models to gain the most insightful information on drug tumour responses, drug metabolism, pharmacodynamic biomarkers etc. prior to clinical translation.

Some of the challenges of developing therapeutic targets in glioblastoma are derived from the lack of universally informative markers to identify GCSCs, as most GCSCs and NSCs share common molecular pathways. Understanding the biology of GCSCs and how these cells interact with their microenvironment in combination with the genetic and epigenetic landscape in GBM will be essential to develop more effective therapies. As there is significant controversy surrounding the use of CD133 as a GCSC marker, SOX2 and Nestin were also used as GCSC markers. SOX2 is critical for the maintenance of stem cell self-renewal and is used for somatic cell reprogramming (384). Abundant SOX2 expression is linked to the maintenance of CSCs in both gliomas and medulloblastomas (385). GCSCs have high SOX2 expression and SOX2 knockdown forfeits both the tumorigenicity and stemness of GCSCs (386, 387). The intermediate filament protein Nestin expression correlates with higher grade gliomas and lower

patient survival rates (388). In addition, it has been observed that Nestin-expressing cells have the ability to differentiate into multiple cell types, implicating Nestin as an effective GCSC marker (389). By multiplexing and using these markers alongside CD133, we have obtained a more accurate picture of the GCSC population as a whole. It also is important to note, that it is the glycosylated form of CD133 which marks CSCs, and the CD133/1 (W6B3C1) Miltenyi Biotec antibody used in this study recognises the glycosylated epitope 1 on the extracellular domain of CD133 (390) ensuring that by using this antibody, only GCSCs were identified during IF staining.

The study by Yahyanejad *et al.* which determined the effect of Notch inhibition alongside the current standard of care in glioblastoma, also assessed the effect of Notch inhibition combined with radiotherapy and TMZ on the expression of GCSC marker expression. Similar to our study, TMZ treatment was shown to increase GCSC marker expression, whilst triple combination treatment (radiotherapy, TMZ, and Notch inhibition) reduces the GCSC population as shown by a reduction in expression of CD133, SOX2, and Nestin (255). In order to make our results more valid, it would have been interesting to assess the GCSC population by flow cytometry, and compare the percentage of CD133+, SOX2+, and Nestin+ cells following single and combination treatments to confirm the results obtained by qPCR and IF.

Another study by Chu *et al*. identified prolonged inhibition of glioblastoma xenograft initiation and clonogenic growth following *in vivo* Notch blockade using the GSI MRK003 in mice. Oral GSI treatment was shown to affect proliferation, expression of Notch targets, NSC, and differentiation markers in the glioblastoma xenografts. The neural stem/progenitor markers Nestin, CD133, BMI1, and Nanog were significantly reduced upon MRK003 treatment compared to control, whilst the glial and neuronal

differentiation markers GFAP and MAP2 were significantly increased (304). Consistent with our results, these findings suggest oral GSI inhibits the expression of stem cell markers in glioblastoma xenografts and induces cellular differentiation. The study also analysed the Ki67 proliferation index by IHC, and found an 18% decrease in proliferation in the GSI treated-tumours (304). This was similar to our IF analysis which identified single DBZ and particularly combination DBZ and TMZ treatment reduced Ki67 staining of CSC-5 neurospheres compared to untreated control. The suppression of GCSC markers could be due, at least in part, to deletion of the GCSC pool from tumours, although other mechanisms are also possible including variation of stem cell marker expression in conjunction with changes in proliferation.

We observed that GSI treatment influenced TMZ enhanced GCSC marker expression, in line with the expected role of Notch signalling in the maintenance of GCSCs (202). Interestingly. It has been reported that endothelial cells in the tumour microenvironment are able to function as a stem cell niche, providing tumour cells with ligands that activate Notch signalling promoting GCSC self-renewal (303, 391). However, if Notch inhibition also reduced the GCSC sub-population either directly or indirectly via endothelial cell signalling was not addressed in this study and as such requires further investigation.

Additionally, a Phase 0/1 clinical trial by Xu *et al*. assessed the molecular and clinical effects of Notch inhibition by the GSI RO4929097 in glioma patients. IHC staining of treated tumours identified RO4929097 treatment resulted in a significant decrease in proliferation (as assessed by Ki67 staining) and expression of NICD in tumour cells and blood vessels. Notably, patient-specific organotypic tumour explant cultures revealed a significant reduction in the CD133+ GCSC population upon treatment with RO4929097

(252). As such, this study underpins the need for further clinical trials investigating the effect of combination Notch inhibition alongside the current standard of care in glioblastoma patients.

Taken together, the results in this chapter provide the rationale for the use of Notch inhibition alongside TMZ treatment for targeting the CSC population in glioblastoma. We have shown that there is little difference between DLL4- and JAG1-induced Notch signalling in GCSCs, and it is active Notch signalling as a whole which appears to be more important. Identification of a subset of patients with active Notch signalling (as identified by for example positive NICD IHC staining of tumour samples) could predict the likelihood of an increased response to anti-Notch therapy. By identifying these individuals, GCSCs could be more successfully targeted resulting in increased patient survival, and decreased rates of recurrence.

Chapter 5

5 DLL4, JAG1, and Glioma Cancer Stem Cell Marker Expression in Paired Primary and Recurrent Glioblastoma

5.1 Introduction

Over recent years, a number of studies have been conducted exploring the potential molecular mechanisms and pathways responsible for the development and progression of glioblastoma. The precise mechanisms of gliomagenesis still remains unclear, however, a distinct cellular hierarchy has been identified. Efforts to personalise treatment are aimed at identifying subsets of patients most likely to benefit from treatment and aiding in avoiding treatment-related morbidity and mortality in patients unlikely to respond to treatment. In previous chapters, we have shown that DLL4- and JAG1-induced Notch signalling results in increased resistance to the alkylating agent TMZ *in vitro* and plays a role in GCSC maintenance and self-renewal. However, whether expression of DLL4 and/or JAG1 can be used as a biomarker to stratify patients for treatment, and whether DLL4 and/or JAG1 expression is correlated with GCSC marker expression in glioblastoma patients remains to be elucidated.

5.1.1 Glioma Grading

Primary tumours of the CNS are classified and graded according to the WHO grading scheme named the WHO classification for CNS tumours (5). The WHO scheme is used in the UK and internationally proving a uniform system of nomenclature, essential for comparative studies and multicentre clinical trials. The most recent 2016 update of the WHO classification of CNS tumours has moved on the from the traditional classification and grading of tumours solely based on the concept of histogenesis, i.e. classification according to the microscopic similarities with putative cells of origin and their

developmental differentiation states (392). Instead, the 2016 WHO classification now incorporates well-established molecular parameters into the classification of tumours of the CNS (5). A more in-depth discussion of glioma grading is given in the introduction of this thesis.

5.1.2 Glioma Biomarkers

A number of molecular biomarkers are used to determine prognosis or guide treatment for glioma (Introduction 1.1.5.2: Glioma Grading). The National Institute for Health and Care Excellence (NICE) in the UK instructs all glioma specimens be reported according to the latest version of the WHO brain tumour classification (5, 22). Alongside histopathological assessment of the tumour, a number of molecular analyses are performed in order to obtain a diagnosis in gliomas. The expression of key molecular markers should be assessed such as: *IDH1* and *IDH2* mutations, *ATRX* mutations to identify *IDH*-mutant astrocytomas and glioblastomas, 1p/19q codeletion to identify oligodendrogliomas, histone H3.3 K27M mutations in midline gliomas, and *BRAF* fusion and gene mutation to identify pilocytic astrocytoma. All high-grade glioma specimens must be tested for *MGMT* promoter methylation in order to inform prognosis and to guide treatment, as well as testing *IDH*-wildtype glioma specimens for *TERT* promoter mutations to inform prognosis (22).

Numerous methods are used to identify these key molecular markers in order to obtain a diagnosis in gliomas. These methods include pyrosequencing analysis of common mutations in codon 132 of the *IDH1* gene, codon 172 of the *IDH2* gene and codons 599, 600 and 601 of the *BRAF* gene; fluorescence *in-situ* hybridisation analysis to identify 1p/19q loss of heterozygosity; and methylation sensitive pyrosequencing analysis of the *MGMT* promoter region (393). The identification of *IDH* R132H

mutation and presence of ATRX can also be easily performed by IHC analysis (394). This integrated diagnosis enables clinicians to provide prognostic and treatment stratification decisions for each patient.

Diagnostic biomarkers enable a more precise tumour classification, prognostic biomarkers inform about a likely outcome (e.g. disease recurrence, disease progression, and overall survival), and predictive biomarkers facilitate patient management by helping tailor treatment strategies to patient-specific biology. Importantly, detailed characterisation of glioblastoma molecular signatures facilitates a personalised approach to treatment, and has contributed to the development of a new generation of anti-glioblastoma therapies such as small molecule inhibitors targeting growth factor receptors (e.g. EGFR), antibody-based drug conjugates, and more recently, immune checkpoint inhibitors (395). However promising these approaches appear, many have shown limited efficacy in increasing patient overall survival compared to the current standard of care.

5.1.3 Notch Signalling in Glioblastoma

As previously discussed in Chapter 1 Introduction (1.3.4), Notch signalling is a major pathway involved in the development of glioblastoma, and expression of Notch receptors and their ligands are critical markers of glioblastoma patient survival. Increased expression of Notch1, Notch4, DLL1, DLL4, JAG1, RBPJ, Hey1, Hey2, and Hes1 is observed in glioblastoma tumour cells compared to normal brain (238-240). A study by Kanamori *et al*. showed the Notch signalling pathway is deregulated in nearly 75% of glioblastomas, and inhibition of Notch signalling can suppress glioblastoma growth. Notch1 is overexpressed in the majority of primary glioblastomas, and elevated levels of cleaved, activated NICD is also observed in 80% of primary glioblastomas (238). The

expression of Notch pathway components exhibits a positive correlation with glioma progression, and high expression is reported to be an independent predictor of poor survival (241, 242). This suggests increased activation of Notch signalling promotes a more undifferentiated and aggressive tumour phenotype.

Activation of the Notch pathway is considered to be a key characteristic of glioblastoma pathogenesis, however limited research has been done to assess the role of Notch receptors and ligands as biomarkers for IHC in glioblastoma. We utilised IHC in paired primary and recurrent glioblastoma samples to determine the role of DLL4 and JAG1 in glioblastoma. This chapter aims to assess the expression of DLL4 and JAG1 in paired primary and recurrent glioblastoma samples and determine if the expression of these ligands correlates with the expression of the GCSC markers Nestin and CD133.

5.2 Methods

Paired primary and recurrent glioblastoma patient samples were provided by the Brain Archive and Information Network UK (BRAIN UK) with ethical approval by the South West Research Ethics committee (REC number: 14/SC/0098; BRAIN UK reference: 17/002).

Immunohistochemical staining of paired primary and recurrent glioblastoma samples was performed as described in Methods 2.9 by the Department of Cellular and Anatomical Pathology, University Hospitals Plymouth. Staining was performed using antibodies to the following: DLL4, JAG1, Nestin, and CD133. A list of antibodies used for IHC staining in this chapter is given below (Table 5.1). IHC staining was assessed semi-quantitatively with the help of consultant neuropathologist Dr David Hilton (Department of Cellular and Anatomical Pathology, University Hospitals Plymouth). A list of all scores for each antibody can be found in Appendix 8.3 IHC Quantification.

All data were presented as mean ± SD and analysed using GraphPad Prism (version 6.01, GraphPad Software Inc., San Diego, USA). The statistical test employed are described in the figure legend of each experiment.

Table 5.1: List of antibodies used for immunohistochemistry in Chapter 5

Primary Antibody	Host	Dilution	Company	Product Code	Antigen Retrieval Method	Detection Kit
CD133/1 (W6B3C1)	Mouse	1:100	Milteyni Biotech	130-092-395	EDTA	Novalink Polymer Detection System
Nestin (10C)	Mouse	1:2000	ThermoFisher Scientific	MA1-110	Citrate	VECTASTAIN Elite ABC HRP Kit
DLL4	Rabbit	1:3000	Abcam	Ab7280	Citrate	VECTASTAIN Elite ABC HRP Kit
JAG1 (28H8)	Rabbit	1:150	Cell Signalling Technology	#2620	EDTA	VECTASTAIN Elite ABC HRP Kit

5.3 Results

A total of 27 paired primary and recurrent glioblastoma specimens were used for staining. Resection was followed by standard TMZ and radiation therapy in all cases. Analysis of patients at diagnosis revealed 2 of the 27 patients (7.4%) were *IDH*-mutant, whilst 10 of the 27 patients (37%) had unmethylated *MGMT* (Appendix 8.3).

5.3.1 DLL4 and JAG1 Staining

DLL4 showed diffuse staining which was finely granular cytoplasmic in tumour cells, endothelial cells, and macrophages (Figure 5.1A-B). DLL4 staining intensity was semi-quantified for each sample and graded as 0 (negative), 1 (weakly positive), 2 (moderately positive), and 3 (strongly positive). Of the 27 paired primary and recurrent samples, for 22 samples staining quantification remained the same, staining intensity increased for 3 paired samples, and decreased in 2 paired samples. We assessed whether there was an association between primary and recurrent DLL4 staining and found this was not significant (Figure 5.1C), suggesting the expression of DLL4 changes between the primary lesion and recurrence.

JAG1 showed weak focal cytoplasmic and membrane staining in tumour cells and endothelial cells (Figure 5.2A-B). Like DLL4, JAG1 staining intensity was semi-quantified for each sample and graded as 0 (negative), 1 (weakly positive), 2 (moderately positive), and 3 (strongly positive). Of the 27 paired primary and recurrent samples, for 13 samples JAG1 staining quantification remained the same, staining intensity increased for 4 paired samples, and decreased in 10 paired samples. We assessed whether there was a correlation between primary and recurrent JAG1 staining and found this was not significant (Figure 5.2C). This suggests JAG1 expression changes between the primary and recurrent tumour.

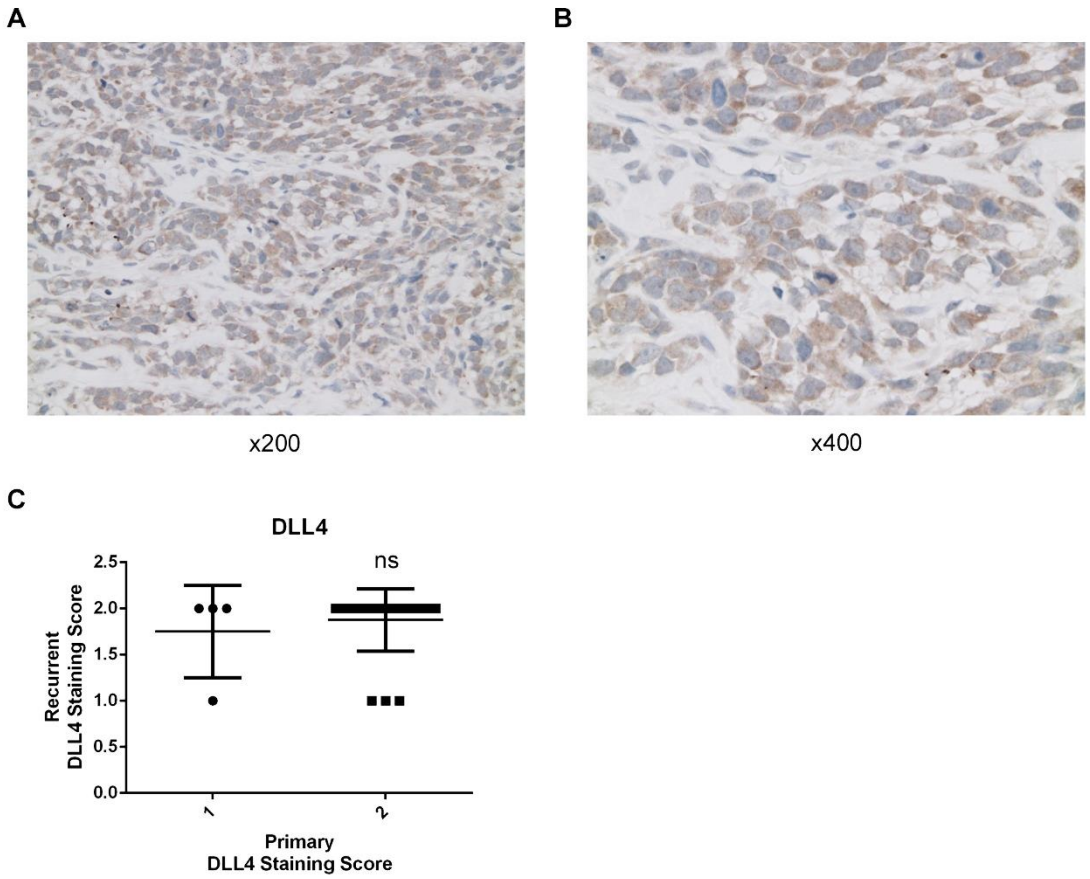

Figure 5.1: Representative IHC staining of the Notch ligand DLL4 in glioblastoma.

In glioblastoma patient samples, DLL4 IHC staining showed diffuse staining which was finely granular cytoplasmic in tumour cells, endothelial cells, and macrophages. **(A)** x200 magnification. **(B)** x400 magnification. **(C)** Comparison between DLL4 staining scores in paired primary and recurrent glioblastoma samples. Immunohistochemical staining was performed on paired primary and recurrent glioblastoma FFPE tissue sections (4 µm) following the standard streptavidin-biotin peroxidase method (VECTASTAIN Elite ABC HRP kit) with citrate heat-mediated antigen retrieval. Primary antibody: rabbit anti-DLL4 (1:3000; Abcam #AB7280). Negative controls were completed in parallel on tonsil and normal brain by omission of primary antibody (data not shown). Staining was assessed semi-quantitatively by a consultant neuropathologist. (Mean ± SD, n = 27, unpaired t-test, ns denotes not significant).

We next assessed whether DLL4 and JAG1 staining scores were associated in both primary and recurrent paired samples, and found this was not significant for either primary (Figure 5.3A) or recurrent glioblastoma (Figure 5.3B). These results suggest DLL4 and JAG1 expression are independent of one another in both primary and recurrent glioblastoma.

5.3.2 Correlation with Nestin Staining

Nestin showed diffuse cytoplasmic staining in both tumour cells and endothelium (Figure 5.4). Nestin staining intensity was semi-quantified for each sample and graded as 0 (negative), 1 (weakly positive), 2 (moderately positive), and 3 (strongly positive). DLL4, JAG1, and Nestin staining scores were compared for primary and recurrent glioblastoma samples. No association was found between either DLL4 and Nestin (Figure 5.5A), and JAG1 and Nestin (Figure 5.5C) staining in primary glioblastoma. However, for recurrent glioblastoma, increased DLL4 and JAG1 staining appears to be associated with increased Nestin staining (Figure 5.5B & D), but this did not reach statistical significance.

5.3.3 Correlation with CD133 Staining

CD133 showed scattered staining in individual tumour cells with both membrane and cytoplasmic staining, and staining was also observed in some macrophages (Figure 5.6). CD133 staining in hot spots was semi-quantified by calculating the percentage of positively stained cells of more than 100 cells counted in areas of highest CD133 staining.

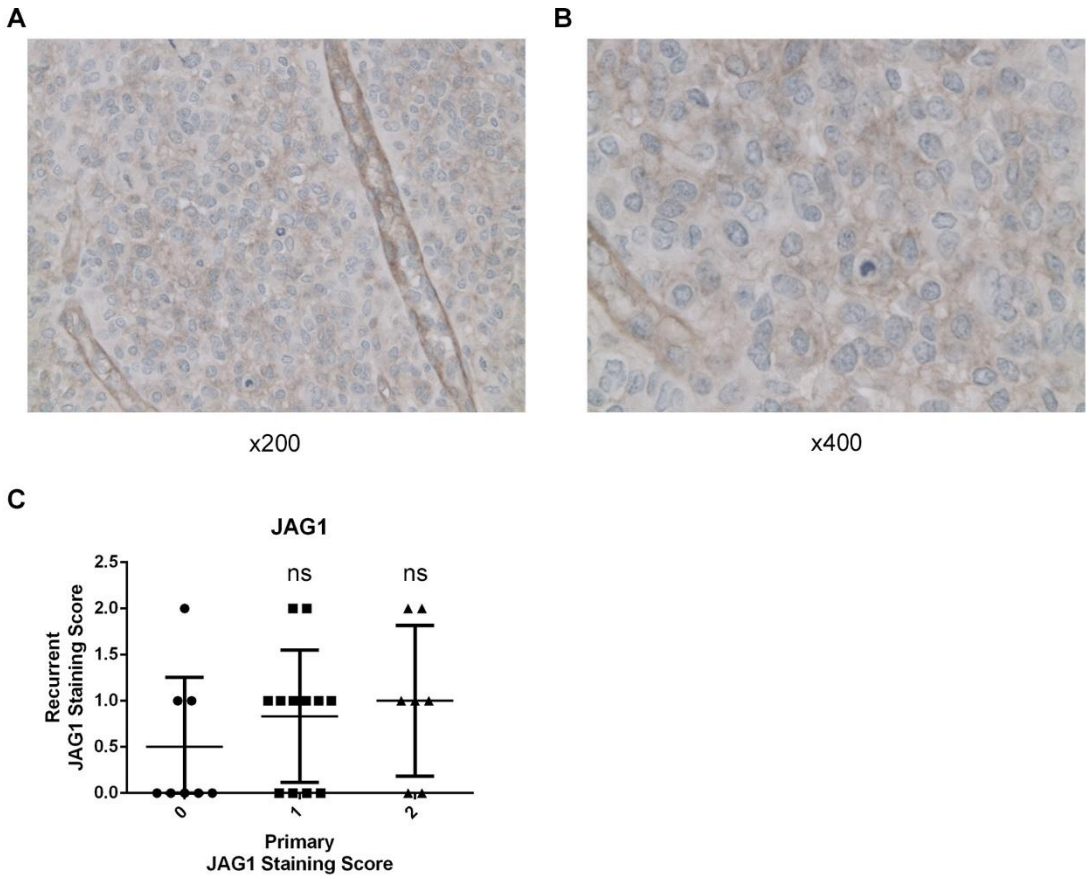

Figure 5.2: Representative IHC staining of the Notch ligand JAG1 in glioblastoma.

In glioblastoma patient samples, JAG1 showed weak focal cytoplasmic and membrane staining in tumour cells and endothelial cells. **(A)** x200 magnification**. (B)** x400 magnification. **(C)** Comparison between JAG1 staining scores in paired primary and recurrent glioblastoma samples. IHC staining was performed on paired primary and recurrent glioblastoma FFPE tissue sections (4 µm) following the standard streptavidin-biotin peroxidase method (VECTASTAIN Elite ABC HRP kit) with EDTA heat-mediated antigen retrieval. Primary antibody: rabbit anti-JAG1 (1:150; Cell Signalling Technology #2620). Negative controls were completed in parallel on tonsil and normal brain by omission of primary antibody (data not shown). Staining was assessed semi-quantitatively by a consultant neuropathologist. (Mean ± SD, n = 27, ordinary one-way ANOVA with Tukey's post-hoc test, ns denotes not significant).

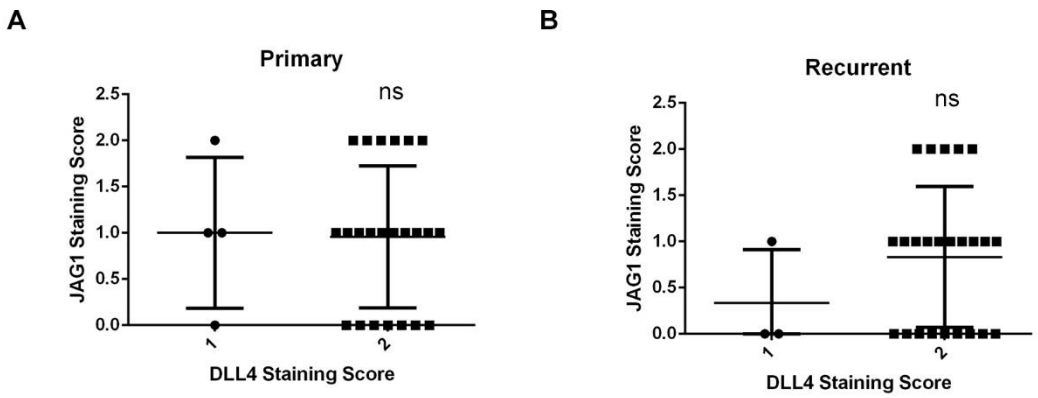

Figure 5.3: Comparison between DLL4 and JAG1 staining scores in (A) primary and (B) recurrent glioblastoma.

Analysis was performed to determine if DLL4 and JAG1 staining scores were related in paired primary and recurrent glioblastoma patient samples. IHC staining was performed on paired primary and recurrent glioblastoma FFPE tissue sections (4 µm) following the standard streptavidin-biotin peroxidase method (VECTASTAIN Elite ABC HRP kit) with citrate/EDTA heat-mediated antigen retrieval. Primary antibodies: rabbit anti-DLL4 (1:3000; Abcam #AB7280) and rabbit anti-JAG1 (1:150; Cell Signalling Technology #2620). Negative controls were completed in parallel on tonsil and normal brain by omission of primary antibody (data not shown). Staining was assessed semi-quantitatively by a consultant neuropathologist. (Mean ± SD, n = 27, unpaired t-test, ns denotes not significant).

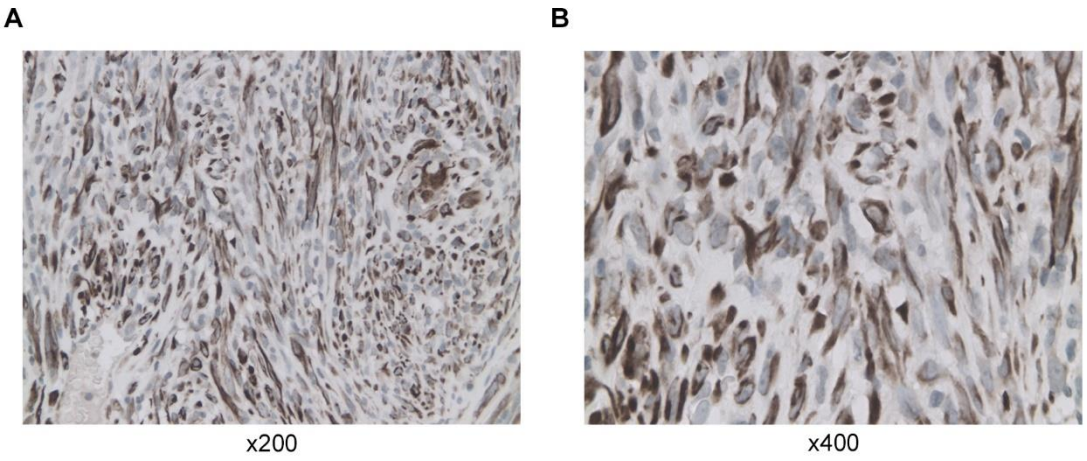

Figure 5.4: Representative IHC staining of the GCSC marker Nestin in glioblastoma.

In glioblastoma patient samples, IHC analysis of the GCSC marker Nestin showed diffuse cytoplasmic staining in both tumour cells and endothelium. **(A)** x200 magnification. **(B)** x400 magnification. IHC staining was performed on paired primary and recurrent glioblastoma FFPE tissue sections (4 µm) following the standard streptavidin-biotin peroxidase method (VECTASTAIN Elite ABC HRP kit) with citrate heat-mediated antigen retrieval. Primary antibody: mouse anti-Nestin (1:2000; ThermoFisher Scientific #MA1-110). Negative controls were completed in parallel on tonsil and normal brain by omission of primary antibody (data not shown). Staining was assessed semi-quantitatively by a consultant neuropathologist.

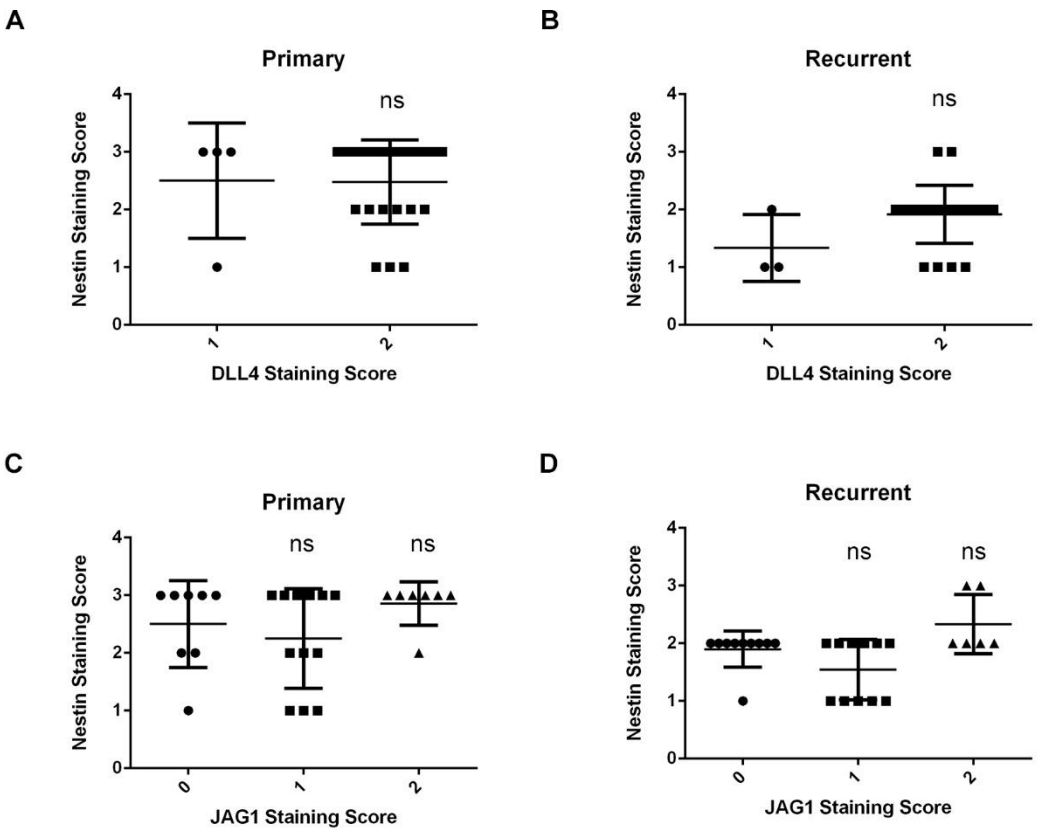

Figure 5.5: Comparison between staining scores for the Notch ligands DLL4 and JAG1 and the glioma cancer stem cell marker Nestin in primary and recurrent glioblastoma.

Comparison between DLL4 and Nestin staining scores in **(A)** primary and **(B)** recurrent glioblastoma samples. Comparison between JAG1 and Nestin staining scores in **(C)** primary and **(D)** recurrent glioblastoma samples. IHC staining was performed on paired primary and recurrent glioblastoma FFPE tissue sections (4 µm) following the standard streptavidin-biotin peroxidase method (VECTASTAIN Elite ABC HRP kit) with citrate/EDTA heat-mediated antigen retrieval. Primary antibodies: rabbit anti-DLL4 (1:3000; Abcam #AB7280), rabbit anti-JAG1 (1:150; Cell Signalling Technology #2620), and mouse anti-Nestin (1:2000; ThermoFisher Scientific #MA1-110). Negative controls were completed in parallel on tonsil and normal brain by omission of primary antibody (data not shown). Staining was assessed semi-quantitatively by a consultant neuropathologist. (Mean ± SD, n = 27, unpaired t-test [A+B], ordinary one-way ANOVA with Tukey's post-hoc test [C+D], ns denotes not significant).

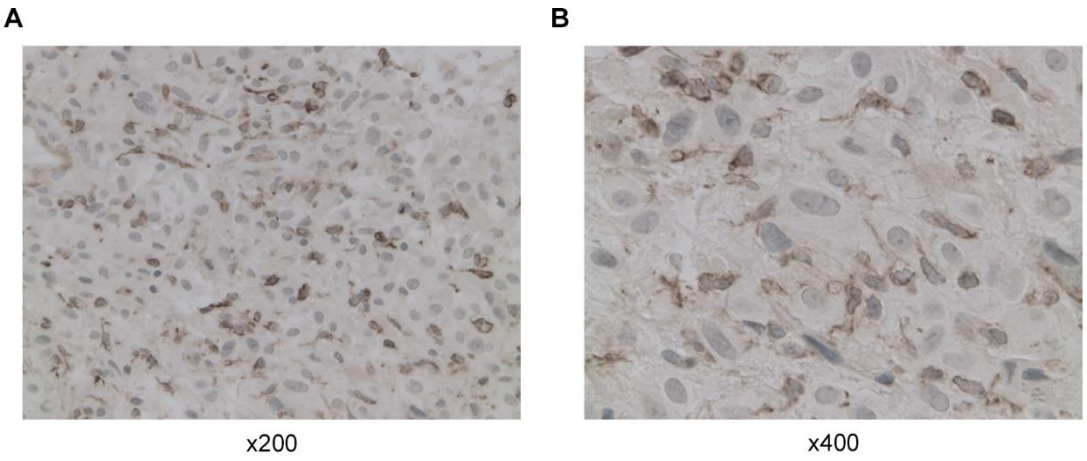

Figure 5.6: Representative IHC staining of the GCSC marker CD133 in glioblastoma.

IHC analysis of the GCSC marker CD133 in glioblastoma patient samples showed scattered staining in individual tumour cells with both membrane and cytoplasmic staining, staining was also observed in some macrophages. **(A)** x200 magnification. **(B)** x400 magnification. IHC staining was performed on paired primary and recurrent glioblastoma FFPE tissue sections (4 µm) following the standard streptavidin-biotin peroxidase method (Novalink Polymer Detection System) with EDTA heat-mediated antigen retrieval. Primary antibody: mouse anti-CD133 (1:100; Milteyni Biotec #130-092-395). Negative controls were completed in parallel on tonsil and normal brain by omission of primary antibody (data not shown). Staining was assessed semi-quantitatively by a consultant neuropathologist.

DLL4, JAG1, and CD133 staining scores were compared for both primary and recurrent glioblastoma samples. No association was found between DLL4 and CD133 staining in both primary and recurrent samples (Figure 5.7A-B). JAG1 and CD133 staining scores were also compared in primary and recurrent glioblastoma samples. In primary glioblastoma, there is no correlation between JAG1 and CD133 staining (Figure 5.7C). However, for recurrent glioblastoma it was identified that increased JAG1 staining score is associated with a significantly higher CD133 staining score (Figure 5.7D).

The correlation between CD133 staining in primary and recurrent samples was also assessed, and it showed a significant positive correlation ($r = 0.7385$, $p < 0.001$; Figure 5.8). This suggests that the number of CD133+ GCSCs in recurrent glioblastoma tumour samples remains the same despite treatment of the primary tumour.

5.3.4 Correlation with MGMT Status

As MGMT is a key mechanism for resistance in glioblastoma, we also assessed whether MGMT status (methylated/unmethylated) is correlated with a higher or lower DLL4 and/or JAG1 expression. MGMT was not found to be associated with either DLL4 or JAG1 staining score in either primary or recurrent glioblastoma in our cohort of samples (Figure 5.9).

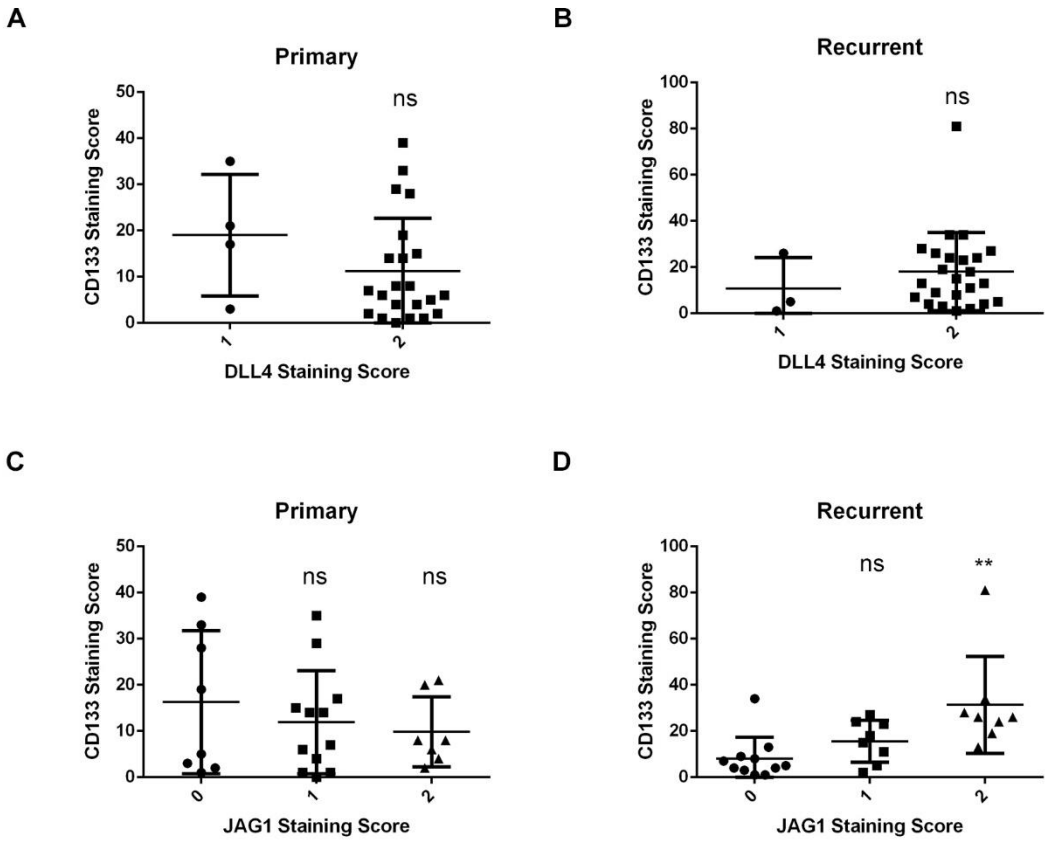

Figure 5.7: Comparison between the Notch ligands DLL4 and JAG1 and the glioma cancer stem cell marker CD133 in primary and recurrent glioblastoma.

Comparison between DLL4 and CD133 staining scores in **(A)** primary and **(B)** recurrent glioblastoma samples. Comparison between JAG1 and CD133 staining scores in **(C)** primary and **(D)** recurrent glioblastoma samples. IHC staining was performed on paired primary and recurrent glioblastoma FFPE tissue sections (4 µm) following the standard streptavidin-biotin peroxidase method (VECTASTAIN Elite ABC HRP kit/Novalink Polymer Detection System) with citrate/EDTA heat-mediated antigen retrieval. Primary antibodies: rabbit anti-DLL4 (1:3000; Abcam #AB7280), rabbit anti-JAG1 (1:150; Cell Signalling Technology #2620), and mouse anti-CD133 (1:100; Milteyni Biotec #130-092-395). Negative controls were completed in parallel on tonsil and normal brain by omission of primary antibody (data not shown). Staining was assessed semi-quantitatively by a consultant neuropathologist (Mean ± SD, n = 27, unpaired t-test [A+B], ordinary one-way ANOVA with Tukey's post-hoc test [C+D], ** $p < 0.01$, and ns denotes not significant).

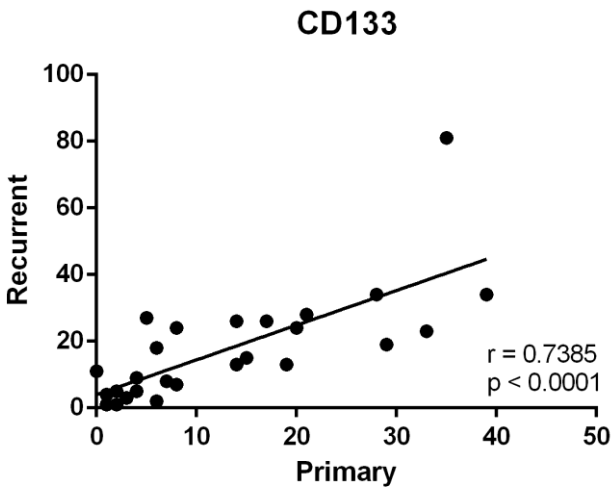

Figure 5.8: Correlation of CD133 staining quantification in primary and recurrent glioblastoma samples.

Correlation analysis showed CD133 staining quantification is correlated in paired primary and recurrent glioblastoma patient samples. IHC staining was performed on paired primary and recurrent glioblastoma FFPE tissue sections (4 µm) following the standard streptavidin-biotin peroxidase method (Novalink Polymer Detection System) with EDTA heat-mediated antigen retrieval. Primary antibody: mouse anti-CD133 (1:100; Milteyni Biotec #130-092-395). Negative controls were completed in parallel on tonsil and normal brain by omission of primary antibody (data not shown). Staining was assessed semi-quantitatively by a consultant neuropathologist. (n = 27, Pearson's correlation, r = 0.7385, r^2 = 0.5453, p < 0.0001).

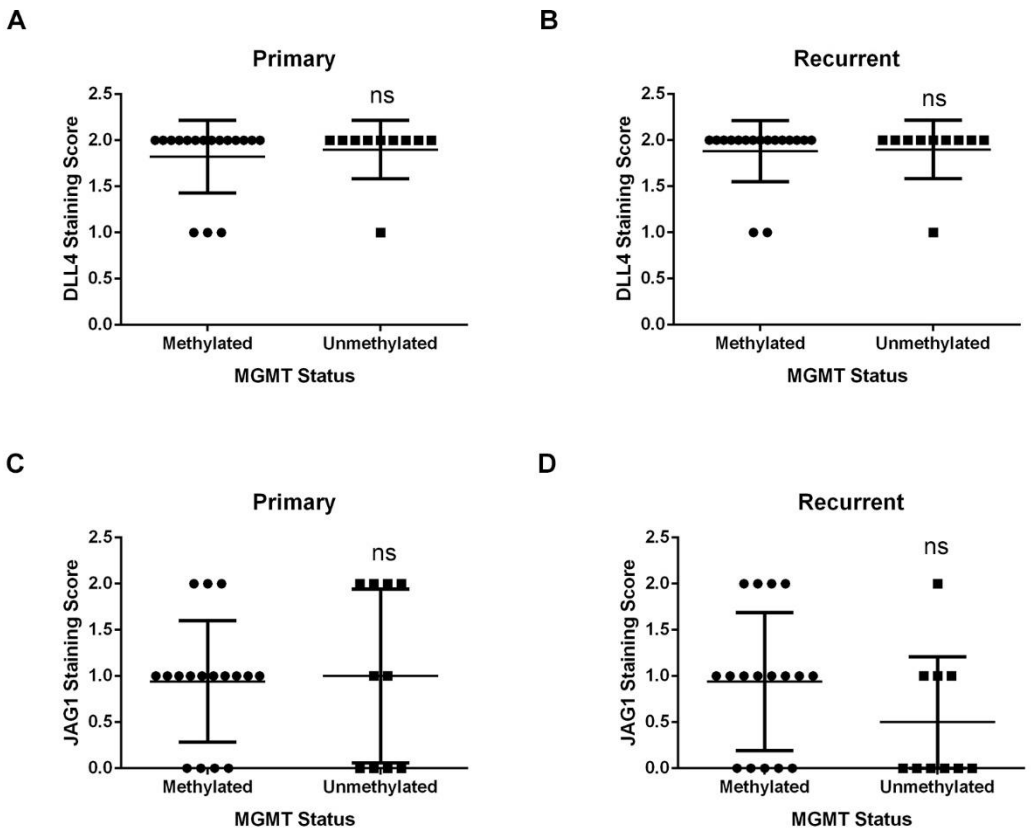

Figure 5.9: Comparison between staining scores for the Notch ligands DLL4 and JAG1 and MGMT status in primary and recurrent glioblastoma.

Comparison between MGMT status and DLL4 staining score in **(A)** primary and **(B)** recurrent glioblastoma samples. Comparison between MGMT status and JAG1 staining score in **(C)** primary and **(D)** recurrent glioblastoma samples. IHC staining was performed on paired primary and recurrent glioblastoma FFPE tissue sections (4 µm) following the standard streptavidin-biotin peroxidase method (VECTASTAIN Elite ABC HRP kit) with citrate/EDTA heat-mediated antigen retrieval. Primary antibodies: rabbit anti-DLL4 (1:3000; Abcam #AB7280) and rabbit anti-JAG1 (1:150; Cell Signalling Technology #2620). Negative controls were completed in parallel on tonsil and normal brain by omission of primary antibody (data not shown). Staining was assessed semi-quantitatively by a consultant neuropathologist. Patient MGMT status was determined following resection of the primary tumour by methylation specific PCR. (Mean ± SD, n = 27, unpaired t-test, ns denotes not significant).

5.4 Discussion

Glioblastomas are highly aggressive tumours that inevitably recur despite current therapies. Knowledge about tumour properties at initial diagnosis and recurrence is essential for a better understanding of tumour evolution and to improve glioblastoma treatment. The analysis of paired glioblastoma tumour samples from the same patient at initial diagnosis and after standard treatment at recurrence provides a unique opportunity to examine this evolution. In our cohort of 27 paired primary and recurrent glioblastoma samples, patients have had standard therapy: maximal tumour resection followed by radiotherapy and concomitant TMZ chemotherapy. In this chapter, we assessed the expression of the Notch ligands DLL4 and JAG1 by IHC in paired primary and recurrent glioblastoma specimens, alongside the expression of the GCSC markers CD133 and Nestin.

We did not find any association between DLL4 and/or JAG1 expression in primary or recurrent glioblastoma samples, suggesting DLL4 and JAG1 expression are independent of one another confirming previous results observed by Jubb *et al.* (307). One of our few significant results showed increased JAG1 staining score in recurrent glioblastoma is associated with increased CD133 staining. An association was also observed between DLL4 and CD133 expression, DLL4 and Nestin expression, as well as JAG1 and Nestin expression in recurrent glioblastoma, however these results did not reach statistical significance. GCSCs are key drivers of treatment resistance and recurrence, therefore recurrent tumours may harbour increased CD133 and/or Nestin positive GCSCs. We hypothesise that it is DLL4- and/or JAG1- induced Notch signalling which increases GCSC self-renewal driving tumour recurrence, hence the correlation between the two.

The lack of significance for some of our results may be due to the small cohort of paired patient samples utilised for IHC staining.

For any retrospective study, this analysis has its limitations. Glioblastomas display high inter- and intra-tumoural heterogeneity and the tissue core taken for staining may not be representative of the entire lesion. It is also worth noting that radiotherapy was used as part of the standard of care for this cohort of patients, and previously we have not assessed the effect of DLL4- and JAG1-induced Notch signalling on radiation treatment resistance in glioblastoma. However, like TMZ chemotherapy, radiotherapy is thought to target the non-GCSC population, and as such enriches the GCSC population (177, 179).

Interestingly, we did observe a significant positive correlation between CD133 IHC staining scores in primary and recurrent glioblastoma samples. This suggests that the number of CD133+ GCSCs remains consistent between primary and recurrent glioblastoma patient samples despite treatment of the primary tumour with radiation and TMZ treatment. This observation suggests these CD133+ cells are resistant to both radiotherapy and TMZ chemotherapy and are able to repopulate the tumour following treatment resulting in tumour recurrence.

MGMT status is a key mechanism of treatment resistance in glioblastoma. High levels of MGMT activity in tumour cells creates a resistant phenotype by inhibiting the therapeutic effect of TMZ and is an important determinant of treatment failure (95, 102, 111). Epigenetic silencing of the *MGMT* gene by promoter methylation is associated with loss of MGMT expression and diminished DNA-repair activity (42, 102). We assessed whether *MGMT* status (methylated/unmethylated) was correlated with DLL4 and/or JAG1 expression in primary and recurrent glioblastoma samples and

found there was no association in our cohort. This suggests that the mechanism by which DLL4 and JAG1 promotes resistance to TMZ in glioblastoma is likely to not be as a result of *MGMT* methylation status, but via a different mechanism.

Additionally, to determine cellular proliferation of these tumours, it would be desirable to assess whether increased DLL4 and/or JAG1 staining correlates with increased Ki-67 staining in both primary and recurrent patient samples, and also if this correlates with GCSC number/marker expression.

There are a number of limitations to the results presented in this chapter. In this study, a semi-quantitative scoring system was used to convert the subjective perception of IHC-marker expression by a histopathologist into quantitative data. One of the main issues with semi-quantitative scoring is that the scoring is the subjective assessment of solely one pathologist. Therefore, to reduce subjectivity, it would have been ideal to have had more than one individual undertake the IHC scoring for this study. Another limitation is the relatively small number of paired glioblastoma samples utilised. As previously discussed, glioblastoma exhibits high inter-and intra-tumoural heterogeneity. By obtaining an increased sample number of paired primary and recurrent glioblastoma samples would enable us to obtain a clearer understanding of the effect of DLL4- and JAG1-induced Notch signalling in patients with regards to both treatment resistance and tumour recurrence.

It would also be of interest to collate the survival data for this cohort of patients to ascertain whether high DLL4 and/or JAG1 expression has an effect on patient overall survival. Previous studies in glioblastoma has shown DLL4 expression correlates with peritumoural brain oedema and poor prognosis (307, 308), whilst JAG1 expression is associated with reduced time to progression and overall survival in primary

glioblastoma patients (309). Similarly, it would be of interest to assess survival data with regards to GCSC marker expression in the cohort. A literature review into CD133 expression in glioblastoma found in ten studies with a total of 715 glioblastoma patients, overall, high CD133 expression is associated with poor overall survival in patients with glioblastoma (396). Like CD133, Nestin plays a role in the survival and proliferation of GCSCs and high expression is associated with a worse overall survival in glioma patients (397). However, further analyses and increased sample numbers will be required to suitably determine if DLL4 and/or JAG1 expression is correlated to increased GCSC marker expression in primary and recurrent glioblastoma.

In glioblastoma, GCSCs are often located regions of hypoxia and perivascular areas. Zhu *et al*. have reported in perivascular regions, Notch ligands present on endothelial cells could increase the GCSC phenotype in neighbouring tumour cells, whilst also enhancing their capacity for self-renewal. Coculture of human brain microvascular endothelial cells or Notch ligand with glioblastoma neurospheres promoted glioma cell growth and increased GCSC self-renewal, suggesting targeting GCSCs via Notch may provide a novel treatment strategy in glioblastoma (303). This would be interesting to assess in our cohort of samples, IF staining could be performed to ascertain the location of GCSCs in relation to cells expressing DLL4 and JAG1, in both primary and recurrent samples. This would help to obtain a clearer picture of the role of DLL4- and JAG1-indced Notch signalling in glioblastoma and GCSCs utilising patient samples.

It would be of interest to perform Notch inhibition studies in mice bearing orthotopic glioblastoma. These mice would be treated with either the current standard of care (radiotherapy and adjuvant TMZ chemotherapy), standard of care plus Notch inhibition treatment (e.g. DBZ), or no treatment control. Upon sacrifice, tumours could be

collected and IHC performed in order to assess the expression of the Notch ligands alongside GCSC markers, to determine if Notch inhibition has an effect on reducing the pool of GCSCs compared to standard treatment alone.

Taken together, these results have shown DLL4 and JAG1 expression in recurrent glioblastoma samples appears to be correlated to GCSC marker (CD133 and Nestin) expression. These findings provide evidence to warrant further investigations of correlations between Notch and GCSC marker expression in primary, and more importantly, recurrent glioblastoma tumour samples.

Chapter 6

6 Discussion

6.1 General Discussion

Glioblastoma is the most commonly diagnosed primary malignant brain tumour in adults, with a median survival of just 14.6 months following diagnosis (9). The existing gold standard treatment is palliative, and despite multimodal aggressive therapy, glioblastoma is uniformly fatal with survival over 3 years being considered long-term (398). In an effort to improve treatment options, glioblastoma has been extensively studied by the Cancer Genome Atlas research network and a number of novel therapies have been developed (360, 399). However, intratumoural and intertumoural heterogeneity remain a huge challenge (375, 376), and despite encouraging preclinical data, novel targeted therapies have failed to increase survival of glioblastoma patients. Due to the poor survival rate of glioblastoma patients, it is therefore vital that novel avenues for therapy are explored to improve patient prognosis.

CSCs are a subpopulation of tumour cells responsible for driving tumourigenesis and recurrence following treatment. They share characteristics with normal stem cells and have the ability undergo self-renewal and differentiate into diverse progeny with limited proliferation potential. Numerous groups have identified and isolated CSCs in glioblastoma (termed GCSCs) (4, 175, 195), and studies have shown GCSCs display increased tumourigenic potential compared to matched non-stem tumour cells when xenotransplanted into the brains of immunocompromised mice (4, 299). GCSCs have also been shown to express elevated levels of VEGF promoting tumour angiogenesis (358), and are resistant to radiation and the alkylating agent TMZ due to enhanced DNA repair capacity (177). Whilst the traditional goal of cancer treatment has been to

kill all neoplastic cells, the CSC hypothesis proposes that it is the subpopulation of CSCs that must be targeted in order to eliminate malignancy.

The Notch signalling pathway regulates numerous processes during embryonic and adult development, including neural stem cell biology (326). Notch pathway activation is considered to be a key characteristic of glioblastoma pathogenesis and a number of studies have shown increased Notch pathway activation in primary glioblastoma compared with low-grade gliomas (243), secondary glioblastomas (244), and normal brain tissue (238-240). There is growing evidence to suggest Notch signalling regulates the self-renewal of GCSCs in glioblastoma (303, 310), and GCSCs are generally believed to mediate tumour recurrence and resistance to treatment (197). However, little is known about the importance of specific Notch ligands. The Notch ligands DLL4 and JAG1 have previously been implicated in tumour angiogenesis, and in glioblastoma, both ligands are upregulated (238-240). But their relative effects and interactions in tumour biology, particularly in response to therapeutic intervention remains unclear. Oon *et al*. recently identified both DLL4 and JAG1 promote tumour growth by modulating angiogenesis, and both mediate tumour resistance to anti-VEGF therapy with bevacizumab (306). In glioblastoma, DLL4 expression in endothelial and tumour cells correlates with peritumoural brain oedema and poor prognosis (307, 308). Similarly, JAG1 expression in tumour and endothelial cells is associated with reduced time to progression and overall survival in primary glioblastoma patients (309).

The main aim of this study was to examine the role of the Notch ligands, DLL4 and JAG1 in the glioblastoma response to TMZ chemotherapy. Initially in Chapter 3, we investigated the effect of DLL4 and JAG1 on 2D cell growth, 3D spheroid growth and TMZ IC50. Following single and combination treatments, our results in 2D monolayer

and 3D spheroid culture show treatment of DLL4 and JAG1 overexpressing cell lines with TMZ resulted in no significant reduction of growth compared to untreated control. However, single DBZ and combination DBZ and TMZ treatment significantly reduced both 2D monolayer and 3D spheroid growth, suggesting DLL4- and JAG1-induced Notch signalling plays a role in TMZ resistance and can be reversed upon treatment with a Notch pathway inhibitor. This result confirms and agrees with findings in the literature. Previous research by Hiddingh *et al*. demonstrated expression of the extracellular matrix protein EFEMP1, which acts via γ-secretase activation of the Notch pathway, is associated with TMZ resistance. Inhibition of Notch signalling by the GSI RO4929097 resulted in sensitisation of glioblastoma to TMZ both *in vitro* and *in vivo* (345). In addition, a study by Yahyanejad *et al.* has shown Notch inhibition in combination with both TMZ and radiotherapy enhances 3D spheroid growth delay *in vitro* and prolongs the survival of mice bearing orthotopic glioblastoma (255).

Utilising 2D monolayer and 3D spheroid culture we identified the overexpression of DLL4 and JAG1 promotes resistance to TMZ by increasing the TMZ IC50. This is the first study to show the IC50 of TMZ is significantly increased following DLL4- and JAG1-induced Notch signalling in the U87 and U251 glioblastoma cell lines. We also showed that this increase in TMZ IC50 can be reversed upon pre-treatment with the Notch pathway inhibitor DBZ. This highlights the role of DLL4- and JAG1-induced Notch signalling in mediating resistance to TMZ in glioblastoma *in vitro,* and these results build on previous studies and are encouraging in developing new combination therapies in order to overcome TMZ resistance in glioblastoma.

To date, clinical trials of Notch inhibition have been largely non-existent with only two published clinical studies utilising GSIs for the treatment of glioblastoma. A Phase I clinical trial conducted by Krop *et al*. assessed both the pharmacology and pharmacodynamics of the GSI MK-0752 in patients with solid tumours who had failed to respond to standard therapies. Dose-dependent inhibition of Notch signalling by MK-0752 was observed. A complete response was seen in a patient with anaplastic astrocytoma, and stable disease in 10 patients with glioblastoma. The study observed MK-0752 has a modest level of activity in patients with gliomas, and provides the first clinical evidence validating Notch as a therapeutic target in gliomas (305). A Phase 0/I clinical trial also assessed the molecular and clinical effects of Notch inhibition in glioma patients using the GSI RO4929097 alongside the current standard of care. The addition of RO4929097 to TMZ and radiotherapy was well tolerated by patients, evidence of target modulation was observed, and the median OS for patients with glioblastoma was 21 months; an increase of 7 months compared to current treatment (252). These clinical studies alongside the data presented in Chapter 3 provide support for further study of Notch pathway inhibitors in patients with gliomas, potentially selecting patients with evidence of overexpression and/or activation of Notch pathway components such as DLL4 and/or JAG1.

GCSCs have been shown to play an important role in mediating treatment resistance and tumour recurrence in glioblastoma, and the Notch pathway facilitates GCSC self-renewal and maintenance. Therefore, the aim of Chapter 4 was to determine the role of DLL4- and JAG1-induced Notch signalling in GCSC self-renewal and resistance to TMZ chemotherapy. We utilised the *in vitro* neurosphere assay to study glioma response to drug treatments because neurospheres resemble the phenotypes and genotypes of

the patients tumours more closely compared to 2D cultured cell lines (299, 315). Our results have shown overexpression of DLL4 and JAG1 promotes the increased self-renewal of glioblastoma cell lines cultured as neurospheres as well as in a patient-derived GCSC cell line (CSC-5). Notably, this increase can be significantly reversed upon combination DBZ and TMZ treatment. Additionally, we also performed shRNA knockdown of DLL4 and JAG1 in the GCSC line resulting in a significant reduction of GCSC self-renewal, strengthening the role of DLL4- and JAG1-induced Notch signalling in GCSC self-renewal and maintenance. We believe DBZ acts in synergy with TMZ in order to induce the differentiation of GCSCs ultimately resulting in cell death of the differentiated GCSCs by TMZ.

The role of Notch signalling in GCSC treatment resistance and tumour recurrence has previously been examined by Gilbert *et al*., whereby inhibition of Notch signalling by a GSI enhanced glioma treatment by inhibiting neurosphere repopulation of cultured patient samples and also xenograft recurrence in mice (197). This study also determined whether scheduling of Notch inhibition and TMZ treatment affected neurosphere recovery. They tested whether treatment with the GSI DAPT administered before, during, or after TMZ treatment would have distinct effects. Interestingly, it was identified that pre-treatment with DAPT decreased the efficacy of TMZ whilst post-treatment significantly inhibited secondary neurosphere formation. This was not something which was assessed during our study; however, our combination treatment results are comparable with those which have previously been published and show a significant reduction in secondary neurosphere formation when DBZ and TMZ are administered concomitantly.

Additionally, in Chapter 4 we have shown DLL4- and JAG1-induced Notch signalling in glioblastoma neurospheres results in the increased expression of the GCSC markers CD133, SOX2, and Nestin at both an mRNA and protein level, and expression of these markers is further increased following TMZ treatment. As there is much debate in the field about what is and is not a GCSC marker, we utilised multiple previously identified in the literature in order to obtain a more accurate picture of the GCSC population (179, 385, 389). Our results confirm the role of Notch in GCSC maintenance and prove that TMZ promotes increased GCSC self-renewal as shown by increased GCSC marker expression. To understand the potential mechanism by which Notch inhibition treatment reduces neurosphere recovery, we performed qPCR and IF staining of treated neurospheres. We identified inhibition of Notch signalling with DBZ resulted in a significant reduction of GCSC marker expression and appears to induce the differentiation of GCSCs as shown by increased GFAP (astrocytes), β-III-tubulin (neurons), and SOX10 (oligodendrocytes) expression at both an mRNA and protein level.

A previous study utilising the GSI RO4949097 in combination with radiation and TMZ also showed decreased expression of CD133, SOX2 and Nestin, inducing neural and astrocytic differentiation (255, 400). Notably, Saito *et al*. showed GCSCs sensitive to the GSIs DAPT, RO4929097, and BMS-708163 have a gene signature enriched in proneural genes such as *OLIG2, SOX2, ERB3, HDAC2, TGFB3, CHIL3I* and *NKX2-2*. The study also showed inhibition of Notch signalling by GSI treatment attenuated both the proliferation and self-renewal of GCSCs, and induced neural and astrocytic differentiation (400). Whilst assessing the clinical effects of Notch inhibition in Glioma patients, Xu *et al*. also revealed patient-specific organotypic tumour explant cultures

treated with RO2929097 resulted in a significant reduction of tumour proliferation, viability, and the CD133+ population (252). Another study by Chu *et al*. identified prolonged inhibition of glioblastoma xenograft initiation and clonogenic growth following *in vivo* Notch blockade using the GSI MRK003 in mice. Oral GSI treatment was shown to affect proliferation, expression of Notch targets, NSC, and differentiation markers in the xenografts. The expression of the neural stem/progenitor markers Nestin, CD133, BMI1, and Nanog were reduced upon MRK003 treatment compared to control, whilst expression of the glial and neuronal differentiation markers GFAP and MAP2 were increased (304). Consistent with our results, these findings suggest GSI treatment inhibits the expression of stem cell markers in glioblastoma and result in GCSC differentiation as shown by the increased expression of markers of neural differentiation.

Finally, in Chapter 5 we utilised IHC to assess the expression of DLL4, JAG1, and the GCSC markers CD133 and Nestin in paired primary and recurrent glioblastoma patient samples, and whether an association exists between these. Our results showed in recurrent glioblastoma samples, increased DLL4 and JAG1 expression appears to be associated with increased GCSC marker (CD133 and Nestin) expression, however due to insufficient sample number some of these results did not reach significance. GCSCs are key drivers of treatment resistance and tumour recurrence, therefore recurrent tumours may harbour increased CD133+/Nestin+ GCSCs. We believe DLL4- and/or JAG1-induced Notch signalling increases GCSCs self-renewal, and thus drives tumour recurrence despite treatment. It is worth noting that radiotherapy was used as part of the standard of care for this cohort of patients, and previously we have not assessed the effect of DLL4- and JAG1-induced Notch signalling on radiation treatment

resistance in glioblastoma. However, like TMZ chemotherapy, radiotherapy is thought to target the non-GCSC population, and as such enriches the GCSC population following treatment (177, 179).

Interestingly, we also identified a significant positive correlation between CD133 staining scores in paired primary and recurrent glioblastoma patient samples. This finding illustrates the number of CD133+ cells in primary versus recurrent glioblastoma tumours remains the same despite treatment of the primary tumour with radiation and TMZ chemotherapy. This observation suggests these CD133+ cells are resistant to both radio- and chemotherapy, and may be responsible for tumour recurrence following treatment, thus highlighting the importance of GCSCs in patient tumours and the need to target this population of cells in order to overcome treatment resistance and tumour recurrence in glioblastoma.

Overall, we have shown DLL4- and JAG1-induced Notch signalling in glioblastoma is responsible for resistance to TMZ chemotherapy, and this can be overcome by the use of Notch inhibition treatment with the GSI DBZ. Our findings are in agreement with the results of previous studies showing the enhanced therapeutic effect of combined Notch inhibition with TMZ. Whilst these findings are important to promote Notch inhibitors as therapeutics for glioblastoma, combination of Notch inhibition to the current standard of care (radiotherapy plus TMZ), has only once been reported. The study previously discussed by Yahyanejad et al., identified Notch inhibition in combination with radiotherapy and TMZ significantly enhanced 3D spheroid growth delay *in vitro*, and prolongs the survival of mice bearing orthotopic glioblastoma in vivo compared with the current standard of care (255). These results alongside ours are encouraging for the development of new combination treatments for glioblastoma.

However, the clinical relevance of our study could be further maximised by the use of patient derived xenografts that are better models of glioblastoma having typical patient histological characteristics (i.e. micro-infiltrative, highly vascularised, palisading necrosis) and mimicking gene expression profiles of the different subtypes of glioblastoma compared to the well-established cultured cell lines.

It has also been reported that endothelial cells function as a stem cell niche to promote the self-renewal of CD133+ cells in glioblastoma by providing Notch ligands that activate Notch signalling. It would therefore be probable, that impeding this relationship between GCSCs and endothelial cells by Notch inhibition would result in significantly reduced tumour growth. However, further study in endothelial-tumour cell co-cultures and animal models would be required to provide further validation of this hypothesis.

Recently, integrated genomic profiling of glioblastoma has led to new classifications with both prognostic and predictive importance (65, 360, 399). Research into targeted therapeutics against actionable targets from this data has however led to limited efficacy in glioblastoma (401). This is believed to be due to the high inter- and intra-tumoural heterogeneity in glioblastoma and clonal expansion driven by treatment or *de novo* acquired mechanisms of resistance (402). Therapies targeting the survival of tumour-initiating cells (GCSCs) are therefore more likely to be a success as they target the so-called “tumour driver” populations. Identification of these populations requires much more research, however our work alongside others highlights the importance of GCSCs in tumour growth, treatment response, and tumour recurrence, alongside the dependence of GCSCs on Notch signalling for maintenance and self-renewal.

6.2 Experimental Limitations

The main limitation of this project is the lack of *in vivo* data which was part of the initial project plan. However due to limitations in both time and funding constraints, *in vivo* animal experiments were unable to be completed.

Another limitation is the use of the U87 and U251 cell lines. 2D cell lines are valuable for generating important biological and mechanistic understanding of cancer targets, as well as for testing anti-cancer therapeutics. However, they do not fully reflect the *in vivo* situation, due to the lack of cellular heterogeneity and the tumour microenvironment, both of which play key roles in glioblastoma pathogenesis. Similarly, only one patient derived GCSC line was utilised during this project. It would have been ideal to have used at least two lines for this study due to the significant heterogeneity between tumours in glioblastoma. However, the results we obtained in the CSC-5 cell line do reflect the results obtained with the U87 and U251 glioblastoma cell lines. Unfortunately, no preclinical model is able to fully recapitulate the complexity of tumours within patients or the physiological parameters which determine intrinsic and acquired drug responses. Therefore, the best approach is to use a combination of models to gain the most insightful information on drug tumour responses prior to clinical translation. We have achieved this during this study by utilising 2D cell lines, 3D spheroid culture models, and by use of the neurosphere recovery assay.

Numerous mechanisms have been suggested to play a role in TMZ resistance in glioblastoma. One such mechanisms is epigenetic silencing of the DNA repair protein MGMT. *MGMT* is silenced by promoter methylation in approximately half of all glioblastoma tumours (42). Both the U87 and U251 cell lines utilised during his study

exhibit *MGMT* promoter methylation (158), therefore MGMT has little effect on TMZ resistance in our cell lines since lack of methylation is associated with resistance. However, it would be of interest to see if performing the experiments in cell lines with unmethylated *MGMT* (such as LN18 and SF767) results in the same outcome. Similarly, *IDH* is a key biomarker in gliomas, and both the U87 and U251 cell lines exhibit wild-type *IDH* (403). Like *MGMT*, it would be interesting to use *IDH*-mutant cell lines to see if this has an effect of Notch-induced TMZ resistance in glioblastoma.

More recently, research has been focused on developing *in vitro* models that better recapitulate the disease *in vivo.* Such models include tumour organoids, glioblastoma cerebral organoids, and patient derived xenografts. Pine *et al.* performed RNA sequencing of glioblastoma models in order to compare the models transcriptional profiles to that of the patients own tumour and found significantly higher correlation with glioblastoma cerebral organoids compared to other model types. Glioblastoma cerebral organoids are of significant interest as the GCSCs within this model are enriched for a neural-progenitor-like cell population and recapitulate the cellular states, heterogeneity, and plasticity found in the corresponding primary parental tumours (404). The models we utilised during this study are useful for understanding basic mechanistic data, but it would be of addition to use models that are more representative of the tumour *in vivo*. It would therefore be of interest to utilise these glioblastoma cerebral organoid models to test our hypothesis, with the hope that this can be further support the results already obtained from our study.

We utilised the GSI DBZ to inhibit Notch signalling in this study. Preferentially, it would be of benefit to use specific DLL4 and JAG1 inhibitors instead such as humanised monoclonal antibodies against DLL4 and JAG1 respectively. As DBZ is a pan-Notch

inhibitor, it is not just DLL4- and JAG1-induced Notch signalling that is inhibited, but Notch signalling as a whole. Also, being pan-Notch inhibitors, *in vivo,* GSIs cause intestinal toxicity via goblet cell metaplasia of the small intestine (329). This could be a limitation for future clinical trials into the value of Notch inhibition as an addition to the current standard of care in glioblastoma. To maximise the therapeutic effects and minimise the systemic Notch-related side effects, improved dosing regimens have been reported in a phase 1 clinical trial testing the antitumour activity of the GSI RO4929097, which has a favourable safety profile with minimal side effects (405). By following this improved dosing regimen, it enables the further study into GSIs and more importantly the safe use of Notch inhibitors in future clinical trials. For example, using specific anti-Notch1 monoclonal antibody (352), or preferentially using specific anti-DLL4 (271, 279) and anti JAG1 (406) monoclonal antibodies.

A further limitation of this study is our models were treated with TMZ only as the standard treatment, however the current standard of care in glioblastoma following tumour resection is radiotherapy and adjuvant TMZ chemotherapy. We were unable to perform radiation therapy in our models due to the lack of facilities for this. However, like TMZ, radiotherapy appears to target the non-GCSC population and as such enriches the GCSC population (177, 179). We believe it is likely that our results would also be valid if radiotherapy was given alongside TMZ as the “control” standard treatment.

6.3 Future Directions

All areas of this project have provided novel and exciting results, which should provide ample support for the research to continue. One of the main future directions of this project is to complete animal studies, to test whether DLL4-and/or JAG1-induced

Notch signalling results in increased tumour growth compared to control, and if combination DBZ and TMZ treatment is able to reverse this. Our 2D cell lines, 3D, and neurosphere culture models lack important factors from the tumour microenvironment known to contribute to the tumour response including tumour vasculature, fibroblasts, and immune cells. It would therefore be of significant interest to exploit an established glioblastoma orthotopic mouse model to address the *in vivo* efficacy of Notch inhibition combined with TMZ.

It would also be of benefit for more patient GCSC lines to be derived to enable further studies into GCSCs using a simple 3D neurosphere model system. GCSC lines better compliment the gene expression profiles of glioblastoma patients and typical histological characteristics compared to established cell lines. These would also give us more insight into mechanisms involved in GCSC maintenance and self-renewal than conventional 2D cell lines, and whether inhibition of Notch signalling in GCSCs results in differentiation. By using multiple patient-derived GCSC lines, it would reflect the heterogeneity between patient tumours and provide a better insight into the role of Notch signalling in GCSCs.

During this study we only assessed the role of DLL4- and JAG1-induced Notch signalling in glioblastoma as these ligands have previously been shown to be upregulated, promote tumour growth by modulating angiogenesis, and mediate tumour resistance to anti-VEGF therapy with bevacizumab (306). It would be of interest to undertake a screen of the other Notch ligands (e.g. DLL1, DLL3 and JAG2) to determine if DLL1/DLL3/JAG2-induced Notch signalling also play a role in mediating TMZ resistance in glioblastoma. This could be achieved by performing an initial screen of cell lines

overexpressing these ligands in a 2D TMZ IC50 (single TMZ and combination TMZ and DBZ treatment) drug assay.

The Notch pathway has been shown to crosstalk with multiple oncogenic signalling pathways including NF-κB, Akt, Hedgehog, mTOR, Ras, Wnt, oestrogen receptor, androgen receptor, EGFR, and PDGFR. It may be that crosstalk between Notch and other signalling pathways plays a role in glioblastoma resistance to TMZ. Therefore, it would be of interest to assess if DLL4- and/or JAG1-induced Notch signalling is required for the maintenance of any of these key pathways in glioblastoma by performing RNA-sequencing of overexpression versus control cells. For example, NF-KB signalling has been shown to be induced upon Notch signalling (407), however, whether this is induced/inhibited following DLL4- and/or JAG1-induced Notch signalling remains to be elucidated. These pathways induced/inhibited by Notch signalling may play a key role in TMZ resistance in glioblastoma. By identifying these significantly upregulated and downregulated pathways, new effective combination treatments options may be found for glioblastoma.

It would also be of interest to acquire more samples for IHC staining and the corresponding patient data to assess the effect of DLL4- and JAG1-Notch signalling in primary and recurrent glioblastoma, and the effect on patient overall survival. The general trend of our results show increased DLL4 and JAG1 expression results in increased expression of GCSC markers in recurrent glioblastoma. This is in line with the hypothesis that GCSCs are responsible for treatment resistance and tumour recurrence in glioblastoma. By obtaining an increased sample number of paired primary and recurrent glioblastoma samples this would enable us to obtain a clearer understanding

of the effect of DLL4- and JAG1-induced Notch signalling in patients with regards to both treatment resistance, tumour recurrence, and patient survival.

The ultimate goal of this project is a phase 1/2 clinical trial in which patients are given Notch inhibition treatment alongside the current standard treatment. It is hoped that the addition of such treatment to the standard of care in glioblastoma will result in increased patient overall survival and decreased tumour recurrence by targeting the GCSC population within the tumour.

6.4 Conclusions

This study has shown DLL4- and JAG1- induced Notch signalling promotes TMZ resistance in glioblastoma in both 2D cell lines and 3D spheroid culture models. The expression of DLL4 and JAG1 promotes increased neurosphere recovery and is reversed upon inhibition of Notch signalling with the GSI DBZ in combination with TMZ treatment. Consequently, Notch inhibition reduces the expression of key GCSC markers and may promote GCSC differentiation. Further research is required to shed light on the prognostic and therapeutic potential of targeting these ligands to overcome TMZ resistance and recurrence of glioblastoma.

7 References

1. Ostrom QT, Gittleman H, Truitt G, Boscia A, Kruchko C, Barnholtz-Sloan JS. CBTRUS Statistical Report: Primary Brain and Other Central Nervous System Tumors Diagnosed in the United States in 2011-2015. Neuro-Oncology. 2018;20(suppl_4):iv1-iv86.

2. Ferlay J, Parkin DM, Steliarova-Foucher E. Estimates of cancer incidence and mortality in Europe in 2008. European Journal of Cancer. 2010;46(4):765-81.

3. Galli R, Binda E, Orfanelli U, Cipelletti B, Gritti A, De Vitis S, et al. Isolation and characterization of tumorigenic, stem-like neural precursors from human glioblastoma. Cancer Research. 2004;64(19):7011-21.

4. Singh SK, Hawkins C, Clarke ID, Squire JA, Bayani J, Hide T, et al. Identification of human brain tumour initiating cells. Nature. 2004;432(7015):396-401.

5. Louis DN, Perry A, Reifenberger G, Von Deimling A, Figarella-Branger D, Cavenee WK, et al. World Health Organization classification of tumors of the central nervous system (revised 4th edition): World Health Organisation; 2016.

6. Weller M, Wick W, Aldape K, Brada M, Berger M, Pfister SM, et al. Glioma. Nature Reviews Disease Primers. 2015;1:15017.

7. Ohgaki H, Kleihues P. The Definition of Primary and Secondary Glioblastoma. Clinical Cancer Research. 2013;19(4):764-72.

8. Wen PY, Kesari S. Malignant gliomas in adults. The New England Journal of Medicine. 2008;359(5):492-507.

9. Stupp R, Mason WP, Van Den Bent MJ, Weller M, Fisher B, Taphoorn MJ, et al. Radiotherapy plus concomitant and adjuvant temozolomide for glioblastoma. The New England Journal of Medicine. 2005;352(10):987-96.

10. Lapointe S, Perry A, Butowski NA. Primary brain tumours in adults. The Lancet. 2018;392(10145):432-46.

11. Alexander BM, Cloughesy TF. Adult Glioblastoma. Journal of Clinical Oncology. 2017;35(21):2402-9.

12. Ron E, Modan B, Boice JD, Jr., Alfandary E, Stovall M, Chetrit A, et al. Tumors of the brain and nervous system after radiotherapy in childhood. The New England Journal of Medicine. 1988;319(16):1033-9.

13. Braganza MZ, Kitahara CM, Berrington de Gonzalez A, Inskip PD, Johnson KJ, Rajaraman P. Ionizing radiation and the risk of brain and central nervous system tumors: a systematic review. Neuro-Oncology. 2012;14(11):1316-24.

14. Campian J, Gutmann DH. CNS Tumors in Neurofibromatosis. Journal of Clinical Oncology. 2017;35(21):2378-85.

15. Carlberg M, Hardell L. Evaluation of Mobile Phone and Cordless Phone Use and Glioma Risk Using the Bradford Hill Viewpoints from 1965 on Association or Causation. BioMed Research International. 2017;2017:9218486.

16. Wang Y, Guo X. Meta-analysis of association between mobile phone use and glioma risk. Journal of Cancer Research and Therapeutics. 2016;12(Supplement):C298-c300.

17. Yang M, Guo W, Yang C, Tang J, Huang Q, Feng S, et al. Mobile phone use and glioma risk: A systematic review and meta-analysis. PLOS One. 2017;12(5):e0175136.

18. Baan R, Grosse Y, Lauby-Secretan B, El Ghissassi F, Bouvard V, Benbrahim-Tallaa L, et al. Carcinogenicity of radiofrequency electromagnetic fields. The Lancet Oncology. 2011;12(7):624-6.

19. Morgan LL, Miller AB, Sasco A, Davis DL. Mobile phone radiation causes brain tumors and should be classified as a probable human carcinogen. International Journal of Oncology. 2015;46(5):1865-71.

20. Kirby S, Purdy RA. Headaches and brain tumors. Neurologic Clinics. 2014;32(2):423-32.

21. Schiff D, Lee EQ, Nayak L, Norden AD, Reardon DA, Wen PY. Medical management of brain tumors and the sequelae of treatment. Neuro-Oncology. 2015;17(4):488-504.

22. NICE. Brain tumours (primary) and brain metastases in adults (NICE Guideline NG99) 2018 [Available from: https://www.nice.org.uk/guidance/ng99/chapter/recommendations#imaging-for-suspected-glioma.

23. la Fougere C, Suchorska B, Bartenstein P, Kreth FW, Tonn JC. Molecular imaging of gliomas with PET: opportunities and limitations. Neuro-Oncology. 2011;13(8):806-19.

24. Louis DN, Ohgaki H, Wiestler OD, Cavenee WK, Burger PC, Jouvet A, et al. The 2007 WHO classification of tumours of the central nervous system. Acta Neuropathologica. 2007;114(2):97-109.

25. Horbinski C, Kofler J, Yeaney G, Camelo-Piragua S, Venneti S, Louis DN, et al. Isocitrate dehydrogenase 1 analysis differentiates gangliogliomas from infiltrative gliomas. Brain Pathology. 2011;21(5):564-74.

26. Bleeker FE, Atai NA, Lamba S, Jonker A, Rijkeboer D, Bosch KS, et al. The prognostic IDH1 (R132) mutation is associated with reduced NADP+-dependent IDH activity in glioblastoma. Acta Neuropathologica. 2010;119(4):487-94.

27. Lee SM, Koh HJ, Park DC, Song BJ, Huh TL, Park JW. Cytosolic NADP(+)-dependent isocitrate dehydrogenase status modulates oxidative damage to cells. Free Radical Biology and Medicine. 2002;32(11):1185-96.

28. Xu W, Yang H, Liu Y, Yang Y, Wang P, Kim SH, et al. Oncometabolite 2-hydroxyglutarate is a competitive inhibitor of alpha-ketoglutarate-dependent dioxygenases. Cancer Cell. 2011;19(1):17-30.

29. He YF, Li BZ, Li Z, Liu P, Wang Y, Tang Q, et al. Tet-mediated formation of 5-carboxylcytosine and its excision by TDG in mammalian DNA. Science. 2011;333(6047):1303-7.

30. Parker SJ, Metallo CM. Metabolic consequences of oncogenic IDH mutations. Pharmacology & Therapeutics. 2015;152:54-62.

31. Cairns RA, Mak TW. Oncogenic isocitrate dehydrogenase mutations: mechanisms, models, and clinical opportunities. Cancer Discovery. 2013;3(7):730-41.

32. van den Bent MJ, Brandes AA, Taphoorn MJ, Kros JM, Kouwenhoven MC, Delattre J-Y, et al. Adjuvant procarbazine, lomustine, and vincristine chemotherapy in newly diagnosed anaplastic oligodendroglioma: long-term follow-up of EORTC brain tumor group study 26951. Journal of Clinical Oncology. 2012;31(3):344-50.

33. Chan AK-Y, Yao Y, Zhang Z, Chung NY-F, Liu JS-M, Li KK-W, et al. TERT promoter mutations contribute to subset prognostication of lower-grade gliomas. Modern Pathology. 2014;28:177.

34. Wesseling P, van den Bent M, Perry A. Oligodendroglioma: pathology, molecular mechanisms and markers. Acta Neuropathologica. 2015;129(6):809-27.

35. Watanabe T, Nakamura M, Kros JM, Burkhard C, Yonekawa Y, Kleihues P, et al. Phenotype versus genotype correlation in oligodendrogliomas and low-grade diffuse astrocytomas. Acta Neuropathologica. 2002;103(3):267-75.

36. Wu G, Broniscer A, McEachron TA, Lu C, Paugh BS, Becksfort J, et al. Somatic histone H3 alterations in pediatric diffuse intrinsic pontine gliomas and non-brainstem glioblastomas. Nature Genetics. 2012;44(3):251-3.

37. Schwartzentruber J, Korshunov A, Liu XY, Jones DT, Pfaff E, Jacob K, et al. Driver mutations in histone H3.3 and chromatin remodelling genes in paediatric glioblastoma. Nature. 2012;482(7384):226-31.

38. Khuong-Quang DA, Buczkowicz P, Rakopoulos P, Liu XY, Fontebasso AM, Bouffet E, et al. K27M mutation in histone H3.3 defines clinically and biologically distinct subgroups of pediatric diffuse intrinsic pontine gliomas. Acta Neuropathologica. 2012;124(3):439-47.

39. Bender S, Tang Y, Lindroth AM, Hovestadt V, Jones DT, Kool M, et al. Reduced H3K27me3 and DNA hypomethylation are major drivers of gene expression in K27M mutant pediatric high-grade gliomas. Cancer Cell. 2013;24(5):660-72.

40. Fontebasso AM, Liu XY, Sturm D, Jabado N. Chromatin remodeling defects in pediatric and young adult glioblastoma: a tale of a variant histone 3 tail. Brain Pathology. 2013;23(2):210-6.

41. Esteller M, Garcia-Foncillas J, Andion E, Goodman SN, Hidalgo OF, Vanaclocha V, et al. Inactivation of the DNA-repair gene MGMT and the clinical response of gliomas to alkylating agents. The New England Journal of Medicine. 2000;343(19):1350-4.

42. Hegi ME, Diserens AC, Gorlia T, Hamou MF, de Tribolet N, Weller M, et al. MGMT gene silencing and benefit from temozolomide in glioblastoma. The New England Journal of Medicine. 2005;352(10):997-1003.

43. Weller M, Stupp R, Hegi ME, Van Den Bent M, Tonn JC, Sanson M, et al. Personalized care in neuro-oncology coming of age: why we need MGMT and 1p/19q testing for malignant glioma patients in clinical practice. Neuro-Oncology. 2012;14(suppl_4):iv100-iv8.

44. Wick W, Hartmann C, Engel C, Stoffels M, Felsberg J, Stockhammer F, et al. NOA-04 randomized phase III trial of sequential radiochemotherapy of anaplastic glioma with procarbazine, lomustine, and vincristine or temozolomide. Journal of Clinical Oncology. 2009;27(35):5874.

45. Zawlik I, Vaccarella S, Kita D, Mittelbronn M, Franceschi S, Ohgaki H. Promoter methylation and polymorphisms of the MGMT gene in glioblastomas: a population-based study. Neuroepidemiology. 2009;32(1):21-9.

46. Hawkins C, Walker E, Mohamed N, Zhang C, Jacob K, Shirinian M, et al. BRAF-KIAA1549 fusion predicts better clinical outcome in pediatric low-grade astrocytoma. Clinical Cancer Research. 2011;17(14):4790-8.

47. Park SH, Won J, Kim SI, Lee Y, Park CK, Kim SK, et al. Molecular Testing of Brain Tumor. Journal of Pathology and Translational Medicine. 2017;51(3):205-23.

48. Malmström A, Grønberg BH, Marosi C, Stupp R, Frappaz D, Schultz H, et al. Temozolomide versus standard 6-week radiotherapy versus hypofractionated radiotherapy in patients older than 60 years with glioblastoma: the Nordic randomised, phase 3 trial. The Lancet Oncology. 2012;13(9):916-26.

49. Ferris SP, Hofmann JW, Solomon DA, Perry A. Characterization of gliomas: from morphology to molecules. Virchows Archiv. 2017;471(2):257-69.

50. Sturm D, Pfister SM, Jones DTW. Pediatric Gliomas: Current Concepts on Diagnosis, Biology, and Clinical Management. Journal of Clinical Oncology. 2017;35(21):2370-7.

51. Cohen SB, Graham ME, Lovrecz GO, Bache N, Robinson PJ, Reddel RR. Protein composition of catalytically active human telomerase from immortal cells. Science. 2007;315(5820):1850-3.

52. Greider CW, Blackburn EH. The telomere terminal transferase of Tetrahymena is a ribonucleoprotein enzyme with two kinds of primer specificity. Cell. 1987;51(6):887-98.

53. Blackburn EH. Structure and function of telomeres. Nature. 1991;350(6319):569-73.

54. Wright WE, Piatyszek MA, Rainey WE, Byrd W, Shay JW. Telomerase activity in human germline and embryonic tissues and cells. Developmental Genetics. 1996;18(2):173-9.

55. Shay JW, Bacchetti S. A survey of telomerase activity in human cancer. European Journal of Cancer. 1997;33(5):787-91.

56. Falchetti ML, Larocca LM, Pallini R. Telomerase in brain tumors. Childs Nervous System. 2002;18(3-4):112-7.

57. Kim NW, Piatyszek MA, Prowse KR, Harley CB, West MD, Ho PL, et al. Specific association of human telomerase activity with immortal cells and cancer. Science. 1994;266(5193):2011-5.

58. Killela PJ, Reitman ZJ, Jiao Y, Bettegowda C, Agrawal N, Diaz LA, Jr., et al. TERT promoter mutations occur frequently in gliomas and a subset of tumors derived from cells with low rates of self-renewal. Proc Natl Acad Sci U S A. 2013;110(15):6021-6.

59. Arita H, Narita Y, Fukushima S, Tateishi K, Matsushita Y, Yoshida A, et al. Upregulating mutations in the TERT promoter commonly occur in adult malignant gliomas and are strongly associated with total 1p19q loss. Acta Neuropathologica. 2013;126(2):267-76.

60. Bell RJ, Rube HT, Kreig A, Mancini A, Fouse SD, Nagarajan RP, et al. The transcription factor GABP selectively binds and activates the mutant TERT promoter in cancer. Science. 2015;348(6238):1036-9.

61. Diplas BH, He X, Brosnan-Cashman JA, Liu H, Chen LH, Wang Z, et al. The genomic landscape of TERT promoter wildtype-IDH wildtype glioblastoma. Nature Communications. 2018;9(1):2087.

62. Henson JD, Hannay JA, McCarthy SW, Royds JA, Yeager TR, Robinson RA, et al. A robust assay for alternative lengthening of telomeres in tumors shows the significance of alternative lengthening of telomeres in sarcomas and astrocytomas. Clinical Cancer Research. 2005;11(1):217-25.

63. Nonoguchi N, Ohta T, Oh JE, Kim YH, Kleihues P, Ohgaki H. TERT promoter mutations in primary and secondary glioblastomas. Acta Neuropathologica. 2013;126(6):931-7.

64. Pekmezci M, Rice T, Molinaro AM, Walsh KM, Decker PA, Hansen H, et al. Adult infiltrating gliomas with WHO 2016 integrated diagnosis: additional prognostic roles of ATRX and TERT. Acta Neuropathologica. 2017;133(6):1001-16.

65. Brat DJ, Verhaak RG, Aldape KD, Yung WK, Salama SR, Cooper LA, et al. Comprehensive, Integrative Genomic Analysis of Diffuse Lower-Grade Gliomas. The New England Journal of Medicine. 2015;372(26):2481-98.

66. Kannan K, Inagaki A, Silber J, Gorovets D, Zhang J, Kastenhuber ER, et al. Whole-exome sequencing identifies ATRX mutation as a key molecular determinant in lower-grade glioma. Oncotarget. 2012;3(10):1194-203.

67. Abedalthagafi M, Phillips JJ, Kim GE, Mueller S, Haas-Kogen DA, Marshall RE, et al. The alternative lengthening of telomere phenotype is significantly associated with loss of ATRX expression in high-grade pediatric and adult astrocytomas: a multi-institutional study of 214 astrocytomas. Modern Pathology. 2013;26(11):1425-32.

68. McGirt MJ, Chaichana KL, Gathinji M, Attenello FJ, Than K, Olivi A, et al. Independent association of extent of resection with survival in patients with malignant brain astrocytoma. Journal of Neurosurgery. 2009;110(1):156-62.

69. Hadjipanayis CG, Widhalm G, Stummer W. What is the Surgical Benefit of Utilizing 5-Aminolevulinic Acid for Fluorescence-Guided Surgery of Malignant Gliomas? Neurosurgery. 2015;77(5):663-73.

70. Eljamel S. 5-ALA Fluorescence Image Guided Resection of Glioblastoma Multiforme: A Meta-Analysis of the Literature. International Journal of Molecular Sciences. 2015;16(5):10443-56.

71. Coburger J, Hagel V, Wirtz CR, Konig R. Surgery for Glioblastoma: Impact of the Combined Use of 5-Aminolevulinic Acid and Intraoperative MRI on Extent of Resection and Survival. PLOS One. 2015;10(6):e0131872.

72. Walker MD, Alexander E, Hunt WE, MacCarty CS, Mahaley MS, Mealey J, et al. Evaluation of BCNU and/or radiotherapy in the treatment of anaplastic gliomas: a cooperative clinical trial. Journal of neurosurgery. 1978;49(3):333-43.

73. Stevens MF, Hickman JA, Stone R, Gibson NW, Baig GU, Lunt E, et al. Antitumor imidazotetrazines. 1. Synthesis and chemistry of 8-carbamoyl-3-(2-chloroethyl)imidazo[5,1-d]-1,2,3,5-tetrazin-4(3 H)-one , a novel broad-spectrum antitumor agent. J Med Chem. 1984;27(2):196-201.

74. Friedman HS, Kerby T, Calvert H. Temozolomide and treatment of malignant glioma. Clinical Cancer Research. 2000;6(7):2585-97.

75. Hickman JA, Stevens MF, Gibson NW, Langdon SP, Fizames C, Lavelle F, et al. Experimental antitumor activity against murine tumor model systems of 8-carbamoyl-3-(2-chloroethyl)imidazo[5,1-d]-1,2,3,5-tetrazin-4(3 H)-one (mitozolomide), a novel broad-spectrum agent. Cancer Res. 1985;45(7):3008-13.

76. Gibson NW, Hickman JA, Erickson LC. DNA Cross-Linking and Cytotoxicity in Normal and Transformed Human Cells Treated in Vitro with 8-Carbamoyl-3-(2-chloroethyl)imidazo[5,1-d]-1,2,3,5-tetrazin-4(3H)-one. Cancer Research. 1984;44(5):1772-5.

77. Gibson NW, Erickson LC. The effects of pretreatment of human tumour cells with MNNG on the DNA crosslinking and cytotoxicity of mitozolomide. Br J Cancer. 1985;52(2):251-8.

78. Newlands ES, Blackledge G, Slack JA, Goddard C, Brindley CJ, Holden L, et al. Phase I clinical trial of mitozolomide. Cancer Treat Rep. 1985;69(7-8):801-5.

79. Stevens MFG, Hickman JA, Langdon SP, Chubb D, Vickers L, Stone R, et al. Antitumor Activity and Pharmacokinetics in Mice of 8-Carbamoyl-3-methyl-imidazo[5,1-d]-1,2,3,5-tetrazin-4(3H)-one (CCRG 81045; M & B 39831), a Novel Drug with Potential as an Alternative to Dacarbazine. Cancer Research. 1987;47(22):5846-52.

80. Stevens MF, Newlands ES. From triazines and triazenes to temozolomide. Eur J Cancer. 1993;29a(7):1045-7.

81. Newlands ES, Blackledge GR, Slack JA, Rustin GJ, Smith DB, Stuart NS, et al. Phase I trial of temozolomide (CCRG 81045: M&B 39831: NSC 362856). Br J Cancer. 1992;65(2):287-91.

82. Yang ZF, Ho DW, Ng MN, Lau CK, Yu WC, Ngai P, et al. Significance of CD90+ cancer stem cells in human liver cancer. Cancer Cell. 2008;13(2):153-66.

83. Portnow J, Badie B, Chen M, Liu A, Blanchard S, Synold TW. The neuropharmacokinetics of temozolomide in patients with resectable brain tumors: potential implications for the current approach to chemoradiation. Clin Cancer Res. 2009;15(22):7092-8.

84. Ostermann S, Csajka C, Buclin T, Leyvraz S, Lejeune F, Decosterd LA, et al. Plasma and cerebrospinal fluid population pharmacokinetics of temozolomide in malignant glioma patients. Clinical Cancer Research. 2004;10(11):3728-36.

85. Denny BJ, Wheelhouse RT, Stevens MF, Tsang LL, Slack JA. NMR and molecular modeling investigation of the mechanism of activation of the antitumor drug temozolomide and its interaction with DNA. Biochemistry. 1994;33(31):9045-51.

86. Loveless A. Possible relevance of O-6 alkylation of deoxyguanosine to the mutagenicity and carcinogenicity of nitrosamines and nitrosamides. Nature. 1969;223(5202):206-7.

87. Newbold RF, Warren W, Medcalf AS, Amos J. Mutagenicity of carcinogenic methylating agents is associated with a specific DNA modification. Nature. 1980;283(5747):596-9.

88. Zhang J, Stevens MF, Bradshaw TD. Temozolomide: mechanisms of action, repair and resistance. Curr Mol Pharmacol. 2012;5(1):102-14.

89. Pegg AE, Dolan ME, Moschel RC. Structure, Function, and Inhibition of O6-Alkylguanine-DNA Alkyltransferase. In: Cohn WE, Moldave K, editors. Progress in Nucleic Acid Research and Molecular Biology. 51: Academic Press; 1995. p. 167-223.

90. Drablos F, Feyzi E, Aas PA, Vaagbo CB, Kavli B, Bratlie MS, et al. Alkylation damage in DNA and RNA--repair mechanisms and medical significance. DNA Repair (Amst). 2004;3(11):1389-407.

91. Karran P, Hampson R. Genomic instability and tolerance to alkylating agents. Cancer Surv. 1996;28:69-85.

92. Thomas A, Tanaka M, Trepel J, Reinhold WC, Rajapakse VN, Pommier Y. Temozolomide in the Era of Precision Medicine. Cancer research. 2017;77(4):823-6.

93. Syro LV, Rotondo F, Camargo M, Ortiz LD, Serna CA, Kovacs K. Temozolomide and Pituitary Tumors: Current Understanding, Unresolved Issues, and Future Directions. Frontiers in endocrinology. 2018;9:318-.

94. Pegg AE. Properties of mammalian O6-alkylguanine-DNA transferases. Mutat Res. 1990;233(1-2):165-75.

95. Christmann M, Verbeek B, Roos WP, Kaina B. O6-Methylguanine-DNA methyltransferase (MGMT) in normal tissues and tumors: Enzyme activity, promoter methylation and immunohistochemistry. Biochimica et Biophysica Acta (BBA) - Reviews on Cancer. 2011;1816(2):179-90.

96. Srivenugopal KS, Yuan XH, Friedman HS, Ali-Osman F. Ubiquitination-dependent proteolysis of O6-methylguanine-DNA methyltransferase in human and murine tumor cells following inactivation with O6-benzylguanine or 1,3-bis(2-chloroethyl)-1-nitrosourea. Biochemistry. 1996;35(4):1328-34.

97. Lindahl T. Instability and decay of the primary structure of DNA. nature. 1993;362(6422):709-15.

98. Lindahl T, Karran P, Wood RD. DNA excision repair pathways. Curr Opin Genet Dev. 1997;7(2):158-69.

99. Krokan HE, Bjoras M. Base excision repair. Cold Spring Harb Perspect Biol. 2013;5(4):a012583.

100. Cahill DP, Levine KK, Betensky RA, Codd PJ, Romany CA, Reavie LB, et al. Loss of the mismatch repair protein MSH6 in human glioblastomas is associated with tumor progression during temozolomide treatment. Clinical Cancer Research. 2007;13(7):2038-45.

101. Hunter C, Smith R, Cahill DP, Stephens P, Stevens C, Teague J, et al. A hypermutation phenotype and somatic MSH6 mutations in recurrent human malignant gliomas after alkylator chemotherapy. Cancer Res. 2006;66(8):3987-91.

102. Liu L, Gerson SL. Targeted Modulation of MGMT: Clinical Implications. Clinical Cancer Research. 2006;12(2):328-31.

103. Plowman J, Waud WR, Koutsoukos AD, Rubinstein LV, Moore TD, Grever MR. Preclinical Antitumor Activity of Temozolomide in Mice: Efficacy against Human Brain Tumor Xenografts and Synergism with 1,3-Bis(2-chloroethyl)-1-nitrosourea. Cancer Research. 1994;54(14):3793-9.

104. O'Reilly SM, Newlands ES, Brampton M, Glaser MG, Rice-Edwards JM, Illingworth RD, et al. Temozolomide: A new oral cytotoxic chemotherapeutic agent

with promising activity against primary brain tumours. European Journal of Cancer. 1993;29(7):940-2.

105. Newlands ES, O'Reilly SM, Glaser MG, Bower M, Evans H, Brock C, et al. The charing cross hospital experience with temozolomide in patients with gliomas. European Journal of Cancer. 1996;32(13):2236-41.

106. Bower M, Newlands ES, Bleehen NM, Brada M, Begent RJ, Calvert H, et al. Multicentre CRC phase II trial of temozolomide in recurrent or progressive high-grade glioma. Cancer Chemother Pharmacol. 1997;40(6):484-8.

107. Yung A, Levin V, Albright R, Olson J, Fredericks R, Fink K, et al., editors. Randomized trial of temodal (TEM) vs. procarbazine (PCB) in glioblastoma multiforme (GBM) at first relapse. Proceedings, annual meeting of the American Society of Clinical Oncology; 1999.

108. Yung WA, Prados MD, Yaya-Tur R, Rosenfeld SS, Brada M, Friedman HS, et al. Multicenter phase II trial of temozolomide in patients with anaplastic astrocytoma or anaplastic oligoastrocytoma at first relapse. Journal of Clinical Oncology. 1999;17(9):2762-71.

109. Friedman HS, McLendon RE, Kerby T, Dugan M, Bigner SH, Henry AJ, et al. DNA Mismatch Repair and O^ 6-Alkylguanine. DNA Alkyltransferase Analysis and Response to Temodal in Newly Diagnosed Malignant Glioma. Journal of Clinical Oncology. 1998;16(12):3851-7.

110. Brandes AA, Franceschi E, Paccapelo A, Tallini G, De Biase D, Ghimenton C, et al. Role of MGMT Methylation Status at Time of Diagnosis and Recurrence for Patients with Glioblastoma: Clinical Implications. Oncologist. 2017;22(4):432-7.

111. Felsberg J, Thon N, Eigenbrod S, Hentschel B, Sabel MC, Westphal M, et al. Promoter methylation and expression of MGMT and the DNA mismatch repair genes MLH1, MSH2, MSH6 and PMS2 in paired primary and recurrent glioblastomas. Int J Cancer. 2011;129(3):659-70.

112. Christmann M, Nagel G, Horn S, Krahn U, Wiewrodt D, Sommer C, et al. MGMT activity, promoter methylation and immunohistochemistry of pretreatment and recurrent malignant gliomas: a comparative study on astrocytoma and glioblastoma. Int J Cancer. 2010;127(9):2106-18.

113. Yip S, Miao J, Cahill DP, Iafrate AJ, Aldape K, Nutt CL, et al. MSH6 mutations arise in glioblastomas during temozolomide therapy and mediate temozolomide resistance. Clinical Cancer Research. 2009;15(14):4622-9.

114. Shinsato Y, Furukawa T, Yunoue S, Yonezawa H, Minami K, Nishizawa Y, et al. Reduction of MLH1 and PMS2 confers temozolomide resistance and is associated with recurrence of glioblastoma. Oncotarget. 2013;4(12):2261-70.

115. Adhikari S, Choudhury S, Mitra PS, Dubash JJ, Sajankila SP, Roy R. Targeting base excision repair for chemosensitization. Anticancer Agents Med Chem. 2008;8(4):351-7.

116. Alexander BM, Pinnell N, Wen PY, D'Andrea A. Targeting DNA repair and the cell cycle in glioblastoma. J Neurooncol. 2012;107(3):463-77.

117. Agnihotri S, Gajadhar AS, Ternamian C, Gorlia T, Diefes KL, Mischel PS, et al. Alkylpurine-DNA-N-glycosylase confers resistance to temozolomide in xenograft models of glioblastoma multiforme and is associated with poor survival in patients. J Clin Invest. 2012;122(1):253-66.

118. Bobola MS, Emond MJ, Blank A, Meade EH, Kolstoe DD, Berger MS, et al. Apurinic endonuclease activity in adult gliomas and time to tumor progression after alkylating agent-based chemotherapy and after radiotherapy. Clinical Cancer Research. 2004;10(23):7875-83.

119. Montaldi AP, Godoy PR, Sakamoto-Hojo ET. APE1/REF-1 down-regulation enhances the cytotoxic effects of temozolomide in a resistant glioblastoma cell line. Mutat Res Genet Toxicol Environ Mutagen. 2015;793:19-29.

120. Silber JR, Bobola MS, Blank A, Schoeler KD, Haroldson PD, Huynh MB, et al. The apurinic/apyrimidinic endonuclease activity of Ape1/Ref-1 contributes to human glioma cell resistance to alkylating agents and is elevated by oxidative stress. Clinical Cancer Research. 2002;8(9):3008-18.

121. Low SY, Ho YK, Too HP, Yap CT, Ng WH. MicroRNA as potential modulators in chemoresistant high-grade gliomas. J Clin Neurosci. 2014;21(3):395-400.

122. Masoudi MS, Mehrabian E, Mirzaei H. MiR-21: A key player in glioblastoma pathogenesis. J Cell Biochem. 2018;119(2):1285-90.

123. Chan JA, Krichevsky AM, Kosik KS. MicroRNA-21 is an antiapoptotic factor in human glioblastoma cells. Cancer Res. 2005;65(14):6029-33.

124. Wong ST, Zhang XQ, Zhuang JT, Chan HL, Li CH, Leung GK. MicroRNA-21 inhibition enhances in vitro chemosensitivity of temozolomide-resistant glioblastoma cells. Anticancer Res. 2012;32(7):2835-41.

125. Shan Z-N, Tian R, Zhang M, Gui Z-H, Wu J, Ding M, et al. miR128-1 inhibits the growth of glioblastoma multiforme and glioma stem-like cells via targeting BMI1 and E2F3. Oncotarget. 2016;7(48):78813-26.

126. Li Y, Liu Y, Ren J, Deng S, Yi G, Guo M, et al. miR-1268a regulates ABCC1 expression to mediate temozolomide resistance in glioblastoma. J Neurooncol. 2018;138(3):499-508.

127. Tian T, Mingyi M, Qiu X, Qiu Y. MicroRNA-101 reverses temozolomide resistance by inhibition of GSK3β in glioblastoma. Oncotarget. 2016;7(48):79584-95.

128. Luo H, Chen Z, Wang S, Zhang R, Qiu W, Zhao L, et al. c-Myc-miR-29c-REV3L signalling pathway drives the acquisition of temozolomide resistance in glioblastoma. Brain. 2015;138(Pt 12):3654-72.

129. Kim YZ. Altered histone modifications in gliomas. Brain tumor research and treatment. 2014;2(1):7-21.

130. Greer EL, Shi Y. Histone methylation: a dynamic mark in health, disease and inheritance. Nat Rev Genet. 2012;13(5):343-57.

131. Xi G, Mania-Farnell B, Lei T, Tomita T. Histone modification as a drug resistance driver in brain tumors. Oncology and Translational Medicine. 2016(2016 05):216-26.

132. Kitange GJ, Mladek AC, Carlson BL, Schroeder MA, Pokorny JL, Cen L, et al. Inhibition of histone deacetylation potentiates the evolution of acquired temozolomide resistance linked to MGMT upregulation in glioblastoma xenografts. Clinical Cancer Research. 2012;18(15):4070-9.

133. Banelli B, Carra E, Barbieri F, Wurth R, Parodi F, Pattarozzi A, et al. The histone demethylase KDM5A is a key factor for the resistance to temozolomide in glioblastoma. Cell Cycle. 2015;14(21):3418-29.

134. Liau BB, Sievers C, Donohue LK, Gillespie SM, Flavahan WA, Miller TE, et al. Adaptive Chromatin Remodeling Drives Glioblastoma Stem Cell Plasticity and Drug Tolerance. Cell Stem Cell. 2017;20(2):233-46.e7.

135. Gottesman MM, Fojo T, Bates SE. Multidrug resistance in cancer: role of ATP-dependent transporters. Nat Rev Cancer. 2002;2(1):48-58.

136. Vasiliou V, Vasiliou K, Nebert DW. Human ATP-binding cassette (ABC) transporter family. Hum Genomics. 2009;3(3):281-90.

137. Munoz JL, Walker ND, Scotto KW, Rameshwar P. Temozolomide competes for P-glycoprotein and contributes to chemoresistance in glioblastoma cells. Cancer Letters. 2015;367(1):69-75.

138. Schaich M, Kestel L, Pfirrmann M, Robel K, Illmer T, Kramer M, et al. A MDR1 (ABCB1) gene single nucleotide polymorphism predicts outcome of temozolomide treatment in glioblastoma patients. Ann Oncol. 2009;20(1):175-81.

139. Emery IF, Gopalan A, Wood S, Chow KH, Battelli C, George J, et al. Expression and function of ABCG2 and XIAP in glioblastomas. J Neurooncol. 2017;133(1):47-57.

140. Agarwal S, Manchanda P, Vogelbaum MA, Ohlfest JR, Elmquist WF. Function of the blood-brain barrier and restriction of drug delivery to invasive glioma cells: findings in an orthotopic rat xenograft model of glioma. Drug Metab Dispos. 2013;41(1):33-9.

141. Hombach-Klonisch S, Mehrpour M, Shojaei S, Harlos C, Pitz M, Hamai A, et al. Glioblastoma and chemoresistance to alkylating agents: Involvement of apoptosis, autophagy, and unfolded protein response. Pharmacology & Therapeutics. 2018;184:13-41.

142. Strik H, Deininger M, Streffer J, Grote E, Wickboldt J, Dichgans J, et al. BCL-2 family protein expression in initial and recurrent glioblastomas: modulation by radiochemotherapy. J Neurol Neurosurg Psychiatry. 1999;67(6):763-8.

143. Codogno P, Meijer AJ. Autophagy and signaling: their role in cell survival and cell death. Cell Death Differ. 2005;12 Suppl 2:1509-18.

144. Kanzawa T, Germano IM, Komata T, Ito H, Kondo Y, Kondo S. Role of autophagy in temozolomide-induced cytotoxicity for malignant glioma cells. Cell Death Differ. 2004;11(4):448-57.

145. Carmo A, Carvalheiro H, Crespo I, Nunes I, Lopes MC. Effect of temozolomide on the U-118 glioma cell line. Oncology letters. 2011;2(6):1165-70.

146. Knizhnik AV, Roos WP, Nikolova T, Quiros S, Tomaszowski KH, Christmann M, et al. Survival and death strategies in glioma cells: autophagy, senescence and apoptosis triggered by a single type of temozolomide-induced DNA damage. PLoS One. 2013;8(1):e55665.

147. Yan Y, Xu Z, Dai S, Qian L, Sun L, Gong Z. Targeting autophagy to sensitive glioma to temozolomide treatment. Journal of Experimental & Clinical Cancer Research. 2016;35(1):23.

148. Du Z, Lovly CM. Mechanisms of receptor tyrosine kinase activation in cancer. Molecular Cancer. 2018;17(1):58.

149. An Z, Aksoy O, Zheng T, Fan QW, Weiss WA. Epidermal growth factor receptor and EGFRvIII in glioblastoma: signaling pathways and targeted therapies. Oncogene. 2018;37(12):1561-75.

150. Taylor TE, Furnari FB, Cavenee WK. Targeting EGFR for treatment of glioblastoma: molecular basis to overcome resistance. Curr Cancer Drug Targets. 2012;12(3):197-209.

151. Nagane M, Levitzki A, Gazit A, Cavenee WK, Huang HJ. Drug resistance of human glioblastoma cells conferred by a tumor-specific mutant epidermal growth factor receptor through modulation of Bcl-XL and caspase-3-like proteases. Proc Natl Acad Sci U S A. 1998;95(10):5724-9.

152. Pang LY, Saunders L, Argyle DJ. Epidermal growth factor receptor activity is elevated in glioma cancer stem cells and is required to maintain chemotherapy and radiation resistance. Oncotarget. 2017;8(42):72494-512.

153. Westphal M, Maire CL, Lamszus K. EGFR as a Target for Glioblastoma Treatment: An Unfulfilled Promise. CNS Drugs. 2017;31(9):723-35.

154. Denduluri SK, Idowu O, Wang Z, Liao Z, Yan Z, Mohammed MK, et al. Insulin-like growth factor (IGF) signaling in tumorigenesis and the development of cancer drug resistance. Genes Dis. 2015;2(1):13-25.

155. Maris C, D'Haene N, Trepant AL, Le Mercier M, Sauvage S, Allard J, et al. IGF-IR: a new prognostic biomarker for human glioblastoma. Br J Cancer. 2015;113(5):729-37.

156. Li L, Wang Y, Peng T, Zhang K, Lin C, Han R, et al. Metformin restores crizotinib sensitivity in crizotinib-resistant human lung cancer cells through inhibition of IGF1-R signaling pathway. Oncotarget. 2016;7(23):34442-52.

157. Yang SH, Li S, Lu G, Xue H, Kim DH, Zhu J-J, et al. Metformin treatment reduces temozolomide resistance of glioblastoma cells. Oncotarget. 2016;7(48):78787-803.

158. Sesen J, Dahan P, Scotland SJ, Saland E, Dang VT, Lemarie A, et al. Metformin inhibits growth of human glioblastoma cells and enhances therapeutic response. PLoS One. 2015;10(4):e0123721.

159. Jawhari S, Ratinaud MH, Verdier M. Glioblastoma, hypoxia and autophagy: a survival-prone 'menage-a-trois'. Cell Death Dis. 2016;7(10):e2434.

160. Brown JM. Tumor microenvironment and the response to anticancer therapy. Cancer Biol Ther. 2002;1(5):453-8.

161. Womeldorff M, Gillespie D, Jensen RL. Hypoxia-inducible factor-1 and associated upstream and downstream proteins in the pathophysiology and management of glioblastoma. Neurosurg Focus. 2014;37(6):E8.

162. Chen C, Pore N, Behrooz A, Ismail-Beigi F, Maity A. Regulation of glut1 mRNA by hypoxia-inducible factor-1. Interaction between H-ras and hypoxia. J Biol Chem. 2001;276(12):9519-25.

163. Han JE, Lim PW, Na CM, Choi YS, Lee JY, Kim Y, et al. Inhibition of HIF1α and PDK Induces Cell Death of Glioblastoma Multiforme. Experimental neurobiology. 2017;26(5):295-306.

164. Ben-Yosef Y, Lahat N, Shapiro S, Bitterman H, Miller A. Regulation of endothelial matrix metalloproteinase-2 by hypoxia/reoxygenation. Circ Res. 2002;90(7):784-91.

165. Abdul Rahim SA, Dirkse A, Oudin A, Schuster A, Bohler J, Barthelemy V, et al. Regulation of hypoxia-induced autophagy in glioblastoma involves ATG9A. Br J Cancer. 2017;117(6):813-25.

166. Colwell N, Larion M, Giles AJ, Seldomridge AN, Sizdahkhani S, Gilbert MR, et al. Hypoxia in the glioblastoma microenvironment: shaping the phenotype of cancer stem-like cells. Neuro Oncol. 2017;19(7):887-96.

167. Heddleston JM, Li Z, McLendon RE, Hjelmeland AB, Rich JN. The hypoxic microenvironment maintains glioblastoma stem cells and promotes reprogramming towards a cancer stem cell phenotype. Cell cycle (Georgetown, Tex). 2009;8(20):3274-84.

168. Lo Dico A, Martelli C, Diceglie C, Lucignani G, Ottobrini L. Hypoxia-Inducible Factor-1α Activity as a Switch for Glioblastoma Responsiveness to Temozolomide. Frontiers in oncology. 2018;8:249-.

169. Chen WL, Wang CC, Lin YJ, Wu CP, Hsieh CH. Cycling hypoxia induces chemoresistance through the activation of reactive oxygen species-mediated B-cell lymphoma extra-long pathway in glioblastoma multiforme. J Transl Med. 2015;13:389.

170. Hsieh CH, Lin YJ, Wu CP, Lee HT, Shyu WC, Wang CC. Livin contributes to tumor hypoxia-induced resistance to cytotoxic therapies in glioblastoma multiforme. Clinical Cancer Research. 2015;21(2):460-70.

171. Chou CW, Wang CC, Wu CP, Lin YJ, Lee YC, Cheng YW, et al. Tumor cycling hypoxia induces chemoresistance in glioblastoma multiforme by upregulating the expression and function of ABCB1. Neuro Oncol. 2012;14(10):1227-38.

172. Tang JH, Ma ZX, Huang GH, Xu QF, Xiang Y, Li N, et al. Downregulation of HIF-1a sensitizes U251 glioma cells to the temozolomide (TMZ) treatment. Exp Cell Res. 2016;343(2):148-58.

173. Persano L, Pistollato F, Rampazzo E, Della Puppa A, Abbadi S, Frasson C, et al. BMP2 sensitizes glioblastoma stem-like cells to Temozolomide by affecting HIF-1alpha stability and MGMT expression. Cell Death Dis. 2012;3:e412.

174. Dirks PB. Brain tumour stem cells: the undercurrents of human brain cancer and their relationship to neural stem cells. Philos Trans R Soc Lond B Biol Sci. 2008;363(1489):139-52.

175. Singh SK, Clarke ID, Terasaki M, Bonn VE, Hawkins C, Squire J, et al. Identification of a cancer stem cell in human brain tumors. Cancer Res. 2003;63(18):5821-8.

176. Bleau AM, Huse JT, Holland EC. The ABCG2 resistance network of glioblastoma. Cell Cycle. 2009;8(18):2936-44.

177. Bao S, Wu Q, McLendon RE, Hao Y, Shi Q, Hjelmeland AB, et al. Glioma stem cells promote radioresistance by preferential activation of the DNA damage response. Nature. 2006;444(7120):756-60.

178. Murat A, Migliavacca E, Gorlia T, Lambiv WL, Shay T, Hamou MF, et al. Stem cell-related "self-renewal" signature and high epidermal growth factor receptor expression associated with resistance to concomitant chemoradiotherapy in glioblastoma. J Clin Oncol. 2008;26(18):3015-24.

179. Liu G, Yuan X, Zeng Z, Tunici P, Ng H, Abdulkadir IR, et al. Analysis of gene expression and chemoresistance of CD133+ cancer stem cells in glioblastoma. Mol Cancer. 2006;5:67.

180. Aponte PM, Caicedo A. Stemness in Cancer: Stem Cells, Cancer Stem Cells, and Their Microenvironment. Stem Cells Int. 2017;2017:5619472.

181. Melton D. Chapter 2 - 'Stemness': Definitions, Criteria, and Standards. In: Lanza R, Atala A, editors. Essentials of Stem Cell Biology (Third Edition). Boston: Academic Press; 2014. p. 7-17.

182. Zhou BB, Zhang H, Damelin M, Geles KG, Grindley JC, Dirks PB. Tumour-initiating cells: challenges and opportunities for anticancer drug discovery. Nat Rev Drug Discov. 2009;8(10):806-23.

183. Nowell P. The clonal evolution of tumor cell populations. Science. 1976;194(4260):23-8.

184. Greaves M, Maley CC. Clonal evolution in cancer. Nature. 2012;481:306.

185. Tan BT, Park CY, Ailles LE, Weissman IL. The cancer stem cell hypothesis: a work in progress. Lab Invest. 2006;86(12):1203-7.

186. Bradshaw A, Wickremsekera A, Tan ST, Peng L, Davis PF, Itinteang T. Cancer Stem Cell Hierarchy in Glioblastoma Multiforme. Frontiers in surgery. 2016;3:21-.

187. Valent P, Bonnet D, De Maria R, Lapidot T, Copland M, Melo JV, et al. Cancer stem cell definitions and terminology: the devil is in the details. Nature Reviews Cancer. 2012;12:767.

188. Lapidot T, Sirard C, Vormoor J, Murdoch B, Hoang T, Caceres-Cortes J, et al. A cell initiating human acute myeloid leukaemia after transplantation into SCID mice. Nature. 1994;367(6464):645-8.

189. Al-Hajj M, Wicha MS, Benito-Hernandez A, Morrison SJ, Clarke MF. Prospective identification of tumorigenic breast cancer cells. Proc Natl Acad Sci U S A. 2003;100(7):3983-8.

190. Collins AT, Berry PA, Hyde C, Stower MJ, Maitland NJ. Prospective identification of tumorigenic prostate cancer stem cells. Cancer Res. 2005;65(23):10946-51.

191. O'Brien CA, Pollett A, Gallinger S, Dick JE. A human colon cancer cell capable of initiating tumour growth in immunodeficient mice. Nature. 2007;445(7123):106-10.

192. Eramo A, Lotti F, Sette G, Pilozzi E, Biffoni M, Di Virgilio A, et al. Identification and expansion of the tumorigenic lung cancer stem cell population. Cell Death Differ. 2008;15(3):504-14.

193. Vescovi AL, Galli R, Reynolds BA. Brain tumour stem cells. Nat Rev Cancer. 2006;6(6):425-36.

194. Das S, Srikanth M, Kessler JA. Cancer stem cells and glioma. Nat Clin Pract Neurol. 2008;4(8):427-35.

195. Chen J, Li Y, Yu T-S, McKay RM, Burns DK, Kernie SG, et al. A restricted cell population propagates glioblastoma growth after chemotherapy. Nature. 2012;488(7412):522-6.

196. Eramo A, Ricci-Vitiani L, Zeuner A, Pallini R, Lotti F, Sette G, et al. Chemotherapy resistance of glioblastoma stem cells. Cell Death Differ. 2006;13(7):1238-41.

197. Gilbert CA, Daou MC, Moser RP, Ross AH. Gamma-secretase inhibitors enhance temozolomide treatment of human gliomas by inhibiting neurosphere repopulation and xenograft recurrence. Cancer Res. 2010;70(17):6870-9.

198. Yan K, Wu Q, Yan DH, Lee CH, Rahim N, Tritschler I, et al. Glioma cancer stem cells secrete Gremlin1 to promote their maintenance within the tumor hierarchy. Genes Dev. 2014;28(10):1085-100.

199. Rinkenbaugh AL, Cogswell PC, Calamini B, Dunn DE, Persson AI, Weiss WA, et al. IKK/NF-kappaB signaling contributes to glioblastoma stem cell maintenance. Oncotarget. 2016;7(43):69173-87.

200. Rheinbay E, Suva ML, Gillespie SM, Wakimoto H, Patel AP, Shahid M, et al. An aberrant transcription factor network essential for Wnt signaling and stem cell maintenance in glioblastoma. Cell Rep. 2013;3(5):1567-79.

201. Gilbertson RJ, Rich JN. Making a tumour's bed: glioblastoma stem cells and the vascular niche. Nat Rev Cancer. 2007;7(10):733-6.

202. Hovinga KE, Shimizu F, Wang R, Panagiotakos G, Van Der Heijden M, Moayedpardazi H, et al. Inhibition of notch signaling in glioblastoma targets cancer stem cells via an endothelial cell intermediate. Stem cells (Dayton, Ohio). 2010;28(6):1019-29.

203. Artavanis-Tsakonas S, Rand MD, Lake RJ. Notch signaling: cell fate control and signal integration in development. Science. 1999;284(5415):770-6.

204. Morgan TH, Bridges CB. Sex-linked inheritance in Drosophila: Carnegie institution of Washington; 1916.

205. Ellisen LW, Bird J, West DC, Soreng AL, Reynolds TC, Smith SD, et al. TAN-1, the human homolog of the Drosophila notch gene, is broken by chromosomal translocations in T lymphoblastic neoplasms. Cell. 1991;66(4):649-61.

206. Rana NA, Haltiwanger RS. Fringe benefits: functional and structural impacts of O-glycosylation on the extracellular domain of Notch receptors. Current Opinion in Structural Biology. 2011;21(5):583-9.

207. Bray SJ. Notch signalling: a simple pathway becomes complex. Nature Reviews Molecular Cell Biology. 2006;7(9):678-89.

208. Kopan R, Ilagan MX. The canonical Notch signaling pathway: unfolding the activation mechanism. Cell. 2009;137(2):216-33.

209. Hori K, Sen A, Artavanis-Tsakonas S. Notch signaling at a glance. Journal of Cell Science. 2013;126(10):2135-40.

210. Gordon WR, Arnett KL, Blacklow SC. The molecular logic of Notch signaling–a structural and biochemical perspective. Journal of Cell Science. 2008;121(19):3109-19.

211. D'Souza B, Meloty-Kapella L, Weinmaster G. Canonical and non-canonical Notch ligands. Current Topics in Developmental Biology. 2010;92:73-129.

212. D'Souza B, Miyamoto A, Weinmaster G. The many facets of Notch ligands. Oncogene. 2008;27(38):5148-67.

213. del Alamo D, Rouault H, Schweisguth F. Mechanism and significance of cis-inhibition in Notch signalling. Curr Biol. 2011;21(1):R40-7.

214. LeBon L, Lee TV, Sprinzak D, Jafar-Nejad H, Elowitz MB. Fringe proteins modulate Notch-ligand cis and trans interactions to specify signaling states. Elife. 2014;3:e02950.

215. Logeat F, Bessia C, Brou C, LeBail O, Jarriault S, Seidah NG, et al. The Notch1 receptor is cleaved constitutively by a furin-like convertase. Proc Natl Acad Sci U S A. 1998;95(14):8108-12.

216. Selkoe DJ, Wolfe MS. Presenilin: running with scissors in the membrane. Cell. 2007;131(2):215-21.

217. Kopan R. Notch signaling. Cold Spring Harb Perspect Biol. 2012;4(10).

218. Imayoshi I, Sakamoto M, Yamaguchi M, Mori K, Kageyama R. Essential roles of Notch signaling in maintenance of neural stem cells in developing and adult brains. J Neurosci. 2010;30(9):3489-98.

219. Basak O, Giachino C, Fiorini E, Macdonald HR, Taylor V. Neurogenic subventricular zone stem/progenitor cells are Notch1-dependent in their active but not quiescent state. J Neurosci. 2012;32(16):5654-66.

220. Lugert S, Basak O, Knuckles P, Haussler U, Fabel K, Gotz M, et al. Quiescent and active hippocampal neural stem cells with distinct morphologies respond selectively to physiological and pathological stimuli and aging. Cell Stem Cell. 2010;6(5):445-56.

221. Bazzoni R, Bentivegna A. Role of Notch Signaling Pathway in Glioblastoma Pathogenesis. Cancers. 2019;11(3):292.

222. Ables JL, Breunig JJ, Eisch AJ, Rakic P. Not(ch) just development: Notch signalling in the adult brain. Nature reviews Neuroscience. 2011;12(5):269-83.

223. Borghese L, Dolezalova D, Opitz T, Haupt S, Leinhaas A, Steinfarz B, et al. Inhibition of notch signaling in human embryonic stem cell-derived neural stem cells delays G1/S phase transition and accelerates neuronal differentiation in vitro and in vivo. Stem Cells. 2010;28(5):955-64.

224. Guentchev M, McKay RD. Notch controls proliferation and differentiation of stem cells in a dose-dependent manner. Eur J Neurosci. 2006;23(9):2289-96.

225. Boareto M, Iber D, Taylor V. Differential interactions between Notch and ID factors control neurogenesis by modulating Hes factor autoregulation. Development. 2017;144(19):3465-74.

226. Engler A, Rolando C, Giachino C, Saotome I, Erni A, Brien C, et al. Notch2 Signaling Maintains NSC Quiescence in the Murine Ventricular-Subventricular Zone. Cell Rep. 2018;22(4):992-1002.

227. Than-Trong E, Ortica-Gatti S, Mella S, Nepal C, Alunni A, Bally-Cuif L. Neural stem cell quiescence and stemness are molecularly distinct outputs of the Notch3 signalling cascade in the vertebrate adult brain. Development. 2018;145(10).

228. Faigle R, Song H. Signaling mechanisms regulating adult neural stem cells and neurogenesis. Biochim Biophys Acta. 2013;1830(2):2435-48.

229. Beatus P, Lendahl U. Notch and neurogenesis. Journal of neuroscience research. 1998;54(2):125-36.

230. Lasky JL, Wu H. Notch signaling, brain development, and human disease. Pediatr Res. 2005;57(5 Pt 2):104r-9r.

231. Henrique D, Hirsinger E, Adam J, Le Roux I, Pourquie O, Ish-Horowicz D, et al. Maintenance of neuroepithelial progenitor cells by Delta-Notch signalling in the embryonic chick retina. Curr Biol. 1997;7(9):661-70.

232. Dorsky RI, Chang WS, Rapaport DH, Harris WA. Regulation of neuronal diversity in the Xenopus retina by Delta signalling. Nature. 1997;385(6611):67-70.

233. Wang S, Sdrulla AD, diSibio G, Bush G, Nofziger D, Hicks C, et al. Notch receptor activation inhibits oligodendrocyte differentiation. Neuron. 1998;21(1):63-75.

234. de la Pompa JL, Wakeham A, Correia KM, Samper E, Brown S, Aguilera RJ, et al. Conservation of the Notch signalling pathway in mammalian neurogenesis. Development. 1997;124(6):1139-48.

235. Swiatek PJ, Lindsell CE, del Amo FF, Weinmaster G, Gridley T. Notch1 is essential for postimplantation development in mice. Genes Dev. 1994;8(6):707-19.

236. Weng AP, Ferrando AA, Lee W, Morris JPt, Silverman LB, Sanchez-Irizarry C, et al. Activating mutations of NOTCH1 in human T cell acute lymphoblastic leukemia. Science. 2004;306(5694):269-71.

237. Ntziachristos P, Lim JS, Sage J, Aifantis I. From fly wings to targeted cancer therapies: a centennial for notch signaling. Cancer Cell. 2014;25(3):318-34.

238. Kanamori M, Kawaguchi T, Nigro JM, Feuerstein BG, Berger MS, Miele L, et al. Contribution of Notch signaling activation to human glioblastoma multiforme. J Neurosurg. 2007;106(3):417-27.

239. Hulleman E, Quarto M, Vernell R, Masserdotti G, Colli E, Kros JM, et al. A role for the transcription factor HEY1 in glioblastoma. J Cell Mol Med. 2009;13(1):136-46.

240. El Hindy N, Keyvani K, Pagenstecher A, Dammann P, Sandalcioglu IE, Sure U, et al. Implications of Dll4-Notch signaling activation in primary glioblastoma multiforme. Neuro Oncol. 2013;15(10):1366-78.

241. Li J, Cui Y, Gao G, Zhao Z, Zhang H, Wang X. Notch1 is an independent prognostic factor for patients with glioma. J Surg Oncol. 2011;103(8):813-7.

242. Hulleman E, Quarto M, Vernell R, Masserdotti G, Colli E, Kros JM, et al. A role for the transcription factor HEY1 in glioblastoma. Journal of cellular and molecular medicine. 2009;13(1):136-46.

243. Margareto J, Leis O, Larrarte E, Idoate MA, Carrasco A, Lafuente JV. Gene expression profiling of human gliomas reveals differences between GBM and LGA related to energy metabolism and notch signaling pathways. J Mol Neurosci. 2007;32(1):53-63.

244. Somasundaram K, Reddy SP, Vinnakota K, Britto R, Subbarayan M, Nambiar S, et al. Upregulation of ASCL1 and inhibition of Notch signaling pathway characterize progressive astrocytoma. Oncogene. 2005;24(47):7073-83.

245. Purow B. Notch inhibition as a promising new approach to cancer therapy. Adv Exp Med Biol. 2012;727:305-19.

246. Olsauskas-Kuprys R, Zlobin A, Osipo C. Gamma secretase inhibitors of Notch signaling. Onco Targets Ther. 2013;6:943-55.

247. Zhang X, Li Y, Xu H, Zhang Y-W. The γ-secretase complex: from structure to function. Frontiers in cellular neuroscience. 2014;8:427-.

248. Fortini ME. Gamma-secretase-mediated proteolysis in cell-surface-receptor signalling. Nat Rev Mol Cell Biol. 2002;3(9):673-84.

249. Haapasalo A, Kovacs DM. The many substrates of presenilin/γ-secretase. J Alzheimers Dis. 2011;25(1):3-28.

250. De Strooper B, Iwatsubo T, Wolfe MS. Presenilins and γ-secretase: structure, function, and role in Alzheimer Disease. Cold Spring Harb Perspect Med. 2012;2(1):a006304.

251. Huynh C, Poliseno L, Segura MF, Medicherla R, Haimovic A, Menendez S, et al. The novel gamma secretase inhibitor RO4929097 reduces the tumor initiating potential of melanoma. PLoS One. 2011;6(9):e25264.

252. Xu R, Shimizu F, Hovinga K, Beal K, Karimi S, Droms L, et al. Molecular and Clinical Effects of Notch Inhibition in Glioma Patients: A Phase 0/I Trial. Clinical Cancer Research. 2016;22(19):4786-96.

253. Luistro L, He W, Smith M, Packman K, Vilenchik M, Carvajal D, et al. Preclinical Profile of a Potent γ-Secretase Inhibitor Targeting Notch Signaling with In vivo Efficacy and Pharmacodynamic Properties. Cancer Research. 2009;69(19):7672-80.

254. Debeb BG, Cohen EN, Boley K, Freiter EM, Li L, Robertson FM, et al. Pre-clinical studies of Notch signaling inhibitor RO4929097 in inflammatory breast cancer cells. Breast Cancer Research and Treatment. 2012;134(2):495-510.

255. Yahyanejad S, King H, Iglesias VS, Granton PV, Barbeau LM, van Hoof SJ, et al. NOTCH blockade combined with radiation therapy and temozolomide prolongs survival of orthotopic glioblastoma. Oncotarget. 2016;7(27):41251-64.

256. Lee SM, Moon J, Redman BG, Chidiac T, Flaherty LE, Zha Y, et al. Phase 2 study of RO4929097, a gamma-secretase inhibitor, in metastatic melanoma: SWOG 0933. Cancer. 2015;121(3):432-40.

257. Peereboom DM, Rich JN, Supko JG, Lamborn K, Ye X, Sloan AE, et al. A phase II and pharmacodynamic trial of RO4929097 for patients with recurrent/progressive glioblastoma. Journal of Clinical Oncology. 2011;29(15_suppl):TPS135-TPS.

258. De Jesus-Acosta A, Laheru D, Maitra A, Arcaroli J, Rudek MA, Dasari A, et al. A phase II study of the gamma secretase inhibitor RO4929097 in patients with previously treated metastatic pancreatic adenocarcinoma. Investigational New Drugs. 2014;32(4):739-45.

259. Sahebjam S, Bedard PL, Castonguay V, Chen Z, Reedijk M, Liu G, et al. A phase I study of the combination of ro4929097 and cediranib in patients with advanced solid tumours (PJC-004/NCI 8503). British Journal of Cancer. 2013;109(4):943-9.

260. Richter S, Bedard PL, Chen EX, Clarke BA, Tran B, Hotte SJ, et al. A phase I study of the oral gamma secretase inhibitor R04929097 in combination with gemcitabine in patients with advanced solid tumors (PHL-078/CTEP 8575). Investigational New Drugs. 2014;32(2):243-9.

261. Diaz-Padilla I, Wilson MK, Clarke BA, Hirte HW, Welch SA, Mackay HJ, et al. A phase II study of single-agent RO4929097, a gamma-secretase inhibitor of Notch signaling, in patients with recurrent platinum-resistant epithelial ovarian cancer: A study of the Princess Margaret, Chicago and California phase II consortia. Gynecologic Oncology. 2015;137(2):216-22.

262. Pan E, Supko JG, Kaley TJ, Butowski NA, Cloughesy T, Jung J, et al. Phase I study of RO4929097 with bevacizumab in patients with recurrent malignant glioma. J Neurooncol. 2016;130(3):571-9.

263. Fleisher AS, Raman R, Siemers ER, Becerra L, Clark CM, Dean RA, et al. Phase 2 Safety Trial Targeting Amyloid β Production With a γ-Secretase Inhibitor in Alzheimer Disease. Archives of Neurology. 2008;65(8):1031-8.

264. Li J-L, Sainson RCA, Oon CE, Turley H, Leek R, Sheldon H, et al. DLL4-Notch Signaling Mediates Tumor Resistance to Anti-VEGF Therapy In Vivo. Cancer Research. 2011;71(18):6073-83.

265. Bender MH, Gao H, Capen AR, Clay JM, Hipskind PA, Reel JK, et al. Novel inhibitor of Notch signaling for the treatment of cancer. AACR; 2013.

266. Massard C, Azaro A, Soria JC, Lassen U, Le Tourneau C, Sarker D, et al. First-in-human study of LY3039478, an oral Notch signaling inhibitor in advanced or metastatic cancer. Ann Oncol. 2018;29(9):1911-7.

267. De Jesus-Acosta A, Laheru D, Maitra A, Arcaroli J, Rudek MA, Dasari A, et al. A phase II study of the gamma secretase inhibitor RO4929097 in patients with previously treated metastatic pancreatic adenocarcinoma. Invest New Drugs. 2014;32(4):739-45.

268. Massard C, Azaro A, Soria JC, Lassen U, Le Tourneau C, Sarker D, et al. First-in-human study of LY3039478, an oral Notch signaling inhibitor in advanced or metastatic cancer. Annals of Oncology. 2018;29(9):1911-7.

269. Johnson M, Rasco D, Schneider B, Shu C, Jotte R, Parmer H, et al. Abstract A081: A phase 1b, open-label, dose escalation and expansion study of demcizumab plus pembrolizumab in patients with locally advanced or metastatic solid tumors. Molecular Cancer Therapeutics. 2018;17(1 Supplement):A081-A.

270. Coleman RL, Handley KF, Burger R, Molin GZD, Stagg R, Sood AK, et al. Demcizumab combined with paclitaxel for platinum-resistant ovarian, primary peritoneal, and fallopian tube cancer: The SIERRA open-label phase Ib trial. Gynecologic Oncology. 2020;157(2):386-91.

271. Chiorean EG, LoRusso P, Strother RM, Diamond JR, Younger A, Messersmith WA, et al. A Phase I First-in-Human Study of Enoticumab (REGN421), a Fully Human Delta-like Ligand 4 (Dll4) Monoclonal Antibody in Patients with Advanced Solid Tumors. Clinical Cancer Research. 2015;21(12):2695-703.

272. Falchook GS, Dowlati A, Naing A, Gribbin MJ, Jenkins DW, Chang LL, et al. Phase I study of MEDI0639 in patients with advanced solid tumors. Journal of Clinical Oncology. 2015;33(15_suppl):3024-.

273. Ferrarotto R, Eckhardt G, Patnaik A, LoRusso P, Faoro L, Heymach JV, et al. A phase I dose-escalation and dose-expansion study of brontictuzumab in subjects with selected solid tumors. Annals of Oncology. 2018;29(7):1561-8.

274. Casulo C, Ruan J, Dang NH, Gore L, Diefenbach C, Beaven AW, et al. Safety and Preliminary Efficacy Results of a Phase I First-in-Human Study of the Novel Notch-1 Targeting Antibody Brontictuzumab (OMP-52M51) Administered Intravenously to Patients with Hematologic Malignancies. Blood. 2016;128(22):5108-.

275. Smith DC, Chugh R, Patnaik A, Papadopoulos KP, Wang M, Kapoun AM, et al. A phase 1 dose escalation and expansion study of Tarextumab (OMP-59R5) in patients with solid tumors. Investigational New Drugs. 2019;37(4):722-30.

276. Bendell J, Cohn AL, Smith L, Strickler JH, Gluck WL, Schmidt WG, et al. Final Results of a Phase 1B of Omp-59R5 (Anti-Notch2/3/Stem Cell Antibody) in Combination with Nab-Paclitaxel and Gemcitabine in Patients with Untreated Metastatic Pancreatic Cancer: Alpine Study. Annals of Oncology. 2014;25:iv233.

277. Hu ZI, Bendell JC, Bullock A, LoConte NK, Hatoum H, Ritch P, et al. A randomized phase II trial of nab-paclitaxel and gemcitabine with tarextumab or placebo in patients with untreated metastatic pancreatic cancer. Cancer Medicine. 2019;8(11):5148-57.

278. Garcia JMP, Cortés J, Stathis A, Mous R, López-Miranda E, Azaro A, et al. First-in-human phase 1-2A study of CB-103, an oral Protein-Protein Interaction Inhibitor

targeting pan-NOTCH signalling in advanced solid tumors and blood malignancies. Journal of Clinical Oncology. 2018;36(15_suppl):TPS2619-TPS.

279. Jia X, Wang W, Xu Z, Wang S, Wang T, Wang M, et al. A humanized anti-DLL4 antibody promotes dysfunctional angiogenesis and inhibits breast tumor growth. Scientific Reports. 2016;6(1):27985.

280. Miles KM, Seshadri M, Ciamporcero E, Adelaiye R, Gillard B, Sotomayor P, et al. Dll4 blockade potentiates the anti-tumor effects of VEGF inhibition in renal cell carcinoma patient-derived xenografts. PloS one. 2014;9(11):e112371.

281. Davis SL, LoRusso P, Xu L, Kapoun AM, Dupont J, Munster P, et al. Abstract B48: A first-in-human Phase I study of the novel cancer stem cell (CSC) targeting antibody OMP-52M51 (anti-Notch1) administered intravenously to patients with certain advanced solid tumors. Molecular Cancer Therapeutics. 2013;12(11 Supplement):B48-B.

282. Agnusdei V, Minuzzo S, Frasson C, Grassi A, Axelrod F, Satyal S, et al. Therapeutic antibody targeting of Notch1 in T-acute lymphoblastic leukemia xenografts. Leukemia. 2014;28(2):278-88.

283. Silkenstedt E, Arenas F, Colom-Sanmartí B, Xargay-Torrent S, Higashi M, Giró A, et al. Notch1 signaling in NOTCH1-mutated mantle cell lymphoma depends on Delta-Like ligand 4 and is a potential target for specific antibody therapy. Journal of Experimental & Clinical Cancer Research. 2019;38(1):446.

284. Yen WC, Fischer MM, Axelrod F, Bond C, Cain J, Cancilla B, et al. Targeting Notch signaling with a Notch2/Notch3 antagonist (tarextumab) inhibits tumor growth and decreases tumor-initiating cell frequency. Clinical Cancer Research. 2015;21(9):2084-95.

285. Moellering RE, Cornejo M, Davis TN, Del Bianco C, Aster JC, Blacklow SC, et al. Direct inhibition of the NOTCH transcription factor complex. Nature. 2009;462(7270):182-8.

286. KleinJan A, Tindemans I, Montgomery JE, Lukkes M, de Bruijn MJW, van Nimwegen M, et al. The Notch pathway inhibitor stapled alpha-helical peptide derived from mastermind-like 1 (SAHM1) abrogates the hallmarks of allergic asthma. Journal of Allergy and Clinical Immunology. 2018;142(1):76-85.e8.

287. González S, Uhm H, Deng SX. Notch Inhibition Prevents Differentiation of Human Limbal Stem/Progenitor Cells in vitro. Scientific Reports. 2019;9(1):10373.

288. Astudillo L, Da Silva TG, Wang Z, Han X, Jin K, VanWye J, et al. The Small Molecule IMR-1 Inhibits the Notch Transcriptional Activation Complex to Suppress Tumorigenesis. Cancer Res. 2016;76(12):3593-603.

289. Weber D, Lehal R, Frismantas V, Bourquin JP, Bauer M, Murone M, et al. Pharmacological activity of CB-103: An oral pan-NOTCH inhibitor with a novel mode of action. Annals of Oncology. 2017;28:v137.

290. Weber D, Lehal R, Frismantas V, Bourquin J, Bauer M, Murone M, et al. PHARMACOLOGICAL ACTIVITY OF CB-103 IN HAEMATOLOGICAL MALIGNANCIES – AN ORAL PAN-NOTCH INHIBITOR WITH A NOVEL MODE OF ACTION. Hematological Oncology. 2017;35(S2):46-.

291. Ma DK, Bonaguidi MA, Ming G-L, Song H. Adult neural stem cells in the mammalian central nervous system. Cell research. 2009;19(6):672-82.

292. Zhu Y, Guignard F, Zhao D, Liu L, Burns DK, Mason RP, et al. Early inactivation of p53 tumor suppressor gene cooperating with NF1 loss induces malignant astrocytoma. Cancer Cell. 2005;8(2):119-30.

293. Zheng H, Ying H, Yan H, Kimmelman AC, Hiller DJ, Chen AJ, et al. p53 and Pten control neural and glioma stem/progenitor cell renewal and differentiation. Nature. 2008;455(7216):1129-33.

294. Takebe N, Miele L, Harris PJ, Jeong W, Bando H, Kahn M, et al. Targeting Notch, Hedgehog, and Wnt pathways in cancer stem cells: clinical update. Nature reviews Clinical oncology. 2015;12(8):445-64.

295. Yoon K, Gaiano N. Notch signaling in the mammalian central nervous system: insights from mouse mutants. Nat Neurosci. 2005;8(6):709-15.

296. Pierfelice TJ, Schreck KC, Eberhart CG, Gaiano N. Notch, neural stem cells, and brain tumors. Cold Spring Harbor symposia on quantitative biology. 2008;73:367-75.

297. Androutsellis-Theotokis A, Leker RR, Soldner F, Hoeppner DJ, Ravin R, Poser SW, et al. Notch signalling regulates stem cell numbers in vitro and in vivo. Nature. 2006;442(7104):823-6.

298. Stump G, Durrer A, Klein AL, Lutolf S, Suter U, Taylor V. Notch1 and its ligands Delta-like and Jagged are expressed and active in distinct cell populations in the postnatal mouse brain. Mech Dev. 2002;114(1-2):153-9.

299. Lee J, Kotliarova S, Kotliarov Y, Li A, Su Q, Donin NM, et al. Tumor stem cells derived from glioblastomas cultured in bFGF and EGF more closely mirror the phenotype and genotype of primary tumors than do serum-cultured cell lines. Cancer Cell. 2006;9(5):391-403.

300. Zhang XP, Zheng G, Zou L, Liu HL, Hou LH, Zhou P, et al. Notch activation promotes cell proliferation and the formation of neural stem cell-like colonies in human glioma cells. Mol Cell Biochem. 2008;307(1-2):101-8.

301. Xie Q, Mittal S, Berens ME. Targeting adaptive glioblastoma: an overview of proliferation and invasion. Neuro Oncol. 2014;16(12):1575-84.

302. Lytle NK, Barber AG, Reya T. Stem cell fate in cancer growth, progression and therapy resistance. Nat Rev Cancer. 2018;18(11):669-80.

303. Zhu TS, Costello MA, Talsma CE, Flack CG, Crowley JG, Hamm LL, et al. Endothelial cells create a stem cell niche in glioblastoma by providing NOTCH ligands that nurture self-renewal of cancer stem-like cells. Cancer Res. 2011;71(18):6061-72.

304. Chu Q, Orr BA, Semenkow S, Bar EE, Eberhart CG. Prolonged inhibition of glioblastoma xenograft initiation and clonogenic growth following in vivo Notch blockade. Clinical Cancer Research. 2013;19(12):3224-33.

305. Krop I, Demuth T, Guthrie T, Wen PY, Mason WP, Chinnaiyan P, et al. Phase I Pharmacologic and Pharmacodynamic Study of the Gamma Secretase (Notch) Inhibitor MK-0752 in Adult Patients With Advanced Solid Tumors. Journal of Clinical Oncology. 2012;30(19):2307-13.

306. Oon CE, Bridges E, Sheldon H, Sainson RCA, Jubb A, Turley H, et al. Role of Delta-like 4 in Jagged1-induced tumour angiogenesis and tumour growth. Oncotarget. 2017;8(25):40115-31.

307. Jubb AM, Browning L, Campo L, Turley H, Steers G, Thurston G, et al. Expression of vascular Notch ligands Delta-like 4 and Jagged-1 in glioblastoma. Histopathology. 2012;60(5):740-7.

308. Qiu XX, Wang CH, Lin ZX, You N, Wang XF, Chen YP, et al. Correlation of high delta-like ligand 4 expression with peritumoral brain edema and its prediction of poor prognosis in patients with primary high-grade gliomas. J Neurosurg. 2015;123(6):1578-85.

309. Qiu XX, Wang CH, You N, Chen BJ, Wang XF, Chen YP, et al. High Jagged1 expression is associated with poor outcome in primary glioblastoma. Med Oncol. 2015;32(1):341.

310. Jeon HM, Kim SH, Jin X, Park JB, Kim SH, Joshi K, et al. Crosstalk between glioma-initiating cells and endothelial cells drives tumor progression. Cancer Res. 2014;74(16):4482-92.

311. Qiang L, Wu T, Zhang HW, Lu N, Hu R, Wang YJ, et al. HIF-1α is critical for hypoxia-mediated maintenance of glioblastoma stem cells by activating Notch signaling pathway. Cell Death & Differentiation. 2012;19(2):284-94.

312. Gil-Ranedo J, Mendiburu-Eliçabe M, García-Villanueva M, Medina D, del Álamo M, Izquierdo M. An Off-Target Nucleostemin RNAi Inhibits Growth in Human Glioblastoma-Derived Cancer Stem Cells. PLOS ONE. 2011;6(12):e28753.

313. Hirschhaeuser F, Menne H, Dittfeld C, West J, Mueller-Klieser W, Kunz-Schughart LA. Multicellular tumor spheroids: an underestimated tool is catching up again. J Biotechnol. 2010;148(1):3-15.

314. Reynolds BA, Weiss S. Generation of neurons and astrocytes from isolated cells of the adult mammalian central nervous system. Science. 1992;255(5052):1707-10.

315. Ernst A, Hofmann S, Ahmadi R, Becker N, Korshunov A, Engel F, et al. Genomic and expression profiling of glioblastoma stem cell-like spheroid cultures identifies

novel tumor-relevant genes associated with survival. Clinical Cancer Research. 2009;15(21):6541-50.

316. Williams CK, Li J-L, Murga M, Harris AL, Tosato G. Up-regulation of the Notch ligand Delta-like 4 inhibits VEGF-induced endothelial cell function. Blood. 2006;107(3):931-9.

317. Graham FL, Smiley J, Russell WC, Nairn R. Characteristics of a human cell line transformed by DNA from human adenovirus type 5. J Gen Virol. 1977;36(1):59-74.

318. DuBridge RB, Tang P, Hsia HC, Leong PM, Miller JH, Calos MP. Analysis of mutation in human cells by using an Epstein-Barr virus shuttle system. Mol Cell Biol. 1987;7(1):379-87.

319. Pear WS, Nolan GP, Scott ML, Baltimore D. Production of high-titer helper-free retroviruses by transient transfection. Proc Natl Acad Sci U S A. 1993;90(18):8392-6.

320. Swift S, Lorens J, Achacoso P, Nolan GP. Rapid Production of Retroviruses for Efficient Gene Delivery to Mammalian Cells Using 293T Cell–Based Systems. Current Protocols in Immunology. 1999;31(1):10.7.4-.7.29.

321. Moore CB, Guthrie EH, Huang MT, Taxman DJ. Short hairpin RNA (shRNA): design, delivery, and assessment of gene knockdown. Methods in Molecular Biology. 2010;629:141-58.

322. Gallego O. Nonsurgical treatment of recurrent glioblastoma. Current Oncology. 2015;22(4):e273-81.

323. Franceschi E, Lamberti G, Visani M, Paccapelo A, Mura A, Tallini G, et al. Temozolomide rechallenge in recurrent glioblastoma: when is it useful? Future Oncology. 2018;14(11):1063-9.

324. Roos WP, Batista LF, Naumann SC, Wick W, Weller M, Menck CF, et al. Apoptosis in malignant glioma cells triggered by the temozolomide-induced DNA lesion O6-methylguanine. Oncogene. 2007;26(2):186-97.

325. Woo P, Li Y, Chan A, Ng S, Loong H, Chan D, et al. A multifaceted review of temozolomide resistance mechanisms in glioblastoma beyond O-6-methylguanine-DNA methyltransferase. Glioma. 2019;2(2):68-82.

326. Aguirre A, Rubio ME, Gallo V. Notch and EGFR pathway interaction regulates neural stem cell number and self-renewal. Nature. 2010;467(7313):323-7.

327. Ranganathan P, Weaver KL, Capobianco AJ. Notch signalling in solid tumours: a little bit of everything but not all the time. Nat Rev Cancer. 2011;11(5):338-51.

328. Hanahan D, Weinberg Robert A. Hallmarks of Cancer: The Next Generation. Cell. 2011;144(5):646-74.

329. Milano J, McKay J, Dagenais C, Foster-Brown L, Pognan F, Gadient R, et al. Modulation of notch processing by gamma-secretase inhibitors causes intestinal goblet

cell metaplasia and induction of genes known to specify gut secretory lineage differentiation. Toxicol Sci. 2004;82(1):341-58.

330. Pai P, Rachagani S, Dhawan P, Sheinin YM, Macha MA, Qazi AK, et al. MUC4 is negatively regulated through the Wnt/β-catenin pathway via the Notch effector Hath1 in colorectal cancer. Genes Cancer. 2016;7(5-6):154-68.

331. Benedito R, Roca C, Sorensen I, Adams S, Gossler A, Fruttiger M, et al. The notch ligands Dll4 and Jagged1 have opposing effects on angiogenesis. Cell. 2009;137(6):1124-35.

332. Li JL, Harris AL. Crosstalk of VEGF and Notch pathways in tumour angiogenesis: therapeutic implications. Front Biosci (Landmark Ed). 2009;14:3094-110.

333. Benhra N, Vignaux F, Dussert A, Schweisguth F, Le Borgne R. Neuralized promotes basal to apical transcytosis of delta in epithelial cells. Mol Biol Cell. 2010;21(12):2078-86.

334. Couturier L, Vodovar N, Schweisguth F. Endocytosis by Numb breaks Notch symmetry at cytokinesis. Nat Cell Biol. 2012;14(2):131-9.

335. Cohen M, Georgiou M, Stevenson NL, Miodownik M, Baum B. Dynamic filopodia transmit intermittent Delta-Notch signaling to drive pattern refinement during lateral inhibition. Developmental Cell. 2010;19(1):78-89.

336. Huang H, Kornberg TB. Myoblast cytonemes mediate Wg signaling from the wing imaginal disc and Delta-Notch signaling to the air sac primordium. Elife. 2015;4:e06114.

337. Shaya O, Binshtok U, Hersch M, Rivkin D, Weinreb S, Amir-Zilberstein L, et al. Cell-Cell Contact Area Affects Notch Signaling and Notch-Dependent Patterning. Developmental Cell. 2017;40(5):505-11.e6.

338. Artavanis-Tsakonas S, Rand MD, Lake RJ. Notch signaling: cell fate control and signal integration in development. Science. 1999;284(5415):770-6.

339. Minchinton AI, Tannock IF. Drug penetration in solid tumours. Nat Rev Cancer. 2006;6(8):583-92.

340. Haas B, Klinger V, Keksel C, Bonigut V, Kiefer D, Caspers J, et al. Inhibition of the PI3K but not the MEK/ERK pathway sensitizes human glioma cells to alkylating drugs. Cancer Cell Int. 2018;18:69.

341. Kanzawa T, Germano IM, Kondo Y, Ito H, Kyo S, Kondo S. Inhibition of telomerase activity in malignant glioma cells correlates with their sensitivity to temozolomide. Br J Cancer. 2003;89(5):922-9.

342. Towner RA, Smith N, Saunders D, Brown CA, Cai X, Ziegler J, et al. OKN-007 Increases temozolomide (TMZ) Sensitivity and Suppresses TMZ-Resistant Glioblastoma (GBM) Tumor Growth. Transl Oncol. 2019;12(2):320-35.

343. Nunes AS, Barros AS, Costa EC, Moreira AF, Correia IJ. 3D tumor spheroids as in vitro models to mimic in vivo human solid tumors resistance to therapeutic drugs. Biotechnology and Bioengineering. 2019;116(1):206-26.

344. Molenaar RJ, Verbaan D, Lamba S, Zanon C, Jeuken JW, Boots-Sprenger SH, et al. The combination of IDH1 mutations and MGMT methylation status predicts survival in glioblastoma better than either IDH1 or MGMT alone. Neuro Oncol. 2014;16(9):1263-73.

345. Hiddingh L, Tannous BA, Teng J, Tops B, Jeuken J, Hulleman E, et al. EFEMP1 induces gamma-secretase/Notch-mediated temozolomide resistance in glioblastoma. Oncotarget. 2014;5(2):363-74.

346. De Strooper B, Saftig P, Craessaerts K, Vanderstichele H, Guhde G, Annaert W, et al. Deficiency of presenilin-1 inhibits the normal cleavage of amyloid precursor protein. Nature. 1998;391(6665):387-90.

347. Marambaud P, Shioi J, Serban G, Georgakopoulos A, Sarner S, Nagy V, et al. A presenilin-1/gamma-secretase cleavage releases the E-cadherin intracellular domain and regulates disassembly of adherens junctions. Embo j. 2002;21(8):1948-56.

348. Ni CY, Murphy MP, Golde TE, Carpenter G. gamma -Secretase cleavage and nuclear localization of ErbB-4 receptor tyrosine kinase. Science. 2001;294(5549):2179-81.

349. Lammich S, Okochi M, Takeda M, Kaether C, Capell A, Zimmer AK, et al. Presenilin-dependent intramembrane proteolysis of CD44 leads to the liberation of its intracellular domain and the secretion of an Abeta-like peptide. J Biol Chem. 2002;277(47):44754-9.

350. Wang R, Tang P, Wang P, Boissy RE, Zheng H. Regulation of tyrosinase trafficking and processing by presenilins: partial loss of function by familial Alzheimer's disease mutation. Proc Natl Acad Sci U S A. 2006;103(2):353-8.

351. Hata S, Taniguchi M, Piao Y, Ikeuchi T, Fagan AM, Holtzman DM, et al. Multiple gamma-secretase product peptides are coordinately increased in concentration in the cerebrospinal fluid of a subpopulation of sporadic Alzheimer's disease subjects. Mol Neurodegener. 2012;7:16.

352. Wu Y, Cain-Hom C, Choy L, Hagenbeek TJ, de Leon GP, Chen Y, et al. Therapeutic antibody targeting of individual Notch receptors. Nature. 2010;464(7291):1052-7.

353. Tejero R, Huang Y, Katsyv I, Kluge M, Lin J-Y, Tome-Garcia J, et al. Gene signatures of quiescent glioblastoma cells reveal mesenchymal shift and interactions with niche microenvironment. EBioMedicine. 2019;42:252-69.

354. Iwadate Y. Plasticity in Glioma Stem Cell Phenotype and Its Therapeutic Implication. Neurologia medico-chirurgica. 2018;58(2):61-70.

355. Wang J, Ma Y, Cooper MK. Cancer stem cells in glioma: challenges and opportunities. Translational Cancer Research. 2013;2(5):429-41.

356. Lan X, Jörg DJ, Cavalli FMG, Richards LM, Nguyen LV, Vanner RJ, et al. Fate mapping of human glioblastoma reveals an invariant stem cell hierarchy. Nature. 2017;549(7671):227-32.

357. Kim J, Lee I-H, Cho Hee J, Park C-K, Jung Y-S, Kim Y, et al. Spatiotemporal Evolution of the Primary Glioblastoma Genome. Cancer Cell. 2015;28(3):318-28.

358. Bao S, Wu Q, Sathornsumetee S, Hao Y, Li Z, Hjelmeland AB, et al. Stem Cell–like Glioma Cells Promote Tumor Angiogenesis through Vascular Endothelial Growth Factor. Cancer Research. 2006;66(16):7843-8.

359. Wakimoto H, Kesari S, Farrell CJ, Curry WT, Zaupa C, Aghi M, et al. Human Glioblastoma–Derived Cancer Stem Cells: Establishment of Invasive Glioma Models and Treatment with Oncolytic Herpes Simplex Virus Vectors. Cancer Research. 2009;69(8):3472-81.

360. Brennan CW, Verhaak RG, McKenna A, Campos B, Noushmehr H, Salama SR, et al. The somatic genomic landscape of glioblastoma. Cell. 2013;155(2):462-77.

361. Ceccarelli M, Barthel FP, Malta TM, Sabedot TS, Salama SR, Murray BA, et al. Molecular profiling reveals biologically discrete subsets and pathways of progression in diffuse glioma. Cell. 2016;164(3):550-63.

362. Batista CM, Mariano ED, Barbosa BJ, Morgalla M, Marie SK, Teixeira MJ, et al. Adult neurogenesis and glial oncogenesis: when the process fails. Biomed Res Int. 2014;2014:438639.

363. Holland EC, Celestino J, Dai C, Schaefer L, Sawaya RE, Fuller GN. Combined activation of Ras and Akt in neural progenitors induces glioblastoma formation in mice. Nature genetics. 2000;25(1):55-7.

364. Zhu Y, Guignard F, Zhao D, Liu L, Burns DK, Mason RP, et al. Early inactivation of p53 tumor suppressor gene cooperating with NF1 loss induces malignant astrocytoma. Cancer cell. 2005;8(2):119-30.

365. Llaguno SA, Chen J, Kwon C-H, Jackson EL, Li Y, Burns DK, et al. Malignant astrocytomas originate from neural stem/progenitor cells in a somatic tumor suppressor mouse model. Cancer cell. 2009;15(1):45-56.

366. Bachoo RM, Maher EA, Ligon KL, Sharpless NE, Chan SS, You MJ, et al. Epidermal growth factor receptor and Ink4a/Arf: convergent mechanisms governing terminal differentiation and transformation along the neural stem cell to astrocyte axis. Cancer cell. 2002;1(3):269-77.

367. Alcantara Llaguno S, Sun D, Pedraza AM, Vera E, Wang Z, Burns DK, et al. Cell-of-origin susceptibility to glioblastoma formation declines with neural lineage restriction. Nature Neuroscience. 2019;22(4):545-55.

368. Kobari L, Giarratana MC, Pflumio F, Izac B, Coulombel L, Douay L. CD133+ cell selection is an alternative to CD34+ cell selection for ex vivo expansion of hematopoietic stem cells. Journal of hematotherapy & stem cell research. 2001;10(2):273-81.

369. Uchida N, Buck DW, He D, Reitsma MJ, Masek M, Phan TV, et al. Direct isolation of human central nervous system stem cells. Proc Natl Acad Sci U S A. 2000;97(26):14720-5.

370. Brescia P, Ortensi B, Fornasari L, Levi D, Broggi G, Pelicci G. CD133 is essential for glioblastoma stem cell maintenance. Stem cells (Dayton, Ohio). 2013;31(5):857-69.

371. Beier D, Hau P, Proescholdt M, Lohmeier A, Wischhusen J, Oefner PJ, et al. CD133(+) and CD133(-) glioblastoma-derived cancer stem cells show differential growth characteristics and molecular profiles. Cancer research. 2007;67(9):4010-5.

372. Kalkan R. Glioblastoma Stem Cells as a New Therapeutic Target for Glioblastoma. Clinical Medicine Insights Oncology. 2015;9:95-103.

373. Li B, McCrudden CM, Yuen HF, Xi X, Lyu P, Chan KW, et al. CD133 in brain tumor: the prognostic factor. Oncotarget. 2017;8(7):11144-59.

374. Sathyan P, Zinn PO, Marisetty AL, Liu B, Kamal MM, Singh SK, et al. Mir-21-Sox2 Axis Delineates Glioblastoma Subtypes with Prognostic Impact. The Journal of neuroscience : the official journal of the Society for Neuroscience. 2015;35(45):15097-112.

375. Meacham CE, Morrison SJ. Tumour heterogeneity and cancer cell plasticity. Nature. 2013;501(7467):328-37.

376. Meyer M, Reimand J, Lan X, Head R, Zhu X, Kushida M, et al. Single cell-derived clonal analysis of human glioblastoma links functional and genomic heterogeneity. Proceedings of the National Academy of Sciences. 2015;112(3):851.

377. Hu YY, Zheng MH, Cheng G, Li L, Liang L, Gao F, et al. Notch signaling contributes to the maintenance of both normal neural stem cells and patient-derived glioma stem cells. BMC Cancer. 2011;11:82.

378. Stockhausen MT, Kristoffersen K, Poulsen HS. The functional role of Notch signaling in human gliomas. Neuro Oncol. 2010;12(2):199-211.

379. Meurette O, Mehlen P. Notch Signaling in the Tumor Microenvironment. Cancer Cell. 2018;34(4):536-48.

380. Man J, Yu X, Huang H, Zhou W, Xiang C, Huang H, et al. Hypoxic Induction of Vasorin Regulates Notch1 Turnover to Maintain Glioma Stem-like Cells. Cell Stem Cell. 2018;22(1):104-18.e6.

381. Middeldorp J, Hol EM. GFAP in health and disease. Prog Neurobiol. 2011;93(3):421-43.

382. Ferreira A, Caceres A. Expression of the class III beta-tubulin isotype in developing neurons in culture. J Neurosci Res. 1992;32(4):516-29.

383. Dai J, Bercury KK, Ahrendsen JT, Macklin WB. Olig1 function is required for oligodendrocyte differentiation in the mouse brain. J Neurosci. 2015;35(10):4386-402.

384. Fong H, Hohenstein KA, Donovan PJ. Regulation of self-renewal and pluripotency by Sox2 in human embryonic stem cells. Stem Cells. 2008;26(8):1931-8.

385. Garros-Regulez L, Garcia I, Carrasco-Garcia E, Lantero A, Aldaz P, Moreno-Cugnon L, et al. Targeting SOX2 as a Therapeutic Strategy in Glioblastoma. Frontiers in oncology. 2016;6:222-.

386. Berezovsky AD, Poisson LM, Cherba D, Webb CP, Transou AD, Lemke NW, et al. Sox2 Promotes Malignancy in Glioblastoma by Regulating Plasticity and Astrocytic Differentiation. Neoplasia. 2014;16(3):193-206.e25.

387. Gangemi RM, Griffero F, Marubbi D, Perera M, Capra MC, Malatesta P, et al. SOX2 silencing in glioblastoma tumor-initiating cells causes stop of proliferation and loss of tumorigenicity. Stem Cells. 2009;27(1):40-8.

388. Zhang M, Song T, Yang L, Chen R, Wu L, Yang Z, et al. Nestin and CD133: valuable stem cell-specific markers for determining clinical outcome of glioma patients. Journal of Experimental & Clinical Cancer Research. 2008;27:85.

389. Ignatova TN, Kukekov VG, Laywell ED, Suslov ON, Vrionis FD, Steindler DA. Human cortical glial tumors contain neural stem-like cells expressing astroglial and neuronal markers in vitro. Glia. 2002;39(3):193-206.

390. Hermansen SK, Christensen KG, Jensen SS, Kristensen BW. Inconsistent immunohistochemical expression patterns of four different CD133 antibody clones in glioblastoma. The journal of histochemistry and cytochemistry : official journal of the Histochemistry Society. 2011;59(4):391-407.

391. Calabrese C, Poppleton H, Kocak M, Hogg TL, Fuller C, Hamner B, et al. A perivascular niche for brain tumor stem cells. Cancer Cell. 2007;11(1):69-82.

392. Louis DN, Perry A, Reifenberger G, von Deimling A, Figarella-Branger D, Cavenee WK, et al. The 2016 World Health Organization Classification of Tumors of the Central Nervous System: a summary. Acta Neuropathol. 2016;131(6):803-20.

393. Howells M. Glioma – IDH1, IDH2, BRAF, 1p/19q LoH, MGMT methylation analysis: NHS Wales; 2018 [Available from: http://www.wales.nhs.uk/sites3/Documents/525/MI-GEN-Glioma.pdf.

394. Brandner S, Jaunmuktane Z, Roncaroli F, Hilton D, Thom M, Ansorge O. Dataset for histopathological reporting of tumours of the central nervous system, including the pituitary gland: The Royal College of Pathologists; 2020 [updated March 2020. 5:[Available from: https://www.rcpath.org/uploads/assets/abc54563-f574-40a0-b6b9a9a2cfbaa89d/g069-dataset-for-histopathological-reporting-of-tumours-of-the-central-nervous-system-in-adults-including-the-pituitary-gland.pdf.

395. Carlsson SK, Brothers SP, Wahlestedt C. Emerging treatment strategies for glioblastoma multiforme. EMBO Mol Med. 2014;6(11):1359-70.

396. Ahmed SI, Javed G, Laghari AA, Bareeqa SB, Farrukh S, Zahid S, et al. CD133 Expression in Glioblastoma Multiforme: A Literature Review. Cureus. 2018;10(10):e3439-e.

397. Wu B, Sun C, Feng F, Ge M, Xia L. Do relevant markers of cancer stem cells CD133 and Nestin indicate a poor prognosis in glioma patients? A systematic review and meta-analysis. Journal of Experimental & Clinical Cancer Research. 2015;34(1):44.

398. Krex D, Klink B, Hartmann C, von Deimling A, Pietsch T, Simon M, et al. Long-term survival with glioblastoma multiforme. Brain. 2007;130(Pt 10):2596-606.

399. TCGA. Comprehensive genomic characterization defines human glioblastoma genes and core pathways. Nature. 2008;455(7216):1061-8.

400. Saito N, Fu J, Zheng S, Yao J, Wang S, Liu DD, et al. A high Notch pathway activation predicts response to γ secretase inhibitors in proneural subtype of glioma tumor-initiating cells. Stem Cells. 2014;32(1):301-12.

401. Prados MD, Byron SA, Tran NL, Phillips JJ, Molinaro AM, Ligon KL, et al. Toward precision medicine in glioblastoma: the promise and the challenges. Neuro Oncol. 2015;17(8):1051-63.

402. Snuderl M, Fazlollahi L, Le LP, Nitta M, Zhelyazkova BH, Davidson CJ, et al. Mosaic amplification of multiple receptor tyrosine kinase genes in glioblastoma. Cancer Cell. 2011;20(6):810-7.

403. Patil V, Pal J, Somasundaram K. Elucidating the cancer-specific genetic alteration spectrum of glioblastoma derived cell lines from whole exome and RNA sequencing. Oncotarget; Vol 6, No 41. 2015.

404. Pine AR, Cirigliano SM, Nicholson JG, Hu Y, Linkous A, Miyaguchi K, et al. Tumor microenvironment is critical for the maintenance of cellular states found in primary glioblastomas. Cancer Discovery. 2020:CD-20-0057.

405. Tolcher AW, Messersmith WA, Mikulski SM, Papadopoulos KP, Kwak EL, Gibbon DG, et al. Phase I study of RO4929097, a gamma secretase inhibitor of Notch signaling, in patients with refractory metastatic or locally advanced solid tumors. J Clin Oncol. 2012;30(19):2348-53.

406. Masiero M, Li D, Whiteman P, Bentley C, Greig J, Hassanali T, et al. Development of Therapeutic Anti-JAGGED1 Antibodies for Cancer Therapy. Molecular Cancer Therapeutics. 2019;18(11):2030-42.

407. Osipo C, Golde TE, Osborne BA, Miele LA. Off the beaten pathway: the complex cross talk between Notch and NF-kappaB. Lab Invest. 2008;88(1):11-7.

408. Ivanov DP, Parker TL, Walker DA, Alexander C, Ashford MB, Gellert PR, et al. Multiplexing Spheroid Volume, Resazurin and Acid Phosphatase Viability Assays for

High-Throughput Screening of Tumour Spheroids and Stem Cell Neurospheres. PLOS ONE. 2014;9(8):e103817.

409. Yen JC, Chang FJ, Chang S. A new criterion for automatic multilevel thresholding. IEEE Trans Image Process. 1995;4(3):370-8.

8 Appendix

8.1 Analysis of Spheroid Volume using ImageJ

Images of spheroids were taken using a Leica DM IL LED microscope with an attached Leica DFC3000G camera. The scale of images was determined using a calibration slide. Images were analysed using the open-source ImageJ (Fiji package) and a macro designed by Ivanov et al. utilised to automate the process (408). The macro works on whole images of folders, converts them the black and white, and uses the Yen thresholding algorithm (409). It proceeds to clean any artefacts from the image, separates it from debris and determines the area of the spheroid. The macro also saves a copy of the file of each analysed image with a blue outline of the spheroids it has detected and an additional file with the numerical measurements for the whole folder. Data from the macro was analysed in Microsoft Excel and the measured area (S) of the 2D projection of the spheroids was used to calculate the radius ($R = \sqrt{\frac{S}{\pi}}$) and the volume ($V = \frac{4}{3}\pi R^3$) of each sphere.

8.1.1 Macro

//This macro aims to automate spheroid size measurement in three-dimensional cell culture. It requires input and output folders with images only, processes the images, records a file with spheroid measurements (Area, Ferret max, Ferret min, etc.) and writes an image with the outline/s of the determined spheroid/s.

//The spheroid detection and size determination function to be repeated for every image is defined below

function action(inputFolder,outputFolder,filename) {

```
open(inputFolder + filename);

//sets scale to predetermined values from calibration slide

run("Set Scale...", "distance=178 known=100 pixel=1 unit=µm global");

run("16-bit");

//run("Brightness/Contrast...");

run("Enhance Contrast", "saturated=0.35");

//Uses Yen thresholding algorithm

setAutoThreshold("Yen");

setOption("BlackBackground", false);

run("Convert to Mask");

//Gets the ratio between black (spheroid) and white (background) pixels. If we assume a single spheroid, the ratio between black and white pixels would allow us to estimate the size of the spheroid.

getHistogram(0,hist,256);

ratio = hist[255]/hist[0];

//If there are more pixels detected as spheroid(black) than background(white) then the spheroid has not been detected due to variations in background

if (ratio>1) {

        // closes the image, reopens it, subtracts the background and proceeds as normal
```

```
close();

open(inputFolder + filename);

run("16-bit");

// Subtract Background is not used in the default function because it can lead to merging of spheroids and debris or it can remove the core of the spheroid leaving a very thin interrupted edge. In certain cases where the edges of a spheroid are very bright removing the background can give better results.

run("Subtract Background...", "rolling=50 light");

setAutoThreshold("Yen");

setOption("BlackBackground", false);

run("Convert to Mask");

run("Remove Outliers...", "radius=15 threshold=0 which=Dark");

getHistogram(0,hist,256);

ratio = hist[255]/hist[0];};

//The strategy here is to act differently according to spheroid size. The general pattern is to expand and then shrink back the spheroids in order to include all cells on the edges. Then a series of functions are used to remove noise and the Watershed function separates fused or superimposed particles. The Analyse particles function is targeted to the specific spheroid size according to the black/white pixel ratio.

if (ratio<0.001) {

run("Maximum...", "radius=8");
```

```
	run("Fill Holes");

	run("Minimum...", "radius=8");

	//small spheroids require a more "gentle" function to clean up noise

	run("Median...", "radius=2");

	run("Maximum...", "radius=25");

	run("Minimum...", "radius=25");

	run("Fill Holes");

	run("Watershed");

	run("Analyse Particles...", "size=4000-Infinity circularity=0.20-1.00
show=[Overlay Outlines] display exclude include summarize");};

if (ratio >=0.001 && ratio<0.01) {

	run("Maximum...", "radius=8");

	run("Fill Holes");

	run("Minimum...", "radius=8");

	//slightly bigger spheroids and a more rigorous function to remove noise

	run("Remove Outliers...", "radius=10 threshold=0 which=Dark");

	run("Watershed");

	run("Analyse Particles...", "size=10000-Infinity circularity=0.20-1.00
show=[Overlay Outlines] display exclude include summarize");};

if (ratio>=0.01 && ratio<0.2) {
```

```
		run("Maximum...", "radius=8");
		run("Fill Holes");
		run("Minimum...", "radius=8");
		run("Remove Outliers...", "radius=15 threshold=0 which=Dark");
		run("Median...", "radius=4");
		run("Watershed");
		run("Analyse Particles...", "size=20000-Infinity circularity=0.20-1.00
show=[Overlay Outlines] display exclude include summarize");};
if (ratio>=0.2 && ratio<1) {
		//Very big spheroids generally do not need to be expanded much to fill up the
edges.
		run("Maximum...", "radius=3");
		run("Fill Holes");
		run("Minimum...", "radius=3");
		//Outliers and noise are removed rigorously
		run("Remove Outliers...", "radius=50 threshold=0 which=Dark");
		run("Minimum...", "radius=30");
		run("Maximum...", "radius=30");
		run("Watershed");
```

```
	run("Analyse Particles...", "size=50000-Infinity circularity=0.20-1.00
show=[Overlay Outlines] display exclude include summarize");};
 if (Overlay.size > 0) {
//Sends particles detected to the ROI manager
run("To ROI Manager");
close();
//Reopens the original image and pastes the outlines of the determined particles onto
it
open(inputFolder + filename);
run("From ROI Manager");
outputPath = outputFolder + filename;
save(outputPath);
close(); }
else {
	close();
};
call("java.lang.System.gc");
};
call("java.lang.System.gc");
run("Clear Results");
```

```
inputFolder = getDirectory("Choose the input folder!");

outputFolder = getDirectory("Choose the output folder!");

//Delete the next line if you want to see how the macro works on the images. However
that will reduce processing speed.

setBatchMode(true);

images = getFileList(inputFolder);

//Sets the measurements that are recorded for each spheroid

run("Set Measurements...", "area centroid shape feret's display add redirect=None
decimal=1");

//That is the cycle that runs through all images

for (i=0; i<images.length; i++) {

 action(inputFolder,outputFolder,images[i]);

 showProgress(i, images.length);

};

//Writes in the Results and Summary windows and saves the data.

selectWindow("Results");

saveAs("Measurements", "" + outputFolder + "Results.txt");

selectWindow("Summary");

saveAs("Text", "" + outputFolder +"Summary.txt");

setBatchMode(false);
```

8.2 ΔΔCT Method for Analysing RT-qPCR Data

ΔΔCT (also known as the Livak method) is a method used for analysing RT-qPCR data and enables the fold change in expression between DLL4/JAG1 overexpression and EV control cells to be calculated. In a qPCR assay, a positive reaction is detected by the accumulation of a fluorescent signal. The cycle threshold (CT) is defined as the number of cycles required for the fluorescent signal to cross the threshold (i.e. exceed background level). CT levels are inversely proportional to the amount of target nucleic acid in the sample, therefore, the lower the CT, the greater the amount of target nucleic acid. The ΔΔCT method requires a reference gene to normalise for possible variations during sample preparation. In this study, GAPDH was used as a reference gene.

Firstly, the average CT is obtained for each sample and for both the reference and target genes. ΔΔCT can then be calculated using the following method:

ΔCT = ΔCT (overexpression sample) – ΔCT (control sample)

Where, ΔCT (sample) = CT (target gene) – CT (reference gene), therefore,

ΔΔCT = (CT (control, target gene) – CT (control, reference gene) – (CT (overexpression, target gene) – CT (overexpression, reference gene)

The fold change of the target gene in the gene overexpression sample relative to the control sample can finally be calculated by calculating $2^{-\Delta\Delta CT}$. An example Microsoft Excel spreadsheet showing these calculations can be seen in Figure 8.1: ΔΔCT method used in this study to analyse qPCR data.

A

		U87-mDLL4			U87-EV										
		1	2	3	1	2	3	Average U87-mDLL4 Ct	Average U87-mDLL4 Ct	Average U87-EV Ct	Average U87-EV Ct	ΔCt (U87-mDLL4)	ΔCt (U87-EV)	Delta Delta Ct	Fold Change
		Ct Value	Ct Value	Ct Value	Ct Value	Ct Value	Ct Value	mDLL4	GAPDH	mDLL4	GAPDH	ΔCTE	ΔCTC	ΔΔCt	2^-ΔΔCt
	GAPDH	15.39	15.64	15.74	15.82	15.63	15.87	-	=AVERAGE(C6:E6)	-	=AVERAGE(F6:H6)	=(I7-J6)	=(K7-L6)	=(M6-N6)	**=2^(-O6)**
	mDLL4	17.23	16.78	17.74	42.82	38.42	36.85	=AVERAGE(C7:E7)	-	=AVERAGE(F7:H7)	-				

B

		U87-mDLL4			U87-EV										
		1	2	3	1	2	3	Average U87-mDLL4 Ct	Average U87-mDLL4 Ct	Average U87-EV Ct	Average U87-EV Ct	ΔCt (U87-mDLL4)	ΔCt (U87-EV)	Delta Delta Ct	Fold Change
		Ct Value	Ct Value	Ct Value	Ct Value	Ct Value	Ct Value	mDLL4	GAPDH	mDLL4	GAPDH	ΔCTE	ΔCTC	ΔΔCt	2^-ΔΔCt
	GAPDH	15.39	15.64	15.74	15.82	15.63	15.87	-	15.59	-	15.77333333	1.66	23.59	-21.93	**3995653.366**
	mDLL4	17.23	16.78	17.74	42.82	38.42	36.85	17.25	-	39.36333333	-				

Figure 8.1: ΔΔCT method used in this study to analyse qPCR data

The LightCycler 480 qPCR system (Roche) was used to performed qPCR and the data obtained was imported into Microsoft Excel for analysis. The average cycle threshold (CT) for each sample was calculated enabling the ΔΔCT, and therefore the $2^{-\Delta\Delta CT}$ to be calculated. (A) An overview of the formulas used in Microsoft Excel to calculate the fold change of mDLL4 overexpression in U87-mDLL4 cells compared to U87-EV control (whereby GAPDH is the housekeeping gene). (B) The values obtained following the method.

8.3 IHC Quantification

The intensity of IHC staining was assessed semi-quantitatively with the help of consultant neuropathologist, Dr David Hilton (Department of Cellular and Anatomical Pathology, University Hospitals Plymouth). DLL4, JAG1, and Nestin staining intensity was semi-quantified for each sample and graded as 0 (negative), 1 (weakly positive), 2 (moderately positive), and 3 (strongly positive). For CD133, IHC staining was semi-quantified by calculating the percentage of positively stained cells of more than 100 cells counted in areas of highest CD133 staining. Staining intensities for each marker for each patient for both primary and recurrent tumour samples, alongside MGMT and IDH status are documented in Figure 8.2.

IHC Staining Quantification

			DLL4		JAG1		Nestin		CD133	
Patient	IDH Status	MGMT Status	Primary	Recurrence	Primary	Recurrence	Primary	Recurrence	Primary	Recurrence
1	WT	M	2	2	1	2	3	2	14	26
2	WT	M	2	2	2	1	3	2	8	24
3	WT	U	2	2	0	1	3	2	33	23
4	WT	M	2	2	1	1	1	1	6	2
5	WT	U	2	2	0	1	2	1	5	27
6	WT	M	2	2	1	2	3	2	14	13
7	WT	U	2	2	2	2	3	2	20	24
8	WT	M	1	2	2	2	3	2	21	28
9	WT	M	2	2	0	2	3	3	39	34
10	Mutant	M	1	1	1	1	1	1	17	26
11	WT	M	2	2	1	1	2	1	29	19
12	WT	M	1	2	1	1	3	1	35	81
13	Mutant	M	2	1	0	0	1	1	2	1
14	WT	M	2	2	1	0	3	2	1	4
15	WT	U	2	2	1	0	2	2	7	8
16	WT	M	2	2	1	1	3	2	15	15
17	WT	M	2	2	2	1	3	2	2	5
18	WT	U	1	2	0	0	3	2	3	3
19	WT	M	2	2	1	0	1	2	1	1
20	WT	U	2	1	1	0	2	2	4	5
21	WT	M	2	2	1	1	3	2	0	11
22	WT	M	2	2	0	0	3	2	19	13
23	WT	U	2	2	2	0	2	2	8	7
24	WT	M	2	2	0	0	2	2	1	4
25	WT	U	2	2	2	0	3	2	4	9
26	WT	U	2	2	0	0	3	3	28	34
27	WT	U	2	2	2	1	3	2	6	18

Figure 8.2: Immunohistochemistry staining quantifications for primary and recurrent glioblastoma samples.

A total of 27 paired glioblastoma (primary and recurrent) tumour samples were assessed by IHC and semi-quantified by a consultant neuropathologist. IDH mutation status (WT; wild-type, M; mutant) and MGMT methylation status (M; methylated, U; unmethylated) were also documented.